https://doi.org/10.35662/unine-thesis-2987

Université de Neuchâtel
Institut de biologie

Faculty of Science, Institute of Biology
Plant Physiology Laboratory

Engineering Light Harvesting Complex II

A dissertation submitted to the
University of Neuchâtel
for the degree of
Doctor of Philosophy in Biological Sciences

Presented by
Hamed SATTARI VAYGHAN

Thesis committee

Prof. Felix Kessler (Thesis director) – University of Neuchâtel, Switzerland
Dr. Fiamma Longoni (Thesis co-director) – University of Neuchâtel, Switzerland
Prof. Roberta Croce – VU University Amsterdam, The Netherlands
Prof. Giovanni Finazzi – CEA Grenoble, France
Prof. Josephus Vermeer – University of Neuchâtel, Switzerland

October 2022

UNIVERSITÉ DE NEUCHÂTEL

Faculté des Sciences
Secrétariat-décanat de Faculté
Rue Emile-Argand 11
2000 Neuchâtel – Suisse
Tél : + 41 (0)32 718 21 00
E-mail : secretariat.sciences@unine.ch

IMPRIMATUR POUR THESE DE DOCTORAT

La Faculté des sciences de l'Université de Neuchâtel autorise l'impression de la présente thèse soutenue par

Monsieur Hamed SATTARI VAYGHAN

Titre:

"Engineering Light Harvesting Complex II"

sur le rapport des membres du jury composé comme suit:

- Prof. Felix Kessler, directeur de thèse, Université de Neuchâtel, Suisse
- Dr Fiamma Longoni, co-directrice de thèse, Université de Neuchâtel, Suisse
- Prof. Joop Vermeer, Université de Neuchâtel, Suisse
- Prof. Roberta Croce, Vrije Universiteit Amsterdam, NL
- Dr Giovanni Finazzi, CNRS (CEA Grenoble), France

Neuchâtel, le 20 octobre 2022

Le Doyen, Prof. R. Bshary

Acknowledgements

Felix
My deepest and sincere gratitude goes to **Prof. Dr. Felix Kessler**, Head of Plant Physiology Lab for providing the golden opportunity to join his lab. I thankfully acknowledge all his support, advice and encouragement during the last four years.

Fiamma
I cannot thank enough my research advisor **Dr. Fiamma Longoni** for believing in me enough to let me work on this exciting project. Her advice, immense knowledge and patience mean more to me than I can express. It was a great privilege and honor to work under her guidance. My completion of this thesis would not have been possible without her support through all the stages of my PhD. I am indebted to Fiamma; As a matter of fact, you did not at any time hesitate to support me. I have learned many things from you.

Committee
Gratitude is also owed to my committee members**: Prof. Roberta Croce**, **Prof. Giovanni Finazzi** and **Prof. Josephus Vermeer** for their insightful comments and suggestions.

Sonia
I would like to express my sincere gratitude to my wife **Sonia Spuri** who was robbed of many precious moments when I was working late in lab or writing alone in my office. Her continuous support, constant encouragement and her Love kept me going and helped overcome difficulties during these last years.

My family
A great heartful thank you to my parents: **Hosein Sattari** and **Ashraf Alamshahi** as well as my sister **Haniye** for all their financial and spiritual support throughout my life. They encouraged me to follow my aspirations during my career.

People from LPV
Last but not least I would like to thanks my former supervisor **Dr. Shanmugabalaji Venkatasalam**, my lab mates **Dr. Thibaut Pralon**, Wayne **Zita**, Sarah **Semeraro** and lab members for their support and useful scientific feedback during lab meeting discussions.

Many people provided immeasurable help in this project, I would like to express my immense appreciation and gratitude for all the support to make this project successful.

Abstract

To sustain the life on Earth solar energy has to be converted into chemical energy, this is possible thanks to the process called photosynthesis. Through a set of interconnected pigment-binding proteins, collectively called “light harvesting complex” (LHC), photon energy is collected and funneled towards the reaction centers (RCs) of the two photosystems. The RCs feed a series of redox reactions that ultimately allow the production of reducing power (NADPH) and ATP, used for the synthesis of organic molecules. Despite having a highly conserved core structure, the light harvesting complex II (LHCII) is capable to acclimate to a wide range of environmental conditions. LHCII can functionally associate to both photosystems thus allowing a fine tuning of the electron transport chain, or act as dissipators of excess light energy protecting the photosystems from photodamage. This dynamic regulation is crucial for the adaptation of plants to different light conditions.

LHCII is mostly composed of homo and hetero trimers of three isoforms: LHCB1, LHCB2 and LHCB3. The first two, through the phosphorylation of a threonine present in the N-terminal domain, are crucial for the regulation of the dynamics of the LHCII network. LHCB2 phosphorylation plays a central role in LHCII association to photosystem I and is thus regarded as the regulatory isoform of LHCII. The role of LHCB1 phosphorylation is less obvious; however, it has an impact in vivo allowing a partial adaptive response also in absence of LHCB2. Thanks to the CRISPR/Cas9 technique, we produced multiple mutants for the clustered genes coding for LHCB1 and LHCB2, thus allowing the production of complete null mutants for these two LHCII isoforms. These mutant lines constitute an ideal platform to study the impact of targeted modifications on the LHCII network via the production of complemented lines.

LHCB1 is the most abundant isoform of LHCII and, consequently, a multiple mutation of the five genes encoding this protein results in a pale phenotype, reduced PSII antenna cross-section, altered thylakoid structure along with lower Photosystem I over Photosystem II reaction center ratio. Interestingly, the loss of one of these two major isoforms results in compensatory effects at the phosphorylation level of the remaining. Loss of LHCB1 results in a de-phosphorylation of the remaining LHCB2, while loss of LHCB2 results in an over-phosphorylation of LHCB1. The complete knock out plants for both LHCB1 and LHCB2 were tested under prolonged fluctuating light, moderate temperature stress and their combination. This revealed an increased susceptibility to only the combined stress for the complete LHCB1 knock out, visible as a clear growth delay, combined with a decrease in the photosynthetic efficiency. Surprisingly, the loss of LHCB2, which impairs the antenna re-allocation between the two photosystems, did not result in any major defect under the combined stress condition.

Modification of the threonine of the phosphorylation site to alanine (non phosphorylable) or aspartate (constitutive negative charge "phospho-mimic») for both LHCB1 and LHCB2 reveals the impact of such irreversible modification on photosynthetic acclimation and on the dynamics of the photosynthetic complexes. We demonstrated that the complete removal of LHCB2 protein or the substitution of its phosphorylation site by alanine or aspartate largely, result in a physiologically overlapping phenotype with sharp reduction of state transitions and decreased LHCII-PSI-LHCI supercomplex formation. These defects result in slower acclimation to fluctuating light. Our results show that only with the phospho-threonine group LHCB2 can fully accomplish state transitions and that the negative charge of the aspartate substitution has no impact on short-term photosynthetic acclimation.

Disentangling the defined role of each antenna isoform, LHCB1 and LHCB2, could shed light in short and long term acclimatory processes. Leading to a better comprehension on how each isoform contributes to LHCII network organization and results in an optimal balance between light capture and photoprotection. The multiple null lines produced during this project are a milestone along this path and open future perspectives towards the design of innovative LHCII complementation studies.

Keywords: Arabidopsis, chloroplasts, CRISPR/Cas9, kinases, photosynthesis, photosynthetic acclimation, protein phosphorylation, electron transport, non-photochemical quenching, NPQ, light-harvesting complexes, LHC, state transitions, thylakoid membranes.

Résumé

Pour maintenir la vie sur Terre, l'énergie solaire doit être convertie en énergie chimique, ce qui est rendu possible grâce au processus appelé : « photosynthèse ». Grâce à un ensemble de protéines de liaison et aux pigments interconnectées, appelées collectivement "complexe de collecte de la lumière" (LHC), l'énergie photonique est collectée et acheminée vers les centres de réaction (CR) des deux photosystèmes. Les CR alimentent une série de réactions redox qui permettent la production de pouvoir réducteur (NADPH) et d'ATP, utilisés pour la synthèse de molécules organiques. Malgré une structure centrale hautement conservée, le complexe de récolte de la lumière II (LHCII) est capable de s'adapter à un large éventail de conditions environnementales. Le LHCII peut s'associer fonctionnellement aux deux photosystèmes, ce qui permet un réglage fin de la chaîne de transport des électrons, ou d'agir en tant que dissipateur d'énergie lumineuse excédentaire, protégeant ainsi les photosystèmes des photodommages. Cette régulation dynamique est cruciale pour l'adaptation des plantes à différentes conditions lumineuses.

LHCII est principalement composé de trimères homo et hétéro de trois isoformes : LHCB1, LHCB2 et LHCB3. Les deux premiers, par la phosphorylation d'une thréonine présente dans le domaine N-terminal, sont cruciaux pour la régulation de la dynamique du réseau LHCII. La phosphorylation de LHCB2 joue un rôle central dans l'association de LHCII au photosystème I et est donc considérée comme l'isoforme régulateur de LHCII. Le rôle de la phosphorylation de LHCB1 est moins évident ; cependant, elle a un impact in vivo permettant une réponse adaptative partielle également en l'absence de LHCB2. Grâce à la technique CRISPR/Cas9, nous avons produit des mutants multiples pour les gènes groupés codant pour LHCB1 et LHCB2, permettant ainsi la production de mutants nuls complets pour ces deux isoformes de LHCII. Ces lignées mutantes constituent une plateforme idéale pour étudier l'impact de modifications ciblées sur le réseau LHCII via la production de lignées complémentées.

LHCB1 est l'isoforme le plus abondante de LHCII et, par conséquent, une mutation multiple des cinq gènes codant pour cette protéine entraîne un phénotype pâle, une section transversale d'antenne PSII réduite, une structure de thylakoïde altérée ainsi qu'un rapport inférieur entre les centres de réaction du Photosystème I et du Photosystème II. Il est intéressant de noter que la perte de l'un de ces deux isoformes majeurs entraîne des effets compensatoires au niveau de la phosphorylation de l'autre. La perte de LHCB1 entraîne une dé-phosphorylation du LHCB2 restant, tandis que la perte de LHCB2 entraîne une sur-phosphorylation de LHCB1. Les plantes knock-out complètes pour LHCB1 et LHCB2 ont été testées sous une lumière fluctuante prolongée, un stress de température modérée et leurs combinaisons. Cela a révélé une susceptibilité accrue au seul stress combiné pour le knock-out complet de LHCB1, visible sous la forme d'un net retard de croissance, associé à une diminution de l'efficacité photosynthétique. Étonnamment, la perte de LHCB2, qui nuit à la réaffectation de l'antenne entre les deux photosystèmes, n'a pas entraîné de défaut majeur dans la condition de stress combiné. La modification de la thréonine du site de phosphorylation en alanine (non phosphorylable) ou en aspartate (charge négative constitutive "phospho-mimique") pour LHCB1 et LHCB2 révèle l'impact d'une telle modification irréversible sur l'acclimatation photosynthétique et sur la dynamique des complexes photosynthétiques. Nous avons démontré que l'élimination complète de la protéine LHCB2 ou la substitution de son site de phosphorylation par de l'alanine ou de l'aspartate en grande partie, entraînent un phénotype physiologiquement superposé avec une forte réduction des transitions d'état et une diminution de la formation du supercomplexe LHCII-PSI-LHCI. Ces défauts entraînent une acclimatation plus lente à la lumière fluctuante. Nos résultats montrent que seul le groupe phospho-thréonine permet à LHCB2 d'accomplir pleinement les transitions d'état et que la charge négative de la substitution aspartate n'a aucun impact sur l'acclimatation photosynthétique à court terme.

Le démêlage du rôle défini de chaque isoforme d'antenne, LHCB1 et LHCB2, pourrait faire la lumière sur les processus d'acclimatation à court et à long terme. Cela conduira à une meilleure compréhension de la façon dont chaque isoforme contribue à l'organisation du réseau LHCII et aboutit à un équilibre optimal entre la capture de la lumière et la photoprotection. Les multiples lignées nulles produites au cours de ce projet constituent une étape importante sur cette voie et ouvrent des perspectives futures vers la conception d'études innovantes sur la complémentation des LHCII.

Mots clés : Arabidopsis, chloroplastes, CRISPR/Cas9, kinases, photosynthèse, acclimatation photosynthétique, phosphorylation des protéines, transport d'électrons, quenching non-photochimique, antennes collectrices de lumière, LHC, transition d'état, membrane des thylakoïdes.

Table of content

Abbreviations

ATP	adenosine triphosphate
ATPase	ATP synthase
ADP	adenosine diphosphate
$C_6H_{12}O_6$	glucose
CO_2	carbon dioxide
Cyt b6f	cytochrome b6f
DCMU	3-(3,4-dichlorophenyl)-1,1-dimethylurea
DGDG	digalactosyldiacylglycerol
DMPBQ	dimethylphytylbenzoquinone
ECS	electrochromic shift
ETC	electron transport chain
e^-	electron
FAR	far-red
FM	maximum fluorescence in dark-adapted state
F0	minimum fluorescence in dark-adapted state
Fd	ferredoxin
FV	variable fluorescence in dark-adapted state
Fm	maximum fluorescence in dark
Fm’	maximum fluorescence in light
FS	steady-state chlorophyll fluorescence in light
FNR	ferredoxin NADP+ reductase
G3P	glyceraldehyde-3-phosphate
HA	human influenza hemagglutinin
H_2O	water
HPLC	high-performance liquid chromatography
kDa	kilodaltons
LEF	linear electron flow
LHC	light-harvesting complex
MGDG	monogalactosyldiacylglycerol
NADP(H)	nicotinamide adenine dinucleotide phosphate
NDH	NAD(P)H dehydrogenase
NPQ	non-photochemical quenching
O_2	molecular oxygen
OEC	oxygen evolving complex
PAR	photosynthetically active radiation
PC	plastocyanin
Pi	inorganic phosphate
PG	phosphatidylglycerol
pmf	proton motive force
PPH1	protein phosphatase 1
PQ	plastoquinone
PQH_2	plastoquinol
PSI	photosystem I
PSII	photosystem II
PTOX	plastid terminal oxidase / plastoquinone terminal oxidase
P680	photosystem II special chlorophyll a pair
P700	photosystem I special chlorophyll a pair
Q_A	plastoquinone strongly bound to photosystem II reaction center
Q_B	plastoquinone exchange site at photosystem II reaction center
Q_I	quinone binding/exchange site of cytochrome b6f at the stromal side

Q_O	quinone binding/exchange site of cytochrome b6f at the lumenal side
qE	energy- or pH-dependent quenching
qI	photoinhibitory quenching
qT	state transitions
Qy max	maximum quantum yield of PSII
qZ	zeaxanthin-dependent quenching
RCs	reaction centers
ROS	reactive oxygen species
Rubisco	ribulose-1,5-bisphosphate carboxylase/oxygenase
STN	state transition kinase
SQDG	sulfoquinovosyldiacylglycerol
TAP38	thylakoid-associated phosphatase 38
TEM	transmission electron microscopy
VI	variable fluorescence at 30 ms
VJ	variable fluorescence at 3 ms
WT	wild type
ΦMAX	maximum photosystem II efficiency
ΦPSII	photosystem II quantum yield

Chapter I

General introduction

Photosynthesis

Primary energy production to sustain life on Earth is largely fueled by photosynthesis, hence it is considered the principal supplier of organic compounds and energy in the biosphere (Hohmann-Marriott & Blankenship, 2011; Janssen et al., 2014; Kiang et al., 2007). Furthermore, it liberates oxygen during water oxidation as a side product, making this process the number one generator of atmospheric O_2. The latter triggered the massive extinction of anaerobic organisms and led to evolution of aerobic life and cellular respiration (Buick, 2008; Lyons et al., 2014) . In a nutshell, life on earth depends directly or indirectly on this process. The general biochemical reaction formula is the following:

$$\text{“}6\ CO_2 + 6\ H_2O + \text{light} \rightarrow C_6H_{12}O_6 + 6\ O_2\text{”}$$

Photoautotrophic organisms convert solar energy which encompasses particle-like packets of light (photons) into chemical energy and later biomass (Croce & van Amerongen, 2014; Stefan Jansson, 1999). Several concomitant physicochemical and biochemical reactions work in series to effect this energy conversion. It consists, essentially, of two successive phases: (I) A photochemical phase, referred to the light reactions ;(II) A biosynthetic phase known as dark reactions. The light-dependent reactions occur at the thylakoid membranes, whereas the dark ones take place in the stroma. The products of the light reactions are reduced nicotinamide adenine dinucleotide phosphate (NADPH), along with the highly energetic molecule, adenosine triphosphate (ATP). As the name suggests this stage depends on light and the photon energy is required to complete the reactions (Rabinowitch & Sons, 1969; Shevela et al., 2017). The light independent reactions are known as Calvin-Benson-Bassham cycle, during these reactions the molecules produced during the light reactions (ATP; NADPH) are used to assimilate carbon dioxide and produce organic compounds thanks to the most abundant enzyme on Earth, ribulose-1,5-bisphosphate carboxylase/oxygenase (Rubisco)(Björn & Govindjee, 2008; Stirbet et al., 2020). The general biochemical reaction formula is the following:

$$3\ CO_2 + 6\ NADPH + 5\ H_2O + 9\ ATP \rightarrow \text{glyceraldehyde-3-phosphate} + 2\ H^+ + 6\ NADP^+ + 9\ ADP + 8\ P_i$$

Chloroplast and thylakoid membrane

In plant cells, the photosynthetic machinery is located within a specialized disk-shaped (∼5 µm in diameter and ∼2.5µm in width) organelle called chloroplast (Figure 1) (Richardson, 2019; Staehelin, 2003). Plant and algal chloroplasts share many characteristics with a photosynthetic cyanobacterium. From an evolutionary point of view, the chloroplast is the outcome of an endosymbiotic event that occurred around 1.5 billion years ago (Maréchal, 2018; McFadden & van Dooren, 2004; Sánchez-Baracaldo et al., 2017). Based on the endosymbiont theory the chloroplast is derived from a free-living photosynthetic prokaryote that was absorbed by a eukaryotic cell. Finally, both cells evolved together stabilizing a mutually beneficial relation during which a large part of the prokaryotic genes were transferred to the eukaryotic nucleus. From the structural point of view the chloroplast is surrounded by an envelope consisting of an inner and outer membrane (Figure 1). As the majority of ancestral genes of the cyanobacterial genome was transferred to the host nucleus, translocon complexes to import nucleus-encoded proteins into the chloroplast emerged at the inner and outer envelope membranes (Kirchhoff, 2019; Strittmatter et al., 2010).

Besides the role of a physical barrier, the envelope membranes enclose a colorless alkaline aqueous matrix called stroma (Block et al., 2007). The stroma contains multiple copies of the circular chloroplast genome, ribosomes, all the enzymes involved in the dark reactions of photosynthesis as well as the components of many other pathways. Furthermore, the stroma encloses an intricate membrane network known as thylakoids where the light reactions of photosynthesis take place (Arnon, 1971). The thylakoids are a complex three-dimensional membrane system. The membrane is composed of a bilayer lipid that constitutes a matrix for the photosynthetic protein complexes and thus supports the electron transport chain.

Free diffusion of ions across the membrane is limited which allows the generation of a proton gradient via photosynthetic activities. Thylakoid lipid composition is highly conserved in photosynthetic organisms. However, lipid stoichiometry and fatty acid tails vary considerably (Anderson et al., 2012; Pribil et al., 2014; Vothknecht & Westhoff, 2001). Four main lipid classes form the thylakoid lipid bilayer. The most abundant is the neutral glycoglycerolipid family making up the bulk of the membrane. The number of galactose residues in their polar head groups allows classification as monogalactosyldiacylglycerols (MGDG) and digalactosyldiacylglycerols DGDG) accounting for ∼50 and ∼30 mole percent of thylakoid lipids, respectively (Domonkos et al., 2008; Mizusawa & Wada, 2012). MGDGs and DGDGs can also be classified by lengths of the esterified fatty acids and their degree of saturation. The remaining two minor anionic lipids are: sulfoquinovosyldiacylglycerol (SQDG) and phosphatidylglycerol (PG), each constitute ∼10 mole percent of total lipids (Lippold et al., 2012; Sato, 2004). Integrity of the thylakoid membrane requires a stable ratio of its constituents under standard growth conditions. The composition, however, can change in response to environmental stress (e.g., temperature variations)(Oakley et al., 2022; Sattari Vayghan et al., 2020; Zheng et al., 2011) . The thylakoid membrane itself is divided into stacks called grana that are connected by stroma exposed non-stacked portions of the membrane called stroma lamellae (Figure 1). The number of grana and stacking size is highly dynamic and the latter varies under different light conditions and as a result of acclimation (Mustárdy & Garab, 2003; Wood et al., 2019). 30 to 60 grana have been reported per mature wild type chloroplast and have a diameter between 0.3 to 0.6 µm (Koochak et al., 2019; Staehelin, 2003). Grana stacks have a highly curved non-appressed region at their periphery that is referred to as grana margin whereas the appressed region is referred to as grana core (Figure 1). The grana margin forms a third functional domain of thylakoids and its identity is highly debated (Anderson, 1989; Koochak et al., 2019).

Apart from lipids, which are the building blocks of the membrane, five major protein complexes together with some cofactors are embedded in this membrane (described in next section).

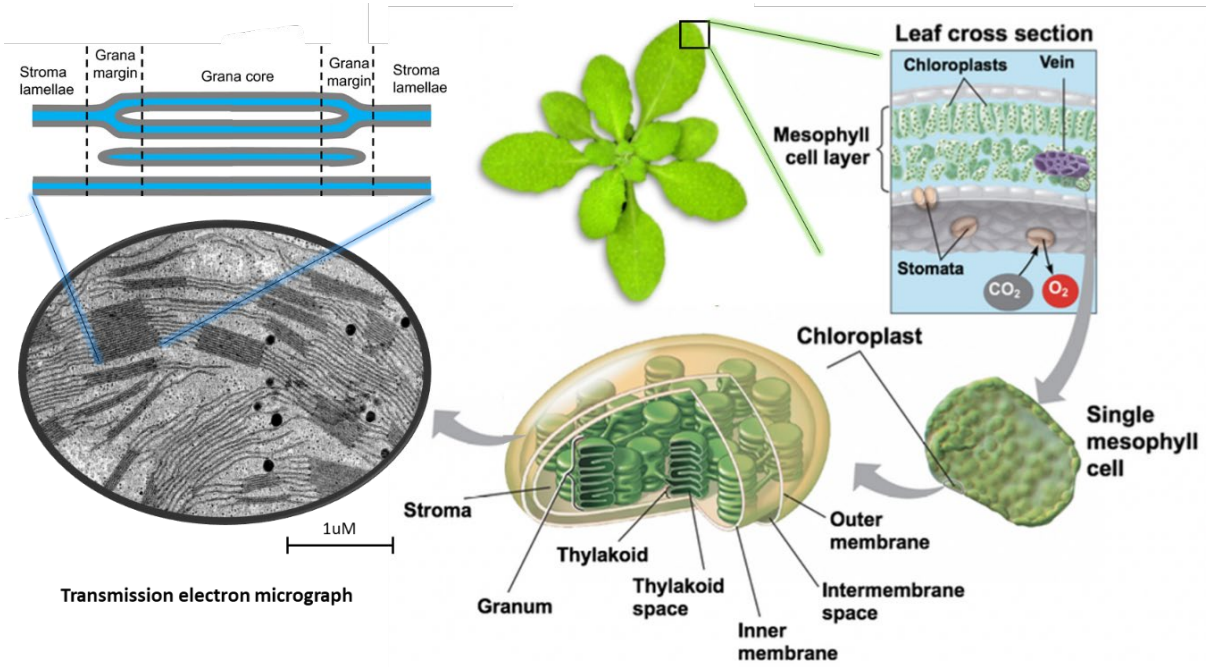

Figure 1 .Scheme of chloroplast location and internal structure of a chloroplast. *Arabidopsis thaliana* leaf contains mesophyll cells between the upper and lower epidermis, single mesophyll cells are rich in chloroplasts ranging from 1 to 50 per cell (Kubínová et al., 2014). The chloroplast comprises three main membrane compartments, namely outer membrane, inner membrane and the thylakoid membrane. The latter creates an internal network organized in grana stacks interconnected by stroma exposed membranes (stroma lamellae). TEM micrographs of Arabidopsis showing the 2 thylakoid membrane subdomains (https://digital.library.wisc.edu/1711.dl/HDTZ7JMHZ5VSU8C). The magnified cartoon view of thylakoid organization highlights a grana stack consisting of the grana core and the highly curved grana margin regions.

Pigment-protein complexes involved in linear and cyclic electron flows

Five major protein complexes are involved in linear electron transport: photosystem II (PSII) and photosystem I (PSI) containing the reaction centers, the light harvesting complexes I (LHCI) and II (LHCII) involved in light capture and transfer of the excitation energy towards the reaction centers, and the cytochrome b6f (Cytb6f) complex connecting PSI with PSII and contributing to the formation of the proton gradient. A separate complex, the ATP synthase produces ATP by dissipating the proton gradient that is formed during the electron transfer redox reactions in the thylakoid membrane(Dekker & Boekema, 2005; Dumas et al., 2016; Hisabori et al., 2013; Natali et al., 2016). Photosystem II absorbs light energy and simultaneously splits a water molecule (Pagliano et al., 2013). Photosystem II is mostly present as a dimer, each monomer is composed of two main core proteins D1(PsbA), D2(PsbD), and two core antenna CP47 (PsbB), CP43 (PsbC). Together with several other subunits (PsbE, PsbF) these form the reaction center of PSII(L. X. Shi & W. P. Schröder, 2004). The oxygen evolving complex (OEC) at the luminal side is essential for water splitting reaction (Renger & Kühn, 2007). Finally, additional extrinsic low molecular mass proteins (PsbH, PsbI, PsbJ, PsbK, PsbL, PsbM, PsbN, PsbR, PsbW, PsbE, psbF) complete the framework of PSII (L.-X. Shi & W. P. Schröder, 2004).

Plant photosystem I is monomeric and 18 different polypeptides constitute the PSI supercomplex. Two main proteins (PsaA, PsaB) form a heterodimer and from the main reaction center. Additional small subunits are involved in the association, stabilization of complex named PSI-A–L, PSI-N, and PSI-O (Jensen et al., 2004; Scheller et al., 2001).

It is worth mentioning that the spatial distribution of these complexes is heterogeneous across the thylakoid membrane (Reinat Nevo et al., 2012) . Photosystem II together with its associated light harvesting complex LHCII is mainly found in the grana stacks while photosystem I and its associated antenna LHCI as well as ATP synthase (ATPase) are only located in stroma-exposed lamellae. Cytochrome b6f (Cyt b6f) is distributed evenly between both sub compartments.

The grana margin is the only part that can host all of these complexes at the same time (Albertsson, 2001; Dekker & Boekema, 2005; Kirchhoff et al., 2017; Staehelin, 2003)(Figure 2A).
One reason for the described uneven distribution is their 3D structure; for instance, the stalk domain of ATP synthase extending on the stomal face is too bulky to fit inside the gap that separates the grana membranes. From a second, evolutionary point of view different kinetics of PSI and PSII may have triggered this compartmentalization; PSI which is a faster photosystem can drain LHCII excitation before arriving at PSII (preventing energy spillover). The distribution of photosynthetic protein complexes in grana margins is under debate and some studies found both photosystems in this region(Anderson, 1981; R. Nevo et al., 2012).

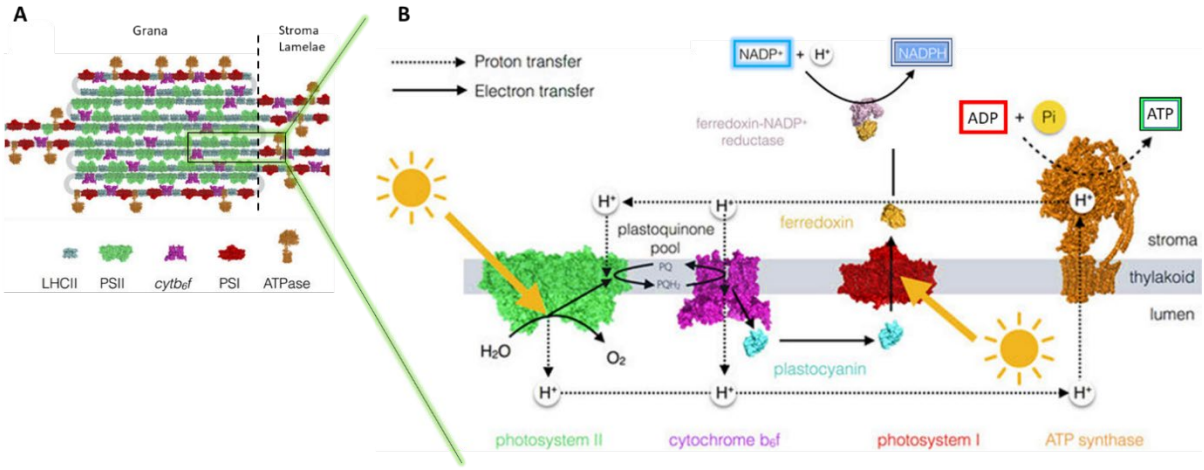

Figure 2. A) Schematic representation of the uneven distribution of the photosynthetic complexes in the thylakoid membrane subdomains. B) Electron and proton pathways in the linear electron transport chain consisting of photosystem II, cytochrome b6f complex, photosystem I and ATP synthase. Solid lines correspond to linear electron transport. Electrons extracted from water in PSII are used to reduce NADP+ to NADPH. Dashed lines represent the proton transfer pathway. During the linear electron transfer a proton gradient across the thylakoid membrane is formed and is used by the ATP synthase to produce ATP. The graphic is modified from (Johnson, 2016; Mullineaux, 2005).

In linear electron flow, light excitation collected by chlorophylls and carotenoids of the antenna is trapped to perform charge separation in PSII and PSI. At PSII, a special pair of chlorophyll a molecule (P680), is located in the reaction center of photosystem II (PSII) and acts as a primary electron donor. This name is due to their absorbance peak at 680 nm(Cardona et al., 2012; Pawlowicz et al., 2007). Lost electrons are replaced by oxidation of tyrosine 161 on D1 (YZ). Electrons lost by oxidation of tyrosine 161 are resupplied by oxidation of water by the manganese cluster (Mn_4CaO_5) inside the water-splitting complex that is coupled to PSII. This reaction also produces molecular oxygen (Pawlowicz et al., 2007). Two-time oxidative turnover of P680 is required to transfer two electrons via the primary electron acceptor pheophytin, to permanently bound plastoquinone molecule Q_A and then to plastoquinone PQ located in the Q_B site. Doubly reduced plastoquinone Q_B^{2-} is then protonated from the stromal side to plastoquinol PQH_2.
Plastoquinone acts as electron carrier along the thylakoid membrane and also contributes to the formation of the proton gradient across the membrane(Satoh et al., 1995; Van Eerden et al., 2017) . PQH_2 binds to the Cytb6f luminal Q_o site where it is oxidized liberating two electrons. During this process two protons are also released in the thylakoid lumen contributing to the proton gradient. The two shuttled electrons have different fates: the first electron will reduce another plastoquinone attached to the stromal Q_i site of cytochrome b6f. This process is known as the Q-cycle(Mitchell, 1975; Van Eerden et al., 2017). The second electron released in this process will be transferred to Rieske Fe_2-S_2 protein and cytochrome f to plastocyanin (PC), which is a water-soluble, copper-containing protein located in the lumen.

It is worth mentioning that plastoquinone oxidation is the rate limiting process under normal light conditions, so that the redox state of the PQ pool involved in the photosynthesis is an indicator of the efficiency of the electron transport (Hasan & Cramer, 2012; Schöttler et al., 2004).
PC carries a single electron to PSI where it reduces the $P700^+$ chlorophyll a at the reaction center, which donates its electron and becomes oxidized upon excitation by a photon. Electrons will be transferred to ferredoxin (Fd) and then to the $NADP^+$ reductase enzyme. The outcome of this electron flux is the production of NADPH from $NAPD^+ + 2H^+$ and the proton motive force (pmf) across the thylakoid membrane. pmf is used by CF1-F0 ATP synthase to produce ATP (Figure 3)(Hahn et al., 2018; Jensen et al., 2007). Aside from LEF which drives electrons from water to CO_2, there is an alternative electron transport pathway called cyclic electron flow (CEF). As the name suggests electrons can be recycled in this process. It takes place around PSI and Cytb6f thus in stromal exposed membranes. It has an important role in maintaining efficiency of photosynthesis and protection of both photosystems (Munekage et al., 2004).
Under non-optimal conditions such as high light stress CEF alleviates oxidative stress in the chloroplast. It has been shown that under fluctuating light conditions the presence of this pathway is crucial to protect PSI against oxidative damage. During CEF, electrons from Fd, instead of being directed to NADP+ reductase, are used to reduce the PQ in Qi site of cytochrome b6f, via an electron transport chain involving PGR5, PGRL1 or NDH-like proteins (Figure 3)(Ishikawa et al., 2016; Munekage et al., 2002). The likely reason for the existence of this pathway is to uncouple the generation of the transmembrane proton motive force (ΔpH) from the linear electron transport. This allows to increase the ATP synthesis in order to compensate for the higher consumption of ATP compared to NADPH in the Calvin cycle. Increased ΔpH also triggers the induction of non-photochemical quenching (NPQ) that will be discussed later (Miyake et al., 2004). Thus, these two pathways limit the overreduction of the acceptor side of photosystem I by providing an additional electron pool. This prevents photosystem I photoinhibition especially under non-optimal conditions.

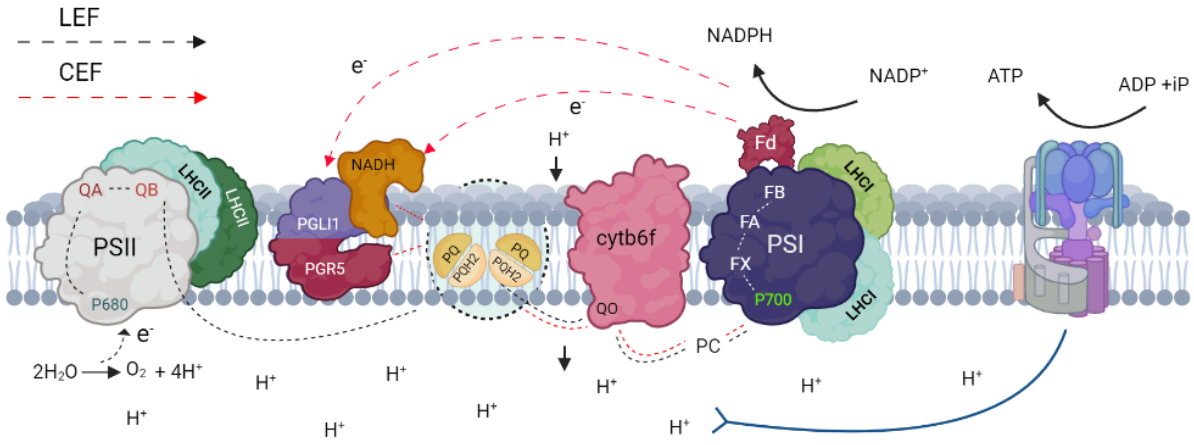

Figure 3. Two main photosynthetic electron transport routes implicate different photosynthetic complex assemblies. The black dashed line corresponds to linear electron flow (LEF) which starts with light excitation capture and funneling by LHCII to the reaction center of photosystem II. During the initial charge separation process, a special pair of Chl (P680) transfers one electron to Q_B site of PSII via Q_A quinone. The lost electron is replaced immediately by an electron extracted from water in the water splitting reaction. At the same time this reaction produces protons (H^+) which acidify the lumen along with molecular oxygen as a byproduct. Two electrons in the QB site are required to doubly reduce the plastoquinone molecule PQ. The reduced plastoquinone molecule is protonated to plastoquinol (PQH_2). Plastoquinol diffuses in the thylakoid membrane to the Q_O site of cytochrome b6f. One of the electrons is transferred to plastocyanin PC which is the water-soluble electron carrier in the lumen bringing it to the P700 chlorophyll in PSI. Light excitation energizes PSI and electrons end up at the final electron acceptor $NADP^+$ to produce NADPH via FX, FA, FB subunits of PSI and finally ferredoxin. Red dashed lines represent the alternative electron pathway known as cyclic election flow (CEF). Electrons from ferredoxin are reinjected into the plastoquinone pool (PQ/PQH_2) instead of being directed to $NADP^+$ reductase. They are used to reduce the PQ in Qi site of cytochrome b6f, via an electron transport chain involving PGR5, PGRL1 or NDH-like proteins. This contributes to the formation of the ΔpH which triggers thermal dissipation. CEF mainly diminishes the overreduction of the acceptor side of PSI when the Calvin cycle activity is impaired under non-optimal conditions.

Light-harvesting complexes in plants

Limited light absorption capacity of the photosystem II reaction center is largely expanded by the light harvesting antenna system proteins. Their ability to rapidly trap photons and transfer chlorophyll excitation (in ~150 picoseconds) allows the charge separation reactions in the PSII reaction center to occur efficiently (Caffarri et al., 2011; van Amerongen & Croce, 2013) . They also have important photoprotective tasks when the light excitation exceeds the electron transport chain capacity. In eukaryotic organisms, concomitant with land colonization, Light-Harvesting Complexes (LHCs) evolved in response to the oxygen-enriched atmosphere, and high and fluctuating photonic environments (Ballottari et al., 2012). LHCs are membrane embedded pigment binding proteins encoded by nuclear genes (Dall'Osto et al., 2015). The members of light-harvesting complexes are similar in structure and pigment organization. However, they can be distinguished by their interactions with the photosystems and their spectroscopic properties (van Oort et al., 2015). They have similar masses of about 25 kDa. An atomic model based on cryo-electron microscopy revealed that each antenna isoforms binds 8 chlorophyll a and 6 chlorophyll b molecules. Furthermore, each antenna also has two lutein molecules, one 9'-cis neoxanthin, assumed to act as accessory light harvesting pigments, and a violaxanthin or zeaxanthin molecule (Liu et al., 2004). Chlorophyll a and b absorption maxima are slightly different, contributing to a wider range absorption in photosynthetically active radiation (PAR)(Saito et al., 2018). In addition to the mentioned pigments a phospholipid molecule is also incorporated into the protein (Nicol et al., 2018). From structural point of view, three transmembrane alpha helices (A, B, C) compose the core part of the protein which binds most of the pigments. They are interconnected with stromal (A-C) and luminal loops (B-C) (Figure 4). The main core of the antenna is not so flexible and similar between different isoforms (Liu et al., 2004).

The major differences between the isoforms are in the two flexible domains, the N-terminal part and the luminal loop. The N-terminal part harbors a threonine residue that is subject to conditional

phosphorylation. The diversification of these two domains hints to distinct functional roles for each isoform (Crepin & Caffarri, 2018; Pietrzykowska et al., 2014) .

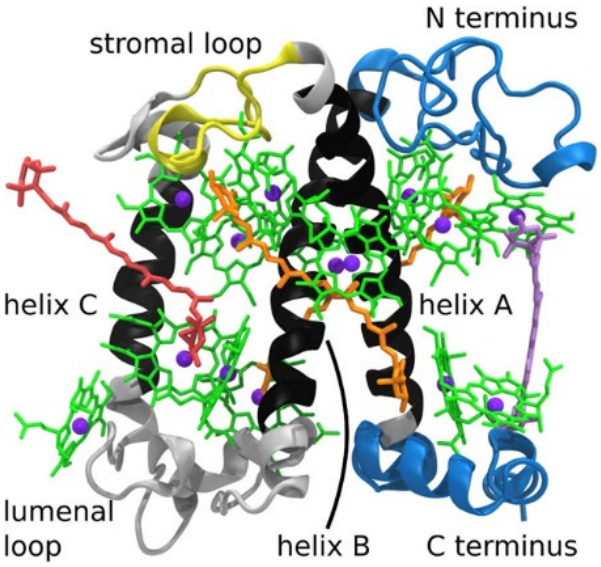

Figure 4. Structure of LHCII monomer with all embedded cofactors. The aliphatic tails of the chlorophylls (green) are omitted for clarity. Neoxanthin is colored red, lutein orange, and violaxanthin light violet. The black bold regions are the three transmembrane helices A, B, and C. N -terminal region is and C terminal are shown in light and dark blue respectively. stomal and luminal loop are shown in yellow and green. Figure adapted from (Thallmair et al., 2019).

Two categories of genes coding for LHCs associate with PSI and PSII respectively called LHCI and LHCII. The major LHCII is the most abundant membrane protein on the Earth and accounts for roughly 30% of the thylakoid membrane proteins and harbors half of the total Chl (Peter & Thornber, 1991; Wientjes & Croce, 2011). It is organized into trimers that are composed of three protein isoforms: LHCB1, LHCB2, and LHCB3. The trimerization of majors LHCII requires the sequence motif WYGPDR at the N terminal region. LHCB1 and LHCB2 can assemble as homotrimers or heterotrimers, including also LHCB3 (Ballottari et al., 2012; Green & Pichersky, 1994). LHCB1 and LHCB2 are the product of multiple genes in plants. For example, in *Arabidopsis thaliana* five genes encode *quasi-identical* LHCB1 proteins. Three genes code for LHCB2 and a single gene for LHCB3 (Leutwiler et al., 1986; McGrath et al., 1992). The most abundant isoform is LHCB1 constituting∼ 70% of the major LHCII, LHCB2 accounts for ∼20% and LHCB3 for about 10% (Galka et al., 2012; Sattari Vayghan et al., 2022). The LHCII comprise also three monomeric antenna CP29, CP26 and CP24 correspond to the genes LHCB4, LHCB5 and LHCB6, respectively and in most case are present in 1:1 stoichiometry with PSI core(Jansson, 1994; Wientjes et al., 2013a).

The monomeric antennas connect the LHCII trimers to photosystem II, therefore the lack of these proteins causes a change in the network of the LHCII that is reflected in a less efficient energy transfer (Chukhutsina et al., 2020; Croce, 2020) . The major LHCII trimers mainly capture and funnel photon excitation energy through minor antenna to the reaction center. Taken together minor and major subunits of LHCII compose one third of the thylakoid proteins in plants.

LHCII trimers can bind to PSII at multiple sites thus creating different PSII-LHCII supercomplexes. Trimeric LHCII associates directly to the dimeric PSII core, interacting with the monomeric LHCB5 or indirectly, bridged through the monomeric antenna proteins LHCB4 and LHCB6. The former trimer is conventionally called “S trimer” for strongly associated and the latter “M trimer” for moderately associated (Sheng et al., 2019; van Amerongen & Croce, 2013) . Dissociation of M trimers from PSII core is suggested to have a protective role under high light conditions (Betterle et al., 2009).There is also a population of loosely bound mobile LHCII, called “L-trimers”.

Due to their loose interaction with PSII, they are not consistently isolated with the PSII-LHCII complexes (Dekker & Boekema, 2005).The L-trimers have been characterized when associated with PSI in the LHCII-PSI-LHCI complex and found to be composed by LHCB1 and LHCB2. Loosely bound trimers serve as the antennae for both Photosystem I and II. Apart from their association to PSII these three types of trimers have a different composition of antenna isoforms, S and L trimers are composed of LHCB1 and LHCB2 isoforms, while the M trimer contains also the LHCB3 isoform (Su et al., 2017). A typical PSII supercomplex visualized with high resolution structure contains two core dimers (C_2), Two strongly associated S trimers (S_2) and two moderately associated M trimers (M_2) forming a so called $C_2S_2M_2$ supercomplex. However, this supercomplex can became even larger by association of one or more L-trimers (L_x) to its periphery constituting a $C_2S_2M_2L_x$ supercomplex (Figure 5 A) (Caffarri et al., 2014; Croce, 2020) .

The light harvesting complex exclusively binding to PSI is called LHCI and it is mainly in dimeric form. The most common PSI-LHCI complex isolated in higher plants contains two heterodimers of LHCI associated with a monomeric PSI core complex (Mazor et al., 2017) . LHCA1 and LHCA4 isoforms form one dimer, while LHCA2 and LHCA3 form the second one (Mazor et al., 2017). Recently, PSI complexes with an additional LHCA1-LHCA4 dimer were observed by electron microscopy so that larger PSI-LHCI complexes may exist *in vivo* (Crepin et al., 2020) .Each of these isoforms is encoded by a single gene in Arabidopsis (Klimmek et al., 2006). It is worth mentioning that two additional genes, named Lhca5 and Lhca6, encode close homologs of the LHCA1-4. However, these genes are rarely expressed, and their protein products are only found in sub-stoichiometric amounts compared to PSI reaction centers. They can be found mostly in PSI-NDH complexes (Otani et al., 2018). Apart for LHCI, PSI antenna can be expanded by the association of a LHCII trimer, constituting the LHCII-PSI-LHCI complex. The dynamic association and dissociation of the LHCII trimer with this complex is crucial to balance the excitation energy between the two photosystems. This regulatory process, called state transitions, will be discussed in detail in the next section (Figure 5 B) (Pan et al., 2018).

Association of light harvesting complexes together with different thylakoid embedded proteins gives rise to different supercomplexes thereby creating a dynamic environment to maintain photosynthesis efficiency. Furthermore, fine tuning of these associations is crucial in fast acclimation processes in response to environmental cues (Duffy & Ruban, 2015; Pietrzykowska et al., 2014). The central determinant for the association of the LHCII trimers with the various supercomplexes is the N-terminal sequence and the phosphorylation level of the isoforms that compose each trimer (Fristedt et al., 2009). In a nutshell, these apoproteins are largely dedicated to light capture; however, they also have important photoprotective and regulatory tasks.

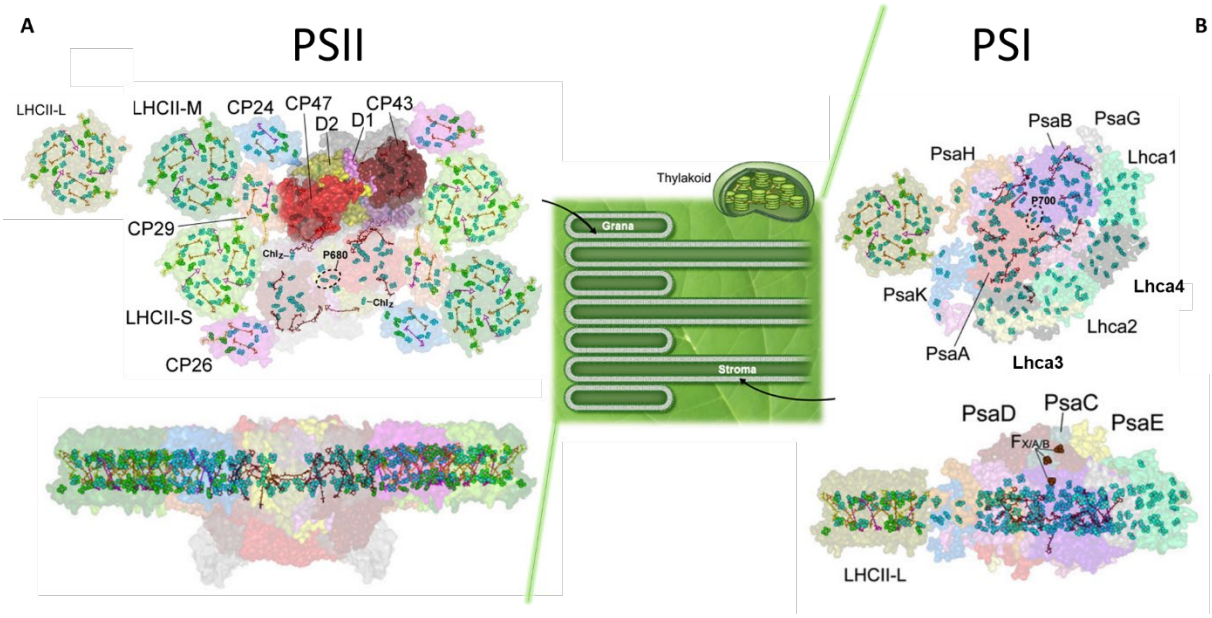

Figure 5. **Schematic representation of the luminal and lateral section of Photosystem II (PSII) and Photosystem I (PSI) supercomplexes and their localization in the thylakoid membrane**. A) Luminal (top) and lateral (down) view of PSII-LHCII supercomplex ($C_2S_2M_2$) associated with one L trimer. The heterodimer of D1 and D2 subunits compose the reaction center of PSII. Two internal antenna CP43 and CP47 are indicated in brown and red and other core proteins are shown in opaque grey. Monomeric LHCII antenna proteins are presented as: CP24, CP26 and CP29 which are in 1:1 stoichiometry with each reaction center core and finally the major LHCII trimers are noted as LHCII-S, -M and -L for strongly, moderately and loosely associated with the complex. B) Luminal (top) and lateral (down) views of the LHCII-PSI-LHCI supercomplex. PsaA and PsaB are the core subunits known as PSI reaction center. Two LHCI heterodimers, composed of Lhca1-Lhca4 and Lhca2-Lhca3, are shown associated to this complex. An extra LHCII L-trimer can bind to the opposite side of the LHCI dimers and enlarge the antenna cross-section. This figure is adapted from (Caffarri et al., 2014; Croce, 2020).

Regulatory mechanisms of photosynthesis

State transitions

Under moderate light conditions, the antenna system gathers light energy and transfers it to the reaction centers in form of chlorophyll excitation. This increases the efficiency of light capture and optimizes the photosynthetic electron transfer (Caffarri et al., 2011). During linear electron transport, photosystem I and photosystem II work in series, hence their excitation level should be balanced to avoid damage and optimize electron transport. Under natural light regimes, changes in the light spectrum may result in an imbalance in the excitation level between the two photosystems. For example, under the canopy, where the far-red light component is enriched, PSI is preferentially excited, due to the predominance of chlorophyll a and stable red shifted pigments present in this complex. Conversely, PSII has a different absorption spectrum that depends on its connection to a large portion of the LHCII, which is enriched in chlorophyll b and therefore increases the absorption efficiency in the blue and red light (Laisk et al., 2014).

To ensure optimal efficiency of electron flow, a reallocation of a fraction of the trimeric LHCII from PSII to PSI allows compensating for this uneven excitation between photosystems. This short term and reversible phenomenon is known as state transitions (qT) (Haldrup et al., 2001; Minagawa, 2011; Murata, 1969). If the imbalance persists long term acclimation processes can follow, for instance a change in photosystem stoichiometry (Dietzel et al., 2011; Pfannschmidt, 2003) .

Due to state transitions, “state 1” is induced during acclimation to far-red light that excites PSI. This state is defined by the connection of most of the LHCII to PSII. It is linked with a low phosphorylation level of LHCII, which favors its association with PSII. These observations are consistent with the conclusion that the excitation cross-section of PSII becomes larger in plants acclimated to “state 1”(Bennett, 1977).

Inversely, “state 2” is induced when plants are exposed to red and blue light that preferentially excite PSII. Opposite phenomena were observed as the room temperature fluorescence decreased. This is due to the fact that in “state 2” a fraction of LHCII binds to PSI, which can also be visualized by a stable LHCII-PSI-LHCI complex (Kouřil et al., 2018; Pan et al., 2018). It is worth mentioning that, in plants acclimated to natural light conditions an intermediate state between State 1 and State 2 is established and LHCII thus serves as an antenna for both photosystems (Wientjes et al., 2013b).

In higher plants, the antenna involved in this energy redistribution is almost exclusively a specific subpopulation of the trimeric LHCII identified as “L-trimers”, which is detached from one photosystem and connected to the other. This reversible transition is regulated by the phosphorylation and dephosphorylation of a threonine located in the N-terminal portion of the LHCII subunits. In a nutshell, any imbalance in the two photosystems’ excitation levels is sensed by the redox poise of the photoactive plastoquinone pool (PQ/PQH_2). If PSII is more excited than PSI, the plastoquinone pool would be mostly in the reduced form (PQH_2), which results a more frequent occupancy of the Q_0 site in the luminal side of cytochrome b6f by PQH_2. This activates STN7, which is the main kinase involved in the phosphorylation of LHCII subunits. It has been shown that STN7 interacts with cytochrome b6f subunit IV and RIESKE protein (Dumas et al., 2017). Furthermore, two highly conserved Cys-residues located near the N-terminus and luminally exposed part of STN7 are suggested to be involved in the redox sensing and regulation process (Lemeille et al., 2009; Rintamäki et al., 2000). STN7 kinase possesses a single membrane-spanning domain and its activation also leads to autophosphorylation (Bellafiore et al., 2005).

Oxidation of plastoquinone is required to inactivate the STN7 kinase. The LHCII antenna is dephosphorylated by the action of the PPH1/TAP38 phosphatase. It has been reported that the redox state of the PQ pool has no impact on its activity, however presence of divalent cation is crucial (Pribil et al., 2010; Shapiguzov et al., 2010).State transition is mainly dependent on the phosphorylation/dephosphorylation of LHCII, with key role attributed to the LHCB2 isoform (Longoni et al., 2015) .

It has been suggested that phosphorylation of LHCII triggers the migration of the antenna from appressed region of the thylakoid membrane (grana) to the non-appressed regions (grana margin and stroma lamellae) which are enriched in PSI complexes.
Some reports suggest that the electrostatic repulsion of the negative charges of the phosphate groups, along with the conformational changes of the LHCII antenna disfavor its binding to PSII and triggers its reallocation towards PSI (Dietzel et al., 2011; Leoni et al., 2013). One of the main points of this modification is the disassociation of a LHCII mobile trimer from the larger PSII-LHCII complexes and its association with PSI. This results in an increase of the PSI relative antenna size upon transition to state2 (Minagawa, 2011). The so-called "L -trimer" of LHCII antenna interacts with the PsaL, PsaO, PsaH subunits of photosystem I on the opposite side of the LHCI belt. The phosphorylated threonine in the third position of the mature form of LHCB2 is proposed to constitute a key residue for the docking with PSI subunits (Amunts et al., 2007; Lunde et al., 2000; Plöchinger et al., 2016). Recently, some evidence suggested that a LHCII trimer, potentially with a different subunit composition than the "L-trimer", can bind PSI trough the LHCI antenna belt (Benson et al., 2015). The presence of extra LHCII associated to PSI is supported by spectroscopic studies demonstrating that up to three LHCII trimers can transfer energy to PSI (Bell et al., 2015; Bos et al., 2017).

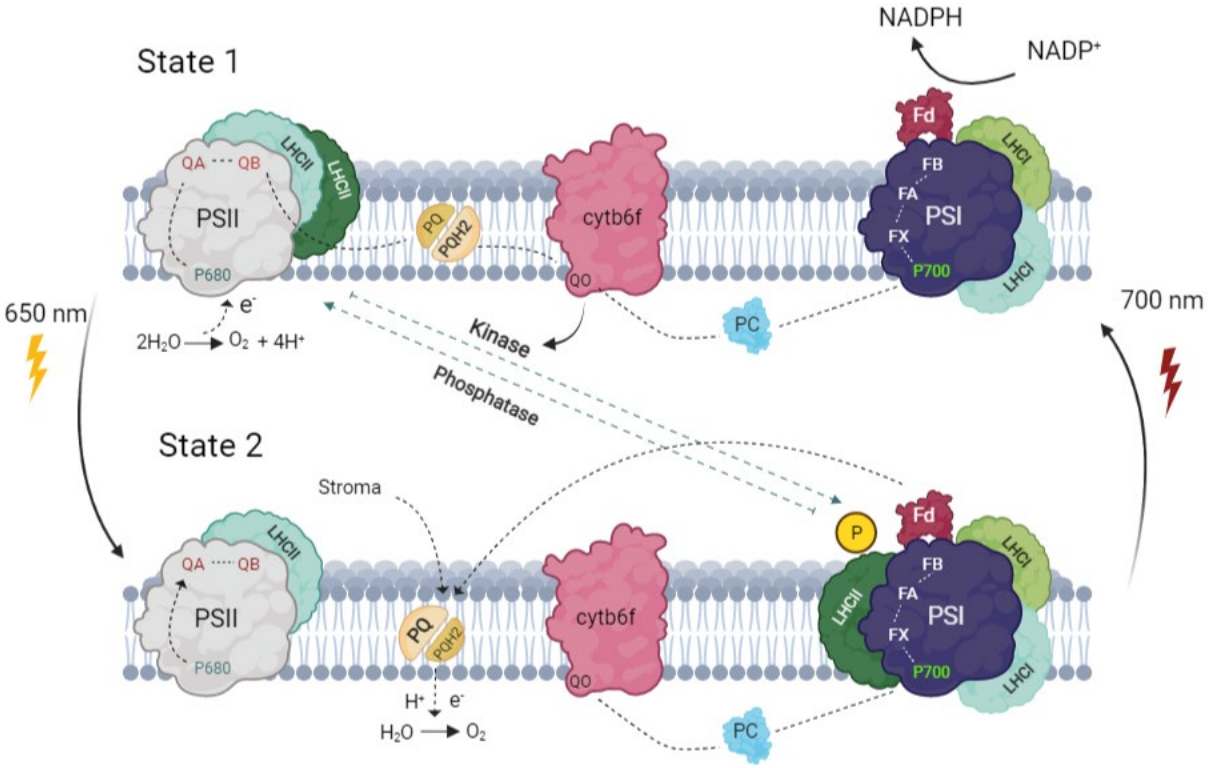

Figure 6. Schematic representation of State transitions regulation adapted from (Rochaix, 2007) . Exposure of plants to different light wavelengths results in excitonic imbalance of the two photosystems. Light with the wavelength~ 650 nm is known as state 2 light and preferentially excites PSII, so that plastoquinone PQ is reduced to plastoquinol (PQH_2). PQH_2 diffuses across the thylakoid membrane and binds to the Qo site of cytochrome b6f. This triggers the activation of the STT7/STN7 kinase and the subsequent phosphorylation of LHCII. Phosphorylation of the antenna along with its conformational change decreases its affinity for PSII and increases its affinity for PSI. Accordingly, a fraction of LHCII antenna detaches from PSII and migrates to bind PSI present in non-appressed regions of the thylakoid membrane. This results in an increase of the PSI antenna cross section, hence, reestablishing the excitonic equilibrium. In contrary, upon exposure to state 1 light (enriched in far-red, 700 nm) the excitation of PSI is favored. This leads to the oxidation of the plastoquinone pool and to the inactivation of STN7. By the action of LHCII-counteracting phosphatase PPH1/TAP38, LHCII is dephosphorylated and re-allocated from PSI to PSII. Dynamic association of LHCII with PSII and PSI alleviates the negative impact of excitation imbalance and is known as state transitions (qT).

Non-Photochemical-Quenching (NPQ)

Besides light capture and state transitions, LHCII is involved in the protection of the photosynthetic apparatus from excess light (Govindjee, 2002). At high light intensity, chlorophyll excitation may overcome the electron transport capacity. This leads to an overreduction of the electron carriers. Therefore, the excited chlorophyll of PSII reaction center may not have any available electron acceptor. A consequence of this condition is the stabilization of the chlorophyll of the reaction center in a singlet state (^{1}Chl*), which in turn can lead to the formation of ^{3}Chl*. This relatively stable form of excited chlorophyll can lead to the production of reactive oxygen species (ROS), which can react with the proteins and lipids surrounding the reaction center and eventually lead to damage of PSII itself (Tripathy & Oelmüller, 2012). When the damage exceeds the repair capacity it results in a drop of PSII maximal quantum yield. As the PSII damage also has a protective effect on the electron transport chain, it is also considered a component of Non-Photochemical-Quenching (NPQ) known as photoinhibition (qI) (Murata et al., 2007). To preempt accumulation of excited chlorophylls and avoid damaging PSII, a rapid response takes place in the photosynthetic complexes. This protective process is the major component of the NPQ (Pinnola & Bassi, 2018). It is a fast-inducible process allowing the dissipation of the excess of light-derived excitation as heat in a harmless fashion.

The decrease of the lumen pH due to the accumulation of the protons translocated across membrane triggers NPQ (Pinnola & Bassi, 2018). In higher plants, the fastest NPQ component requires the protonation of the transmembrane protein PsbS. This small protein of 22 kDa belongs to the LHC superfamily.

Four highly conserved glutamates in the luminal side of this protein are crucial for its pH sensing (Stefan Jansson, 1999; X. P. Li et al., 2002) . PsbS protonation triggers a conformational change of LHCII and its oligomerization along with supercomplex reorganization that favors the energy quenching (qE)(X. P. Li et al., 2002; Ruban, 2016). It could be reverted within seconds to minutes in the dark and is called energy dependent quenching due to energization of thylakoid (*i.e.* ΔpH). NPQ switches off when the electron transport slows down and the proton gradient is dissipated by the ATP synthase.

A second NPQ component, also induced by the lumen acidification, is known as the xanthophyll cycle. It represents an efficient mechanism to protect the photosynthetic machinery under overexciting conditions. Some carotenoids of this cycle act as direct quenchers of (1Chl*). However, the most common and intensively studied mechanism is the de-epoxidation of the violaxanthin associated with LHCII to zeaxanthin (Niyogi et al., 1998) . The catalytic enzyme responsible for this conversion is violaxanthin de-epoxidase (VDE) and is located in thylakoid lumen and can be activated upon its protonation. Zeaxanthin is considered a 'quencher' by the fact that its S_1 energy is below that of Chl a(Holt et al., 2005; Kress & Jahns, 2017). The activation and relaxation of this quenching mechanism are much slower than that of qE. It can take up to hours to completely reconvert all the bound zeaxanthin to violaxanthin to completely relax the qZ component (Johnson et al., 2009; Li et al., 2000). This reaction is catalyzed by the zeaxanthin epoxidase (ZE), which counteracts the VDE activity. The xanthophyll cycle needs a structural re-arrangement of the light harvesting complex and of the protein-lipid interaction to operate efficiently (for a recent review see (Goss & Latowski, 2020) .

The precise site of NPQ is under debate and poorly defined. However, the chlorophylls associated to the LHCII trimer along with the lutein are likely to create the quenching site. The NPQ is thus a multifactorial process that requires the change in ΔpH as a trigger, dedicated catalytical proteins as PsbS, and possibly also other partners such as the thylakoid membrane lipids, but the contribution of these remains still largely unclear (Holt et al., 2004; X.-P. Li et al., 2002; Sylak-Glassman et al., 2014). Even though NPQ is an essential protective process, its activation decreases the quantum yield of PSII, its fine tuning is thus required to ensure the optimization of the photosynthesis in all light conditions and therefore to maximize plant productivity (Holt et al., 2004).

LHCII phosphorylation and its role in the thylakoid organization

In higher plants phosphorylable isoforms of major LHCII trimers are composed of LHCB1 and LHCB2. LHCB3 lacks any obvious phosphorylation site and is most likely involved in light energy transfer from the main LHCB1/LHCB2 antennae to the PSII core (Grieco et al., 2012; Longoni & Goldschmidt-Clermont, 2021). In *Arabidopsis thaliana* both phosphorylable isoforms contain a threonine residue at the N-terminal part of the mature protein which can undergo reversible phosphorylation, mainly by the action of the STN7 kinase (Tikkanen & Aro, 2012) . The sequence surrounding the LHCB2 threonine is highly conserved among different species, which is consistent with its specific role in state transitions, as previously discussed (Longoni et al., 2015). The LHCB1 N-terminal sequence, on the contrary, has more variations across different species, and also between duplicate genes in the same species. For instance, among the 5 genes coding for LHCB1, Lhcb1.4 codes for a protein with a different N-terminal sequence lacking the threonine residue that is phosphorylated (S. Jansson, 1999). Although this is a relatively unique feature of Arabidopsis, it is still unclear whether this specific LHCB1 isoform has a unique role in LHCII regulation (Crepin & Caffarri, 2018). The specific role of LHCB1 phosphorylation is poorly understood, however its phosphorylation is suggested to be linked to heat dissipation (Pietrzykowska et al., 2014). The absolute extents of phosphorylation of LHCB1 and LHCB2 also vary in different trimers associated either with PSI or PSII. For instance, LHCB2 in the pool of LHCII trimers associated with PSI-LHCI-LHCII supercomplex is extensively phosphorylated (>98%).

Interestingly, the phosphorylation of the LHCB1 isoform in this trimer is almost non-detectable (Leoni et al., 2013; Longoni et al., 2015) . Phosphorylated LHCB1 has been observed in the “S and M trimers” associated to PSII (Crepin & Caffarri, 2015) .LHCII phosphorylation is also involved in thylakoid reorganization. This process may be important in allowing the LHCII “L trimers” and the PSII-LHCII complexes to migrate from the center of the grana stacks to their margins.
This process may facilitate the equilibration of energy between the two photosystems facilitating the formation of LHCII-PSI-LHCI and/or LHCII-PSII-PSI-LHCI complexes. Non-identical extent of phosphorylation of these two isoforms in different supercomplexes suggests that they have a specific role during dynamic light acclimation (Grieco et al., 2012). Despite the difference in the final phosphorylation level and their distribution within supercomplexes, the kinetics of LHCB1 and LHCB2 phosphorylation remain similar during the shift from far-red to blue light (Longoni et al., 2015).

Aim of the project

The main goal of my thesis is to investigate the role of the two most abundant LHCII isoforms Lhcb1 and Lhcb2 in the dynamic organization of the LHCII network. Said organisation is important to maintain an optimal balance between the light-derived excitation of the two photosystems to enhance the photosynthetic yield but also to activate mechanisms preventing photodamage such as NPQ, which mostly occurs at the level of LHCII. My aim is to elucidate the role of these two major LHCII subunits and their reversible phosphorylation on the dynamics and regulation of the LHCII network.

To address this question stable knock-out lines for all the genes encoding Lhcb1 and for the genes encoding Lhcb2 will be produced using CRISPR/Cas9 directed mutagenesis. The first goal will be to characterize these mutants and compare their phenotype with previously described knock-down antenna mutants. To detail the impact of this multiple mutation the knock-out lines will be tested for any kind of impairment in growth, development and acclimation to different light regimes (constant or fluctuating light). Lhcb1 and Lhcb2 knock-out lines will also be complemented with a HA-tagged version of the protein carrying a point mutation leading to the substitution of the phosphorylated threonine to a non-phosphorylable amino acid to address the role of this phosphorylation. The goal is to understand how this post-translational modification of the N-terminally located threonine influences the organisation of the LHCII, its connectivity to the photosystems and, consequently, the ability of the plant to acclimate to different environmental conditions.

The in-depth investigation of all these mutant and complemented lines will be realised by analysing thylakoid protein accumulation, photosynthetic parameters, protein phosphorylation levels, lipidomic profile changes, super complex reorganisation by Native gel and Mass spectrometry analysis, the antenna size and connectivity, as well as the PSII/PSI ratio.

The ultimate goal is to gain a deeper understanding of the dynamics of the organization of the major component of the LHCII antenna system, the role of the regulatory residues of LHCII subunits and how these aspects impact plant photosynthetic efficiency and productivity.

References

Albertsson, P. (2001). A quantitative model of the domain structure of the photosynthetic membrane. *Trends Plant Sci*, *6*(8), 349-358. https://doi.org/10.1016/s1360-1385(01)02021-0

Amunts, A., Drory, O., & Nelson, N. (2007). The structure of a plant photosystem I supercomplex at 3.4 Å resolution. *Nature*, *447*(7140), 58-63. https://doi.org/10.1038/nature05687

Anderson, J. M. (1981). Consequences of spatial separation of photosystem 1 and 2 in thylakoid membranes of higher plant chloroplasts. *FEBS Letters*, *124*(1), 1-10. https://doi.org/https://doi.org/10.1016/0014-5793(81)80041-5

Anderson, J. M. (1989). The grana margins of plant thylakoid membranes. *Physiologia Plantarum*, *76*(2), 243-248. https://doi.org/https://doi.org/10.1111/j.1399-3054.1989.tb05640.x

Anderson, J. M., Horton, P., Kim, E. H., & Chow, W. S. (2012). Towards elucidation of dynamic structural changes of plant thylakoid architecture. *Philos Trans R Soc Lond B Biol Sci*, *367*(1608), 3515-3524. https://doi.org/10.1098/rstb.2012.0373

Arnon, D. I. (1971). The Light Reactions of Photosynthesis. *Proceedings of the National Academy of Sciences*, *68*(11), 2883-2892. https://doi.org/doi:10.1073/pnas.68.11.2883

Ballottari, M., Girardon, J., Dall'Osto, L., & Bassi, R. (2012). Evolution and functional properties of Photosystem II light harvesting complexes in eukaryotes. *Biochimica et Biophysica Acta (BBA) - Bioenergetics*, *1817*(1), 143-157. https://doi.org/https://doi.org/10.1016/j.bbabio.2011.06.005

Bell, A. J., Frankel, L. K., & Bricker, T. M. (2015). High Yield Non-detergent Isolation of Photosystem I-Light-harvesting Chlorophyll II Membranes from Spinach Thylakoids: IMPLICATIONS FOR THE ORGANIZATION OF THE PS I ANTENNAE IN HIGHER PLANTS. *J Biol Chem*, *290*(30), 18429-18437. https://doi.org/10.1074/jbc.M115.663872

Bellafiore, S., Barneche, F., Peltier, G., & Rochaix, J.-D. (2005). State transitions and light adaptation require chloroplast thylakoid protein kinase STN7. *Nature*, *433*(7028), 892-895. https://doi.org/10.1038/nature03286

Bennett, J. (1977). Phosphorylation of chloroplast membrane polypeptides. *Nature*, *269*(5626), 344-346. https://doi.org/10.1038/269344a0

Benson, S. L., Maheswaran, P., Ware, M. A., Hunter, C. N., Horton, P., Jansson, S., Ruban, A. V., & Johnson, M. P. (2015). An intact light harvesting complex I antenna system is required for complete state transitions in Arabidopsis. *Nature Plants*, *1*(12), 15176. https://doi.org/10.1038/nplants.2015.176

Betterle, N., Ballottari, M., Zorzan, S., de Bianchi, S., Cazzaniga, S., Dall'Osto, L., Morosinotto, T., & Bassi, R. (2009). Light-induced Dissociation of an Antenna Hetero-oligomer Is Needed for Non-photochemical Quenching Induction. *Journal of Biological Chemistry*, *284*(22), 15255-15266. https://doi.org/https://doi.org/10.1074/jbc.M808625200

Björn, L. O., & Govindjee. (2008). The Evolution of Photosynthesis and Its Environmental Impact. In L. O. Björn (Ed.), *Photobiology: The Science of Life and Light* (pp. 255-287). Springer New York. https://doi.org/10.1007/978-0-387-72655-7_12

Block, M. A., Douce, R., Joyard, J., & Rolland, N. (2007). Chloroplast envelope membranes: a dynamic interface between plastids and the cytosol. *Photosynth Res*, *92*(2), 225-244. https://doi.org/10.1007/s11120-007-9195-8

Bos, I., Bland, K. M., Tian, L., Croce, R., Frankel, L. K., van Amerongen, H., Bricker, T. M., & Wientjes, E. (2017). Multiple LHCII antennae can transfer energy efficiently to a single Photosystem I. *Biochimica et Biophysica Acta (BBA) - Bioenergetics*, *1858*(5), 371-378. https://doi.org/https://doi.org/10.1016/j.bbabio.2017.02.012

Buick, R. (2008). When did oxygenic photosynthesis evolve? *Philos Trans R Soc Lond B Biol Sci*, *363*(1504), 2731-2743. https://doi.org/10.1098/rstb.2008.0041

Caffarri, S., Broess, K., Croce, R., & van Amerongen, H. (2011). Excitation energy transfer and trapping in higher plant Photosystem II complexes with different antenna sizes. *Biophys J*, *100*(9), 2094-2103. https://doi.org/10.1016/j.bpj.2011.03.049

Caffarri, S., Tibiletti, T., Jennings, R. C., & Santabarbara, S. (2014). A comparison between plant photosystem I and photosystem II architecture and functioning. *Curr Protein Pept Sci*, *15*(4), 296-331. https://doi.org/10.2174/1389203715666140327102218

Cardona, T., Sedoud, A., Cox, N., & Rutherford, A. W. (2012). Charge separation in photosystem II: a comparative and evolutionary overview. *Biochim Biophys Acta*, *1817*(1), 26-43. https://doi.org/10.1016/j.bbabio.2011.07.012

Chukhutsina, V. U., Liu, X., Xu, P., & Croce, R. (2020). Light-harvesting complex II is an antenna of photosystem I in dark-adapted plants. *Nature Plants*, *6*(7), 860-868. https://doi.org/10.1038/s41477-020-0693-4

Crepin, A., & Caffarri, S. (2015). The specific localizations of phosphorylated Lhcb1 and Lhcb2 isoforms reveal the role of Lhcb2 in the formation of the PSI-LHCII supercomplex in Arabidopsis during state transitions. *Biochimica et Biophysica Acta (BBA) - Bioenergetics*, *1847*(12), 1539-1548. https://doi.org/https://doi.org/10.1016/j.bbabio.2015.09.005

Crepin, A., & Caffarri, S. (2018). Functions and Evolution of Lhcb Isoforms Composing LHCII, the Major Light Harvesting Complex of Photosystem II of Green Eukaryotic Organisms. *Curr Protein Pept Sci*, *19*(7), 699-713. https://doi.org/10.2174/1389203719666180222101534

Crepin, A., Kučerová, Z., Kosta, A., Durand, E., & Caffarri, S. (2020). Isolation and characterization of a large photosystem I–light-harvesting complex II supercomplex with an additional Lhca1–a4 dimer in Arabidopsis. *The Plant Journal*, *102*(2), 398-409. https://doi.org/https://doi.org/10.1111/tpj.14634

Croce, R. (2020). Beyond 'seeing is believing': the antenna size of the photosystems in vivo. *New Phytol*, *228*(4), 1214-1218. https://doi.org/10.1111/nph.16758

Croce, R., & van Amerongen, H. (2014). Natural strategies for photosynthetic light harvesting. *Nature Chemical Biology*, *10*(7), 492-501. https://doi.org/10.1038/nchembio.1555

Dall'Osto, L., Bressan, M., & Bassi, R. (2015). Biogenesis of light harvesting proteins. *Biochim Biophys Acta*, *1847*(9), 861-871. https://doi.org/10.1016/j.bbabio.2015.02.009

Dekker, J. P., & Boekema, E. J. (2005). Supramolecular organization of thylakoid membrane proteins in green plants. *Biochim Biophys Acta*, *1706*(1-2), 12-39. https://doi.org/10.1016/j.bbabio.2004.09.009

Dietzel, L., Bräutigam, K., Steiner, S., Schüffler, K., Lepetit, B., Grimm, B., Schöttler, M. A., & Pfannschmidt, T. (2011). Photosystem II Supercomplex Remodeling Serves as an Entry Mechanism for State Transitions in Arabidopsis *The Plant Cell*, *23*(8), 2964-2977. https://doi.org/10.1105/tpc.111.087049

Domonkos, I., Laczkó-Dobos, H., & Gombos, Z. (2008). Lipid-assisted protein-protein interactions that support photosynthetic and other cellular activities. *Prog Lipid Res*, *47*(6), 422-435. https://doi.org/10.1016/j.plipres.2008.05.003

Duffy, C. D. P., & Ruban, A. V. (2015). Dissipative pathways in the photosystem-II antenna in plants. *Journal of Photochemistry and Photobiology B: Biology*, *152*, 215-226. https://doi.org/https://doi.org/10.1016/j.jphotobiol.2015.09.011

Dumas, L., Chazaux, M., Peltier, G., Johnson, X., & Alric, J. (2016). Cytochrome b 6 f function and localization, phosphorylation state of thylakoid membrane proteins and consequences on cyclic electron flow. *Photosynth Res*, *129*(3), 307-320. https://doi.org/10.1007/s11120-016-0298-y

Dumas, L., Zito, F., Blangy, S., Auroy, P., Johnson, X., Peltier, G., & Alric, J. (2017). A stromal region of cytochrome b(6)f subunit IV is involved in the activation of the Stt7 kinase in Chlamydomonas. *Proc Natl Acad Sci U S A*, *114*(45), 12063-12068. https://doi.org/10.1073/pnas.1713343114

Fristedt, R., Willig, A., Granath, P., Crèvecoeur, M. l., Rochaix, J.-D., & Vener, A. V. (2009). Phosphorylation of Photosystem II Controls Functional Macroscopic Folding of Photosynthetic Membranes in Arabidopsis *The Plant Cell*, *21*(12), 3950-3964. https://doi.org/10.1105/tpc.109.069435

Galka, P., Santabarbara, S., Khuong, T. T., Degand, H., Morsomme, P., Jennings, R. C., Boekema, E. J., & Caffarri, S. (2012). Functional analyses of the plant photosystem I-light-harvesting complex II supercomplex reveal that light-harvesting complex II loosely bound to photosystem II is a very efficient antenna for photosystem I in state II. *Plant Cell*, *24*(7), 2963-2978. https://doi.org/10.1105/tpc.112.100339

Goss, R., & Latowski, D. (2020). Lipid Dependence of Xanthophyll Cycling in Higher Plants and Algae [Review]. *Frontiers in Plant Science*, *11*. https://doi.org/10.3389/fpls.2020.00455

Govindjee. (2002). A role for a light-harvesting antenna complex of photosystem II in photoprotection. *Plant Cell*, *14*(8), 1663-1668. https://doi.org/10.1105/tpc.140810

Green, R. R., & Pichersky, E. (1994). Hypothesis for the evolution of three-helix Chl a/b and Chl a/c light-harvesting antenna proteins from two-helix and four-helix ancestors. *Photosynth Res*, *39*(2), 149-162. https://doi.org/10.1007/bf00029382

Grieco, M., Tikkanen, M., Paakkarinen, V., Kangasjärvi, S., & Aro, E. M. (2012). Steady-state phosphorylation of light-harvesting complex II proteins preserves photosystem I under fluctuating white light. *Plant Physiol*, *160*(4), 1896-1910. https://doi.org/10.1104/pp.112.206466

Hahn, A., Vonck, J., Mills, D. J., Meier, T., & Kühlbrandt, W. (2018). Structure, mechanism, and regulation of the chloroplast ATP synthase. *Science*, *360*(6389). https://doi.org/10.1126/science.aat4318

Haldrup, A., Jensen, P. E., Lunde, C., & Scheller, H. V. (2001). Balance of power: a view of the mechanism of photosynthetic state transitions. *Trends in Plant Science*, *6 7*, 301-305.

Hasan, S. S., & Cramer, W. A. (2012). On rate limitations of electron transfer in the photosynthetic cytochrome b6f complex. *Phys Chem Chem Phys*, *14*(40), 13853-13860. https://doi.org/10.1039/c2cp41386h

Hisabori, T., Sunamura, E., Kim, Y., & Konno, H. (2013). The chloroplast ATP synthase features the characteristic redox regulation machinery. *Antioxid Redox Signal*, *19*(15), 1846-1854. https://doi.org/10.1089/ars.2012.5044

Hohmann-Marriott, M. F., & Blankenship, R. E. (2011). Evolution of Photosynthesis. *Annual Review of Plant Biology*, *62*(1), 515-548. https://doi.org/10.1146/annurev-arplant-042110-103811

Holt, N. E., Fleming, G. R., & Niyogi, K. K. (2004). Toward an Understanding of the Mechanism of Nonphotochemical Quenching in Green Plants. *Biochemistry*, *43*(26), 8281-8289. https://doi.org/10.1021/bi0494020

Holt, N. E., Zigmantas, D., Valkunas, L., Li, X. P., Niyogi, K. K., & Fleming, G. R. (2005). Carotenoid cation formation and the regulation of photosynthetic light harvesting. *Science*, *307*(5708), 433-436. https://doi.org/10.1126/science.1105833

Ishikawa, N., Takabayashi, A., Noguchi, K., Tazoe, Y., Yamamoto, H., von Caemmerer, S., Sato, F., & Endo, T. (2016). NDH-Mediated Cyclic Electron Flow Around Photosystem I is Crucial for C4 Photosynthesis. *Plant Cell Physiol*, *57*(10), 2020-2028. https://doi.org/10.1093/pcp/pcw127

Janssen, P. J., Lambreva, M. D., Plumeré, N., Bartolucci, C., Antonacci, A., Buonasera, K., Frese, R. N., Scognamiglio, V., & Rea, G. (2014). Photosynthesis at the forefront of a sustainable life. *Front Chem*, *2*, 36. https://doi.org/10.3389/fchem.2014.00036

Jansson, S. (1994). The light-harvesting chlorophyll ab-binding proteins. *Biochimica et Biophysica Acta (BBA) - Bioenergetics*, *1184*(1), 1-19. https://doi.org/https://doi.org/10.1016/0005-2728(94)90148-1

Jansson, S. (1999). A guide to the Lhc genes and their relatives in Arabidopsis. *Trends in Plant Science*, *4*(6), 236-240. https://doi.org/https://doi.org/10.1016/S1360-1385(99)01419-3

Jansson, S. (1999). A guide to the Lhc genes and their relatives in Arabidopsis/IT>. *Trends Plant Sci*, *4*(6), 236-240. https://doi.org/10.1016/s1360-1385(99)01419-3

Jensen, P. E., Bassi, R., Boekema, E. J., Dekker, J. P., Jansson, S., Leister, D., Robinson, C., & Scheller, H. V. (2007). Structure, function and regulation of plant photosystem I. *Biochim Biophys Acta*, *1767*(5), 335-352. https://doi.org/10.1016/j.bbabio.2007.03.004

Jensen, P. E., Haldrup, A., Zhang, S., & Scheller, H. V. (2004). The PSI-O Subunit of Plant Photosystem I Is Involved in Balancing the Excitation Pressure between the Two Photosystems*. *Journal of Biological Chemistry*, *279*(23), 24212-24217. https://doi.org/https://doi.org/10.1074/jbc.M403147200

Johnson, M. P. (2016). Photosynthesis. *Essays Biochem*, *60*(3), 255-273. https://doi.org/10.1042/ebc20160016

Johnson, M. P., Pérez-Bueno, M. L., Zia, A., Horton, P., & Ruban, A. V. (2009). The zeaxanthin-independent and zeaxanthin-dependent qE components of nonphotochemical quenching involve common conformational changes within the photosystem II antenna in Arabidopsis. *Plant Physiol*, *149*(2), 1061-1075. https://doi.org/10.1104/pp.108.129957

Kiang, N. Y., Siefert, J., Govindjee, & Blankenship, R. E. (2007). Spectral signatures of photosynthesis. I. Review of Earth organisms. *Astrobiology*, *7*(1), 222-251. https://doi.org/10.1089/ast.2006.0105

Kirchhoff, H. (2019). Chloroplast ultrastructure in plants. *New Phytologist*, *223*(2), 565-574. https://doi.org/https://doi.org/10.1111/nph.15730

Kirchhoff, H., Li, M., & Puthiyaveetil, S. (2017). Sublocalization of Cytochrome b(6)f Complexes in Photosynthetic Membranes. *Trends Plant Sci*, *22*(7), 574-582. https://doi.org/10.1016/j.tplants.2017.04.004

Klimmek, F., Sjödin, A., Noutsos, C., Leister, D., & Jansson, S. (2006). Abundantly and rarely expressed Lhc protein genes exhibit distinct regulation patterns in plants. *Plant Physiol*, *140*(3), 793-804. https://doi.org/10.1104/pp.105.073304

Koochak, H., Puthiyaveetil, S., Mullendore, D. L., Li, M., & Kirchhoff, H. (2019). The structural and functional domains of plant thylakoid membranes. *Plant J*, *97*(3), 412-429. https://doi.org/10.1111/tpj.14127

Kouřil, R., Nosek, L., Semchonok, D., Boekema, E. J., & Ilík, P. (2018). Organization of Plant Photosystem II and Photosystem I Supercomplexes. *Subcell Biochem*, *87*, 259-286. https://doi.org/10.1007/978-981-10-7757-9_9

Kress, E., & Jahns, P. (2017). The Dynamics of Energy Dissipation and Xanthophyll Conversion in Arabidopsis Indicate an Indirect Photoprotective Role of Zeaxanthin in Slowly Inducible and Relaxing Components of Non-photochemical Quenching of Excitation Energy. *Front Plant Sci*, *8*, 2094. https://doi.org/10.3389/fpls.2017.02094

Kubínová, Z., Janácek, J., Lhotáková, Z., Kubínová, L., & Albrechtová, J. (2014). Unbiased estimation of chloroplast number in mesophyll cells: advantage of a genuine three-dimensional approach. *J Exp Bot*, *65*(2), 609-620. https://doi.org/10.1093/jxb/ert407

Laisk, A., Oja, V., Eichelmann, H., & Dall'Osto, L. (2014). Action spectra of photosystems II and I and quantum yield of photosynthesis in leaves in State 1. *Biochimica et Biophysica Acta (BBA) - Bioenergetics*, *1837*(2), 315-325. https://doi.org/https://doi.org/10.1016/j.bbabio.2013.12.001

Lemeille, S., Willig, A., Depège-Fargeix, N., Delessert, C., Bassi, R., & Rochaix, J.-D. (2009). Analysis of the Chloroplast Protein Kinase Stt7 during State Transitions. *PLOS Biology*, *7*(3), e1000045. https://doi.org/10.1371/journal.pbio.1000045

Leoni, C., Pietrzykowska, M., Kiss, A. Z., Suorsa, M., Ceci, L. R., Aro, E. M., & Jansson, S. (2013). Very rapid phosphorylation kinetics suggest a unique role for Lhcb2 during state transitions in Arabidopsis. *Plant J*, *76*(2), 236-246. https://doi.org/10.1111/tpj.12297

Leutwiler, L. S., Meyerowitz, E. M., & Tobin, E. M. (1986). Structure and expression of three light-harvesting chlorophyll a/b-binding protein genes in Arabidopsis thaliana. *Nucleic Acids Res*, *14*(10), 4051-4064. https://doi.org/10.1093/nar/14.10.4051

Li, X.-P., Björkman, O., Shih, C., Grossman, A. R., Rosenquist, M., Jansson, S., & Niyogi, K. K. (2000). A pigment-binding protein essential for regulation of photosynthetic light harvesting. *Nature*, *403*(6768), 391-395. https://doi.org/10.1038/35000131

Li, X.-P., Müller-Moulé, P., Gilmore, A. M., & Niyogi, K. K. (2002). PsbS-dependent enhancement of feedback de-excitation protects photosystem II from photoinhibition. *Proceedings of the National Academy of Sciences*, *99*(23), 15222-15227. https://doi.org/doi:10.1073/pnas.232447699

Li, X. P., Phippard, A., Pasari, J., & Niyogi, K. K. (2002). Structure-function analysis of photosystem II subunit S (PsbS) in vivo. *Funct Plant Biol*, *29*(10), 1131-1139. https://doi.org/10.1071/fp02065

Lippold, F., vom Dorp, K., Abraham, M., Hölzl, G., Wewer, V., Yilmaz, J. L., Lager, I., Montandon, C., Besagni, C., Kessler, F., Stymne, S., & Dörmann, P. (2012). Fatty acid phytyl ester synthesis in chloroplasts of Arabidopsis. *Plant Cell*, *24*(5), 2001-2014. https://doi.org/10.1105/tpc.112.095588

Liu, Z., Yan, H., Wang, K., Kuang, T., Zhang, J., Gui, L., An, X., & Chang, W. (2004). Crystal structure of spinach major light-harvesting complex at 2.72 A resolution. *Nature*, *428*(6980), 287-292. https://doi.org/10.1038/nature02373

Longoni, F. P., & Goldschmidt-Clermont, M. (2021). Thylakoid Protein Phosphorylation in Chloroplasts. *Plant and Cell Physiology*, *62*(7), 1094-1107. https://doi.org/10.1093/pcp/pcab043

Longoni, P., Douchi, D., Cariti, F., Fucile, G., & Goldschmidt-Clermont, M. (2015). Phosphorylation of the Light-Harvesting Complex II Isoform Lhcb2 Is Central to State Transitions *Plant Physiology*, *169*(4), 2874-2883. https://doi.org/10.1104/pp.15.01498

Lunde, C., Jensen, P. E., Haldrup, A., Knoetzel, J., & Scheller, H. V. (2000). The PSI-H subunit of photosystem I is essential for state transitions in plant photosynthesis. *Nature*, *408*(6812), 613-615. https://doi.org/10.1038/35046121

Lyons, T. W., Reinhard, C. T., & Planavsky, N. J. (2014). The rise of oxygen in Earth's early ocean and atmosphere. *Nature*, *506*(7488), 307-315. https://doi.org/10.1038/nature13068

Maréchal, E. (2018). Primary Endosymbiosis: Emergence of the Primary Chloroplast and the Chromatophore, Two Independent Events. *Methods Mol Biol*, *1829*, 3-16. https://doi.org/10.1007/978-1-4939-8654-5_1

Mazor, Y., Borovikova, A., Caspy, I., & Nelson, N. (2017). Structure of the plant photosystem I supercomplex at 2.6 Å resolution. *Nat Plants*, *3*, 17014. https://doi.org/10.1038/nplants.2017.14

McFadden, G. I., & van Dooren, G. G. (2004). Evolution: red algal genome affirms a common origin of all plastids. *Curr Biol*, *14*(13), R514-516. https://doi.org/10.1016/j.cub.2004.06.041

McGrath, J. M., Terzaghi, W. B., Sridhar, P., Cashmore, A. R., & Pichersky, E. (1992). Sequence of the fourth and fifth Photosystem II type I chlorophyll a/b-binding protein genes of Arabidopsis thaliana and evidence for the presence of a full complement of the extended CAB gene family. *Plant Mol Biol*, *19*(5), 725-733. https://doi.org/10.1007/bf00027069

Minagawa, J. (2011). State transitions—The molecular remodeling of photosynthetic supercomplexes that controls energy flow in the chloroplast. *Biochimica et Biophysica Acta (BBA) - Bioenergetics*, *1807*(8), 897-905. https://doi.org/https://doi.org/10.1016/j.bbabio.2010.11.005

Mitchell, P. (1975). The protonmotive Q cycle: a general formulation. *FEBS Lett*, *59*(2), 137-139. https://doi.org/10.1016/0014-5793(75)80359-0

Miyake, C., Shinzaki, Y., Miyata, M., & Tomizawa, K.-i. (2004). Enhancement of Cyclic Electron Flow Around PSI at High Light and its Contribution to the Induction of Non-Photochemical Quenching of Chl Fluorescence in Intact Leaves of Tobacco Plants. *Plant and Cell Physiology*, *45*(10), 1426-1433. https://doi.org/10.1093/pcp/pch163

Mizusawa, N., & Wada, H. (2012). The role of lipids in photosystem II. *Biochim Biophys Acta*, *1817*(1), 194-208. https://doi.org/10.1016/j.bbabio.2011.04.008

Mullineaux, C. W. (2005). Function and evolution of grana. *Trends Plant Sci*, *10*(11), 521-525. https://doi.org/10.1016/j.tplants.2005.09.001

Munekage, Y., Hashimoto, M., Miyake, C., Tomizawa, K., Endo, T., Tasaka, M., & Shikanai, T. (2004). Cyclic electron flow around photosystem I is essential for photosynthesis. *Nature*, *429*(6991), 579-582. https://doi.org/10.1038/nature02598

Munekage, Y., Hojo, M., Meurer, J., Endo, T., Tasaka, M., & Shikanai, T. (2002). PGR5 is involved in cyclic electron flow around photosystem I and is essential for photoprotection in Arabidopsis. *Cell*, *110*(3), 361-371. https://doi.org/10.1016/s0092-8674(02)00867-x

Murata, N. (1969). Control of excitation transfer in photosynthesis I. Light-induced change of chlorophyll a fluoresence in Porphyridium cruentum. *Biochimica et Biophysica Acta (BBA) - Bioenergetics*, *172*(2), 242-251. https://doi.org/https://doi.org/10.1016/0005-2728(69)90067-X

Murata, N., Takahashi, S., Nishiyama, Y., & Allakhverdiev, S. I. (2007). Photoinhibition of photosystem II under environmental stress. *Biochimica et Biophysica Acta (BBA) - Bioenergetics*, *1767*(6), 414-421. https://doi.org/https://doi.org/10.1016/j.bbabio.2006.11.019

Mustárdy, L., & Garab, G. (2003). Granum revisited. A three-dimensional model--where things fall into place. *Trends Plant Sci*, *8*(3), 117-122. https://doi.org/10.1016/s1360-1385(03)00015-3

Natali, A., Gruber, J. M., Dietzel, L., Stuart, M. C., van Grondelle, R., & Croce, R. (2016). Light-harvesting Complexes (LHCs) Cluster Spontaneously in Membrane Environment Leading to Shortening of Their Excited State Lifetimes. *J Biol Chem*, *291*(32), 16730-16739. https://doi.org/10.1074/jbc.M116.730101

Nevo, R., Charuvi, D., Tsabari, O., & Reich, Z. (2012). Composition, architecture and dynamics of the photosynthetic apparatus in higher plants. *Plant J*, *70*(1), 157-176. https://doi.org/10.1111/j.1365-313X.2011.04876.x

Nevo, R., Charuvi, D., Tsabari, O., & Reich, Z. (2012). Composition, architecture and dynamics of the photosynthetic apparatus in higher plants. *The Plant Journal*, *70*(1), 157-176. https://doi.org/https://doi.org/10.1111/j.1365-313X.2011.04876.x

Nicol, L., Croce, R., van Grondelle, R., van Amerongen, H., & van Stokkum, I. (2018). Light harvesting in higher plants and green algae. In *Light Harvesting in Photosynthesis* (pp. 59-76). CRC Press.

Niyogi, K. K., Grossman, A. R., & Björkman, O. (1998). Arabidopsis mutants define a central role for the xanthophyll cycle in the regulation of photosynthetic energy conversion. *Plant Cell*, *10*(7), 1121-1134. https://doi.org/10.1105/tpc.10.7.1121

Oakley, C. A., Pontasch, S., Fisher, P. L., Wilkinson, S. P., Keyzers, R. A., Krueger, T., Dove, S., Hoegh-Guldberg, O., Leggat, W., & Davy, S. K. (2022). Thylakoid fatty acid composition and response to short-term cold and heat stress in high-latitude Symbiodiniaceae. *Coral Reefs*, *41*(2), 343-353. https://doi.org/10.1007/s00338-022-02221-2

Otani, T., Kato, Y., & Shikanai, T. (2018). Specific substitutions of light-harvesting complex I proteins associated with photosystem I are required for supercomplex formation with chloroplast NADH dehydrogenase-like complex. *Plant J*, *94*(1), 122-130. https://doi.org/10.1111/tpj.13846

Pagliano, C., Saracco, G., & Barber, J. (2013). Structural, functional and auxiliary proteins of photosystem II. *Photosynth Res*, *116*(2-3), 167-188. https://doi.org/10.1007/s11120-013-9803-8

Pan, X., Ma, J., Su, X., Cao, P., Chang, W., Liu, Z., Zhang, X., & Li, M. (2018). Structure of the maize photosystem I supercomplex with light-harvesting complexes I and II. *Science*, *360*(6393), 1109-1113. https://doi.org/10.1126/science.aat1156

Pawlowicz, N. P., Groot, M. L., van Stokkum, I. H. M., Breton, J., & van Grondelle, R. (2007). Charge Separation and Energy Transfer in the Photosystem II Core Complex Studied by Femtosecond Midinfrared Spectroscopy. *Biophysical Journal*, *93*(8), 2732-2742. https://doi.org/https://doi.org/10.1529/biophysj.107.105452

Peter, G. F., & Thornber, J. P. (1991). Biochemical composition and organization of higher plant photosystem II light-harvesting pigment-proteins. *J Biol Chem*, *266*(25), 16745-16754.

Pfannschmidt, T. (2003). Chloroplast redox signals: how photosynthesis controls its own genes. *Trends Plant Sci*, *8*(1), 33-41. https://doi.org/10.1016/s1360-1385(02)00005-5

Pietrzykowska, M., Suorsa, M., Semchonok, D. A., Tikkanen, M., Boekema, E. J., Aro, E.-M., & Jansson, S. (2014). The Light-Harvesting Chlorophyll a/b Binding Proteins Lhcb1 and Lhcb2 Play Complementary Roles during State Transitions in Arabidopsis *The Plant Cell*, *26*(9), 3646-3660. https://doi.org/10.1105/tpc.114.127373

Pinnola, A., & Bassi, R. (2018). Molecular mechanisms involved in plant photoprotection. *Biochem Soc Trans*, *46*(2), 467-482. https://doi.org/10.1042/bst20170307

Plöchinger, M., Torabi, S., Rantala, M., Tikkanen, M., Suorsa, M., Jensen, P. E., Aro, E. M., & Meurer, J. (2016). The Low Molecular Weight Protein PsaI Stabilizes the Light-Harvesting Complex II Docking Site of Photosystem I. *Plant Physiol*, *172*(1), 450-463. https://doi.org/10.1104/pp.16.00647

Pribil, M., Labs, M., & Leister, D. (2014). Structure and dynamics of thylakoids in land plants. *Journal of Experimental Botany*, *65*(8), 1955-1972. https://doi.org/10.1093/jxb/eru090

Pribil, M., Pesaresi, P., Hertle, A., Barbato, R., & Leister, D. (2010). Role of Plastid Protein Phosphatase TAP38 in LHCII Dephosphorylation and Thylakoid Electron Flow. *PLOS Biology*, *8*(1), e1000288. https://doi.org/10.1371/journal.pbio.1000288

Rabinowitch, E. G. J. W., & Sons. (1969). *Photosynthesis*. John Wiley & Sons.

Renger, G., & Kühn, P. (2007). Reaction pattern and mechanism of light induced oxidative water splitting in photosynthesis. *Biochimica et Biophysica Acta (BBA) - Bioenergetics*, *1767*(6), 458-471. https://doi.org/https://doi.org/10.1016/j.bbabio.2006.12.004

Richardson, L. G. L. (2019). Decoding Natural Variation in Chloroplast Size. *Plant Physiology*, *181*(3), 840-842. https://doi.org/10.1104/pp.19.01159

Rintamäki, E., Martinsuo, P., Pursiheimo, S., & Aro, E.-M. (2000). Cooperative regulation of light-harvesting complex II phosphorylation via the plastoquinol and ferredoxin-thioredoxin system in chloroplasts. *Proceedings of the National Academy of Sciences*, *97*(21), 11644-11649. https://doi.org/doi:10.1073/pnas.180054297

Rochaix, J.-D. (2007). Role of thylakoid protein kinases in photosynthetic acclimation. *FEBS Letters*, *581*(15), 2768-2775. https://doi.org/https://doi.org/10.1016/j.febslet.2007.04.038

Ruban, A. V. (2016). Nonphotochemical Chlorophyll Fluorescence Quenching: Mechanism and Effectiveness in Protecting Plants from Photodamage. *Plant Physiology*, *170*(4), 1903-1916. https://doi.org/10.1104/pp.15.01935

Saito, K., Suzuki, T., & Ishikita, H. (2018). Absorption-energy calculations of chlorophyll a and b with an explicit solvent model. *Journal of Photochemistry and Photobiology A: Chemistry*, *358*, 422-431. https://doi.org/https://doi.org/10.1016/j.jphotochem.2017.10.003

Sánchez-Baracaldo, P., Raven, J. A., Pisani, D., & Knoll, A. H. (2017). Early photosynthetic eukaryotes inhabited low-salinity habitats. *Proceedings of the National Academy of Sciences*, *114*(37), E7737-E7745. https://doi.org/doi:10.1073/pnas.1620089114

Sato, N. (2004). Roles of the acidic lipids sulfoquinovosyl diacylglycerol and phosphatidylglycerol in photosynthesis: their specificity and evolution. *Journal of Plant Research*, *117*(6), 495-505. https://doi.org/10.1007/s10265-004-0183-1

Satoh, K., Oh-hashi, M., Kashino, Y., & Koike, H. (1995). Mechanism of Electron Flow through the QB Site in Photosystem II. 1. Kinetics of the Reduction of Electron Acceptors at the QB and Plastoquinone Sites in Photosystem II Particles from the Cyanobacterium Synechococcus vulcanus. *Plant and Cell Physiology*, *36*(4), 597-605. https://doi.org/10.1093/oxfordjournals.pcp.a078799

Sattari Vayghan, H., Nawrocki, W. J., Schiphorst, C., Tolleter, D., Hu, C., Douet, V., Glauser, G., Finazzi, G., Croce, R., Wientjes, E., & Longoni, F. (2022). Photosynthetic Light Harvesting and Thylakoid Organization in a CRISPR/Cas9 Arabidopsis Thaliana LHCB1 Knockout Mutant [Original Research]. *Frontiers in Plant Science*, *13*. https://doi.org/10.3389/fpls.2022.833032

Sattari Vayghan, H., Tavalaei, S., Grillon, A., Meyer, L., Ballabani, G., Glauser, G., & Longoni, P. (2020). Growth Temperature Influence on Lipids and Photosynthesis in Lepidium sativum [Original Research]. *Frontiers in Plant Science*, *11*. https://doi.org/10.3389/fpls.2020.00745

Scheller, H. V., Jensen, P. E., Haldrup, A., Lunde, C., & Knoetzel, J. (2001). Role of subunits in eukaryotic Photosystem I. *Biochimica et Biophysica Acta (BBA) - Bioenergetics*, *1507*(1), 41-60. https://doi.org/https://doi.org/10.1016/S0005-2728(01)00196-7

Schöttler, M. A., Kirchhoff, H., & Weis, E. (2004). The role of plastocyanin in the adjustment of the photosynthetic electron transport to the carbon metabolism in tobacco. *Plant Physiol*, *136*(4), 4265-4274. https://doi.org/10.1104/pp.104.052324

Shapiguzov, A., Ingelsson, B., Samol, I., Andres, C., Kessler, F., Rochaix, J.-D., Vener, A. V., & Goldschmidt-Clermont, M. (2010). The PPH1 phosphatase is specifically involved in LHCII dephosphorylation and state transitions in Arabidopsis. *Proceedings of the National Academy of Sciences*, *107*(10), 4782-4787. https://doi.org/doi:10.1073/pnas.0913810107

Sheng, X., Watanabe, A., Li, A., Kim, E., Song, C., Murata, K., Song, D., Minagawa, J., & Liu, Z. (2019). Structural insight into light harvesting for photosystem II in green algae. *Nature Plants*, *5*(12), 1320-1330. https://doi.org/10.1038/s41477-019-0543-4

Shevela, D., Björn, L. O., & Govindjee. (2017). *Photosynthesis* [doi:10.1142/10522]. WORLD SCIENTIFIC. https://doi.org/doi:10.1142/10522

Shi, L.-X., & Schröder, W. P. (2004). The low molecular mass subunits of the photosynthetic supracomplex, photosystem II. *Biochimica et Biophysica Acta (BBA) - Bioenergetics*, *1608*(2), 75-96. https://doi.org/https://doi.org/10.1016/j.bbabio.2003.12.004

Shi, L. X., & Schröder, W. P. (2004). The low molecular mass subunits of the photosynthetic supracomplex, photosystem II. *Biochim Biophys Acta*, *1608*(2-3), 75-96. https://doi.org/10.1016/j.bbabio.2003.12.004

Staehelin, L. A. (2003). Chloroplast structure: from chlorophyll granules to supra-molecular architecture of thylakoid membranes. *Photosynth Res*, *76*(1-3), 185-196. https://doi.org/10.1023/a:1024994525586

Stirbet, A., Lazár, D., Guo, Y., & Govindjee, G. (2020). Photosynthesis: basics, history and modelling. *Ann Bot*, *126*(4), 511-537. https://doi.org/10.1093/aob/mcz171

Strittmatter, P., Soll, J., & Bölter, B. (2010). The chloroplast protein import machinery: a review. *Methods Mol Biol*, *619*, 307-321. https://doi.org/10.1007/978-1-60327-412-8_18

Su, X., Ma, J., Wei, X., Cao, P., Zhu, D., Chang, W., Liu, Z., Zhang, X., & Li, M. (2017). Structure and assembly mechanism of plant C₂S₂M₂-type PSII-LHCII supercomplex. *Science*, *357*(6353), 815-820. https://doi.org/doi:10.1126/science.aan0327

Sylak-Glassman, E. J., Malnoë, A., De Re, E., Brooks, M. D., Fischer, A. L., Niyogi, K. K., & Fleming, G. R. (2014). Distinct roles of the photosystem II protein PsbS and zeaxanthin in the regulation of light harvesting in plants revealed by fluorescence lifetime snapshots. *Proceedings of the National Academy of Sciences*, *111*(49), 17498-17503. https://doi.org/doi:10.1073/pnas.1418317111

Thallmair, S., Vainikka, P. A., & Marrink, S. J. (2019). Lipid Fingerprints and Cofactor Dynamics of Light-Harvesting Complex II in Different Membranes. *Biophys J*, *116*(8), 1446-1455. https://doi.org/10.1016/j.bpj.2019.03.009

Tikkanen, M., & Aro, E. M. (2012). Thylakoid protein phosphorylation in dynamic regulation of photosystem II in higher plants. *Biochim Biophys Acta*, *1817*(1), 232-238. https://doi.org/10.1016/j.bbabio.2011.05.005

Tripathy, B. C., & Oelmüller, R. (2012). Reactive oxygen species generation and signaling in plants. *Plant Signal Behav*, *7*(12), 1621-1633. https://doi.org/10.4161/psb.22455

van Amerongen, H., & Croce, R. (2013). Light harvesting in photosystem II. *Photosynthesis Research*, *116*(2), 251-263. https://doi.org/10.1007/s11120-013-9824-3

Van Eerden, F. J., Melo, M. N., Frederix, P. W. J. M., Periole, X., & Marrink, S. J. (2017). Exchange pathways of plastoquinone and plastoquinol in the photosystem II complex. *Nature Communications*, *8*(1), 15214. https://doi.org/10.1038/ncomms15214

van Oort, B., van Grondelle, R., & van Stokkum, I. H. M. (2015). A Hidden State in Light-Harvesting Complex II Revealed By Multipulse Spectroscopy. *The Journal of Physical Chemistry B*, *119*(16), 5184-5193. https://doi.org/10.1021/acs.jpcb.5b01335

Vothknecht, U. C., & Westhoff, P. (2001). Biogenesis and origin of thylakoid membranes. *Biochim Biophys Acta*, *1541*(1-2), 91-101. https://doi.org/10.1016/s0167-4889(01)00153-7

Wientjes, E., & Croce, R. (2011). The light-harvesting complexes of higher-plant Photosystem I: Lhca1/4 and Lhca2/3 form two red-emitting heterodimers. *Biochem J*, *433*(3), 477-485. https://doi.org/10.1042/bj20101538

Wientjes, E., van Amerongen, H., & Croce, R. (2013a). LHCII is an antenna of both photosystems after long-term acclimation. *Biochimica et Biophysica Acta (BBA)-Bioenergetics*, *1827*(3), 420-426.

Wientjes, E., van Amerongen, H., & Croce, R. (2013b). LHCII is an antenna of both photosystems after long-term acclimation. *Biochimica et Biophysica Acta (BBA) - Bioenergetics*, *1827*(3), 420-426. https://doi.org/https://doi.org/10.1016/j.bbabio.2012.12.009

Wood, W. H. J., Barnett, S. F. H., Flannery, S., Hunter, C. N., & Johnson, M. P. (2019). Dynamic Thylakoid Stacking Is Regulated by LHCII Phosphorylation but Not Its interaction with PSI. *Plant Physiology*, *180*(4), 2152-2166. https://doi.org/10.1104/pp.19.00503

Zheng, G., Tian, B., Zhang, F., Tao, F., & Li, W. (2011). Plant adaptation to frequent alterations between high and low temperatures: remodelling of membrane lipids and maintenance of unsaturation levels. *Plant Cell Environ*, *34*(9), 1431-1442. https://doi.org/10.1111/j.1365-3040.2011.02341.x

Chapter II

Growth Temperature Influence on Lipids and Photosynthesis in *Lepidium sativum*

Hamed Sattari Vayghan[1], Shahrzad Tavalaei[1], Armand Grillon[1], Léa Meyer[1], Gent Ballabani[1], Gaëtan Glauser[2] and Paolo Longoni[1]*

[1]Laboratory of Plant Physiology, Institute of Biology, University of Neuchâtel, Neuchâtel, Switzerland
[2]Neuchâtel Platform of Analytical Chemistry, University of Neuchâtel, Neuchâtel, Switzerland

Front. Plant Sci., 04 June 2020: https://doi.org/10.3389/fpls.2020.00745, Sec. Plant Physiology

Received: 26 November 2019; **Accepted:** 11 May 2020
Published: 04 June 2020.
Edited by: Yoshitaka Nishiyama, Saitama University, Japan
Reviewed by: Koichi Kobayashi, Osaka Prefecture University, Japan, Esa Tyystjärvi, University of Turku, Finland

***Correspondence**: Fiamma.longoni@unine.ch, longonifiamm@gmail.com

Temperature has a major impact on plant development and growth. In temperate climates, the seasonal temperature displays large variations that can affect the early stages of plant growth and development. Sessile organisms need to be capable of responding to these conditions, so that growth temperature induces morphological and physiological changes in the plant. Besides development, there are also important molecular and ultrastructural modifications allowing to cope with different temperatures. The chloroplast plays a crucial role in plant energetic metabolism and harbors the photosynthetic apparatus. The photosynthetic light reactions are at the interface between external physical conditions (light, temperature) and the cell biochemistry. Therefore, photosynthesis requires structural flexibility to be able to optimize its efficiency according to the changes of the external conditions. To investigate the effect of growth temperature on the photosynthetic apparatus, we followed the photosynthetic performances and analyzed the protein and lipid profiles of *Lepidium sativum* (cress) grown at three different temperatures. This revealed that plants developing at temperatures above the optimum have a lower photosynthetic efficiency. Moreover, plants grown under elevated and low temperatures showed a different galactolipid profile, especially the amount of saturated galactolipids decreased at low temperature and increased at high temperature. From the analysis of the chlorophyll a fluorescence induction, we assessed the impact of growth temperature on the re-oxidation of plastoquinone, which is the lipidic electron carrier of the photosynthetic electron transport chain. We show that, at low temperature, along with an increase of unsaturated structural lipids and plastochromanol, there is an increase of the plastoquinone oxidation rate in the dark. These results emphasize the importance of the thylakoid membrane composition in preserving the photosynthetic apparatus under non-optimal temperatures.

Keywords: photosynthesis, thylakoid membrane, membrane lipids, plastoquinone, temperature stress, electron transport

Introduction

Plant metabolism must respond to daily and seasonal temperature variations. Photosynthesis, which is the main energetic process allowing plants to produce organic carbon, chemical energy, and reducing power, is no exception. Furthermore, the photosynthetic process is peculiar in the fact that uses light as the energy source of the primary photosynthetic reactions. As temperature differences affect the biochemical reactions but not the pigment excitation, the conversion of light energy into chemical energy needs to be finely tuned to be adapted to different temperatures (Yamori et al., 2014). Light energy conversion requires a series of pigment–protein complexes, namely photosystem II (PSII), cytochrome b6f ($Cytb_6f$), and photosystem I (PSI). These complexes are functionally connected constituting an electron transport chain (Rochaix, 2011). The electrons obtained from the water-splitting reaction at PSII are transferred to plastoquinone (PQ), which is reduced to plastoquinol (reduced PQ). Reduced PQ diffuses into the membrane until $Cytb_6f$. This complex oxidizes the reduced PQ, splitting the two electrons obtained from the oxidation, one toward the plastocyanin and the other to a second PQ molecule. The electrons from plastocyanin are then transferred to PSI and from this complex to the final acceptor NADP via ferredoxin. The water-splitting and the cycle of the PQ during the electron transport increase the proton concentration in the thylakoid lumen generating a pH gradient across the membrane (ΔpH). ΔpH is used by the ATP synthase complex to produce ATP. The light absorption capacity of PSI and PSII reaction centers is extended by the light harvesting complex II (LHCII), a complex of trimeric and monomeric proteins binding chlorophylls and carotenoids that are capable to capture photons converting them into excitation energy. LHCII proteins can also act as dissipators of excess light energy by releasing part of the excitation energy as heat. Fine regulation of this energy dissipation has an important impact on plant growth and productivity (Kromdijk et al., 2016; Ware et al., 2016). The transmembrane ΔpH is the trigger of the thermal dissipation (Wraight and Crofts, 1970), the presence and abundance of the protein PsbS promote its induction (Li et al., 2000), while the xanthophylls, primarily lutein and zeaxanthin, are the main pigments acting as dissipators (Dall'Osto et al., 2010; Leuenberger et al., 2017). The processes allowing the dissipation of light excess as heat take collectively the name of non-photochemical quenching (NPQ).

The photosynthetic proteins involved in the electron transport chain are sensitive to changes in temperature. Prolonged low temperature results in the increase of the trimeric LHCII over monomeric LHCII in maize (Caffarri et al., 2005), and high temperature induces a change in the phosphorylation of the thylakoid proteins and by this also their localization in the thylakoid membrane subdomains (Rokka et al., 2000). Furthermore, the electron flux toward alternative pathways increases at suboptimal temperatures resulting in a lower efficiency of photosynthetic electron transport (Ivanov et al., 2012). These alternative electron routes, such as chlororespiration through the plastidic terminal oxidase (PTOX), water–water cycle, cyclic electron flow, and mitochondrial oxidative electron transport, may act collectively in reducing the excitation pressure on the photosystems and thus protecting the photosynthetic proteins from photodamage (Ivanov et al., 2012; Sunil et al., 2019).

Light reactions of the photosynthesis depend also on the lipids constituting the membrane in which the protein complexes are embedded. The membrane lipid composition influences PQ diffusion, and this may affect its functionality as electron transporter (Kirchhoff et al., 2002). The structural lipids of the thylakoid membrane are mostly galactolipids: Monogalactosyldiacylglycerols (MGDGs), representing around 50% of the total thylakoid lipids by weight, and digalactosyldiacylglycerols (DGDGs), constituting about 26%. Anionic lipids phosphatidylglycerol (PG) and sulfoquinovosyldiacylglycerol (SQDG) constitute most of the remaining lipid fraction of the thylakoid membrane (Dörmann, 2013). The temperature influences thylakoid membrane composition as well. At high temperature, the thylakoid membrane accumulates structural lipids with a higher degree of saturation (Falcone et al., 2004; Higashi et al., 2015). In addition to the structural lipids, the thylakoid membrane also contains antioxidant molecules such as tocopherols and plastochromanol (Mène-Saffrané et al., 2010; Spicher et al., 2016).

These antioxidants have been shown to have an important role in the preservation of the photosynthetic apparatus during stress conditions such as high light (Rastogi et al., 2014), high temperature (Spicher et al., 2016), and their combination (Spicher et al., 2017).
Furthermore, the chloroplast ultrastructure was also reported to change in response to temperature, for instance, following a temperature increase, the *Arabidopsis thaliana* chloroplast was reported to swell and the number and size of the internal lipid droplets, known as plastoglobules, was reported to increase (Zhang et al., 2010).
Here we investigate the impact of two growth temperatures, one above (30°C) and one below (10°C) the optimal growth temperature (22°C), on the photosynthetic apparatus of *Lepidium sativum* (cress). Cress is a fast-growing species belonging to the Brassicaceae family. We will focus on the differences in thylakoid membrane lipids and on the alternative pathways for the photosynthetic electrons as an adaptive strategy to reduce the excitation pressure and thus the damage of the photosynthetic apparatus.

Materials and Methods

Plant Growth and Stress Condition

Seeds of *L. sativum* were obtained from a local supplier. The seeds were put on soil and kept overnight at 6–8°C in the dark for stratification. The seeded pots were then transferred at 22°C under long day illumination (16 h L/8 h D, photosynthetic photon flux density in photoactive radiation PAR spectrum 86 µmol photons m^{-2} s^{-1}) and allowed to germinate for 48 h. After germination, the plants were moved to 10°C or 30°C under the same light conditions, or maintained at 22°C, and grown for 5 additional days. Warm and cold conditions were produced within a FitoClima 600 (Aralab) climatic chamber. The length of the hypocotyl was measured manually for each plant. The leaf area per plant was calculated with ImageJ (NIH) measuring the green area of each plant from a top view picture using a scale for reference as previously described (Longoni et al., 2019). Five samples constituting the epigeal part of three plants were collected at the end of the growth to measure the average plant dry weight. For that, the samples were lyophilized for 120 h (FreeZone 2.5, Labconco, Kansas City, MO, United States) before weighing. To calculate the dry weight percentage over fresh weight, five samples per temperature, containing only the leaves collected from three plants, were weighted before and after 120 h of lyophilization.

Photosynthetic Parameters

Each batch of plants was kept in the dark for at least 10 min before the measurements. Room temperature chlorophyll fluorescence was measured with a MF800 Fluorcam (Photon System Instrument, Czechia)[1] employing a personalized light protocol (Pralon et al., 2020). The protocol is composed of blue light (470 nm) steps of 1 min with increasing intensity (35, 125, 315, 500, 690, and 875 µmol photons m^{-2} s^{-1} of PAR intensity). F_M' for each light intensity was measured with a saturating pulse at the end of the corresponding light step. After every light step, the actinic light was turned off for 10 s. During the first 2 s, far-red light was turned on to oxidize the photosynthetic electron transport chain. F_0' for each step was measured during the remaining part of the dark period. F_S is the steady-state fluorescence recorded at each light condition before the saturating light pulse. PSII quantum yield under light (ΦPSII) was calculated as $\Phi PSII = (F_M' - F_S)/F_M'$. The fraction of the open PSII centers (qL) was calculated with the following formula: $qL = [(F_M' - F_S)/(F_M' - F_0')]^*(F_0'/F_S)$ (Kramer et al., 2004). The non-photochemical energy dissipation was measured as $NPQ = (F_M - F_M')/F_M'$. The average fluorescence signal of each plant was used for the calculation of the photosynthetic parameters. Rapid chlorophyll fluorescence induction of PSII was measured on detached leaves with Plant Efficiency Analyser (M-PEA 2; Hansatech Ltd). The following protocol was used: after an initial saturating pulse (3000 µmol photons m^{-2} s^{-1}, 700 ms, red light, dominant λ625 nm), the saturating light pulse was repeated after sequentially longer dark intervals (0.05, 4, 8, 12, 16, 20, and 24 s) for a total of eight pulses.

After the eighth pulse, far-red light (20%) was turned on, and the leaf sample was submitted to a second series of saturating pulses separated by increasing time intervals (0.05, 0.1, 0.2, 0.4, 0.8, and 1.6 s) with continuous far-red light in between the pulses. For each saturating pulse, the parameters of the fast chlorophyll fluorescence curve were extrapolated by the M-PEA 2 software (Hansatech Ltd). The variable fluorescence at 3 ms (V_J) and the Fo normalized over the maximal fluorescence (F_O/F_M) were analyzed by plotting them over the time interval between the pulses.

Protein Analysis

Plant samples were ground to a fine powder in a 1.5 ml plastic tube with glass beads in an Ivoclar Vivadent shaker (Silamat). The proteins were extracted adding 10 µl per mg FW of lysis buffer [100 mM Tris–HCl, pH 8.5, 2% SDS, 10 mM NaF, 0.05% of protease inhibitor cocktail for plants (Sigma)], vortexing and incubating the sample at 37°C for 30 min. Plant debris was removed by centrifugation (5 min at 16,000 × *g*) at room temperature. The samples were diluted four times in water and supplemented with gel loading buffer (50 mM Tris–HCl, pH 6.8, 100 mM dithiothreitol, 2% SDS, 0.1% bromophenol blue, 10% glycerol). After denaturation at 75°C for 10 min, an aliquot of 10 µl of the diluted sample was loaded in the gel. The protein separation was performed following the standard SDS-PAGE protocol in a 12% acrylamide bis acrylamide (37.5:1) gel (Laemmli, 1970). The proteins were transferred on a nitrocellulose membrane, stained for 30 s with amido black solution (15% isopropanol, 10% acetic acid, 0.1% w/v amido black), and destained with a destaining solution (40% ethanol, 10% acetic acid). An image of the stained membrane was taken for the quantification of the total proteins in each lane. The membrane was blocked with 5% milk in TBS-0.05% Tween and then decorated with the following antibodies: anti-Lhcb2 (Agrisera, AS01 003), anti-Lhcb1 (Agrisera, AS01 004), anti-D1 (PsbA) (Agrisera, AS05 084), anti-PetC (Agrisera, AS08 330); anti-PsaD (Agrisera, AS09 461), anti-RbcL (Agrisera, AS03 037A); a secondary antibody anti-rabbit conjugated with HRP (Merk) was used to allow the detection of the protein by chemioluminescence (ECL). The ECL signal was recorded with a CCD camera (Amersham Imager 600 Amersham Biosciences, Inc.), set on automatic detection time. Band intensity was measured with ImageQuant TL 8.1 Software (GE Healthcare Life Sciences). The obtained values were normalized over the sum of the amido black band intensities measured with the same software using a minimum profile subtraction method. The protein extraction was performed on leaf samples harvested during at least two independent biological replicates (9 total samples for PsbA and PsaD, 6 samples for RbcL and PetC, 5 for Lhcb2 and 4 for Lhcb1). For PTOX detection (Agrisera, AS16 3692), the membrane was blocked in 6% BSA in TBS-0.05% Tween; the same solution was used for the preparation of the primary and secondary antibody dilutions.

Pigments and Lipid Profiling

The sample used for chlorophyll quantification and lipidomic profiling is constituted of at least two leaves collected from two different plants grown at the same temperature. Chlorophyll extraction was performed in 80% acetone by adding 10 µl of solvent per mg of FW of leaf sample. The sample was further diluted twofold in 80% acetone before measuring the absorbance at multiple wavelengths (470, 646, 663 nm). The quantification of chlorophyll *a* and *b* was performed according to Lichtenthaler and Wellburn (1983). The measured chlorophyll concentration was adjusted to the dry weight based on the average leaf water content measured for each growth temperature. The measure was repeated on 15 samples from different plants obtained from five independent experiments. Extraction of the lipid fraction was performed on 12 samples from different plants obtained from three independent experiments. In brief, after grinding, the lipids were extracted in 10 µl of tetrahydrofuran: methanol 50:50 (v/v) per mg of FW, plant debris was separated by centrifugation (3 min, 14,000 × *g*), and the supernatant was carefully transferred to an HPLC vial.
The lipids were separated by ultra-high pressure liquid chromatography and identified by a coupled atmospheric pressure chemical ionization-quadrupole time-of-flight mass spectrometry (UHPLC-APCI-QTOF-MS) as previously described (Spicher et al., 2016).

Lipids were separated on a reverse-phase Acquity BEH C18 column (50 × 2.1 mm, 1.7 µm) maintained at 60°C. The elution was as follows: solvent A = water; solvent B = methanol; 80–100% B in 3 min, 100% B for 2 min, re-equilibration at 80% B for 2.0 min.
The flow rate was 0.8 ml min^{-1} and the injection volume was 2.5 µl. Data were acquired using MassLynx version 4.1 (Waters) and further processed with QuanLynx (Waters). Compound identity was determined based on reference standards that were also used for the quantification curve (Spicher et al., 2016).
Violaxanthin and neoxanthin could be resolved neither in the chromatographic nor in the mass dimensions under the conditions employed; therefore, the measured peak corresponds to the sum of these compounds. The same applies for lutein and zeaxanthin. MGDG 36:6, 36:5, 36:4, 34:6, 34:5, 34:4 and DGDG 36:6, 36:5, 36:4, 36:3, 34:6, 34:3, 34:2, 34:1 identities were confirmed comparing the peak of the extract with a standard plant MGDG mix and DGDG mix (Avanti Polar Lipids). The calibration curves of MGDG 36:6, MGDG 34:6, DGDG 36:6, and DGDG 34:6 were used for the quantification of all MGDG 36:x, MGDG 34:x, DGDG 36:x and DGDG 34:x, respectively (Supplementary Figure S1). To avoid any bias due to signal saturation in the quantification of the most abundant DGDGs, the samples were measured a second time following a tenfold dilution in tetrahydrofuran: methanol 50:50 (v/v). The values obtained by the calibration curves were corrected by the percentage of each molecule composing the standard mix, as reported by the manufacturer (Avanti Polar Lipids). The molecules not detected in the standard mix were tentatively characterized based on m/z and retention time characteristics, which vary proportionally to the degree of acyl chain length and saturation (Li et al., 2008).

Statistical Analysis

The normal distribution of the residuals of each data set was tested before any other statistical analysis. If this assumption was met, an ANOVA model was utilized; otherwise, a Kruskal–Wallis rank sum test was performed. If the results were significant, we used *post hoc* Tukey's HSD test for multiple comparisons. The reported *p*-values were obtained with the latter. The calculations were performed with RStudio (Version 1.2.5019 RStudio Inc).

Results

Growth Temperature Affects Photosynthetic Efficiency

The plants of *L. sativum* grown at different temperatures had a slightly different morphology. The leaf area was smaller in the plants grown at 10°C and 30°C compared with the control condition. The hypocotyl was longer in the plants grown at 30°C, while there was no significant difference in the other two conditions. However, both the plants grown at 10°C and 30°C produced less dry biomass per plant (Supplementary Figure S2). The entire pot, containing 24 plants, was analyzed by chlorophyll fluorescence to determine the impact of the different growth temperatures on the overall functionality of the photosynthetic electron transport chain. The first parameter observed was the maximal quantum yield of the photosystem II (F_V/F_M), a decrease in this value would suggest the presence of persistent damage on PSII. The maximum quantum yield was slightly lower in the plants grown at 10°C ($p < 0.0001$) compared to the other two growth temperatures (Figure 1). However, the average value of 0.83 measured at 10°C, which is PSII efficiency reported for healthy plants, suggests that there was no major damage during the growth at this suboptimal temperature (Maxwell and Johnson, 2000). The negligible effect on the maximum yield of PSII allowed investigating further the photosynthetic activity and adaptation under increasing actinic light intensity.
Chlorophyll *a* fluorescence was measured at 22°C by red flashes while stepwise increasing the actinic light intensity. The use of a saturating pulse at the end of each light step allowed the calculation of the fraction of the energy dissipated as heat (NPQ) at each light intensity (Caffarri et al., 2005). Plants grown at 30°C had a higher NPQ value compared to those grown under control temperature (Figure

2A). This effect was evident already at the lower light intensity tested (35 µmol photons m^{-2} s^{-1}) (p < 0.0001 compared to both 10°C and 22°C), a condition in which the NPQ of the plants grown at 10°C was statistically lower than the control (p = 0.0005). Only at 315 µmol photons m^{-2} s^{-1}, the plants grown at 10°C appear to have a slightly higher NPQ compared with the control condition (p = 0.11); otherwise, there was no statistically significant difference between these two conditions. The changes in the NPQ are symmetrically reflected in the quantum yield of photosystem II photochemistry (ΦPSII, Figure 2B). The plants grown at 30°C had constantly a lower yield of PSII compared to the control growth temperature. ΦPSII of those grown at 10°C was also lower, especially at 125 and 315 µmol photons m^{-2} s^{-1} (p < 0.0001). While at higher light intensities, ΦPSII difference between the plants grown at 10°C and those at 22°C became smaller.

Therefore, at the higher light intensities tested, the plants grown at 10°C had a higher ΦPSII compared to the plants grown at 30°C. Analysis of the fraction of open PSII centers (qL) revealed that the plants grown at 30°C had a steady increase in the fraction of closed PSII as measured by the qL parameter (Baker, 2008). Surprisingly, this is not the case for the plants grown at 10°C, which have a similar qL level compared to the control temperature (22°C) (Figure 2C). Since these differences may underlay a change in the organization of the electron transport chain, we further analyzed the protein and the lipid composition of the plants grown at the different temperatures.

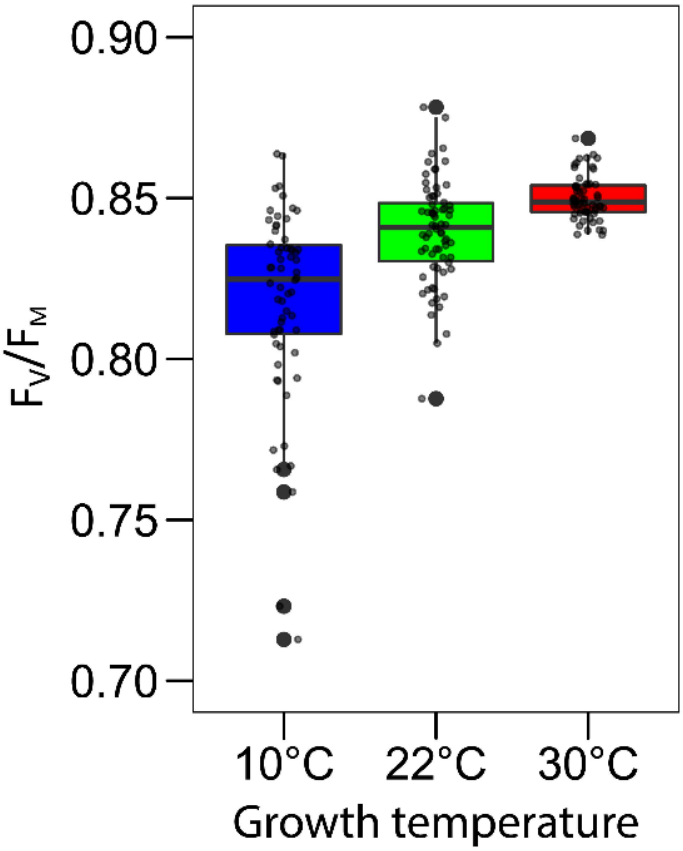

FIGURE 1. Growth temperature has a minimal impact on the Photosystem II maximum efficiency. The maximum PSII quantum yield was measured in trays containing 20–24 plants, grown at three different temperatures (10, 22, and 30°C) for 5 days. Before measuring, the plants were incubated 10 min in the dark at room temperature. Gray points represent the average value for each single plant. In the box plots, the lower and upper hinges correspond to the first and third quartiles (the 25th and 75th percentiles). The whiskers extend from the hinge to the farthest value no further than 1.5 times the distance between the first and third quartiles from the hinge. Farther points are considered as "outliers" and plotted individually as solid black points.

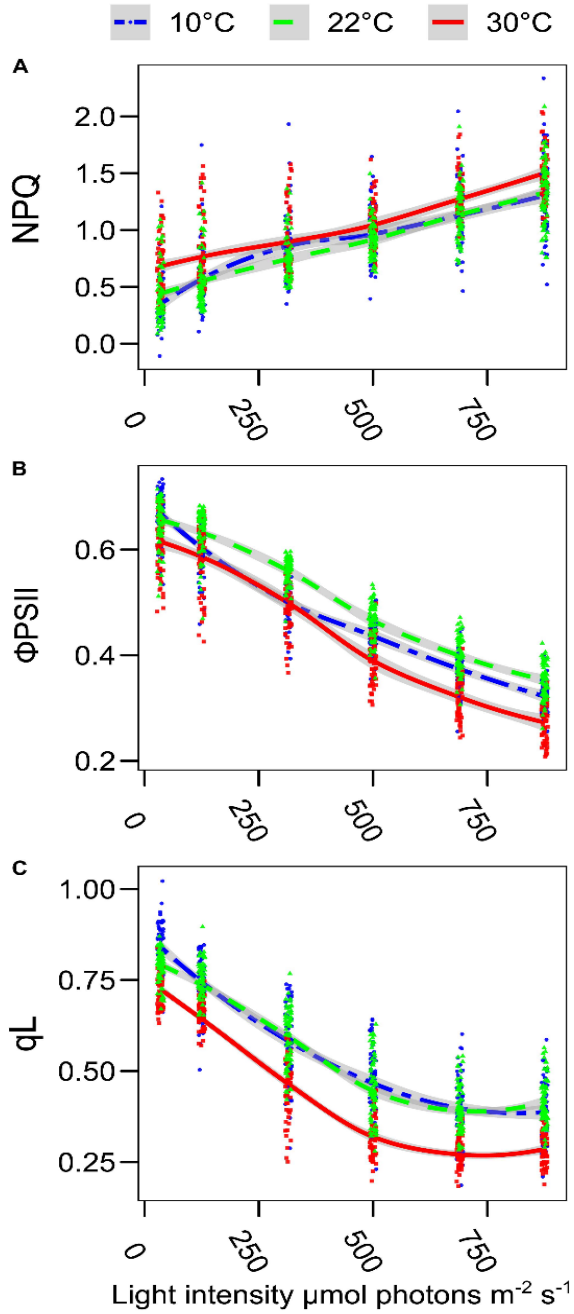

FIGURE 2. Growth temperature affects the photosynthetic electron transport chain in *Lepidium sativum*. The room temperature fluorescence was measured on trays with 20–24 plants, grown at the three different temperatures (10°C blue, 22°C green, and 30°C red). Prior to the measurement, the plants were incubated 10 min in the dark at room temperature and directly used for the measure of the chlorophyll a fluorescence kinetic. (A) Level of thermal dissipation measured as NPQ for the three growth conditions after 1 min of exposure to increasing light intensity. (B) Photosystem II quantum yield (ΦPSII) measured at the end of each 1-min light intensity step. (C) Fraction of the open PSII reaction centers (qL) after 1 min of exposure to increasing light intensities. The light intensities are expressed as µmol photons m–2 s–1 of blue light (470 nm), and the same scale is used for the three graphs. The points were fitted with a local regression algorithm based on a polynomial quadratic function to visually represent the data distribution in function of the light intensities with a continuous error estimate. The fit is shown for the three growth conditions (10°C, blue double dashed line, 22°C green dashed line, and 30°C red continuous line). The standard error of the interpolation is shown as a gray area around the curve. All the data points from the 30°C growth are statistically different from the 22°C control conditions (Post Hoc analysis, $p < 0.0001$). The three parameters were measured simultaneously, and they originated from two independent experimental replicates (30°C, n = 60; 22°C, n = 70; 10°C, n = 62)

Effect of Growth Temperature on Major Thylakoid Pigments and Proteins

The stoichiometry of the different photosynthetic complexes of the thylakoid membrane, namely the two photosystems (PSI and PSII), the cytochrome b6f ($Cytb_6f$), and the light harvesting complex II (LHCII), may vary upon acclimation of the photosynthetic machinery to the environment. To test the impact of the growth temperature on the organization of the major thylakoid proteins, the total chlorophyll content was measured along with the chlorophyll a to b ratio. This gives an indication of the ratio between the LHCII antenna complex, enriched in chlorophyll b, and the two photosystems, which have a higher chlorophyll a/b ratio. The chlorophyll concentration was adjusted to the average calculated dry mass of the sample, which corresponds to 7% at 22°C and 8% both at 30 and 10°C of the respective fresh weight (n = 5). The chlorophyll concentrations of the plants grown at the three temperatures differed a little. Plants grown at 10°C had a slightly lower chlorophyll concentration compared to those grown at 30°C (p = 0.0626, n = 15) and at 22°C (p = 0.1338, n = 15) (Figure 3A). A clear difference was instead observed by comparing the chlorophyll a/b ratio. In both the plants grown at 30°C and at 10°C, the a/b ratio was significantly lower than the one observed at control temperature (22°C–30°C, p = 0.0004, n = 15; 10°C–22°C, p = 0.0343, n = 15) (Figure 3B). This suggests that the relative amount of chlorophyll b rich proteins, such as LHCII, increased in the plants grown in both non-optimal temperatures. The carotenoids were quantified by mass spectrometry (UHPLC-APCI-QTOF-MS). For the carotenoids analyzed, we observed a general trend toward lower accumulation at 10°C compared to the other two growth temperatures. However, these differences appeared not to be statistically significant. β-carotene was the compound showing the most consistent difference among biological replicates when comparing plants grown at 10°C with those grown at the control temperature of 22°C (p = 0.1382, n = 11) (Figure 3C). Other carotenoids associated with the photosynthetic proteins, instead, do not show a differential level of accumulation at the different temperatures; this is the case for lutein and zeaxanthin and for the combination of neoxanthin and violaxanthin (Figures 3D,E).

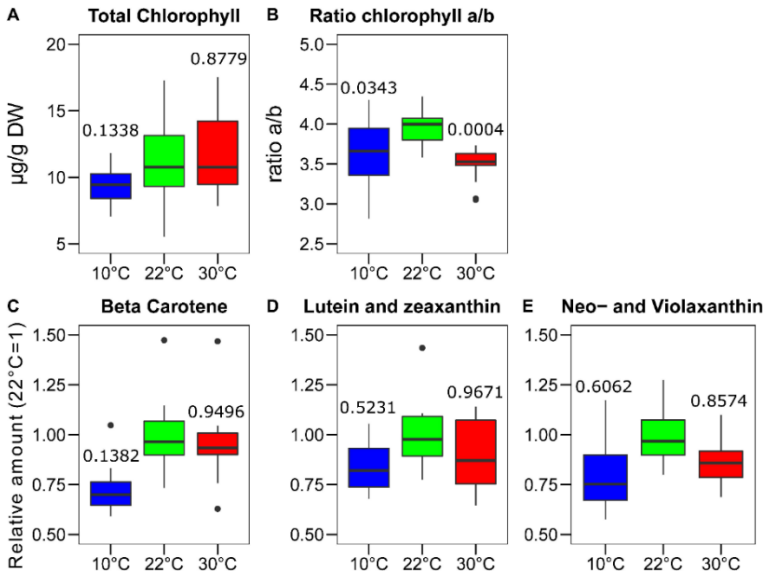

FIGURE 3. Changes in pigments content after the growth of *Lepidium sativum* at different temperatures. The chlorophyll content was measured in a sample constituted of two leaves collected from different plants grown in the same condition. (A) Content in total chlorophyll measured after the growth at three different temperatures normalized on the leaf dry weight. (B) Chlorophyll a/b ratio measured in the same samples shown in (A) (n = 15). Carotenoids analysis was performed by chromatography coupled with mass spectrometry (n = 11). The values are reported in terms of differences from the average value at 22°C for (C) Beta-carotene, (D) Lutein and zeaxanthin, and (E) neoxanthin and violaxanthin. The carotenoids in the blots (D) and (E) were indistinguishable in time or m/z and therefore are plotted as the sum of the two. In the box plots, the lower and upper hinges correspond to the first and third quartiles (the 25th and 75th percentiles). The whiskers extend from the hinge to the farthest value no further than 1.5 times the distance between the first and third quartiles from the hinge. Farther points are considered as "outliers" and plotted individually. The p-value derived from a post hoc test comparing the data with the value at 22°C is shown above each box.

The changes in the accumulation of the major photosynthetic complex were estimated by immunodetection of the subunits of each complex in total protein extracts. Interestingly, it appeared that growth at 10°C, compared to the control at 22°C, results in a lower accumulation, on a total protein basis, of PSII (PsbA/D1) ($p < 0.0001$, $n = 9$), PSI (PsaD) ($p = 0.0001$, $n = 9$), $Cytb_6f$ (PetC) ($p = 0.02$, $n = 6$). For the trimeric LHCII (Lhcb2 and Lhcb1), the reduction was milder so that we did not observe a significant difference in the detected protein compared to the 22°C condition (Lhcb1 $p = 0.29$, $n = 4$; Lhcb2 $p = 0.82$, $n = 5$) (Figure 4). At 30°C, the only significant difference observed by immunodetection was for PetC of the $Cytb_6f$, which was reduced similarly to the 10°C condition (10°C–30°C, $p = 0.76$; 22°C–30°C, $p = 0.1$) (Figure 4).

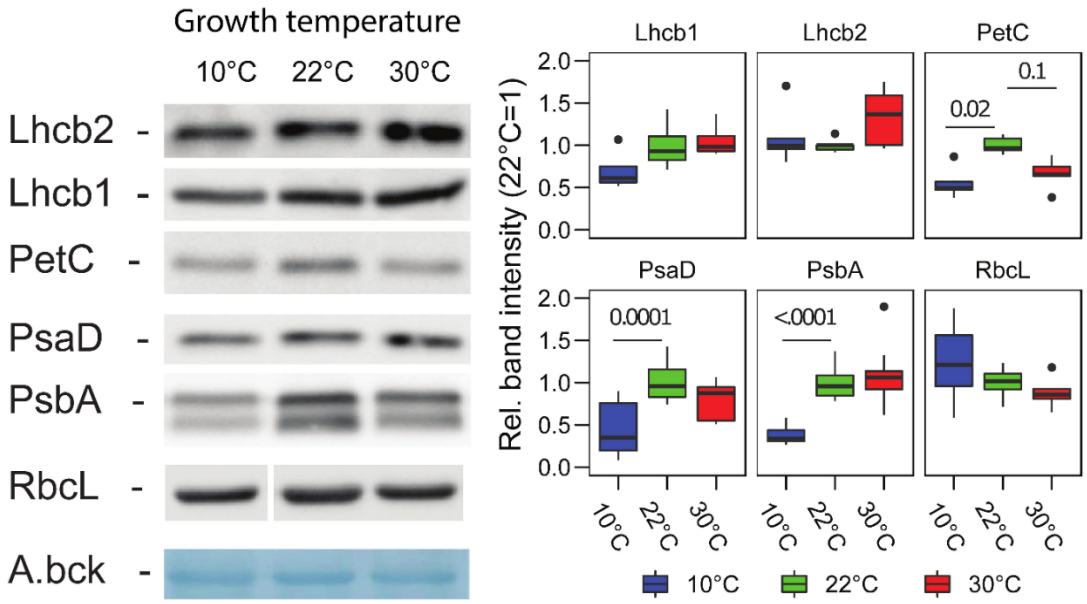

FIGURE 4. Photosynthetic protein accumulation in *Lepidium sativum* at different growth temperatures. Representative proteins for the complexes of the electron transport chain, PSII (PsbA), PSI (PsaD), $Cytb_6f$ (PetC), and LHCII (Lhcb1, Lhcb2) were analyzed by immunodetection in samples normalized on fresh weight. A representative blot is shown for each protein along with a representative band of the total transferred proteins stained with amido black (A.bck) as a protein loading control. The box plots show the band intensity, normalized over the total amido black lane staining, compared to the control condition (22°C) (average intensity 22°C = 1). PSII (PsbA/D1) ($n = 9$), PSI (PsaD) ($n = 9$), $Cytb_6f$ (PetC) ($n = 6$), LHCII (Lhcb2) ($n = 5$), Lhcb1 ($n = 4$), and RbcL ($n = 6$). In the box plots, the lower and upper hinges correspond to the first and third quartiles (the 25th and 75th percentiles). The whiskers extend from the hinge to the farthest value no further than 1.5 times the distance between the first and third quartiles from the hinge. Farther points are considered as "outliers" and plotted individually.

Temperature-Dependent Changes in the Lipids of the Thylakoid Membrane

Alpha-tocopherol and plastochromanol, major antioxidants present in the thylakoid membrane, were measured by mass spectrometry following chromatographic separation (Mène-Saffrané et al., 2010; Spicher et al., 2017; Figure 5). The amount of α-tocopherol, on a dry weight basis, was higher in both non-optimal temperatures compared to the plants grown at 22°C (10°C–22°C, $p = 0.0001$; 30°C–22°C, $p = 0.0077$; $n = 11$). The difference between 10 and 30°C was not statistically significant for this compound ($p = 0.4834$) (Figure 5A). Similarly, plastochromanol concentration was higher, 1.5-fold to twofold, in both temperature conditions (10°C–22°C, $p < 0.0001$; 30°C–22°C, $p = 0.0046$), with a tendency toward a greater amount at 10°C compared to 30°C ($p = 0.1061$) (Figure 5C). The accumulation of the two precursors of these molecules, γ-tocopherol and PQ, was measured as well. Despite a large difference between replicates, the concentration of γ-tocopherol was found to be higher at 10°C and slightly lower at 30°C compared to the control temperature (10°C, $p < 0.0001$; 30°C, $p = 0.0924$) (Figure 5B).

This may suggest that at 10°C there could be an incomplete conversion of γ-tocopherol into α-tocopherol as vegetative tissues do not normally accumulate γ-tocopherol (Abbasi et al., 2007). This conversion may be possibly faster at 30°C, and this leading to the lower accumulation was observed. On the contrary, the amount of PQ was not significantly different in the three temperatures tested, even if a tendency toward higher PQ concentrations was observed in the plants grown at 30°C and toward lower concentrations in those grown at 10°C creating a significant difference between the two conditions (10°C–30°C, p = 0.0564) (Figure 5D).

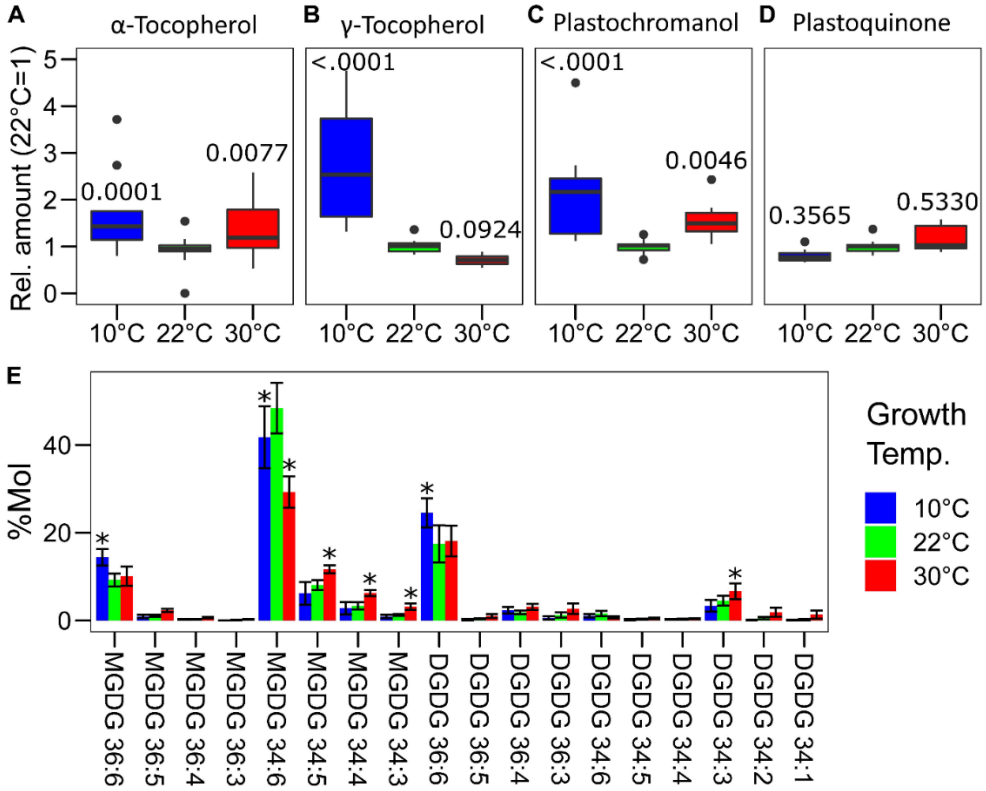

FIGURE 5. Profile of the galacto- and prenyl-lipids in *Lepidium sativum* grown at different temperatures. Total lipids were extracted from pooled leaf samples, separated by liquid chromatography and identified by mass spectrometry. Eleven leaf samples from three independent growth replicates were used. Relative concentration of the principal antioxidants of the thylakoid membrane (A) α-tocopherol, (B) γ-tocopherol, (C) plastochromanol, and its precursors (D) plastoquinone, the latter also serves as an electron carrier in the electron transport chain. In the box plots, the lower and upper hinges correspond to the first and third quartiles (the 25th and 75th percentiles). The whiskers extend from the hinge to the farthest value no further than 1.5 times the distance between the first and third quartiles from the hinge. Farther points are considered as "outliers" and plotted individually. The p-value derived from a post hoc test comparing the data with the value at 22°C is shown above each box. (E) Profile of the monogalactosyldiacylglycerols (MGDG) and digalactosyldiacylglycerols (DGDG) expressed as % molecules over the total of the measured galactolipids. The compounds are listed by the length and degree of saturation of the acyl chains, and significant differences from the control temperature 22°C ($p < 0.05$) are highlighted with an asterisk (n = 11).

The saturation degree of the lipids composing the biological membrane is known to change depending on temperature (Falcone et al., 2004). This is also the case for the major structural lipids of the thylakoid membrane that are monogalactosyldiacylglycerols (MGDG) and digalactosyldiacylglycerols (DGDG) (Block et al., 1983). The growth temperature had a wide impact on the profile of the galactolipids (Figure 5E). At 10°C, long-chained unsaturated mono- and digalactolipids (36:6) were relatively more abundant compared to the control temperature. The effect was opposite for the plants grown at 30°C in which there was a higher proportion of galactolipids with 34 carbons and particularly of those which are more saturated (34:3, 34:2), compared to the control condition at 22°C (Figure 5E).

A specific difference was observed for MGDG 34:6, which is the most abundant galactolipid; its level was maximal in the plants grown at 22°C but lower at both 10 and 30°C (Figure 5E). Also, the MGDG/DGDG ratio was different in the plants grown at non-optimal temperatures.
In fact, over the total of the measured galactolipids, the MGDG fraction was 72 ± 4% in the control condition (22°C) but it decreased to 67 ± 4% and 63 ± 3% at 10 and 30°C, respectively (10°C–22°C, $p = 0.0184$; 30°C–22°C, $p < 0.0001$; $n = 11$). Furthermore, there was also a different accumulation of the galactolipids originating from the endoplasmic reticulum (ER), containing two 18 carbon acyl chains (C18/C18), and those of plastid origin containing one 18 carbon chain and the second with 16 carbons (C18/C16) (Boudière et al., 2014). Considering the molar fraction of the measured galactolipids, in control condition (22°C), 32 ± 5% had two acyl chains of 18 carbons. In the cress plants grown at 10°C, the fraction of the C18/C18 galactolipids increased to 43 ± 5%, significantly higher than in the control condition ($p < 0.0001$, $n = 11$). An intermediate state was observed at 30°C with C18/C18 galactolipids representing 38 ± 3% of the total, differing from the cress grown at 22°C ($p = 0.0092$, $n = 11$) and at 10°C ($p = 0.0214$, $n = 11$). The average number of desaturations per molecule of the measured galactolipids was significantly lower ($p < 0.0001$, $n = 11$) in the plants grown at 30°C (5.1 ± 0.2) compared to the control condition (5.5 ± 0.1) and to the 10°C temperature (5.7 ± 0.1). The difference in the average number of desaturations per molecule was bigger considering only DGDGs, and the average number of desaturations per molecule at 22°C was 5.09 ± 0.2, significantly higher at 10°C (5.44 ± 0.2; 10°C–22°C, $p = 0.0123$) and lower at 30°C (4.62 ± 0.4; 30°C–22°C, $p = 0.0009$).

Plastoquinone Oxidation Is Altered at Low Temperature

The alteration of the lipid composition may have a functional impact on electron transport and on the PQ dynamics. We therefore assessed the re-oxidation kinetics of the photoactive PQ pool using an indirect method based on PSII fluorescence induction curve. It has been shown that the fluorescence level at 3 ms (Fj) correlates with the redox state of the QB site of photosystem II, and the latter is in equilibrium with the photoactive PQ pool (Tóth et al., 2007). Therefore, the relative fluorescence at 3 ms (VJ) and its kinetics after a dark or far red-light period of increasing length were taken as a proxy of the PQ oxidation over time. In the dark, the PQ oxidation is performed by electron pathways alternative to the photosynthetic electron transport chain, mostly via the plastid terminal oxidase (PTOX) (Pralon et al., 2020). Conversely, far-red will activate PSI allowing a photochemical oxidation of PQ (Rochaix, 2011). As expected, PQ oxidation under far-red light was faster than the oxidation observed in the dark, PTOX being a much slower oxidizer than PSI (Tóth et al., 2007). The PQ oxidation in the dark, as inferred by the VJ parameter, was faster in the plants grown at 10°C compared to both other conditions ($p < 0.001$), which, on the contrary, did not differ significantly (Figure 6A). When the oxidation of the photoactive PQ pool was performed by the electron transport chain, exciting PSI with far-red light, the plants grown at 30°C showed a faster initial re-oxidation, up to 0.4 s ($p = 0.0513$), while further followed the same kinetics as the plants grown at 22°C. For the plants grown at 10°C, the effect was reversed; in fact, the kinetics up to 0.2 s were identical to the plants grown at 22°C, while the following re-oxidation kinetics appeared to be slower, so that the VJ was significantly higher at the 0.4 and 0.8 s time points ($p = 0.0005$ and $p = 0.0015$, respectively; Figure 6B). The fluorescence in the dark, before the saturating pulse (FO) calculated by the M-PEA instrument, does also decline with increasing time intervals between the pulses. However, the FO value normalized over the FM does not show the same difference between the samples as observed for VJ (Supplementary Figure S3), suggesting that the two parameters are partially independent.

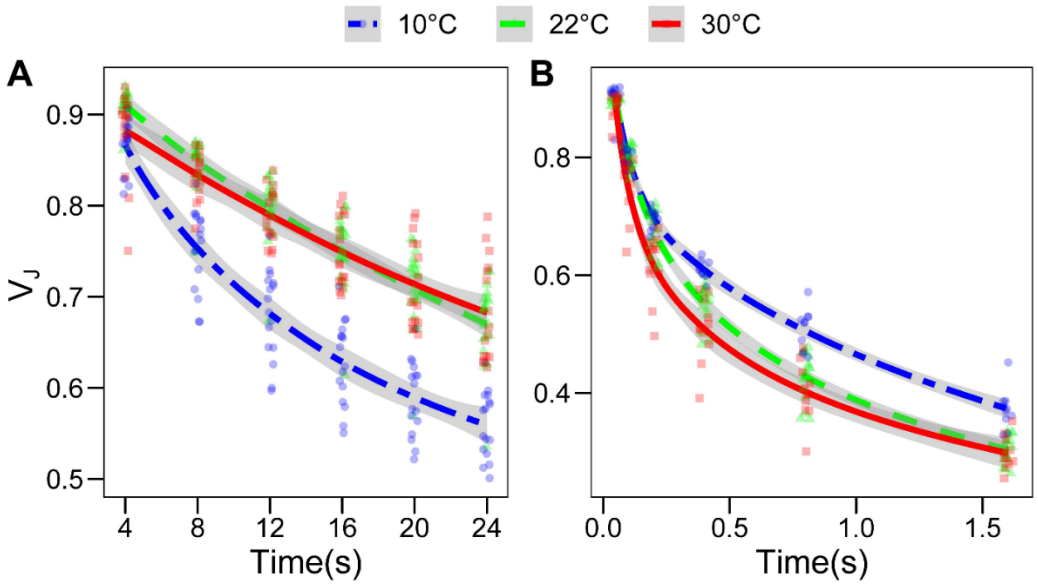

FIGURE 6. Fluorescence relaxation in the dark is faster in *Lepidium sativum* grown at low temperature. The fluorescence value measured at 3 ms during a 700 ms saturating pulse was normalized over the maximal fluorescence to obtain the VJ parameter. This parameter was used as a proxy of the redox state of the photoactive plastoquinone pool. (A) Evolution of the VJ parameter upon sequential incubations of the sample in the dark, for the three growth conditions. The points were fitted with a local regression algorithm based on a logarithmic function to visually represent the data distribution in function of the time with a continuous error estimate (10°C, blue double dashed line, 22°C green dashed line, 30°C red continuous line). The standard error of the interpolation is shown as a gray area around the curve. (B) Evolution of the VJ parameter upon sequential incubation with far-red light exciting preferentially the photosystem I. The statistical significance of the difference between non-overlapping error areas of the interpolation was confirmed by a post hoc test ($p < 0.001$) (10°C, n = 10; 30°C, n = 11; 22°C, n = 16). Different X and Y axes are used in (A) and (B) to highlight the differences between the growth temperatures.

Discussion

Temperature is a challenge for the photosynthetic apparatus, affecting enzymatic kinetics, as well as membrane dynamics and organization (Yamori et al., 2014). It is therefore essential for the plant to adopt strategies to protect its photosynthetic apparatus while maximizing light utilization at the non-optimal temperature condition. Here we explored the response on the early growth of a fast-developing species: *L. sativum*, which belongs to the same family, Brassicaceae, as model organism A. thaliana and important crop species.

The total chlorophyll concentration displayed minor differences compared with those previously reported using other plant species that were exposed to high and low temperature (Grimaud et al., 2013; Spicher et al., 2016). This is possibly because the temperatures employed in this experiment were milder, and therefore, a strong detrimental stress to the photosynthetic apparatus was avoided. This is in line with the limited effect on the maximum quantum yield of PSII observed in the plants grown at 10°C (Figure 1). However, both the plants grown at 10 and 30°C showed an alteration in the measured photosynthetic parameters compared to the control temperature (Figure 2). It has to be underlined that all the photosynthetic measurements were performed at 22°C, i.e., the temperature at which the control plants were grown, and it is therefore not surprising that plants grown at the same temperature are the best performers at this temperature. The average PSII redox state under light was inferred from the qL parameter, representing the probability of a photon to be transferred to an open PSII reaction center in an interconnected lake model (Kramer et al., 2004). Surprisingly, for the plants grown at 30°C, the qL was smaller compared to the plant grown at the two other temperatures (Figure 2).

This result is consistent with the protein amount, as the plants grown at 30°C appear to have a lower level of the $Cytb_6f$ complex (PetC), which is the rate limiting step of the electron transport chain under moderate light condition and in the presence of CO2 (Rochaix, 2011). This downregulation has been hypothesized to serve as a protective mechanism for the photosystems (Krieger-Liszkay et al., 2000).
In this regard, the specific relative loss of $Cytb_6f$ at 30°C may be part of the regulation mechanism to protect PSI challenged by the high temperature, by slowing down the electron flow toward PSI, while PSII repair cycle and the higher constitutive NPQ maintain PSII efficiency (Yamane et al., 1997). At 10°C, all the three complexes involved in the electron transport appear to be diminished to a similar extent compared to the control temperature. Therefore, there should be no effect on the relative electron transport capacity per PSII. Consistently, the fraction of open PSII reaction centers (qL) in 35 to 875 µmol photons m–2 s–1 of PAR intensity range is comparable to the control (Figure 2C). Another protective mechanism of PSII is the thermal dissipation of the light excess (NPQ), which also appears to be induced in the plants grown at 30°C that display a stronger thermal dissipation component already at the lowest light intensity used in the fluorescence measurement (Figure 2A). The growth at lower temperature results in a minor change of the thermal dissipation at moderately high intensity; however, the NPQ at higher light intensities (above 500 µmol photons m–2 s–1) was similar to the NPQ of the plants grown at control temperature (22°C). As NPQ induction is dependent on the transmembrane ΔpH (Wraight and Crofts, 1970), this observation suggests that plants grown at higher temperature could be less efficient in the dissipation of the ΔpH, or alternatively that the components of the NPQ machinery are over-accumulated in these plants. However, PsbS, which is the protein responsible for the fast NPQ component (Li et al., 2000), was reported not to respond to temperature as it is not induced in low temperature (Rorat et al., 2001; Norén et al., 2003). Furthermore, the PSBS gene expression was not altered upon changes in the growth temperature, neither by increasing nor by lowering it, in A. thaliana (Kilian et al., 2007). In the plants grown at the higher temperature, there was no increase in the concentration of the two xanthophylls, lutein and zeaxanthin, which are directly involved in the dissipation of the chlorophyll excitation energy, compared with the control (Figure 3; Leuenberger et al., 2017). Therefore, a tentative explanation for the higher NPQ observed in the plants grown at 30°C is the aggregation of LHCII (Tang et al., 2007); this effect should produce a constitutive energy dissipation that would explain the quenching detected already at low light intensity. A relative increase of LHCII over the photosystems would also explain the lower chlorophyll a/b ratio (Figure 3B). A tendency over a higher Lhcb2 accumulation was observed at 30°C ($p = 0.14$, Figure 4). The lack of a quantitative confirmation of this increased accumulation by immunodetection may be explained by an interference of the N-terminal phosphorylation of the antenna on the protein recognition by the antibodies (Longoni et al., 2015). Indeed, the Lhcb2 protein tends to be more phosphorylated when plants were grown at 30°C (Supplementary Figure S4). The level of NPQ affects also directly the quantum yield of PSII (ΦPSII). The plants grown at 30°C induced the most NPQ and had a lower ΦPSII in all the light conditions tested (Figure 2B). The factor limiting ΦPSII in cress grown at low temperature, on the contrary, does not appear to be the NPQ. Most likely in this case unrepaired damage on PSII is responsible for the lower efficiency (Grimaud et al., 2013). This hypothesis would be consistent with the slightly lower FV/FM value measured in the plants grown at lower temperature (Figure 1). This shows that, despite both un-optimal temperatures affecting photosynthesis, the response to the temperature change is different, and not necessarily symmetrical, between lower and higher temperatures.
Membrane lipid composition, including galactolipids of the thylakoid membrane, varies in response to temperature (Falcone et al., 2004; Spicher et al., 2016). As expected, we observed a tendency toward the accumulation of long-chained unsaturated galactolipids (36:6) at 10°C, while the opposite (i.e., accumulation of 34 acyl-carbons and more saturated lipids) was true at higher temperature. This change is most likely necessary to have a similar level of membrane fluidity at different temperatures (Barber et al., 1984). The average number of desaturations per acyl chain in the measured galactolipids was significantly higher at 30°C and lower at 10°C compared to 22°C. The mode by which galactolipid desaturation influences the thylakoid membrane fluidity is not yet defined unambiguously.

However, the level of galactolipid saturation does change in different plant species in response to a temperature shift (Falcone et al., 2004).
Consistently, modification of the level of lipid saturation by knocking down or overexpressing individual fatty acid desaturases results in an altered resistance of the plants to extreme temperatures (Penfield, 2008).
This suggests that the differences observed in the acyl chain saturation are part of cress acclimation to growth temperature. At both non-optimal temperatures, the cress accumulated a larger proportion of MGDG and DGDG originating from the ER (i.e., containing two acyl chains at 18 carbons (C18/C18)] over the galactolipids of plastid origin (i.e., containing one acyl chain of 18 carbons and one of 16 carbons (C18/C16)] (Figure 5; Boudière et al., 2014). The induction of the ER-derived eukaryotic pathway for chloroplast galactolipids upon heat stress has been reported in several species (Higashi and Saito, 2019). Furthermore, a previous report showed an increase of the ER-derived galactolipids and the key role of the ACYL-LIPID DESATURASE2 located in the ER in the acclimation to low temperature in A. thaliana (Chen and Thelen, 2013). The reported difference in the relative abundance of the galactolipid acyl chains supports the hypothesis that a shift from the plastid to the ER pathway for membrane lipid biosynthesis is part of the plant response to non-optimal temperatures. Considering the MGDG/DGDG ratio observed at 10°C, the relative DGDG content was higher than at 22°C. This is consistent with previous reports showing that, during acclimation to prolonged cold periods, the MGDG/DGDG ratio became smaller, while minor changes were observed in the concentration of the other major thylakoid membrane components PG and SQDG (Hendrickson et al., 2006). However, PG and SQDG may also have an impact on thylakoid membrane structure and dynamics depending on the desaturation of the acyl chains. In fact, PG accumulation and desaturation may be critical for photosynthetic acclimation to low temperature (Gao et al., 2015).
The differences in the galactolipid levels may affect the thylakoid organization. For instance, a larger DGDG fraction may strengthen the stacking of the thylakoid membranes by the interactions between facing headgroups of these galactolipids (Demé et al., 2014; Kanduè et al., 2017). However, a lower MGDG/DGDG ratio could also affect the stacking of the LHCII-rich portions of the thylakoid membranes (Seiwert et al., 2018). As the relative level of DGDG was higher at 30°C than in the other two growth temperature, it is plausible that the increased proportion of DGDG strengthens the membrane interactions. This, along with the lower average number of desaturations per molecule, may increase the thermal stability of the thylakoid membrane and may also have a direct effect on the NPQ component acting on the aggregation of LHCII (Krumova et al., 2010).
High temperature may directly affect the photosystem II electron transport efficiency and its structure causing the production of ROS (Pospíšil, 2016). Low temperature hampers PSII repair cycle, leading to photoinhibition and activation of ROS signaling pathways (Grimaud et al., 2013). Consistently, previous reports have shown that temperature changes lead to an increase in the concentration of antioxidant compounds embedded in the thylakoid membrane (Mène-Saffrané et al., 2010; Spicher et al., 2016). In a previous report on tomato, α-tocopherol and plastochromanol were shown to accumulate following a temperature increase, while minor to no change was observed in plants grown at low temperature (Spicher et al., 2016). This study, conversely, found a similar increase in α-tocopherol and plastochromanol concentrations in the plants grown at 10 and 30°C compared to the control condition at 22°C (Figure 5). It is interesting to note that PQ re-oxidation in the dark was faster in the plants grown at 10°C compared to the other two growth temperatures, as inferred by the chlorophyll a fluorescence parameter VJ. In the absence of light, the oxidation of PQ is mostly dependent on the activity of the plastid terminal oxidase PTOX (Carol and Kuntz, 2001). In A. thaliana an accumulation of the PTOX protein was reported in plants acclimated to low temperature (Ivanov et al., 2012). However, the commercial antibody against PTOX detects multiple bands even on cress protein sample obtained from purified thylakoid (Supplementary Figure S5). Lacking any genomic data of *L. sativum*, it is not possible to exclude that different forms of PTOX exist in this species, although the majority of the sequenced higher plants contain a single PTOX gene (Nawrocki et al., 2015).

These uncertainties do not allow drawing a conclusion on the accumulation of PTOX in cress at different temperatures. High level of PTOX protein was hypothesized to be responsible for an increase in the non-photochemical oxidation of PQ in the high mountain plant species *Ranunculus glacialis* as a strategy allowing a better acclimation to low temperatures combined with high irradiation (Streb et al., 2005). However, in this species low temperature alone was not sufficient to induce PTOX protein accumulation (Laureau et al., 2013).
Furthermore, considering studies where an ectopic overexpression of the PTOX protein was achieved, it appears that the PTOX protein level is not the unique determinant of the non-photochemical PQ oxidation rate (Johnson and Stepien, 2016).
The crowded thylakoid membrane poses major limitations to the mobility of PQ and therefore may physically hamper its oxidation in the dark (Tremmel et al., 2003). Considering this, the differences in the galactolipid profile (Figure 5) and the change in the photosynthetic protein accumulation (Figure 4) observed at 10°C may be functional in facilitating PQ mobility and therefore its oxidation by PTOX (Pralon et al., 2020). Furthermore, the accumulation of plastochromanol, which appears to be tendentially higher at 10°C than at 30°C, would allow to contrast more efficiently membrane lipid peroxidation (Figure 5; Nowicka et al., 2013). Accumulation of lipid peroxides, in fact, would reduce the membrane fluidity and therefore the mobility of PQ (Niki, 2009). Accumulation of α-tocopherol, necessary to protect from ROS in both temperature condition, would, on the contrary, stabilize the membrane (Arora et al., 2000). The accumulation of γ-tocopherol, observed at 10°C (Figure 5A), may be a hint of a downregulation of α-tocopherol biosynthesis, functional to control its concentration and thus preserve the membrane fluidity. Membrane fluidity, and the mobility of PQ, may also explain the difference in qL observed between the plants grown at 10°C and those at 30°C (Figure 2). Lipid circulation would facilitate the access of oxidized PQ to PSII. The difference in the VJ kinetics in the dark between these two temperatures is consistent with a difference in long-distance PQ mobility (Figure 6). Increased fluidity may also facilitate the movement of PTOX to the grana stacks, as in *Eutrema salsugineum* under salt stress (Stepien and Johnson, 2018).
The presumed higher thylakoid membrane fluidity of the plants developed at 10°C compared to the other growth temperatures had, if any, a negative impact on PQ oxidation under far-red. Plants developed at 10°C displayed a slower photochemical PQ oxidation compared to 22°C. While in the plants grown at 30°C, PQ oxidation under far-red appears to be slightly faster than in those grown at 22°C (Figure 5B). This difference may be rationalized assuming that the accumulation of more saturated galactolipids and α-tocopherol observed at 30°C results in the stabilization of the thylakoid membrane structure and grana stacking (Arora et al., 2000; Krumova et al., 2010). In this scenario, the photochemical oxidation of PQ would be accelerated by the stabilization of PQ microdomains inside the grana allowing a more efficient circulation of PQ between PSII and $Cytb_6f$ (Kirchhoff et al., 2002). Conversely, the stabilization of the membrane may reduce PQ exchange between microdomains and between different portions of the thylakoid membrane, thus limiting the total PQ pool available per PSII and resulting in the lower ΦPSII and qL observed in the plants grown at 30°C (Figure 2). A hypothetic destabilization of the membrane domains, possibly due to the lower degree of galactolipid saturation, could explain the opposite effect on PQ mobility at 10°C compared to the 30°C scenario.
The dark re-oxidation rate, inferred from the VJ parameter, appears to be two order of magnitude slower than the one under far-red. In this scenario, the contribution of PTOX as an efficient alternative sink of electrons to protect the photosystems appears doubtful. Nevertheless, it has been shown that Arabidopsis plants lacking PTOX had a more severe variegation phenotype at lower temperature, suggesting that PTOX contribution is more critical at low temperature (Rosso et al., 2009). The increased non-photochemical oxidation of PQ may then serve to sustain the biosynthesis of carotenoids allowing to compensate for the enzymatic activity limitation imposed by the lower temperature (Norris et al., 1995). Consistently with this hypothesis, the accumulation of the most abundant carotenoids, on a dry weight basis, was only slightly lower in the plants grown at 10°C compared to the other conditions tested (Figure 3).

The differences observed in plants grown at higher and lower temperature are not symmetrical, but show some common differences, such as the higher level of the membrane antioxidants and a lower MGDG/DGDG ratio. However, at lower temperature, the acclimation is a trade-off between membrane fluidity and protection from ROS, which results in a detectable damage to PSII, while at higher temperature, membrane fluidity is not a constraint allowing to a more efficient protection.
Furthermore, in the plants grown at lower temperature, the non-photochemical oxidation of PQ was faster compared to those at 22 and 30°C. This supports the model in which the activation of alternative electron pathways is an important strategy to protect the photosynthetic apparatus under cold stress.

Data Availability Statement
The datasets generated for this study can be found in the Zenodo repository https://doi.org/10.5281/zenodo.3839245.

Author Contributions
HS, ST, AG, LM, and PL designed the experimental plan. HS, ST, AG, LM, GB, and PL performed the experiments. GG performed the lipid profile analysis. ST and PL performed the statistical analysis of the data. PL wrote the manuscript. All authors read and approved the manuscript.

Funding
This work was supported by the University of Neuchâtel and the Swiss National Science Foundation (31003A_179417).

Conflict of Interest
The authors declare that the research was conducted in the absence of any commercial or financial relationships that could be construed as a potential conflict of interest.

Acknowledgments
The authors would like to acknowledge Felix Kessler, for hosting the research in his laboratory, Michel Goldschmidt Clermont for his critical reading of the manuscript, and Veronique Douet, Gautier Pizzolon, and Jenny Pego Morales for their technical assistance.

References

Abbasi, A.-R., Hajirezaei, M., Hofius, D., Sonnewald, U., and Voll, L. M. (2007). Specific Roles of α- and γ-tocopherol in abiotic stress responses of transgenic tobacco. Plant Phys. 143, 1720–1738. doi: https://10.1104/pp.106.094771

Arora, A., Byrem, T. M., Nair, M. G., and Strasburg, G. M. (2000). Modulation of liposomal membrane fluidity by flavonoids and isoflavonoids. Arch. Biochem. Biophys. 373, 102–109. doi: https://10.1006/abbi.1999.1525

Baker, N. R. (2008). Chlorophyll fluorescence: a probe of photosynthesis in vivo. Annu. Rev. Plant Biol. 59, 89–113. doi: 10.1146/annurev.arplant.59.032607.092759

Barber, J., Ford, R. C., Mitchell, R. A., and Millner, P. A. (1984). Chloroplast thylakoid membrane fluidity and its sensitivity to temperature. Planta 161, 375–380. doi: https://10.1007/bf00398729

Block, M. A., Dorne, A. J., Joyard, J., and Douce, R. (1983). Preparation and characterization of membrane fractions enriched in outer and inner envelope membranes from spinach chloroplasts. II. Biochemical characterization. J. Biol. Chem. 258, 13281–13286.

Boudière, L., Michaud, M., Petroutsos, D., Rébeillé, F., Falconet, D., Bastien, O., et al. (2014). Glycerolipids in photosynthesis: composition, synthesis and trafficking. Biochim. Biophys. Acta 1837, 470–480. doi: https://10.1016/j.bbabio.2013.09.007

Caffarri, S., Frigerio, S., Olivieri, E., Righetti, P. G., and Bassi, R. (2005). Differential accumulation of Lhcb gene products in thylakoid membranes of Zea mays plants grown under contrasting light and temperature conditions. Proteomics 5, 758–768. doi: https://10.1002/pmic.200402008

Carol, P., and Kuntz, M. (2001). A plastid terminal oxidase comes to light: implications for carotenoid biosynthesis and chlororespiration. Trends Plant Sci. 6, 31–36. doi: https://10.1016/s1360-1385(00)01811-2

Chen, M., and Thelen, J. J. (2013). ACYL-LIPID DESATURASE2 is required for chilling and freezing tolerance in Arabidopsis. Plant Cell 25, 1430–1444. doi: https://10.1105/tpc.113.111179

Dall'Osto, L., Cazzaniga, S., Havaux, M., and Bassi, R. (2010). Enhanced Photoprotection by protein-bound vs free xanthophyll pools: a comparative analysis of chlorophyll b and xanthophyll biosynthesis mutants. Mol. Plant 3, 576–593. doi: https://10.1093/mp/ssp117

Demé, B., Cataye, C., Block, M. A., Maréchal, E., and Jouhet, J. (2014). Contribution of galactoglycerolipids to the 3-dimensional architecture of thylakoids. FASEB J. 28, 3373–3383. doi: https://10.1096/fj.13-247395

Dörmann, P. (2013). "Galactolipids in plant membranes," in eLS (Chichester: John Wiley & Sons, Ltd.). doi: https://10.1002/9780470015902.a0020100.pub2

Falcone, D. L., Ogas, J. P., and Somerville, C. R. (2004). Regulation of membrane fatty acid composition by temperature in mutants of Arabidopsis with alterations in membrane lipid composition. BMC Plant Biol. 4:17. doi: https://10.1186/1471-2229-4-17

Gao, J., Wallis, J. G., and Browse, J. (2015). Mutations in the prokaryotic pathway rescue the fatty acid biosynthesis1 mutant in the cold. Plant Physiol. 169, 442–452. doi: https://10.1104/pp.15.00931

Grimaud, F., Renaut, J., Dumont, E., Sergeant, K., Lucau-Danila, A., Blervacq, A.-S., et al. (2013). Exploring chloroplastic changes related to chilling and freezing tolerance during cold acclimation of pea (Pisum sativum L.). J. Proteomics 80, 145–159. doi: https://10.1016/j.jprot.2012.12.030

Hendrickson, L., Vlèková, A., Selstam, E., Huner, N., Öquist, G., and Hurry, V. (2006). Cold acclimation of the Arabidopsis dgd1 mutant results in recovery from photosystem I-limited photosynthesis. FEBS Lett. 580, 4959–4968. doi: https://10.1016/j.febslet.2006.07.081

Higashi, Y., Okazaki, Y., Myouga, F., Shinozaki, K., and Saito, K. (2015). Landscape of the lipidome and transcriptome under heat stress in Arabidopsis thaliana. Sci. Rep. 5, 1–11. doi: 10.1038/srep10533

Higashi, Y., and Saito, K. (2019). Lipidomic studies of membrane glycerolipids in plant leaves under heat stress. Prog. Lipid Res. 75:100990. doi: https://10.1016/j.plipres.2019.100990

Ivanov, A. G., Rosso, D., Savitch, L. V., Stachula, P., Rosembert, M., Oquist, G., et al. (2012). Implications of alternative electron sinks in increased resistance of PSII and PSI photochemistry to high light stress in cold-acclimated Arabidopsis thaliana. Photosyn. Res. 113, 191–206. doi: https://10.1007/s11120-012-9769-y

Johnson, G. N., and Stepien, P. (2016). Plastid terminal oxidase as a route to improving plant stress tolerance: known knowns and known unknowns. Plant Cell Physiol. 57, 1387–1396.

Kanduè, M., Schlaich, A., de Vries, A. H., Jouhet, J., Maréchal, E., Demé, B., et al. (2017). Tight cohesion between glycolipid membranes results from balanced water-headgroup interactions. Nat. Commun. 8:14899. doi: https://10.1038/ncomms14899

Kilian, J., Whitehead, D., Horak, J., Wanke, D., Weinl, S., Batistic, O., et al. (2007). The AtGenExpress global stress expression data set: protocols, evaluation and model data analysis of UV-B light, drought and cold stress responses. Plant J. 50, 347–363.

Kirchhoff, H., Mukherjee, U., and Galla, H.-J. (2002). Molecular architecture of the thylakoid membrane: lipid diffusion space for plastoquinone. Biochemistry 41, 4872–4882.

Kramer, D. M., Johnson, G., Kiirats, O., and Edwards, G. E. (2004). New fluorescence parameters for the determination of QA redox state and excitation energy fluxes. Photosyn. Res. 79:209. doi: https://10.1023/B:PRES.0000015391.99477.0d

Krieger-Liszkay, A., Kienzler, K., and Johnson, G. N. (2000). Inhibition of electron transport at the cytochrome b6f complex protects photosystem II from photoinhibition. FEBS Lett. 486, 191–194.

Kromdijk, J., Głowacka, K., Leonelli, L., Gabilly, S. T., Iwai, M., Niyogi, K. K., et al. (2016). Improving photosynthesis and crop productivity by accelerating recovery from photoprotection. Science 354, 857–861.

Krumova, S. B., Laptenok, S. P., Kovács, L., Tóth, T., van Hoek, A., Garab, G., et al. (2010). Digalactosyl-diacylglycerol-deficiency lowers the thermal stability of thylakoid membranes. Photosyn. Res. 105, 229–242. doi: https://10.1007/s11120-010-9581-5

Laemmli, U. K. (1970). Cleavage of structural proteins during the assembly of the head of bacteriophage T4. Nature 227, 680–685.

Laureau, C., Paepe, R. D., Latouche, G., Moreno−Chacón, M., Finazzi, G., Kuntz, M., et al. (2013). Plastid terminal oxidase (PTOX) has the potential to act as a safety valve for excess excitation energy in the alpine plant species Ranunculus glacialis L. Plant Cell Environ. 36, 1296–1310. doi: https://10.1111/pce.12059

Leuenberger, M., Morris, J. M., Chan, A. M., Leonelli, L., Niyogi, K. K., and Fleming, G. R. (2017). Dissecting and modeling zeaxanthin- and lutein-dependent nonphotochemical quenching in Arabidopsis thaliana. Proc. Natl. Acad. Sci. U.S.A. 114, E7009–E7017. doi: https://10.1073/pnas.1704502114

Li, H., Yan, X., Xu, J., and Zhou, C. (2008). Precise identification of photosynthetic glycerolipids in microalga Tetraselmis chuii by UPLC-ESI-Q-TOF-MS. Sci. China C Life Sci. 51, 1101–1107. doi: https://10.1007/s11427-008-0138-1

Li, X.-P., Björkman, O., Shih, C., Grossman, A. R., Rosenquist, M., Jansson, S., et al. (2000). A pigment-binding protein essential for regulation of photosynthetic light harvesting. Nature 403, 391–395.

Lichtenthaler, H. K., and Wellburn, A. R. (1983). Determinations of total carotenoids and chlorophylls a and b of leaf extracts in different solvents. Biochem. Soc. Trans. 11, 591–592.

Longoni, P., Douchi, D., Cariti, F., Fucile, G., and Goldschmidt-Clermont, M. (2015). Phosphorylation of the light-harvesting complex II Isoform Lhcb2 Is central to state transitions. Plant Physiol. 169, 2874–2883. doi: https://10.1104/pp.15.01498

Longoni, P., Samol, I., and Goldschmidt-Clermont, M. (2019). The kinase STATE TRANSITION 8 phosphorylates light harvesting complex II and contributes to light acclimation in Arabidopsis thaliana. Front. Plant Sci. 10:1156. doi: https://10.3389/fpls.2019.01156

Maxwell, K., and Johnson, G. N. (2000). Chlorophyll fluorescence—a practical guide. J. Exp. Bot. 51, 659–668.

Mène-Saffrané, L., Jones, A. D., and DellaPenna, D. (2010). Plastochromanol-8 and tocopherols are essential lipid-soluble antioxidants during seed desiccation and quiescence in Arabidopsis. Proc. Natl. Acad. Sci. U.S.A. 107, 17815–17820. doi: https://10.1073/pnas.1006971107

Nawrocki, W. J., Tourasse, N. J., Taly, A., Rappaport, F., and Wollman, F.-A. (2015). The plastid terminal oxidase: its elusive function points to multiple contributions to plastid physiology. Annu. Rev. Plant. Biol. 66, 49–74. doi: https://10.1146/annurev-arplant-043014-114744

Niki, E. (2009). Lipid peroxidation: physiological levels and dual biological effects. Free Radic. Biol. Med. 47, 469–484. doi: https://10.1016/j.freeradbiomed.2009.05.032

Norén, H., Svensson, P., Stegmark, R., Funk, C., Adamska, I., and Andersson, B. (2003). Expression of the early light-induced protein but not the PsbS protein is influenced by low temperature and depends on the developmental stage of the plant in field-grown pea cultivars. Plant Cell Environ. 26, 245–253.

Norris, S. R., Barrette, T. R., and DellaPenna, D. (1995). Genetic dissection of carotenoid synthesis in Arabidopsis defines plastoquinone as an essential component of phytoene desaturation. Plant Cell 7, 2139–2149.

Nowicka, B., Gruszka, J., and Kruk, J. (2013). Function of plastochromanol and other biological prenyllipids in the inhibition of lipid peroxidation—a comparative study in model systems. Biochim. Biophys. Acta 1828, 233–240. doi: https://10.1016/j.bbamem.2012.08.018

Penfield, S. (2008). Temperature perception and signal transduction in plants. New Phytol. 179, 615–628. doi: https://10.1111/j.1469-8137.2008.02478.x

Pospíšil, P. (2016). Production of reactive oxygen species by photosystem II as a response to light and temperature stress. Front. Plant Sci. 7:1950. doi: https://10.3389/fpls.2016.01950

Pralon, T., Collombat, J., Pipitone, R., Ksas, B., Shanmugabalaji, V., Havaux, M., et al. (2020). Mutation of the atypical kinase ABC1K3 partially rescues the proton gradient regulation 6 Phenotype in Arabidopsis thaliana. Front. Plant Sci. 11:337. doi: https://10.3389/fpls.2020.00337

Rastogi, A., Yadav, D. K., Szymańska, R., Kruk, J., Sedláøová, M., and Pospíšil, P. (2014). Singlet oxygen scavenging activity of tocopherol and plastochromanol in Arabidopsis thaliana: relevance to photooxidative stress. Plant Cell Environ. 37, 392–401. doi: https://10.1111/pce.12161

Rochaix, J.-D. (2011). Regulation of photosynthetic electron transport. Biochim. Biophys. Acta 1807, 375–383. doi: https://10.1016/j.bbabio.2010.11.010

Rokka, A., Aro, E.-M., Herrmann, R. G., Andersson, B., and Vener, A. V. (2000). Dephosphorylation of photosystem II reaction center proteins in plant photosynthetic membranes as an immediate response to abrupt elevation of temperature. Plant Physiol. 123, 1525–1536.

Rorat, T., Havaux, M., Irzykowski, W., Cuiné, S., Becuwe, N., and Rey, P. (2001). PSII-S gene expression, photosynthetic activity and abundance of plastid thioredoxin-related and lipid-associated proteins during chilling stress in Solanum species differing in freezing resistance. Physiol. Plant 113, 72–78.

Rosso, D., Bode, R., Li, W., Krol, M., Saccon, D., Wang, S., et al. (2009). Photosynthetic redox imbalance governs leaf sectoring in the Arabidopsis thaliana variegation mutants immutans, spotty, var1, and var2. Plant Cell 21, 3473–3492. doi: https://10.1105/tpc.108.062752

Seiwert, D., Witt, H., Ritz, S., Janshoff, A., and Paulsen, H. (2018). The nonbilayer lipid MGDG and the major light-harvesting complex (LHCII) promote membrane stacking in supported lipid bilayers. Biochemistry 57, 2278–2288. doi: https://10.1021/acs.biochem.8b00118

Spicher, L., Almeida, J., Gutbrod, K., Pipitone, R., Dörmann, P., Glauser, G., et al. (2017). Essential role for phytol kinase and tocopherol in tolerance to combined light and temperature stress in tomato. J. Exp. Bot. 68, 5845–5856. doi: https://10.1093/jxb/erx356

Spicher, L., Glauser, G., and Kessler, F. (2016). Lipid antioxidant and galactolipid remodeling under temperature stress in tomato plants. Front. Plant Sci. 7:167. doi: https://10.3389/fpls.2016.00167

Stepien, P., and Johnson, G. N. (2018). Plastid terminal oxidase requires translocation to the grana stacks to act as a sink for electron transport. Proc. Natl. Acad. Sci. U.S.A. 115, 9634–9639. doi: https://10.1073/pnas.1719070115

Streb, P., Josse, E.-M., Gallouët, E., Baptist, F., Kuntz, M., and Cornic, G. (2005). Evidence for alternative electron sinks to photosynthetic carbon assimilation in the high mountain plant species Ranunculus glacialis. Plant Cell Environ. 28, 1123–1135.

Sunil, B., Saini, D., Bapatla, R. B., Aswani, V., and Raghavendra, A. S. (2019). Photorespiration is complemented by cyclic electron flow and the alternative oxidase pathway to optimize photosynthesis and protect against abiotic stress. Photosyn. Res. 139, 67–79. doi: https://10.1007/s11120-018-0577-x

Tang, Y., Wen, X., Lu, Q., Yang, Z., Cheng, Z., and Lu, C. (2007). Heat stress induces an aggregation of the light-harvesting complex of photosystem II in spinach plants. Plant Physiol. 143, 629–638.

Tóth, S. Z., Schansker, G., and Strasser, R. J. (2007). A non-invasive assay of the plastoquinone pool redox state based on the OJIP-transient. Photosyn. Res. 93, 193–203.

Tremmel, I. G., Kirchhoff, H., Weis, E., and Farquhar, G. D. (2003). Dependence of plastoquinol diffusion on the shape, size, and density of integral thylakoid proteins. Biochim. Biophys. Acta 1607, 97–109.

Ware, M. A., Dall'Osto, L., and Ruban, A. V. (2016). An in vivo quantitative comparison of photoprotection in Arabidopsis xanthophyll mutants. Front. Plant Sci. 7:841. doi: https://10.3389/fpls.2016.00841

Wraight, C. A., and Crofts, A. R. (1970). Energy-dependent quenching of chlorophyll a fluorescence in isolated chloroplasts. Eur. J. Biochem. 17, 319–327.

Yamane, Y., Kashino, Y., Koike, H., and Satoh, K. (1997). Increases in the fluorescence Fo level and reversible inhibition of Photosystem II reaction center by high-temperature treatments in higher plants. Photosyn. Res. 52, 57–64.

Yamori, W., Hikosaka, K., and Way, D. A. (2014). Temperature response of photosynthesis in C3, C4, and CAM plants: temperature acclimation and temperature adaptation. Photosyn. Res. 119, 101–117. doi: https://10.1007/s11120-013-9874-6

Zhang, R., Wise, R. R., Struck, K. R., and Sharkey, T. D. (2010). Moderate heat stress of Arabidopsis thaliana leaves causes chloroplast swelling and plastoglobule formation. Photosyn. Res. 105, 123–134. doi: https://10.1007/s11120-010-9572-6

Supplementary Material

The Supplementary Material for this article can be found online at: https://www.frontiersin.org/articles/10.3389/fpls.2020.00745/full#supplementary-material

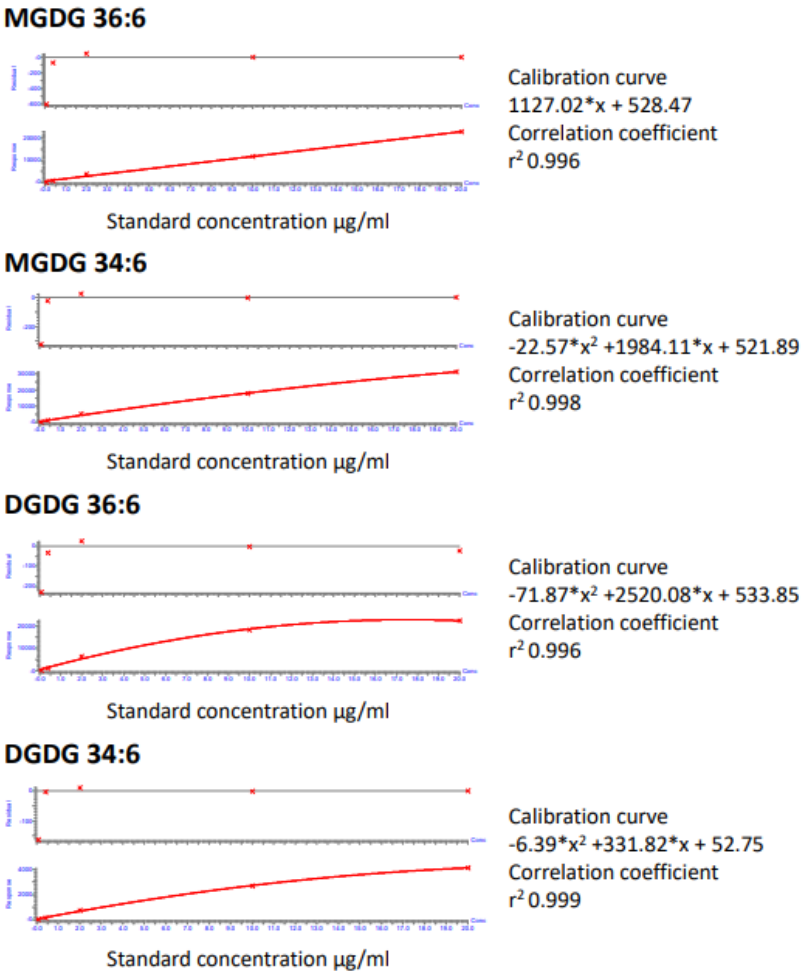

Supplementary Figure 1. Calibration curves for galactolipids quantification.

The graphs show the correlation between the response, based on peak height, and the concentration of the standard mixture for the four molecules used for the quantification of the mono- (MGDG 36:6, MGDG 34:6) and di- (DGDG 36:6, DGDG 34:6) galactosyldiacylglycerols. Upper panel, residuals from the calibration; lower panel, measured points and calibration curve. The calibration was performed with TargetLynx XS (Waters) using a linear or a second-degree polynomial function. The equations of the functions and the correlation coefficients are shown on the right side of each graph

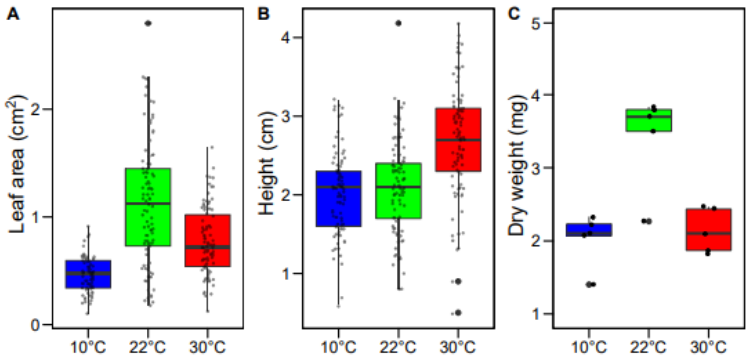

Supplementary Figure 2. Analysis of *L. sativum* grown at different temperatures

A) The average leaf area per plant was measured using ImageJ, based on the elaboration of a digital image taken for each pot and for each condition. The leaf area is significantly different for each growth condition ($p < 0.0001$). **B)** Length of the hypocotyl for each individual was measured manually. The hypocotyl length of the plants grown at 30°C is significantly different from the other two conditions ($p < 0.0001$). the same set of plants was used for the measure of these two parameters (10°C n=76, 22°C n=93, 30°C n=87). **C)** Average dry weight of a single cress plant after 120 hours of lyophilization, the data show the distribution of 5 samples for each growth temperature composed of three plants each, only the epigeal portion of the plant was considered. Both the plants grown at 10°C and at 30°C have a dry mass significantly lower than the control at 22°C ($p < 0.005$). In the box plots, the lower and upper hinges correspond to the first and third quartiles (the 25th and 75th percentiles). The whiskers extend from the hinge to the farthest value no further than 1.5 times the distance between the first and third quartiles from the hinge. Farther points are considered as "outliers" and plotted individually.

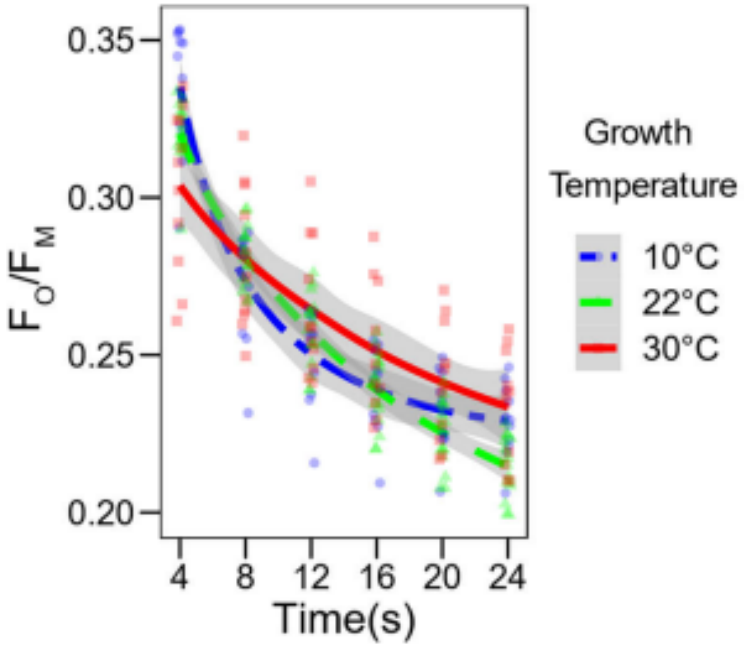

Supplementary Figure 3. Decrease of the Fo during dark incubation.

The Fo was calculated from the M-PEA (Hansatec) from the first pointe of the fluorescence rise during a 700 ms saturating pulse for all the time points shown in Figure 6. Between the pulses the leaf was kept in the dark. The points were interpolated with a logarithmic function (10°C, blue double dashed line, 22°C green dashed line, 30°C red continuous line). The standard error of the interpolation is shown as a grey area around the curve.

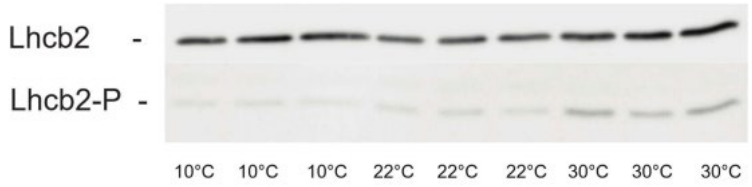

Supplementary Figure 4. Phosphorylation of Lhcb2 increases at higher temperature. in *L. sativum*.

A membrane loaded with three protein samples prepared for different individuals grown at the same temperature (10°C, 22°C and 30°C) was decorated with the antibody against A) Lhcb2 and B) the phosphorylated form of the same protein (Lhcb2-P) (Agrisera AS13 2705). The position of the expected signal is shown on the left.

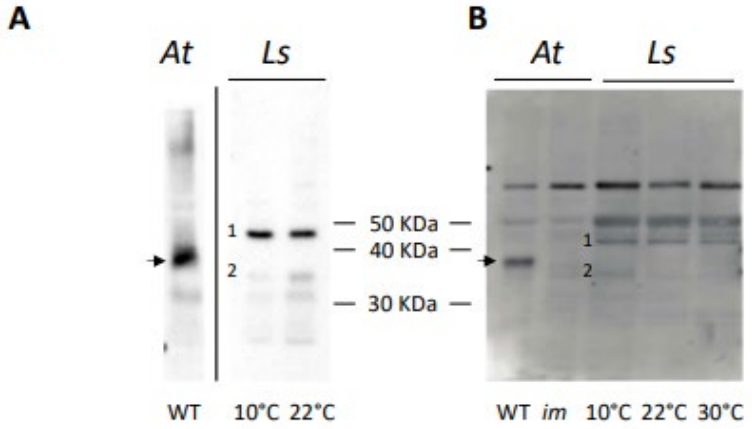

Supplementary Figure 5. Detection of the PTOX/im protein in *L. sativum*. Membranes containing extracts from *Arabidopsis thaliana* and *Lepidium sativum* were decorated with the commercial PTOX/im antibody (Agrisera) and revealed by ECL. A) The protein sample is derived from a thylakoid preparation from *Arabidopsis thaliana* (*At*) and *Lepidium sativum* (*Ls*) grown at 10°C and 22°C. The thylakoid preparation was performed according to Longoni et al. 2015. The samples were loaded by equal chlorophyll amount. Two differential bands were detected in the *L. sativum* samples, marked with 1 and 2, having a size consistent with the expected PTOX size (the average predicted size of the mature PTOX for the sequenced members of the Brassicaceae family is 35 KDa). The PTOX protein in the samples from *Arabidopsis thaliana* is highlighted with an arrow. B) representative immunoblot of the analysis of total protein extracts from *Arabidopsis thaliana* (*At*) and *Lepidium sativum* (*Ls*) grown at 10°, 22°C and 30°C. The mutant im (lacking the PTOX protein) was included to confirm the identification of the protein in *A. thaliana*. The bands 1 and 2 identified in the thylakoid preparation are shown in the total extracts according to their size.

Chapter III

Photosynthetic Light Harvesting and Thylakoid Organization in a CRISPR/Cas9 Arabidopsis Thaliana LHCB1 Knockout Mutant

Hamed Sattari Vayghan1, Wojciech J. Nawrocki2, Christo Schiphorst3, Dimitri Tolleter4, Chen Hu2, Veronique Douet1, Gaëtan Glauser5, Giovanni Finazzi4, Roberta Croce2, Emilie Wientjes3 and Fiamma Longoni1*

[1]Laboratory of Plant Physiology, Institute of Biology, University of Neuchâtel, Neuchâtel, Switzerland
[2]Department of Physics and Astronomy, Faculty of Science, Vrije Universiteit Amsterdam, Amsterdam, Netherlands
[3]Laboratory of Biophysics, Wageningen University, Wageningen, Netherlands
[4]Univ. Grenoble Alpes, CNRS, CEA, INRAE, IRIG, LPCV, Grenoble, France
[5]Neuchâtel Platform of Analytical Chemistry, University of Neuchâtel, Neuchâtel, Switzerland

Front. Plant Sci., 07 March 2022: https://doi.org/10.3389/fpls.2022.833032, Sec. Plant Physiology

Received: 10 December 2021; Accepted: 28 January 2022;
Published: 07 March 2022.
Edited by: Harvey J. M. Hou, Alabama State University, United States
Reviewed by: Heiko Lokstein, Charles University, Czechia,Jianfeng Yu, Imperial College London, United Kingdom

***Correspondence:** Fiamma Longoni, Fiamma.longoni@unine.ch, longonifiamm@gmail.com

Light absorbed by chlorophylls of Photosystems II and I drives oxygenic photosynthesis. Light-harvesting complexes increase the absorption cross-section of these photosystems. Furthermore, these complexes play a central role in photoprotection by dissipating the excess of absorbed light energy in an inducible and regulated fashion. In higher plants, the main light-harvesting complex is trimeric LHCII. In this work, we used CRISPR/Cas9 to knockout the five genes encoding LHCB1, which is the major component of LHCII. In absence of LHCB1, the accumulation of the other LHCII isoforms was only slightly increased, thereby resulting in chlorophyll loss, leading to a pale green phenotype and growth delay. The Photosystem II absorption cross-section was smaller, while the Photosystem I absorption cross-section was unaffected. This altered the chlorophyll repartition between the two photosystems, favoring Photosystem I excitation. The equilibrium of the photosynthetic electron transport was partially maintained by lower Photosystem I over Photosystem II reaction center ratio and by the dephosphorylation of LHCII and Photosystem II. Loss of LHCB1 altered the thylakoid structure, with less membrane layers per grana stack and reduced grana width. Stable LHCB1 knockout lines allow characterizing the role of this protein in light harvesting and acclimation and pave the way for future *in vivo* mutational analyses of LHCII.

Keywords: photosynthesis, light harvesting, CRISPR/Cas9, LHCII, chloroplast, Arabidopsis

Introduction

Light is the source of energy for photosynthetic organisms and largely fuels the synthesis of organic molecules in the biosphere. Light excites the chlorophyll (Chl) molecules of the photosynthetic complexes embedded in the thylakoid membrane. The light energy is used by Photosystem II (PSII) for the photo-oxidation of water. The released electrons move from PSII through the electron transport chain (ETC) *via* plastoquinol/plastoquinone (PQ), cytochrome b_6f (cytb6f), plastocyanin (Pc), to Photosystem I (PSI). Light absorbed by PSI drives the electron transport through ferredoxin to reduce $NADP^+ + H^+$ to NADPH (reviewed in Merchant and Sawaya, 2005).
This process is coupled with the generation of a proton gradient between the lumen and the stroma side of the thylakoid membrane, a gradient used by the ATP synthase for the generation of ATP (Boyer, 1993). Light is an inconstant source of energy, and photosynthetic organisms experience shifts in light spectrum and intensity. To cope with these changes and optimize the photosynthetic efficiency, the organization of the pigment-protein complexes must be dynamic (for a recent review, see Rantala et al., 2020). The dynamism of the ETC is also helped by the non-homogeneous distribution of thylakoid membrane proteins. The stacked domains of the thylakoids, called grana, are enriched in PSII, while other domains, composed of non-appressed membranes, are enriched in PSI and are collectively referred to as stroma lamellae. The stacked and unstacked portions of thylakoids are dynamic and contribute to the acclimation to changes in environmental conditions (for a recent review, see Johnson and Wientjes, 2020).
Light is harvested *via* pigment protein complexes embedded in the thylakoid membrane and associated with the two photosystems. The members of these light-harvesting complexes are similar in structure and pigment organization. They can be distinguished by their interactions with the photosystems and spectroscopic properties into (i) LHCI, tightly bound to PSI, (ii) the minor antenna complexes LHCB4 (CP29), LHCB5 (CP26), and LHCB6 (CP24) associated with PSII, and (iii) LHCII, which acts as an antenna of both photosystems (Jansson et al., 1992; Wientjes et al., 2013; Bos et al., 2019; Chukhutsina et al., 2020). LHCI is composed of protein dimers. In higher plants, the most common PSI-LHCI complex contains two heterodimers of LHCI associated with a monomeric PSI core complex (Mazor et al., 2017). These two dimers are composed of different LHCI isoforms: LHCA1 and LHCA4 form one dimer, while LHCA2 and LHCA3 form the second one (Wientjes and Croce, 2011). Each of these isoforms is encoded by a single gene in Arabidopsis (Klimmek et al., 2006). Two additional genes, named *Lhca5* and *Lhca6*, encode close homologs. However, these genes are rarely expressed, and their protein products are only found in sub-stoichiometric amounts compared to PSI reaction centers (Klimmek et al., 2006).
LHCII is the most abundant membrane protein in photosynthetic eukaryotes, accounting for roughly 30% of the thylakoid membrane proteins and harbors half of the total Chl (Peter and Thornber, 1991). The amino acid sequence and the structure of LHCII are highly conserved across plant species. The LHCII, in higher plants, is composed of homo- and heterotrimers of three protein isoforms: LHCB1, LHCB2, and LHCB3 (Caffarri et al., 2004), which share more than 50% sequence identity (reviewed in Barros and Kühlbrandt, 2009; Crepin and Caffarri, 2018). Trimeric LHCII and monomeric antennae LHCB4, LHCB5, and LHCB6 play a central role in the structure of the PSII-LHCII supercomplexes. Two classes of LHCII trimers are present in stable PSII-LHCII supercomplexes. The strongly associated trimers (S-trimers), composed of LHCB1 and LHCB2, interact with the monomeric LHCB4 and LHCB5 isoforms and the inner antenna of PSII. The moderately bound trimers (M-trimers), containing also the LHCB3 isoform, interact only with the monomeric antennae LHCB6 and LHCB4, the latter being connected to the PSII core (for recent reviews, see Croce and Amerongen, 2020; Pan et al., 2020).
An extra pool of LHCII trimers (L-trimers) exists in the thylakoid membranes. These trimers have a loose interaction with PSII and, therefore, are not consistently isolated with the PSII-LHCII complexes (Dekker and Boekema, 2005). The L-trimers have been characterized when associated with PSI in the PSI-LHCI-LHCII complex and found to be composed by LHCB1 and LHCB2 (Kouřil et al., 2005; Galka et al., 2012). The LHCII trimers can thus serve both as antennae of PSII and PSI (Wientjes et al., 2013).

The amount of LHCII associated with each photosystem is dynamic and, in part, regulated *via* the phosphorylation of a threonine residue located close to the N-terminus of the LHCII protein (Allen, 1992; Wientjes et al., 2013). In particular, the phosphorylated N-terminus of LHCB2 is capable to interact with PSI (Pan et al., 2018), while LHCB1, in the stable PSI-LHCI-LHCII complex, is mostly non-phosphorylated (Pietrzykowska et al., 2014; Crepin and Caffarri, 2015; Longoni et al., 2015). Despite this difference between LHCB1 and LHCB2, the STN7 kinase (Bellafiore et al., 2005) and the PPH1/TAP38 phosphatase (Pribil et al., 2010; Shapiguzov et al., 2010) regulate the phosphorylation level of both isoforms (Leoni et al., 2013; Longoni et al., 2015). The phosphorylation level of LHCB1 and LHCB2 is linked to the redox state of the PQ pool present in the ETC.
In a simplified model, an increased reduction of PQ activates STN7 and thus induces the phosphorylation of its targets (recently reviewed in Longoni and Goldschmidt-Clermont, 2021; Malone et al., 2021). Furthermore, the activity of STN7 is regulated *via* thioredoxins (Ancin et al., 2019) so that the kinase is inactive when plants are exposed to high light intensity, and by the protein amount, for instance, a prolonged over-excitation of PSI by far-red light leads to degradation of STN7 (Willig et al., 2011). While the contribution of LHCB2 and its phosphorylation to the dynamics of the photosynthetic complexes has been described and appears to be conserved across higher plants, the contribution of phosphorylated LHCB1 is less obvious.
LHCB1 is the most abundant isoform composing the trimeric LHCII, based on proteomic analysis a ratio of 7:4:1 for LHCB1:LHCB2:LHCB3 was calculated for Arabidopsis (Galka et al., 2012; Crepin and Caffarri, 2018). In Arabidopsis, there are five genes coding for LHCB1: three genes form a cluster on Chromosome 1 (named *Lhcb1.1*, *Lhcb1.2*, and *Lhcb1.3*), with *Lhcb1.1* and *Lhcb1.3* sharing a common bidirectional promoter (Leutwiler et al., 1986). These three genes encode identical mature proteins with few amino acid differences in the sequence of the transit peptide. The remaining two genes (*Lhcb1.4* and *Lhcb1.5*) form a cluster on Chromosome 2 and code for slightly different mature proteins characterized by three amino acid substitutions compared to the products of the genes on Chromosome 1 (McGrath et al., 1992). Furthermore, the product of *Lhcb1.4* has three extra amino acid substitutions and one deletion in the N-terminal portion of the mature protein that also removes the phosphorylable threonine.
The earlier mutants characterized by a decrease of the LHCII were the mutant of Chl *b* synthesis. These mutants resulted in lower Chl and antenna protein content (Krol et al., 1995; Espineda et al., 1999). However, in these mutants, different antenna isoforms were differentially affected, and previous reports showed an inconsistent effect; further investigations led to the hypothesis that the different isoforms of the light harvesting complex were affected, depending on the growth light intensity (Kim et al., 2009). To investigate the role of the LHCB1 isoform, a more targeted approach was thus required. Almost complete depletion of LHCB1 has been previously obtained by transforming Arabidopsis plants with specific artificial miRNA (*Lhcb1amiRNA*) (Pietrzykowska et al., 2014). This knock-down line revealed that this isoform is contributing *via* STN7-dependent phosphorylation to regulate the photosynthetic electron transport upon light quality changes (Pietrzykowska et al., 2014). However, the study on multiple mutants, lacking both STN7 and PPH1/TAP38, revealed that LHCB1 can also be phosphorylated by the STN7 homolog STN8 (Longoni et al., 2019). The analysis of *Lhcb1amiRNA* showed that LHCB1 is required for the accumulation of trimeric LHCII, and it is important for non-photochemical quenching (NPQ), a collective definition of mechanisms protecting the photosystems from excessive light irradiance (reviewed in Horton and Ruban, 2005; Bassi and Dall'Osto, 2021). Strong reduction of LHCB1, along with LHCB2, was obtained by the introduction of an Lhcb2 antisense gene (Andersson et al., 2003). More recently, by crossing the *Lhcb1amiRNA* with a mutant containing an artificial miRNA targeting LHCB2-coding genes, plants without LHCII trimers and with lower NPQ were obtained (Nicol et al., 2019).
However, there is still no information on the impact of LHCB1 loss on the excitation equilibrium between PSI and PSII, or about the distribution of the photosystems in a "LHCII-depleted" thylakoid membrane. Furthermore, knock-down mutants are prone to changes in gene expression, allowing a leaky accumulation of the target protein, which is not the case for a complete knockout.

To investigate the role of LHCB1, we used a CRISPR/Cas9-based approach to mutate simultaneously the five genes encoding this protein. The potential of said approach was previously presented, allowing to reduce the LHCB1 protein amount below the detection limit (Ordon et al., 2020). By targeting identical regions shared between the five *Lhcb1* genes, it was possible to use only two synthetic gRNAs to generate stable mutant lines deprived of LHCB1. We describe how the constitutive and complete loss of LHCB1 affects the antenna organization around the photosystems, its phosphorylation, and the thylakoid structure.

Materials and Methods

Plant Material and Mutant Production

For the production of multiple mutant lines, two synthetic gRNAs (sgRNA) were designed based on the Arabidopsis genomic sequence, using the software chop-chop (Montague et al., 2014). The highest ranking sgRNA sequences, targeting multiple *Lhcb1* genes, were further analyzed with E-CRISP (Heigwer et al., 2014). The sgRNA sequences with the highest efficacy score were cloned in a binary vector for the stable transformation of wild type Arabidopsis plants (ecotype: Col0), containing the Cas9 gene under the control of the synthetic EC1 promoter that confers expression in egg cells (Durr et al., 2018). The insertion of two sgRNA was performed following the method described by Xing et al. (2014).

The seed obtained from the transformed plants was germinated on 1/2 MS, containing 33 μg ml^{-1} Hygromycin. After 10 days, resistant plants were transferred to soil. The genomic DNA was extracted from a leaf sample, and a PCR was performed to confirm the presence of the T-DNA insert. The plants containing the T-DNA were led to flowering and the collected seeds germinated on 1/2 MS; the seedlings were screened by Chl *a* fluorescence measurement (detailed below) to detect low NPQ individuals within mixed populations (Supplementary Figure 1). Those individuals were transferred to soil and further analyzed for presence of the T-DNA insert and for the presence of the mutation in the Lhcb1.1–5 genes.

The plants on plates were grown under white light LEDs (120 μmol photons $m^{-2}s^{-1}$PAR) with a 16-h-light 8-h-dark daily cycle in a climatic chamber set at 22°C (ARALAB FitoClima 600 PL). The plants in soil were grown under white neon tubes (120 μmol photons $m^{-2}s^{-1}$PAR) with a 16-h-light 8-h-dark day cycle in a walk-in climatic chamber set at 22°C. Total Chl extraction was performed on samples composed of three 14 day-old plantlets, which were weighted to measure the total fresh weight, frozen in liquid nitrogen, and grounded to fine powder. The total pigments were extracted in 80% acetone buffered with Tris-HCl pH 7.4 and the Chl *a* and *b* concentration measured by multi-wave length absorbance according to Porra (2002).

Protein Analysis and Immunodetection

Protein samples were prepared from entire 14 days-old plantlets. Each sample was composed of at least three individuals, the fresh weight recorded, and the plantlets were then flash frozen in liquid nitrogen. The frozen samples were grounded to fine powder using glass beads, mixing in an IvoclarVivadent shaker (Silamat) two times for 10 s. The extraction was performed by homogenizing the sample powder in a lysis buffer, containing 100 mM Tris-HCl, pH 7.8, 2% SDS, 50-mM NaF, and 1 × Protease Inhibitor Cocktail for Plant (Sigma-Aldrich) and then incubating for 30 min at 37°C. The supernatant was clarified by centrifugation and added to a mix composed by 25% of a protein sample, 50% of deionized water, and 25% of a 4x sample buffer (0.2 M Tris/HCl pH 6.8, 0.4 M Dithiotreitol, 8% w/v SDS, 0.4% w/v Bromophenol Blue, 40% v/v Glycerol). The mix was loaded on a Tris-Gly SDS-PAGE 12% acrylamide gel. For the separation of the phosphorylated form of the protein, we used the same gel system to which we added 30 μM Phos-tag (Wako Chemicals) and 60 μM $MnCl_2$. The proteins were separated by electrophoresis on the gel and transferred to a nitrocellulose membrane for immuno-detection.

The nitrocellulose membranes were blocked with commercial skim-milk 5% (M) in TBS Tween (0.25%), except for the membranes used for the detection of LHCB2, which were blocked with 3% BSA (Applichem) in TBS Triton X-100 (0.1%) to allow the membrane dephosphorylation before the incubation with the primary antibody, detailed in Longoni et al. (2015). After the blocking, the membranes were decorated with primary antibodies for the detection of relevant proteins. The antibodies recognizing the following proteins were obtained from Agrisera: LHCB1 (AS09 522), LHCB2 (AS01 003), LHCB2-P (AS13 2705), LHCB3 (AS01 002), LHCB4 (CP29) (AS04 045), LHCB5 (CP26) (AS01 009), LHCB6 (CP24) (AS04 010), D1 (PsbA) (AS05 084), PsbA-P (AS13 2669), D2 (PsbD) (AS06 146), PsbC (CP43) (AS06 111), PsbB (CP47) (AS04 038), PETC (AS08 330), PsaB (AS10 695), PsaC (AS10 939), PSAD (AS09 461), PSAH (AS06 105), LHCA1 (AS01 005), LHCA2 (AS01 006), LHCA3 (AS01 007), LHCA4 (AS01 008), STN7 (AS16 4098), PPH1 (AS16 4084), STN8 (AS10 1601), ATPC (Agrisera, AS08 312). The antibody recognizing ACT2 (Actin) (A0480) was from Sigma-Aldrich; the anti-PBCP antibody was a gift from Michel Goldschmidt-Clermont. Secondary antibodies (anti-rabbit (Merck, AP132P) or anti-mouse (Sigma, A5278) conjugated with HRP were used for the detection of the primary antibody by enhanced chemiluminescence (ECL); the light signal was recorded using an imager for chemiluminescence (Amersham Imager 600, Amersham Biosciences, Inc.). Band intensity was measured with ImageQuant software (Amersham) and the protein amount estimated based on the signals measured on a dilution scale of the WT sample.

Thylakoid Preparation and Fractionation

Thylakoid preparation was performed according to Arnold et al. (2014) from adult (4 weeks old) full rosettes. Separation of supercomplexes by blue native polyacrylamide gel electrophoresis was performed as previously described (Järvi et al., 2011), using SERVAGel™ N 3–12, Vertical Native Gels (Serva). The grana and the stroma lamellae fractions were obtained by solubilization of the thylakoid preparation (0.5 mg ml^{-1}) with 1% water soluble digitonin (Serva), followed by sequential ultracentrifugation 40,000 × g for 40 min to pellet the grana and 180,000 × g for 90 min to pellet the stroma lamellae.

Lipid Analysis

The total lipid extraction was performed on samples composed by three 14-days-old plantlets. After measurement of the total fresh weight (FW), the samples were flash frozen in liquid nitrogen and stored at –80°C. The frozen samples were grounded to fine powder using glass beads, mixing in an IvoclarVivadent shaker (Silamat) two times for 10 s. Total lipids were extracted from the powder by adding 10 µl of a tetrahydrofuran: methanol 50:50 (v/v) solution per mg of FW. Plants debris were pelleted by centrifugation (3 min, 14,000 × g); finally, clear supernatant was pipetted to an HPLC vial to perform an ultra-high pressure liquid chromatography separation, followed by atmospheric pressure chemical ionization-quadrupole time-of-flight mass spectrometry (UHPLC-APCI-QTOF-MS) according to Spicher et al. (2016) and Sattari Vayghan et al. (2020). Briefly, the separation was performed on a reverse-phase Acquity BEH C18 column (50 × 2.1 mm, 1.7 µm) maintained at 60°C and analyzed in negative APCI. Mass data were acquired using MassLynx version 4.1 (Waters), and TargetLynx (Waters) was used for processing. Compound identity was determined based on reference standards, which were used for the quantification curves as well (Spicher et al., 2016). Lutein and zeaxanthin, as well as violaxanthin and neoxanthin, could be resolved neither by chromatography nor by mass spectrometry under the conditions employed; therefore, the measured peak corresponds to the sum of both compounds. For the identification of the galactolipids, a commercial DGDG and MGDG mix (Avanti Polar Lipids) was used as a standard, and the linearity of the detection was confirmed as previously reported (Sattari Vayghan et al., 2020).

Chlorophyll Fluorescence Analysis

Before the measurements, the plants were dark acclimated for at least 15 min. The Chl *a* fluorescence was recorded with MF800 Fluorcam (Photon System Instrument) using a personalized light protocol (Pralon et al., 2020). Briefly, the maximum fluorescence of dark-adapted plants was first measured during a saturating light pulse (F_M). Subsequently, the plants were exposed to steps of increasing blue light intensity. The length of the steps was 1 min for the seedling screening (92; 208; 335; 846; 1,365; and 1,878 µmol photons m^{-2} s^{-1} of PAR intensity), and 5 min for the analyses on adult plants (40, 95, 150, 380, 620, and 850 µmol photons m^{-2} s^{-1} of PAR intensity). At the end of each step, the maximal fluorescence of light-acclimated plants (F_M') was measured during a saturating light pulse. After each step, the actinic light was turned off; the plants were then exposed for 2 s to far-red light to oxidize the photosynthetic ETC; after that, the recorder fluorescence value was used as F_0'. To calculate the derived parameters, we used the fluorescence recorded just before the saturating light pulse as F_S. The non-photochemical energy dissipation was measured as NPQ = (F_M–F_M')/F_M'. PSII quantum yield under light (ΦPSII) was calculated as ΦPSII = (F_M'-F_S)/F_M' (Papageorgiou and Govindjee, 2004). The fraction of the closed PSII centers (1-qL) was calculated with the following formula: 1-qL = 1–[(F_M'–F_S)/(F_M'–F_0')]*(F_0'/F_S) (Kramer et al., 2004). The Chl fluorescence was also measured with a portable device (Multispeq v2, PhotosynQ, Firmware 2.1), with a modified protocol available at this address: https://photosynq.org/protocols/npq_phi2_from_simple_fluor_light_curve_with_recovery. Due to the LED limitations of this instrument, the time for each light intensity was reduced to 30 s (40, 95, 150, 380, 620, 850 µmol photons m^{-2} s^{-1} of PAR intensity). State transitions and NPQ kinetics were measured on adult plants (4 weeks old) in pots. The state transitions protocol was performed essentially as described using MF800 Fluorcam (Photon System Instrument) (Willig et al., 2011). After 30 min of dark adaptation and the measure of the Fm, 25 µmol photons m^{-2} s^{-1} of red light were used to induce State 2 and red light supplemented with far red light to induce State 1. Each light condition lasted 10 min. The maximal fluorescence was recorded during a saturating light pulse (500 ms) at the end of each light phase. The qT was calculated as (FmSt1-FmSt2)/FmSt1. The NPQ induction and the relaxation curve were measured with the same MF800 Fluorcam, using a protocol adapted from Nicol et al. (2019). Briefly, after the measurement of the Fm in plants dark adapted for 1 h, the plants were exposed to 10 min of 1,000 µmol photons m^{-2} s^{-1} actinic light (837 µmol photons m^{-2} s^{-1} blue and 165 µmol photons m^{-2} s^{-1} red light). The light was turned off, allowing the relaxation of the NPQ for 10 min. During the light and dark periods, the maximal fluorescence was measured with saturating light pulses (500 ms, 100% intensity) at intervals of 20 s. For the second light induction, the same light, dark, and measurement protocol was repeated.

Rapid Chl *a* fluorescence induction was measured on detached leaves with the Plant Efficiency Analyzer (M-PEA 2; Hansatech Ltd.). The following protocol was used: after an initial saturating pulse (3,000 µmol photons m^{-2} s^{-1}, 700 ms, red light, dominant λ625 nm), the same pulse was repeated after sequentially longer dark intervals (0.05, 4, 8, 12, 16, 20, and 24 s) for a total of eight pulses. After the eighth pulse, far-red light (20%) was turned on, and the sample was submitted to a second series of saturating pulses separated by increasing far-red light intervals (0.05, 0.1, 0.2, 0.4, 0.8, and 1.6 s). For each pulse, the fast Chl fluorescence curve was extrapolated by the M-PEA2 software (Hansatech Ltd.). The variable fluorescence at 3 ms (Vj) was analyzed by plotting as a function of the time between pulses.

To assess the functional antenna size of PSII, fluorescence induction measurements upon a transition from darkness to low light were performed on DCMU [3-(3,4-dichlorophenyl)-1,1-dimethylurea]-infiltrated leaves according to Nicol et al. (2019). In brief, in the presence of DCMU, the rise to the fluorescence maximum (F_M) represents a single, stable charge separation in PSII, the rate of the latter being directly proportional to the PSII absorption cross-section at a given light intensity. The reciprocal of the integrated area above the induction curve yields the maximal initial rate of PSII (when all PSIIs are open) (Papageorgiou and Govindjee, 2004).

FLIM measurements were performed on whole leaves incubated with DCMU with the same setup as the confocal images (see section "Confocal Microscopy"), except that it was coupled to a PicoHarp 300 time-correlated single photon counting (TCSPC) module (PicoQuant, Berlin, Germany) as described in Wientjes et al. (2017). The samples were excited with 633-nm light (40-MHz rep. rate), and fluorescence emission was detected at 710–750 nm. Each image was recorded for 1 min. The total image size was 116 * 116 µm, with 128*128 pixels. The time step for the TCSPC detection was 32 ps/channel. Decay traces were fitted with three exponentials $F(t) = a1*e^{(-t/\tau1)} + a2*e^{(-t/\tau2)} + a3*e^{(-t/\tau3)}$ with (a) the amplitude and (τ) the lifetimes (τ1 = 100 ps, τ2 = 900 ps, and τ3 = 2 ns) using the FLIMfit software tool (Warren et al., 2013). Based on the amplitude of the PSI lifetime (100 ps), the ratio of Chls associated with PSI compared to PSII can be calculated according to PSI/(PSI + PSII) = c*a1/(1-a1 + c*a1) with c being a previously determined correction factor for this specific setup (*c* = 0.49) (Wientjes et al., 2017).

Absorption Spectroscopy in vivo

For the calculation of the ratio of CEF over LEF, we used the protocol described in Kramer et al. (2021). Briefly, the plants were grown under long-day conditions and initially dark incubated for 60 min and then 5 min before transfer into actinic light with 630-µmol photons m^{-2} s^{-1} PAR for light acclimation. After 10, 20, 40, 60 s or 5 min of illumination, LEF and CEF were measured by following the relaxation kinetics of the carotenoid electrochromic bandshift at 520 nm (corrected for the signal at 546 nm) using a JTS-10 spectrophotometer (Biologic, France). The ECS spectral change is a shift in the pigment absorption bands, which is linearly correlated with the light-induced generation of a membrane potential across the thylakoid membranes (Bailleul et al., 2010). Under steady-state continuous illumination, the ECS signal stems from transmembrane potential generation by PSII, the cytb6f complex, and PSI and from transmembrane potential dissipation by the ATP synthase CF_0-F_1. When light is switched off, reaction centers' activity stops immediately, while ATPase and the cytb6f complex activities remain (transiently) unchanged. Therefore, the initial rate of ECS decay is proportional to the rate of PSI and PSII photochemistry (i.e., to the rate of "total" electron flow). This can be calculated by dividing this rate (expressed as $-\Delta I/I$ per unit of time) by the amplitude of the ECS signal (again expressed as $-\Delta I/I$) induced by the transfer of one charge across the membrane (e.g., one PSI turnover). The rate of CEF can be evaluated using the same approach under conditions where PSI only is excited by exposure to saturating far red light (λ > 720 nm) for enough time to be at the steady state (5 min in our condition). Results were expressed as electrons^{-1} s^{-1} and estimated from the amplitude of the electrochromic shift signal upon excitation with a saturating single turnover flash [5 ns Nd:YAG laser flash, Continuum Minilite, 532-nm flash exciting 4-(dicyanomethylene)-2-methyl-6-(p-dimethylaminostyryl)-4H-pyran (DCM), emission peak at 630 nm]. Total electron flow was measured following a pulse of actinic light (λ = 640 ± 20 nm FWHM) at 1,100 µmol photons m^{-2} s^{-1}, while CEF was measured with a pulse of far-red light at the maximum setting (estimated as 1,400 µmol photons m^{-2} s^{-1} by the manufacturer). Functional antenna size of PSII and PSI was assessed using ECS as described in Hu et al. (2021). In brief, similar to the light-to-dark transition described above, the initial slope of the ECS signal during the onset of light is directly proportional to the absorption-limited, maximal rate of charge separation by fully open PSII + PSI. Addition of DCMU and hydroxylamine by vacuum infiltration of the leaf inhibited PSII activity (systematically verified with fluorescence measurements), allowing to separately quantify the rates of both PSII and PSI. The rates in e^- s^{-1} PSI^{-1} (or e^- s^{-1} $PSII^{-1}$) were obtained by dividing the slope by the ECS signal obtained 140 µs after a saturating, single-turnover laser flash (see above), corresponding to 1 charge separation PS^{-1}.

Confocal Microscopy

Confocal images were recorded on an (inverted) confocal Leica TCS SP8 system equipped with a 63 × 1.20 NA water immersion objective. Chloroplasts were freshly isolated, and Chls were excited at 633 nm with a pulsed laser (40 MHz) and an intensity of 100 nW. The fluorescence was detected at 650–680 nm (PSII-maximum) and 710–750 nm (PSI-maximum) with internal hybrid detectors. The total image size was 9.2 * 9.2 µm, with 128*128 pixels.

Transmission Electron Microscopy

Samples preparation and analysis were performed as previously described (Martinis et al., 2013), with minor modifications. Leaves from 14-day-old WT and L1ko plants were fixed in a fixative buffer [5% (W/V) glutaraldehyde and 4% (W/V) formaldehyde in a 100-mM phosphate buffer (pH 6.8)] overnight at 4°C, rinsed several times in a phosphate buffer, and post fixed for 2 h with 1% (W/V) osmium tetroxide in a phosphate buffer at 20°C. After two further washing steps in a phosphate buffer and distilled water, the samples were dehydrated in ethanol and embedded in Spurr's low-viscosity resin (Polyscience). Ultrathin sections of 50–70 nm were cut with a diamond knife (Ultracut-E microtome-Reihtert-Jung), mounted on uncoated copper grids. The sections were post stained with Uranyless and Reynold's lead citrate stain (Delta Microscopies). Sections were observed with a Philips CM 100 transmission electron microscope operating at 60 kV (Philips Electron Optics BV, Eindhoven, the Netherlands).

Statistical Analysis

The normal distribution of the residuals of each data set was tested before any other statistical analysis. If this assumption was met, an ANOVA model was utilized; otherwise, a Kruskal–Wallis rank sum test was performed. If the results were significant, we used *post hoc* Student's *t*-test for multiple comparisons. The reported *p*-values were obtained with the latter. The effect of genotypes on the correlation between the number of stacks per grana or grana width was tested using analyses of covariance, with number of stacks as a response variable, and the genotypes by grana, or by grana width as factors. We used a generalized linear model (GLM) with Poisson distribution for assessing the numbers of stacks, and a linear model for grana width. The calculations were performed with RStudio (Version 1.2.5019 RStudioInc).

Results

Production of Lines Deprived of LHCB1

The Arabidopsis genome contains five genes encoding quasi-identical LHCB1 proteins. These genes are organized in two close regions. Chromosome 1 contains Lhcb1.1 (AT1G29920), Lhcb1.2 (AT1G29910), and Lhcb1.3 (AT1G29930). The remaining two, *Lhcb1.4* (AT2G34430) and *Lhcb1.5* (AT2G34420), are located on Chromosome 2. Due to their close proximity, it would not be possible to obtain multiple insertional mutants by crossing. A CRISPR/Cas9 approach was used to insert simultaneously a mutation in all the genes. As these genes have a largely identical nucleotide sequence, it was possible to design two gRNAs targeting all of them (Figure 1A). Five plants were transformed with the construct containing the two gRNAs and the gene encoding the Cas9 endonuclease. From each plant, we obtained two to four resistant progenies (T1 generation), which were screened for NPQ, as a loss of *Lhcb1* should lower the photoprotective capacity (Pietrzykowska et al., 2014; Supplementary Figure 1). The candidates were self-crossed to obtain stable T2 lines. To characterize the nature of the mutation, we sequenced each targeted gene of two independently selected T2 lines.

In the line named D2, five different knockout mutations were identified: *Lhcb1.2* (AT1G29910), which has a single nucleotide deletion in the codon for Tyr 191; *Lhcb1.1* (AT1G29920), containing a single nucleotide insertion in the codon for Ser 140; *Lhcb1.3* (AT1G29930), with a single nucleotide insertion in the Pro 192 codon; in *Lhcb1.4* (AT2G34430), a single nucleotide insertion occurred in the codon for Ser 139, and, finally, *Lhcb1.5* (AT2G34420), harboring a large deletion from the Ser 138 codon to the Pro190 codon. A second line, named C2, displayed a deletion/rearrangement between the genes *Lhcb1.2* (AT1G29910) and *Lhcb1.1* (AT1G29920) that made impossible to amplify the gene sequences plus a single nucleotide deletion in the codon for Pro 192 of *Lhcb1.3* (AT1G29930). The mutations on *Lhcb1.4* (AT2G34430), single nucleotide insertion in Ser 139 codon, and *Lhcb1.5* (AT2G34420), single nucleotide insertion in Ser 138 codon, were heterozygous in the T2 line. Therefore, this line was further self-crossed to obtain two T3 lines: one with no mutation in these two genes (C2a) and one carrying the mutations in both genes (C2b). However, even in the presence of non-mutated Lhcb1 genes on Chromosome 2, in both C2-derived lines, there was no detectable LHCB1 protein nor a detectable band by total protein staining at the LHCII level (Figure 1B). We will refer to the multiple LHCB1 mutants, lacking any detectable LHCB1 protein, as L1ko mutants.

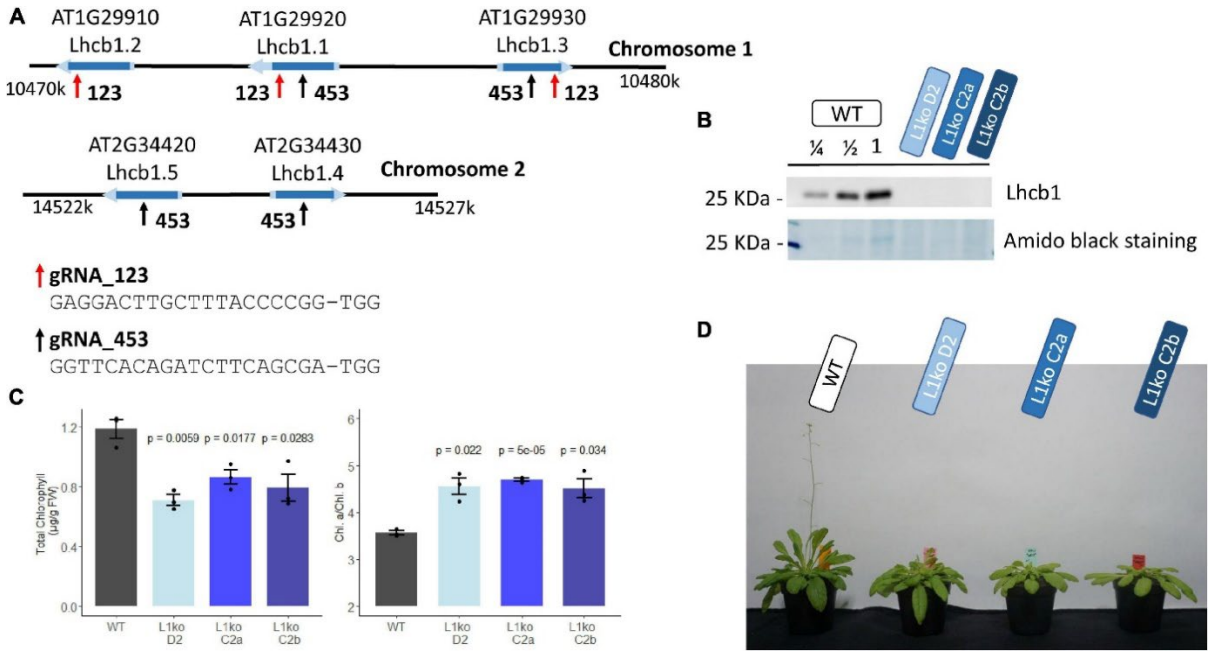

FIGURE 1. Generation of total knock-out lines for the five genes encoding LHCB1. (A) Schematic representation of the Lhcb1 gene clusters, showing the regions targeted by the two sgRNAs; the sequence of the sgRNAs is reported below. **(B)** Protein accumulation of the produced mutant lines; the representative immunoblot shows the detection of LHCB1 in a dilution series of WT total protein extract and in the L1ko mutants. Below, the staining of the membrane with amidoblack shows the differential band at 25 KDa that corresponds to the LHCII protein. **(C)** Total Chl accumulation normalized over the plant fresh weight, left, and the Chl *a*/*b* ratio, right, in WT and in the three L1ko mutant lines. The error bar indicates the standard error, and individual replicates are plotted as points (n = 3) above each L1ko line are reported the p-value of a Student's t-test comparison with WT. **(D)** The representative flowering phenotype of adult plants of the WT and the three independent L1ko lines.

The L1ko mutant plants have a pale green phenotype, with an average Chl per fresh weight content corresponding to 66 ± 6% of the WT (Figure 1C). Consistent with the notion that LHCII is enriched in Chl b, this loss was uneven between Chl a and b, and caused an increase in the Chl a/b ratio in L1ko lines compared to the WT (Figure 1C). Furthermore, the plant growth was also slower, resulting in a smaller rosette and a delay in flowering (Figure 1D).

To compare the generated mutant lines, we analyzed their photosynthetic performance in a range of increasing light intensities. This analysis revealed that there was no statistically significant difference between the three L1ko lines in terms of NPQ, quantum yield of the photosystem II (ΦPSII), and the fraction of the closed PSII reaction centers (1-qL) (Supplementary Figure 2).In summary, the CRISPR/Cas9 system based on two sgRNAs allowed for the simultaneous mutation of multiple LHCB1-encoding genes. Multiple stable lines produced are characterized by an undetectable amount of the LHCB1 protein and a pale phenotype. All the L1ko lines have a similar photosynthetic activity profile, showing that the loss of LHCB1 correlates with the photosynthetic defect, independently of the presence of non-mutated *Lhcb1.4* and *Lhcb1.5* genes.

A Profile of Thylakoid Proteins in L1ko

It was previously reported that the removal of LHCB1 by miRNA has a limited impact on the accumulation of other thylakoid proteins, with the exception of LHCB2 (Pietrzykowska et al., 2014). We investigated if the protein accumulation (relative to fresh weight) was modified in the stable L1ko lines compared to WT (Supplementary Figure 3). Figure 2 reports the average of the three independent lines D2, C2a, and C2b to highlight differences in protein accumulation due to the loss of the LHCB1 protein, independently of the genetic background. In the L1ko lines, we observed a significant increase in the accumulation of LHCB2 (1.42 ± 0.33-fold change) and a small one in LHCB4 (1.27 ± 0.15-fold change) compared to WT. There was, however, little to no detectable difference in the accumulation of LHCB5 (1.24 ± 0.40-fold change), LHCB6 (1.01 ± 0.19-fold change) or LHCB3 (0.89 ± 0.15-fold change) (Figure 2). Taken together, these results show that the loss of LHCB1 did not cause any large—and thus detectable by immunoblotting—compensatory changes at the protein level of the minor LHCBs. The larger variation is at the level of LHCB2, whose accumulation is slightly increased in a fashion similar to the previous report on the *amiLhcb1* line (Pietrzykowska et al., 2014). We also assessed the accumulation of the subunits of the core of PSII (PsbA to D); these proteins did not display any significant difference when compared to WT levels of accumulation (Figure 2).

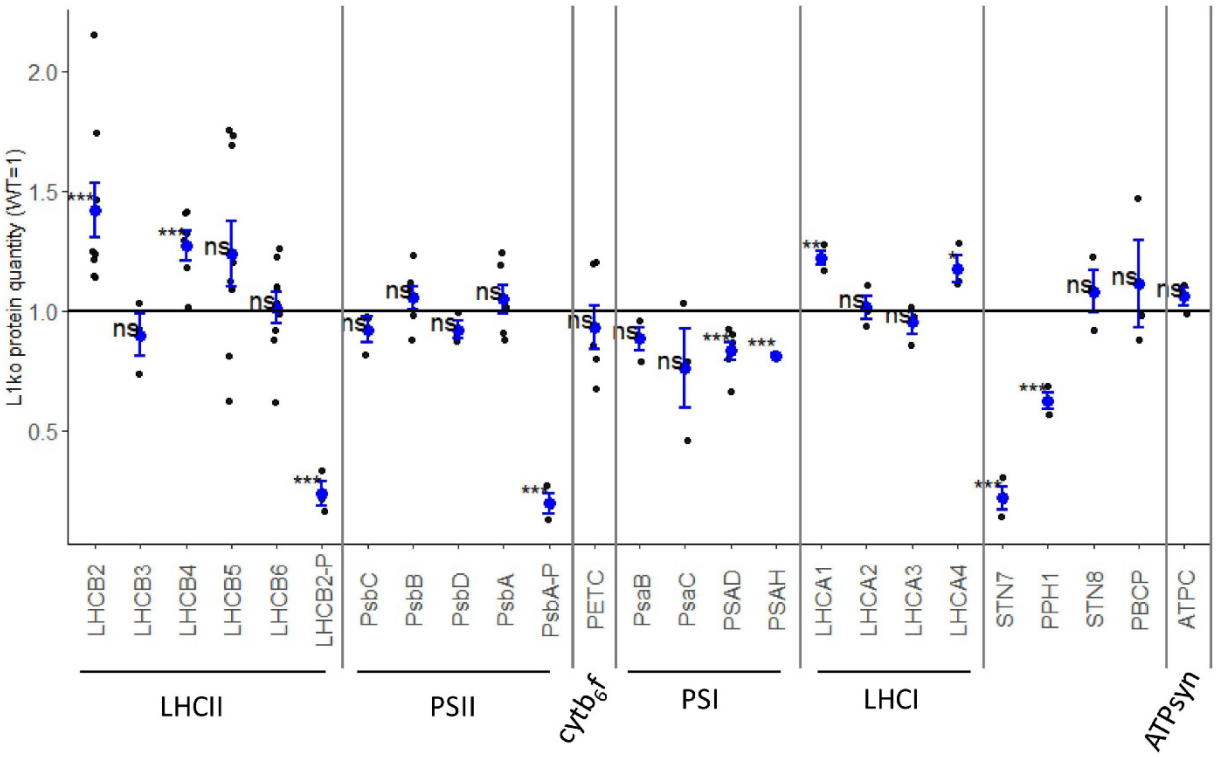

FIGURE 2. Few thylakoid proteins are affected by the loss of LHCB1. The accumulation of proteins was assessed in 14-days-old seedlings of WT and L1ko lines by immunoblotting. The relative protein accumulation, normalized over the actin, was measured compared to the WT level. Each point represents the quantification of the relevant protein in an individual biological replicate; we analyzed one sample per genotype for proteins with low variation between lines and two or three samples for proteins with larger variation. The blue dot represents the average and the blue bars the standard error of the distribution. The proteins were divided into the complexes to which they are associated (LHCII, PSII, cytb6f, PSI, LHCI, and ATPsyn). The accumulation kinases and phosphatase mainly involved in the regulation of the phosphorylation of LHCII and PSII were also measured. The measured levels were compared to the average of 1, corresponding to the protein accumulation in WT extracts *via* a Student's *t*-test; asterisks indicate *p*-value thresholds ($0.0001 < p < 0.001$ "***", $0.001 < p < 0.05$ "**", $0.05 < p < 0.10$ "*", $0.10 < p$ "ns") (see **Supplementary Figures 3A,B**).

As for the subunits of PSI, we could not detect a significant difference in the core subunits PsaB and PsaC despite a general tendency toward a lower level of accumulation in L1ko lines compared to WT (0.88 ± 0.09 and 0.76 ± 0.29-fold change, respectively). The decrease was instead significant for the peripheral subunits PsaD (0.83 ± 0.09-fold change) and PsaH (0.81 ± 0.01-fold change), as their signal was consistently lower in L1ko lines compared to the WT (Figure 2).
It has to be highlighted that this difference between the core and peripheral subunits of PSI may stem from the semi-quantitative nature of the immunodetection rather than of a physiological difference.
Conversely, two of the four proteins composing the PSI antenna, LHCA1 and LHCA4, appeared to be slightly, but significantly, more abundant in L1ko lines compared to WT (1.22 ± 0.06 and 1.17 ± 0.10-fold change, respectively), while no significant difference was observed for LHCA2 and LHCA3. We measured the level of PETC protein as a proxy for the cytb6f complex amount; this protein did not show any significant difference in accumulation between L1ko lines and the WT. Similarly, there was no difference in the accumulation level of ATPC, used as a proxy for the ATP synthase complex.
The phosphorylation level of LHCB2 and of the two PSII subunits, PsbA and PsbC, was clearly lower in L1ko lines compared to the WT (Figure 2 and Supplementary Figure 4), as assessed by antibodies recognizing the phosphorylated form of these two proteins and by phos-tag gels.
Following on the altered phosphorylation of LHCB2 and PSII in L1ko, we assessed the accumulation of the relevant kinases and phosphatases. The accumulation of STN7 (i.e., the kinase mainly involved in LHCII phosphorylation) was strikingly lower in the L1ko lines compared to the WT (0.22 ± 0.08-fold change). This was also the case for the phosphatase TAP38/PPH1, which counters the activity of STN7, which was less accumulated in L1ko lines compared to the WT (0.62 ± 0.06-fold change). Conversely, the second kinase/phosphatase pair, consisting of the thylakoid kinase STN8 and its counteracting phosphatase PBCP, did not show any significant difference in accumulation in L1ko compared to WT.
Taken together, these results show that LHCB1 mutation caused a minor change in the composition of the photosynthetic proteins. Protein analysis suggests that most of the compensatory responses occur at the level of ETC proteins activity and interaction, notably, by changing the phosphorylation level. As the potential difference in the PSII and PSI relative accumulation and antenna size between L1ko and WT should be rather minor, the immunodetection based on chemio-luminescence is not sufficient to assess it conclusively. This prompted us to pursue further biophysical analysis.

Decrease of PSII Antenna Size in L1ko Is Partially Compensated by the Increased PSII/PSI Ratio

LHCII antenna has the important role to equilibrate the excitation between the two photosystems. This dynamic equilibrium allows the photosynthetic apparatus to optimize the linear electron transport and to respond to variations in light intensity and quality (Allen, 1992; Ballottari et al., 2012). As the L1ko mutants showed an important loss of the LHCII complex (Supplementary Figure 5), we investigated the ratio of the photosystems and their relative antenna size. To assess which proportion of the antenna was connected to the two photosystems in the mutant background, the photochemical rate of both photosystems was measured by electrochromic shift (ECS) and fluorescence rise time. This analysis showed that the PSII maximal photochemical rate at 80 µmol photons m^{-2} s^{-1} was 25% lower in L1ko on a per-photosystem basis (14.95 ± 1.78 electrons·s^{-1}·PS^{-1}) compared to WT (20.25 ± 4.55 electrons·s^{-1}·PS^{-1}). Note that the absolute value of maximal PSII rate at 80 µmol·photons·m^{-2}·s^{-1} obtained with both fluorescence- and ECS-based methods is identical (Figure 3A). The PSI maximal photochemical rate was unchanged (WT, 39.98 ± 5.48 electrons·s^{-1}·PS^{-1}; L1ko, 46.14 ± 6.56 electrons·s^{-1}·PS^{-1}) (Figure 3B). The relative amount of the two photosystems partially compensated for the difference in the photochemical rate. The PSII/PSI reaction centers ratio was 1.37 ± 0.25 in the WT and 1.71 ± 0.09 in L1ko (Figure 3C). By multiplying the average photochemical rate measured for PSI and PSII by the average PSII/PSI reaction centers ratio, we can estimate a global PSI/(PSI + PSII) Chl ratio of 0.59 for WT and 0.64 for L1ko. This difference in the global Chl ratio between the two photosystems in WT and L1ko was found also by analyzing the fluorescence decay. The calculated PSI/(PSI + PSII) Chl ratio was of 0.52 ± 0.01 for WT and 0.60 ± 0.01 in L1ko (Figure 3D and Supplementary Figure 6).

The difference between PSI and PSII Chls is also reflected in the rate of Q_B oxidation as estimated by the Vj parameter, which is the relative fluorescence measured at 3 ms during a saturating light pulse, normalized over the maximal fluorescence (Toth et al., 2007). In fact, in a leaf exposed to far-red light, the decrease of the Vj value over time is faster in L1ko (the Vj trend over time, –0.303) compared to the WT (–0.281) (Figure 3E).

The same does not occur in the dark; in this situation, the slope of the Vj decrease over time is comparable between the two genotypes: –0.149 for L1ko and –0.147 for WT (Supplementary Figure 7). This supports the idea that the faster oxidation of the photoactive plastoquinone is due to the higher activity of PSI over PSII and not to an increased activity of the non-photochemical plastid oxidase (Nawrocki et al., 2015). The different distributions in the excitation of the photosystems did not result in a change in the proportion of the two main photosynthetic electron transport routes; in fact, the proportion of the cyclic electron flow (CEF) around PSI to the linear electron flow (LEF) was comparable between L1ko and WT (Figure 3F).

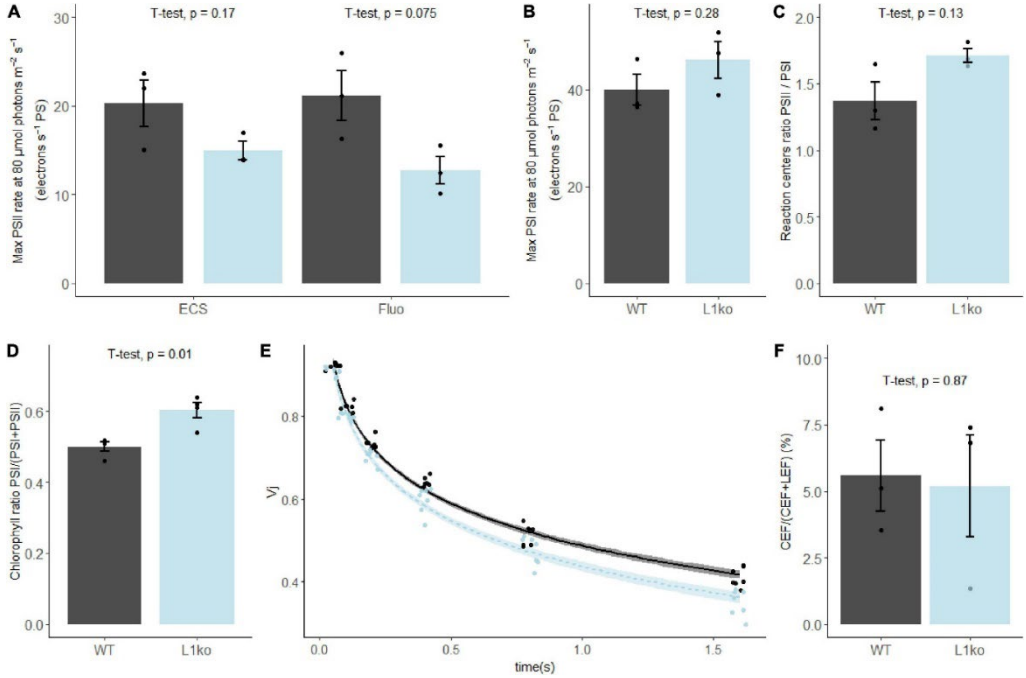

FIGURE 3. In plants lacking LHCB1, the chlorophyll repartition is shifted toward PSI. (A) The maximal photochemical rate of PSII, measured by electrochromic shift (ECS) and fluorescence (fluo) and **(B)** PSI measured by ECS. **(C)** The ratio of PSI/PSII reaction centers measured by a single turnover flash. **(D)** The average PSI/(PSI + PSII) Chl ratio determined from the 100 ps component of the fluorescence decay measured in fully expanded leaves, excitation wavelength at 633 nm and fluorescence emission at 710–750 nm (see Supplementary Figure 5). **(E)** Fluorescence value measured at 3 ms during a 700 ms saturating pulse normalized over the maximal fluorescence (VJ), upon sequential incubations of the sample with far-red light with increasing time intervals. The points were fitted with a local regression algorithm based on a logarithmic function to visually represent the data distribution in function of the time with a continuous error estimate (black continuous line WT, light blue L1ko). The standard error of the interpolation is shown as a gray area around the curves. **(F)** Contribution of CEF to the total electron flow in WT and L1ko expressed as a percentage of the electron flow. Individual biological replicates are plotted as points, the histogram shows the average, and the error bars represent the standard error (n = 3, n = 4 for **E**). The averages of the distributions were compared with Student's t-test, and the p-value of the comparison between WT and L1ko reported above the bars.

The faster PQ oxidation in far-red and the higher PSI/(PSI + PSII) Chl ratio measured in L1ko plants should result in a larger ΦPSII and open PSII reaction centers under light-limiting conditions. To assess that, we performed a follow-up experiment using adult plants.

The room temperature Chl *a* fluorescence transient on WT and L1ko exposed to a range of increasing light intensities (from 40 to 850 µmol·photons·m^{-2}·s^{-1} PAR) was measured with a fluorescence camera as well as a portable device. Consistently, with our hypothesis, the ΦPSII resulted to be higher, especially in the initial range of light intensities used in L1ko compared to WT. The higher quantum yield in L1ko correlated with a larger fraction of open PSII reaction centers estimated by the 1-qL parameter (Figure 4). Furthermore, in agreement with previous results during the screening for L1ko mutants and the literature (Pietrzykowska et al., 2014; Nicol et al., 2019), the NPQ amplitude was lower in L1ko compared to WT (Figure 4). The same trends for NPQ and ΦPSII parameters were confirmed by a second measurement with the portable device (Supplementary Figure 8).
The measurement of the state transitions by fluorescence in WT and L1ko is in agreement with the previous observation (Figure 4). In L1ko, the state transitions amplitude (qT) is reduced compared to WT. The change in the PSI/(PSI + PSII) Chl ratio could also be responsible for the lack of the transient reduction of the ETC that is visible in the WT as an increase of the Chl *a* fluorescence upon a switch from State 1 to State 2 light (Figure 4).

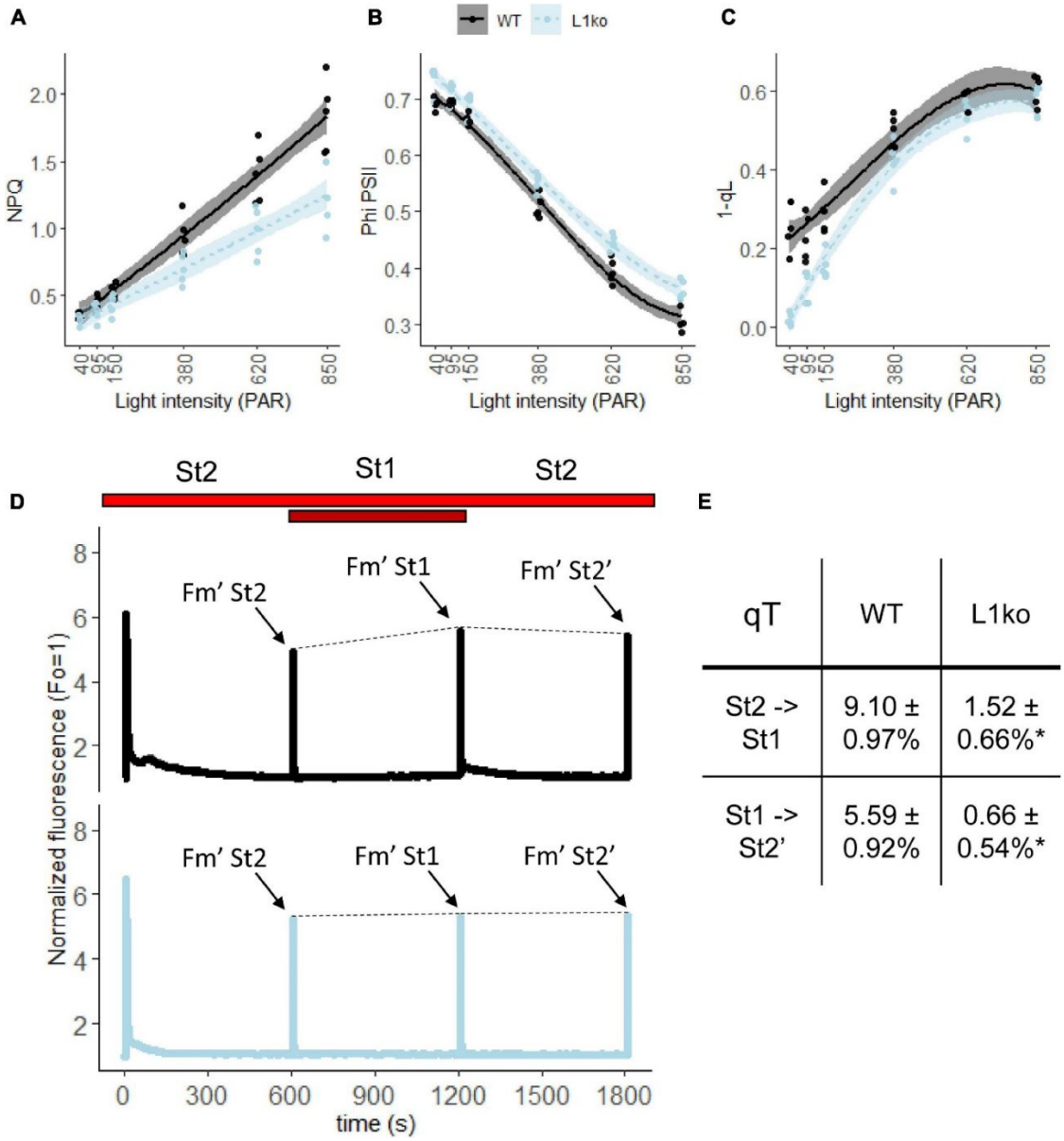

FIGURE 4. Loss of LHCB1 alters the equilibrium of the LEF between PSII and PSI. The LEF was monitored by room temperature Chl fluorescence on adult WT (black lines) and L1ko (light blue lines) plants. The plants were exposed to a range of increasing light intensities, each lasting 5 min. **(A)** Non-photochemical quenching (NPQ), **(B)** quantum efficiency of PSII, referred as ΦPSII in the main text. **(C)** Fraction of closed PSII centers estimated by the 1 qL parameter. Each experimental point is displayed as a dot. The measured points were fitted with a second-degree polynomial function for NPQ, a third-degree polynomial for ΦPSII and 1-qL to visually represent the data distribution and the standard error for WT (the black line and the gray area) and L1ko (the blue dotted line and the light blue area). *Post hoc* analysis of the models shows that there is a significant difference between L1ko and WT ($p < 0.001$). **(D)** Chl *a* fluorescence traces measured during shifts from State 2 (St2) to State 1 (St1), light and back. The line represents the average fluorescence and the area the standard deviation ($n = 3$) for WT (upper, the black line) and L1ko (lower, the blue line). The bars at the top indicate illumination with red (shown in red) and far-red (dark red) light. The dashed line connecting the Fm' peaks was added to highlight the state transitions. **(E)** qT values calculated as (Fm'St1-Fm'St2)/Fm'St2 ± SD ($n = 3$), the peaks used for the calculation are highlighted in **(D)**, and the values indicated with an * are statistically different ($p < 0.01$).

However, the loss of qT is not enough to explain the difference in NPQ observed between WT and L1ko as, at higher light intensities, the NPQ governs the redox state of the ETC. We, therefore, conducted a follow-up analysis measuring the NPQ induction and relaxation kinetics (Figure 5 and Supplementary Figure 9). We observed that L1ko had a significantly lower induction of the rapidly reversible component of NPQ (qE).

In fact, at the end of the light phase, the total NPQ is still a significantly lower in L1ko (1.38 ± 0.08) compared to WT (1.95 ± 0.07), but, after 5 min of dark relaxation, both L1ko (0.27 ± 0.05) and WT (0.27 ± 0.02) had comparable levels of NPQ. The second phase of NPQ induction after 10 min of dark relaxation shows a faster induction in both L1ko and WT. This is due to the persistence of the Zeaxanthin-dependent NPQ component due to the kinetics of the zeaxanthin conversion back to violaxanthin in the dark (Siefermann and Yamamoto, 1975).

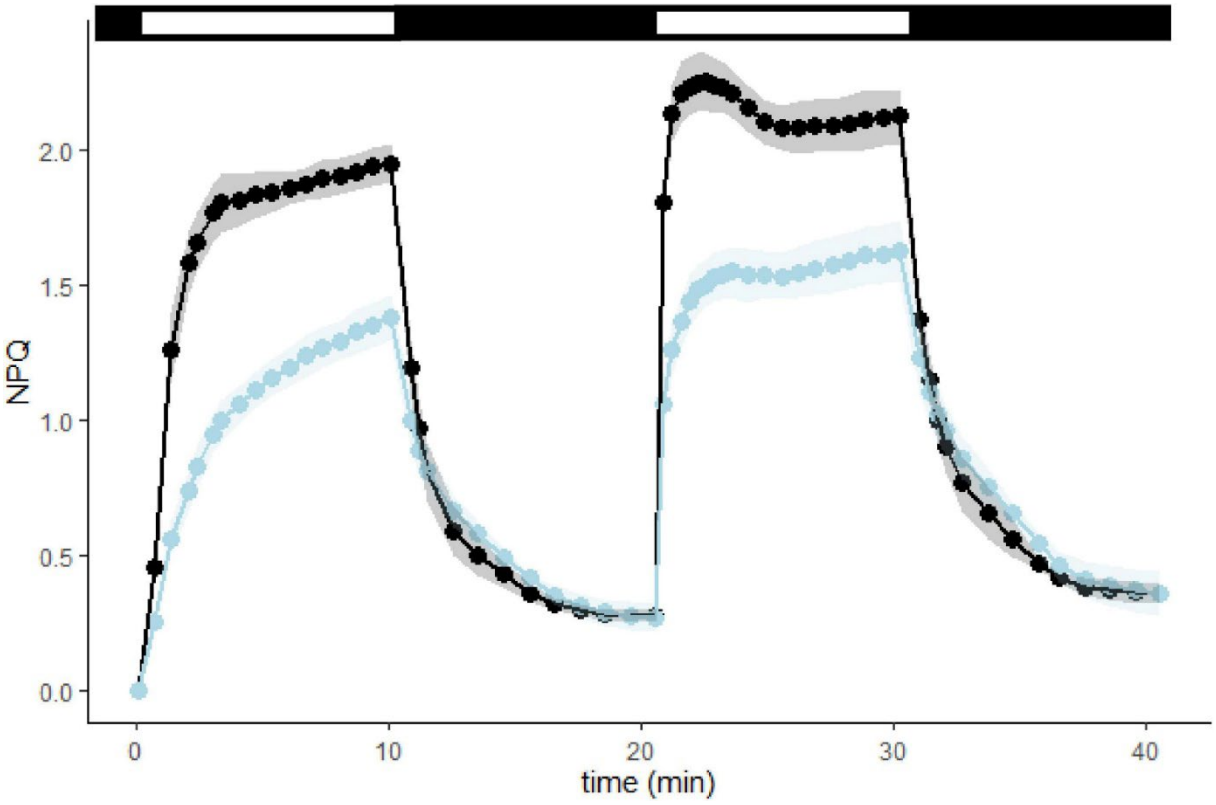

FIGURE 5. L1ko is affected in the rapidly reversible component of NPQ (qE). NPQ kinetics with two periods of light induction, both at 1,000 µmol photons m^{-2} s^{-1}, measured in WT and L1ko adult plants. The top bar shows the light exposition periods (white bars) and the dark relaxation (black bars). The points and the lines correspond to the average NPQ value recorded for each time from five biological replicates. The lines and areas show a continuous estimate of the average and the standard deviation for WT (the black line and the gray area) and L1ko (the blue line and the light blue area). The corresponding fluorescence traces are shown in Supplementary Figure 9.

In conclusion, the loss of LHCB1 has a larger impact on the photochemical rate of PSII than on that of PSI. This imbalance is partly compensated by an increase of the relative PSII/PSI reaction centers ratio. However, this does not allow L1ko plants to reach the same photosynthetic equilibrium of the WT. The photoprotection is also impaired in L1ko, as seen by a lower extent of qE and qT induction.

Loss of LHCB1 Alters the Thylakoid Organization

The trimeric LHCII is a large component of the thylakoid membrane. Consequently, a change in the shape and organization of the thylakoid membrane is expected upon removing LHCB1, which constitutes a large portion of LHCII. Therefore, the chloroplast ultrastructure was investigated in the mutant lines by transmission electron microscopy (TEM) and confocal microscopy.

While confocal microscopy allows to observe the overall chloroplasts topology and the distribution of the photosystems, the TEM images allow to observe the fine structure of the thylakoids (Figure 6). Confocal microscopy images of isolated chloroplasts were acquired using two detection ranges to preferentially detect either the emission of PSII (650–680 nm, green), or of PSI (710–750 nm, red) (Figure 6A and Supplementary Figure 10).

These images showed relatively more Chl connected to PSI and smaller grana in L1ko compared to the WT (yellow areas in Figure 6A and Supplementary Figure 11). Since the spatial resolution of confocal microscopy is too low, TEM images were used to measure the grana widths and number of grana layers per stack (Figure 6B and Supplementary Figure 12). These analyses showed that the loss of LHCB1 leads to fewer stacks per grana on average (3.75) compared to the WT (4.57). Covariance analysis showed a significant negative correlation between the number of grana and the number of stacks for both the WT and L1ko (z-value = –13.8, $p < 0.001$), but such correlation was different across genotypes (interaction term: z-value = 3.12, $p = 0.002$), which results in an average of 21% less stacks per grana in L1ko compared to WT (genotype effect; z-value = –3.4, $p = 0.001$). Concerning grana width, the variance analysis shows a significant difference between the genotypes ($p < 0.001$), with an average grana width for the WT of 500 nm and an average width of 356 nm for the L1ko mutant. Consistently, with the observation of the reduced grana width and stacks number, upon separation of the grana stacks from total thylakoids by digitonin, the grana fraction from WT thylakoids contained 66 ± 4% of the total Chl, while, in L1ko, this percentage was reduced to 40 ± 14% (Supplementary Figure 13).

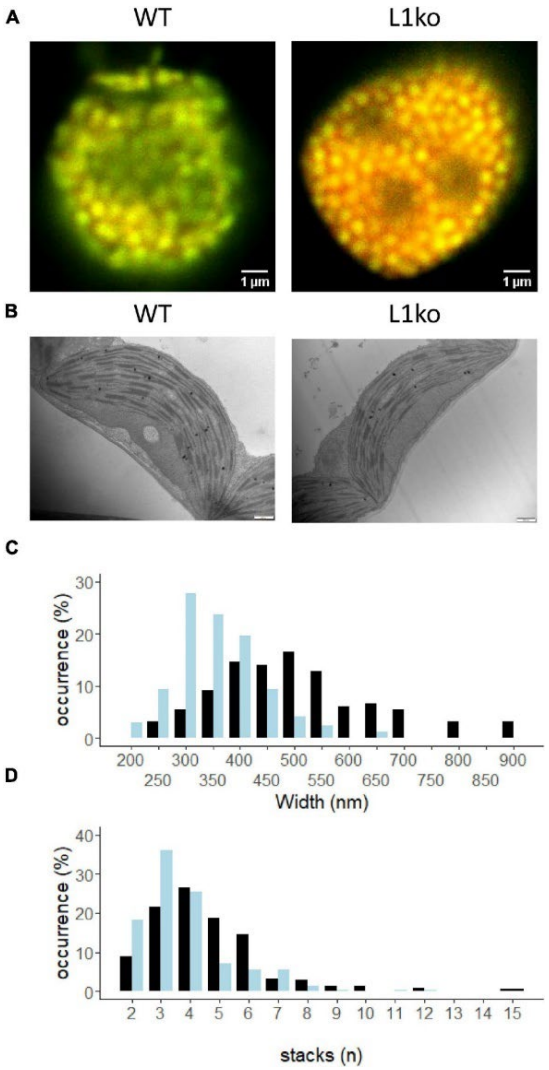

FIGURE 6. LHCB1 mutation affects the thylakoid structure. (A) Confocal microscopy on isolated chloroplasts of WT and L1ko. Excitation at 633 nm and detection at 650–680 nm are shown in green (PSII-maximum), while 710–750 nm detection in red (PSI-maximum). Red channel intensity has been increased 10 times in comparison to the green channel to compensate for decreased sensitivity of the detector and decreased fluorescence emission in the far-red region (see Supplementary Figure 10). (B) Representative images of chloroplasts from WT and L1ko leaves obtained by transmission electron microscopy. The scale bar is 500 nm (see Supplementary Figure 12). (C) Distribution of the grana width in WT and L1ko based on the measurement of 164 and 173 grana for WT and L1ko, respectively. (D) Distribution of the grana stacks divided by the number of layers based on the analysis of 215 and 241 grana for WT and L1ko, respectively. The chloroplast images used for the analysis were obtained from two independent biological samples. The statistical analysis of the grana stack number and width distributions is presented in the text.

To assess whether the change in the LHCII content had an impact on the lipid portion of the thylakoid membrane, we measured the total content of the two main classes of galactolipids, monogalactosyldiacylglycerols (MGDGs), and digalactosyldiacylglycerols (DGDGs). This analysis showed that the total galactolipid content, normalized over the fresh weight, was unchanged between the L1ko lines and the WT. In addition, the relative abundance of the different molecules sorted by the degree of saturation and length of the acyl chains was comparable between the L1ko lines and the WT (Supplementary Figure 14). The main prenyl lipids found in the thylakoid membrane were also accumulated to the same level in L1ko and WT; only the xanthophylls, which are mostly associated with LHCII proteins (i.e., violaxanthin, neoxanthin, zeaxanthin, and lutein) were clearly less abundant in the L1ko lines compared to the WT. Conversely, there was no change in β-carotene content (Supplementary Figure 14).

Discussion

Three of the Five Genes Encoding LHCB1 Are the Major Contributors to the Protein Accumulation

Stable multiple mutant lines are fundamental to study the function and the role of the major components of the LHCII. The two major isoforms, LHCB1 and LHCB2, are coded by multiple genes; therefore, the production of these mutant lines requires an approach targeting simultaneously multiple genes. The CRISPR/Cas9 technique provided such a tool, allowing the mutation of entire gene families with a single transformation event by using multiple gRNAs along with the Cas9 endonuclease (Ordon et al., 2020). In this report, we targeted conserved sequences, shared by multiple LHCB1-coding genes, to design two gRNAs capable of knocking down the five genes. The pale green phenotype and the previously reported lower NPQ level in plants in which LHCB1 was depleted by artificial miRNA (*amiLhcb1*) (Pietrzykowska et al., 2014) facilitated the screening procedure, allowing rapid identification of multiple mutant lines characterized by a complete loss of LHCB1. The selected mutants were all mutated in Chromosome 1 genes (therefore, lacking the Lhcb1.1, Lhcb1.2, and Lhcb1.3 *genes*). Conversely, mutations in *Lhcb1.4* and *Lhcb1.5* CDS were not present in all the lines even if there was no detectable LHCB1 protein. However, it has to be noted that the primary amino acid sequence of the *Lhcb1.4* product is slightly different from the other LHCB1 protein isoforms. This difference, present at the level of the N-terminal portion of the mature protein, may affect the antibody binding and lead to underestimation of the *Lhcb1.4* product (Jansson, 1999). However, the line containing no detectable mutation in the *Lhcb1.4* and *Lhcb1.5* genes, named L1ko "C2a," did not show any significant difference in Chl content or NPQ when compared to the other L1ko lines (Supplementary Figure 2). This can be explained by a low contribution of *Lhcb1.4* and *Lhcb1.5* to the LHCB1 protein content in our growth condition, despite being reported as relatively highly expressed genes (Jansson, 1999), or by the effect of an undetected mutation outside the CDS that affects these genes.

Change in Protein Phosphorylation and Photosystem Stoichiometry Partially Compensates for the Loss of LHCB1

Being the most abundant isoform in L1ko lines, the loss of LHCB1 results in the almost complete absence of the trimeric LHCII complex. The differences in antenna and photosynthetic proteins accumulation between L1ko and WT are minor; and, within the expected error of an immunoblot detection, this may hide some significant changes but overall suggests that the mutation caused only limited alterations in terms of protein amount. However, considering the LHCII, the accumulation of LHCB2 increased, while the LHCB3 level showed no significant difference between L1ko and WT. These moderate changes cannot compensate for the LHCB1 loss and align well with the *amiLhcb1* line phenotype (Pietrzykowska et al., 2014). Except for LHCB4, the accumulation of which increased only by around 20% in L1ko compared to WT; the monomeric antennae also show no significant increase. A previous report suggested that the loss of trimeric LHCII was compensated by an increase in the LHCB5 protein (Ruban et al., 2003). LHCB5 was proposed to be integrated into the trimeric LHCII, thanks to the presence of an N-proximal trimerization motif (Hobe et al., 1995). However, a higher accumulation of LHCB5 does not seem to be induced in the L1ko lines as well as in the *amiLhcb1* line (Pietrzykowska et al., 2014) and in the noLHCII mutant (Nicol et al., 2019).
Overall, these observations suggest that LHCB5 has no specific role, nor that the accumulation of a specific antenna isoform is induced to compensate the loss of the isoforms composing the LHCII trimers. Despite similarities between the L1ko mutation *via* CRISPR/Cas9 and the *amiLhcb1* line, differences exist between the two genotypes, notably at the level of STN7 accumulation. In fact, in the *amiLhcb1* line, the amount of the STN7 protein was higher compared to WT (Pietrzykowska et al., 2014). In the mutant lines produced *via* CRISPR/Cas9, we clearly observed the opposite response (Figure 2).

The decrease of STN7 in L1ko compared to WT is consistent with the previously reported long-term regulation of STN7 abundance in response to light conditions. Exposure of plants to far-red light, a condition that enhances excitation of PSI over PSII, for a long period, leads to a decrease in the amount of the STN7 kinase (Willig et al., 2011).
Therefore, the decrease of STN7 in L1ko can be explained as a consequence of the oxidation of the photosynthetic ETC, as, in the L1ko line, the Chl distribution is shifted in favor of PSI (Figures 3, 4). Conversely, the lower level of TAP38/PPH1, observed in the L1ko lines, is less obvious. In previous reports, the protein levels of STN7 and TAP38/PPH1 were shown to be oppositely regulated; i.e., a decrease of the STN7 kinase was coupled with an increase of the TAP38/PPH1 phosphatase (Wunder et al., 2013). The observation that both STN7 and the counteracting phosphatase are less accumulated in L1ko suggests the existence of another layer of regulation of the protein accumulation, besides the previously documented redox status of the photosynthetic ETC. Consistently, a reduction of the TAP38/PPH1 level was also observed in *amiLhcb1* lines (although to a lesser extent) (Pietrzykowska et al., 2014), which led to the hypothesis that TAP38/PPH1 abundance is also regulated by the presence of its substrate LHCB1 (Suorsa et al., 2016). The observation that the phosphorylation level of the thylakoid protein was lower in L1ko is in agreement with previous reports linking the thylakoid protein phosphorylation to the redox state of the photosynthetic PQ pool more than to the accumulation of the relevant kinases and phosphatases (Suorsa et al., 2016). This appeared to be particularly true for the PSII kinase STN8, as PSBA and PSBC, which are the main targets of this kinase, showed strongly decreased phosphorylation in L1ko compared to WT. However, the lower phosphorylation level was not coupled with a decrease of the relevant kinase, STN8, or the PBCP phosphatase. This supports the hypothesis that their activity is regulated in response to changes in the redox status, previously formulated based on the observation of plants overexpressing the STN8 kinase (Wunder et al., 2013).

Photosynthetic Electron Transport in L1ko

The clear reduction in STN7 accumulation and phosphorylation of the main thylakoid phospho-proteins in L1ko compared to WT may be related to an imbalance in the redox equilibrium of the photosynthetic ETC. We, therefore, investigated the status of the ETC using Chl fluorescence and transient absorption spectroscopy to detail the impact of the LHCB1 loss on the photosynthetic activity. The first expected impact of the absence of LHCB1, and thus a decrease of LHCII trimers, is a reduction of the PSII physical and functional antenna size (Terao and Katoh, 1996). Consistently, both Chl fluorescence and ECS measurements confirmed that, in L1ko, the maximal PSII photochemical rate measured at a light-limiting intensity of 80-µmol photons m^{-2} s^{-1} was lower in L1ko compared to WT (Figure 3A). Besides the interaction with PSII, several reports have shown that LHCII also contributes to the excitation of PSI (Wientjes et al., 2013; Bos et al., 2017; Chukhutsina et al., 2020). Therefore, we used ECS-based methods to investigate whether the absence of LHCB1 affects the antenna size of PSI. Our data showed that the maximal PSI rate at 80-µmol photons m^{-2} s^{-1} in L1ko is comparable, with a tendency to be larger than that in the WT (Figure 3B). Therefore, no major difference in PSI antenna size should be present between these two genotypes. This can be explained by the relative increase of the LHCA1 and LHCA4 proteins, part of LHCI antenna, over the PSI core (Figure 2). Increased LHCI could compensate for the loss of LHCII, preserving the PSI antenna size. This hypothesis fits well with a previous report showing that an extra LHCI dimer, composed by LHCA1 and LHCA4, can functionally connect to PSI (Crepin et al., 2020). However, both the increase of these LHCI proteins and the decrease of PSI subunits, under our growth conditions, are minimal and thus difficult to confirm by immunodetection. Therefore, we further defined if there was an excitation imbalance between photosystems in L1ko by an indirect measurement of the rate of PQ oxidation by far-red light based on Chl fluorescence rise (Vj) (Toth et al., 2007; Pralon et al., 2020). The result showed that PQ oxidation is faster in L1ko, supporting the idea that the difference between PSI and PSII excitation in far-red light is larger in L1ko compared to the WT background (Figure 3E).

The same analysis conducted in the dark showed no difference, suggesting that the difference in the PQ oxidation between L1ko and WT is due to a different relative excitation of PSI and not to an increased contribution of the non-photochemical oxidation of the PQ pool (Supplementary Figure 7; Nawrocki et al., 2015).
Consistent with this result, the analysis of the fluorescence decay shows a bigger contribution of the faster component, which is interpreted as the decay of PSI excitation (Wientjes et al., 2017).
This confirms that, in L1ko, the global relative Chl pool connected to PSI over PSII is larger compared to the WT; therefore, the decrease in PSII antenna size is not fully compensated by the change in the PSII/PSI reaction center ratio. The increase in the PSII/PSI reaction center ratio is a compensatory response previously observed in Chl *b* mutants as well as in no-LHCII mutants (Terao and Katoh, 1996; Nicol et al., 2019). The PSII/PSI reaction center ratio has also been shown to be adjusted in function of the antenna size by transient induction of Chl *b* synthesis in the Chl *b*-less mutant (Jia et al., 2016). In terms of maintaining the equilibrium of the PQ pool redox state, the excess excitation of PSI could have been partially compensated by an increase of the CEF/LEF ratio. However, there was no significant difference in the CEF over the LEF ratio between the L1ko and WT, suggesting that the CEF/LEF ratio does not play a major role in balancing the ETC redox equilibrium in L1ko (Figure 3F). As the relative PSI/PSII Chl ratio is higher in L1ko than the WT, this should lead to higher oxidation of the photoactive PQ pool under light-limiting condition in the mutant. The oxidation of the photoactive PQ can be inferred by a smaller fraction of closed PSII reaction centers (Krause and Weis, 1984). Consistently, when L1ko plants were analyzed by room temperature fluorescence, we observed a smaller fraction of closed PSII centers as determined by the 1-qL parameter (Kramer et al., 2004), and a higher ΦPSII compared to the WT (Figure 4 and Supplementary Figure 8). As discussed in the previous paragraph, the constitutive over-oxidation of the PQ pool could explain the low phosphorylation of the thylakoid proteins and the low level of STN7 accumulation in L1ko. The qT analysis supports the hypothesis of oxidation of the photosynthetic PQ pool in L1ko. In fact, the changes in the light spectrum that alter the Chl *a* fluorescence, showing a transient peak after the switch from State 1 to State 2 light in WT, have no measurable effect in L1ko (Figure 4). Lack of LHCII caused a low reduction of the PQ pool and, therefore, did not activate STN7 also in the barley *chlorina f2* mutant (Bhalla and Bennett, 1987). This resulted in no measurable quenching related to state transition in this mutant (Lokstein et al., 1994). Consistently, we observed limited phosphorylation of LHCB2 and a minor change in the antenna connected to PSII and PSI in L1ko, calculated from the maximal fluorescence as qT. The relative increase of LHCB2 abundance, therefore, is not sufficient to compensate for the lack of LHCII heterotrimers in L1ko, as shown also by the lack of a visible PSI-LHCI-LHCII complex in this line by native gel separation (Supplementary Figure 5). These observations are consistent with the previous report showing that both *amiLhcb1* and *amiLhcb2* lines had limited state transitions even if the PQ pool was oxidized in the *amiLhcb1* line and reduced in amiLhcb2 (Pietrzykowska et al., 2014). Besides regulating the qT, STN7 activity has also been shown to regulate the grana stacks diameter (Hepworth et al., 2021). With this regard, the low level and activity of STN7 can also have a role in compensating the smaller grana observed in L1ko (discussed below) and contribute to maintain the equilibrium between LEF and CEF in this mutant as proposed in Hepworth et al. (2021).
The extent of NPQ induction in L1ko is lower than in WT; this phenomenon was observed in the amiLhcb1 line (Pietrzykowska et al., 2014), in the asLhcb2 line, which is lacking both LHCB1 and LHCB2 proteins (Johnson et al., 2008), and in mutants of Chl *b* synthesis such as the *chlorina f2* mutant of barley, which lacks specifically of the fast inducible component qE (Lokstein et al., 1993, 1994) and the *ch1-1* mutant of Arabidopsis (Havaux et al., 2007). This further supports the observation of the important role of LHCII proteins as quenching sites (Dall'Osto et al., 2010). The kinetics of NPQ induction and relaxation are slower in L1ko compared with the WT; this is consistent with previous observations made with the mutants lacking both LHCB1 and LHCB2 (Johnson et al., 2008; Nicol et al., 2019), suggesting that the trimeric LHCII, by its structure or abundance, has an important role in NPQ dynamics.

Lack of the LHCB1 Isoform Alters the Thylakoid Organization

The trimeric LHCII occupies a large part of the thylakoid membrane surface (Kirchhoff et al., 2002). Therefore, it has been proposed to play a major role in the structure of the thylakoids and, in particular, in the grana stacking (Barber, 1980; Daum et al., 2010; Albanese et al., 2020). However, plants deprived of the two major isoforms, LHCB1 and LHCB2, still have grana stacks (Andersson et al., 2003; Nicol et al., 2019).

Mutants of Chl *b* synthesis in Arabidopsis, despite having a strong reduction in LHCII protein content, have been reported to still have stacked grana but with lesser stacks and thus occupying a smaller surface of the chloroplast (Murray and Kohorn, 1991; Ruban et al., 2003; Kim et al., 2009). The grana were present also in *amiLhcb1*, depleted only of LHCB1, but with less grana stacks on average when compared to the WT (Pietrzykowska et al., 2014). Our investigation by TEM found that L1ko contains statistically less stacks per grana compared to WT, and, on average, a smaller diameter (Figure 6). This was, in part, expected as, by losing LHCII, the PSII particles in the grana would be smaller and packed more tightly and thus occupy a smaller area (Goral et al., 2012). LHCII phosphorylation by STN7 was linked to the regulation of the grana diameter as discussed earlier (Hepworth et al., 2021). However, also, the STN8/PBCP kinase and phosphatase were proposed to play a role in regulating grana dynamics. In particular, the mutation of STN8, the kinase mainly involved in the phosphorylation of PSII core protein, was associated with an increase in the grana diameter (Fristedt et al., 2009). Further studies have shown that the CURVATURE 1 (CURT1) protein, which is also phosphorylated in an STN8-dependent fashion, is directly involved in regulating the grana diameter and may be responsible for the change of grana width in the *stn8* mutant (Armbruster et al., 2013; Trotta et al., 2019). Therefore, as for STN7, also, the low level of STN8 activity may have a compensatory function in terms of grana width and stability in the L1ko background.

Although the relationship between the protein composition of the thylakoid membrane and the grana structure has been described in detail, there is a less clear consensus about the role played by the membrane lipids in shaping the thylakoid membrane. In this report, we analyzed the galactolipids present in L1ko, and we found no significant difference with the WT (Supplementary Figure 14). The amount of galactolipids does not follow the decrease of the LHCII proteins thus changing the protein to the lipid ratio in the thylakoids of L1ko. This change may affect not only the ultrastructure of the thylakoids but also the electron transport routes by interfering with the lipid mobility and thus hampering the PQ diffusion between PSII and the cytb6f, antagonizing the acclimation strategies of L1ko discussed in the previous paragraph (Johnson et al., 2014; Tyutereva et al., 2017). Quantification of the carotenoids revealed that, in the L1ko lines, the lutein and violaxanthin/neoxanthin content was lower than in the WT (Supplementary Figure 14). This is not surprising since the large majority of the xanthophylls are expected to be bound to LHCII, while most of the β-carotene, which is not decreasing in L1ko compared to WT, is associated with the photosystems core and, mostly, to PSI (Qin et al., 2015). The same decrease in xanthophyll content was not observed in the *asLhcb2* line, which is lacking both LHCB1 and LHCB2 proteins (Andersson et al., 2003), while the carotenoid content decreased to the same extent in the crossed *amiLhcb1*/*amiLhcb2* line (Nicol et al., 2019). A similar response is observed in the Arabidopsis Chl *b* mutant *ch1-3* where, on a Chl *a* basis, the β-carotene content increased, while the xanthophylls lutein and neoxanthin were less accumulated (Kim et al., 2009). Hinting that, in these lines, a signaling mechanism is in place to coordinate the carotenoid metabolism with the antenna biosynthesis (Li et al., 2009).

Conclusion

In conclusion, we report that the stable loss of LHCB1 induces compensatory mechanisms in the plant. These mechanisms include the alteration of the kinase and phosphatases, regulating the equilibrium of the photosynthetic ETC. Taken together, these data show that loss of LHCB1 cannot be compensated by the other LHCII isoforms, and that this isoform, by its nature or level of accumulation, has a unique role in shaping the thylakoid membrane and maintaining the equilibrium between the two photosystems. Besides, this mutant gives the first possibility for a mutational analysis on the major LHCII, something that, up until now, has been impossible due to the clustered gene organization. Since trimeric LHCII is essential for the plasticity of the photosynthetic machinery that allows the rapid acclimation to changing light conditions, these mutants are not only of vital importance for fundamental research but also for applied projects aiming at increasing crop productivity by improving the light use efficiency.

Data Availability Statement

The raw data and the pictures used for this manuscript are available at https://zenodo.org/record/5729177#.YaDZILrjKUk. Further data, and the described lines, can be provided by the authors upon reasonable request.

Author Contributions

HS and FL designed the experimental plan and performed the other experiments. RC, WN, and CH measured the photochemical rate of photosystems. GF and DT performed the CEF/LEF analysis. HS and VD produced the electron microscopy pictures. EW analyzed the images. EW and CS performed confocal microscopy and FLIM analysis. GG performed the lipid profile analysis. FL performed the statistical analysis of the data. All authors contributed in the redaction, read, and approved the manuscript.

Funding

HS and FL's work was supported by the University of Neuchâtel and the Swiss National Science Foundation (31003A_179417). EW and CS were supported by the Dutch Organization for Scientific Research (NWO) *via* a Vidi grant no. VI.Vidi 192.042 (EW). The work at the Vrije Universiteit Amsterdam was supported by the Dutch Organization for Scientific Research *via* a TOP grant (714.018.001) to RC.

Conflict of Interest

The authors declare that the research was conducted in the absence of any commercial or financial relationships that could be construed as a potential conflict of interest.

Publisher's Note

All claims expressed in this article are solely those of the authors and do not necessarily represent those of their affiliated organizations, or those of the publisher, the editors and the reviewers. Any product that may be evaluated in this article, or claim that may be made by its manufacturer, is not guaranteed or endorsed by the publisher.

Acknowledgments

We thank Sergio Rasmann for his assistance in the statistical analysis of the grana stack and width distribution, and Jenny Pego Magalhaes for her technical help in TEM analysis.

References

Albanese, P., Tamara, S., Saracco, G., Scheltema, R. A., and Pagliano, C. (2020). How paired PSII-LHCII supercomplexes mediate the stacking of plant thylakoid membranes unveiled by structural mass-spectrometry. Nat. Commun. 11:1361. doi: https://10.1038/s41467-020-15184-1

Allen, J. F. (1992). Protein phosphorylation in regulation of photosynthesis. Biochim. Biophys. Acta 1098, 275–335.

Ancin, M., Fernandez-San Millan, A., Larraya, L., Morales, F., Veramendi, J., Aranjuelo, I., et al. (2019). Overexpression of thioredoxin m in tobacco chloroplasts inhibits the protein kinase STN7 and alters photosynthetic performance. J. Exp. Bot. 70, 1005–1016. doi: https://10.1093/jxb/ery415

Andersson, J., Wentworth, M., Walters, R. G., Howard, C. A., Ruban, A. V., Horton, P., et al. (2003). Absence of the Lhcb1 and Lhcb2 proteins of the light-harvesting complex of photosystem II - effects on photosynthesis, grana stacking and fitness. Plant J. 35, 350–361. doi: https://10.1046/j.1365-313x.2003.01811.x

Armbruster, U., Labs, M., Pribil, M., Viola, S., Xu, W., Scharfenberg, M., et al. (2013). Arabidopsis CURVATURE THYLAKOID1 proteins modify thylakoid architecture by inducing membrane curvature. Plant Cell 25, 2661–2678. doi: https://10.1105/tpc.113.113118

Arnold, J., Shapiguzov, A., Fucile, G., Rochaix, J.-D., Goldschmidt-Clermont, M., and Eichacker, L. A. (2014). Separation of membrane protein complexes by native LDS-PAGE. Methods Mol. Biol. 1072, 667–676. doi: https://10.1007/978-1-62703-631-3_46

Bailleul, B., Cardol, P., Breyton, C., and Finazzi, G. (2010). Electrochromism: a useful probe to study algal photosynthesis. Photosynth. Res. 106, 179–189. doi: https://10.1007/s11120-010-9579-z

Ballottari, M., Girardon, J., Dall'Osto, L., and Bassi, R. (2012). Evolution and functional properties of photosystem II light harvesting complexes in eukaryotes. Biochim. Biophys. Acta 1817, 143–157. doi: https://10.1016/j.bbabio.2011.06.005

Barber, J. (1980). An explanation for the relationship between salt-induced thylakoid stacking and the chlorophyll fluorescence changes associated with changes in spillover of energy from photosystem II to photosystem I. FEBS Lett. 118, 1–10. doi: https://10.1016/0014-5793(80)81207-5

Barros, T., and Kühlbrandt, W. (2009). Crystallisation, structure and function of plant light-harvesting Complex II. Biochim. Biophys. Acta 1787, 753–772. doi: https://10.1016/j.bbabio.2009.03.012

Bassi, R., and Dall'Osto, L. (2021). Dissipation of Light Energy Absorbed in Excess: the Molecular Mechanisms. Ann. Rev. Plant Biol. 72, 47–76. doi: https://10.1146/annurev-arplant-071720-015522

Bellafiore, S., Barneche, F., Peltier, G., and Rochaix, J. D. (2005). State transitions and light adaptation require chloroplast thylakoid protein kinase STN7. Nature 433, 892–895. doi: https://10.1038/nature03286

Bhalla, P., and Bennett, J. (1987). Chloroplast phosphoproteins: Phosphorylation of a 12-kDa stromal protein by the redox-controlled kinase of thylakoid membranes. Arch. Biochem. Biophys. 252, 97–104. doi: https://10.1016/0003-9861(87)90012-9

Bos, I., Bland, K. M., Tian, L., Croce, R., Frankel, L. K., van Amerongen, H., et al. (2017). Multiple LHCII antennae can transfer energy efficiently to a single Photosystem I. Biochim. Biophys. Acta 1858, 371–378. doi: https://10.1016/j.bbabio.2017.02.012

Bos, P., Oosterwijk, A., Koehorst, R., Bader, A., Philippi, J., van Amerongen, H., et al. (2019). Digitonin-sensitive LHCII enlarges the antenna of Photosystem I in stroma lamellae of Arabidopsis thaliana after far-red and blue-light treatment. Biochim. Biophys. Acta 1860, 651–658. doi: https://10.1016/j.bbabio.2019.07.001

Boyer, P. D. (1993). The binding change mechanism for ATP synthase—some probabilities and possibilities. Biochim. Biophys. Acta 1140, 215–250. doi: https://10.1016/0005-2728(93)90063-l

Caffarri, S., Croce, R., Cattivelli, L., and Bassi, R. (2004). A look within LHCII: differential analysis of the Lhcb1-3 complexes building the major trimeric antenna complex of higher-plant photosynthesis. Biochemistry 43, 9467–9476. doi: https://10.1021/bi036265i

Chukhutsina, V. U., Liu, X., Xu, P., and Croce, R. (2020). Light-harvesting complex II is an antenna of photosystem I in dark-adapted plants. Nat. Plants 6, 860–868. doi: https://10.1038/s41477-020-0693-4

Crepin, A., and Caffarri, S. (2015). The specific localizations of phosphorylated Lhcb1 and Lhcb2 isoforms reveal the role of Lhcb2 in the formation of the PSI-LHCII supercomplex in Arabidopsis during state transitions. Biochim. Biophys. Acta 1847, 1539–1548. doi: https://10.1016/j.bbabio.2015.09.005

Crepin, A., and Caffarri, S. (2018). Functions and evolution of Lhcb isoforms composing LHCII, the major light harvesting complex of photosystem II of green eukaryotic organisms. Curr. Protein Peptide Sci. 19, 699–713. doi: https://10.2174/1389203719666180222101534

Crepin, A., Kucerova, Z., Kosta, A., Durand, E., and Caffarri, S. (2020). Isolation and characterization of a large photosystem I-light-harvesting complex II supercomplex with an additional Lhca1-a4 dimer in Arabidopsis. Plant J. 102, 398–409. doi: https://10.1111/tpj.14634

Croce, R., and Amerongen, H. V. (2020). Light harvesting in oxygenic photosynthesis: structural biology meets spectroscopy. Science 369, eaay2058. doi: https://10.1126/science.aay2058

Dall'Osto, L., Cazzaniga, S., Havaux, M., and Bassi, R. (2010). Enhanced photoprotection by protein-bound vs free xanthophyll pools: a comparative analysis of chlorophyll b and xanthophyll biosynthesis mutants. Mol. Plant 3, 576–593. doi: https://10.1093/mp/ssp117

Daum, B., Nicastro, D., Austin, J., McIntosh, J. R., and Kühlbrandt, W. (2010). Arrangement of photosystem II and ATP synthase in chloroplast membranes of spinach and pea. Plant Cell 22, 1299–1312. doi: https://10.1105/tpc.109.071431

Dekker, J. P., and Boekema, E. J. (2005). Supramolecular organization of thylakoid membrane proteins in green plants. Biochim. Biophys. Acta 1706, 12–39. doi: https://10.1016/j.bbabio.2004.09.009

Durr, J., Papareddy, R., Nakajima, K., and Gutierrez-Marcos, J. (2018). Highly efficient heritable targeted deletions of gene clusters and non-coding regulatory regions in Arabidopsis using CRISPR/Cas9. Sci. Rep. 8, 1–11. doi: https://10.1038/s41598-018-22667-1

Espineda, C. E., Linford, A. S., Devine, D., and Brusslan, J. A. (1999). The AtCAO gene, encoding chlorophyll a oxygenase, is required for chlorophyll b synthesis in Arabidopsis thaliana. Proc. Natl. Acad. Sci. 96, 10507–10511. doi: https://10.1073/pnas.96.18.10507

Fristedt, R., Willig, A., Granath, P., Crevecoeur, M., Rochaix, J.-D., and Vener, A. V. (2009). Phosphorylation of photosystem II controls functional macroscopic folding of photosynthetic membranes in Arabidopsis. Plant Cell 21, 3950–3964. doi: https://10.1105/tpc.109.069435

Galka, P., Santabarbara, S., Khuong, T. T. H., Degand, H., Morsomme, P., Jennings, R. C., et al. (2012). Functional analyses of the plant photosystem I–light-harvesting complex II supercomplex reveal that light-harvesting complex II loosely bound to photosystem II is a very efficient antenna for photosystem I in state II. Plant Cell 24, 2963–2978. doi: https://10.1105/tpc.112.100339

Goral, T. K., Johnson, M. P., Duffy, C. D., Brain, A. P., Ruban, A. V., and Mullineaux, C. W. (2012). Light-harvesting antenna composition controls the macrostructure and dynamics of thylakoid membranes in Arabidopsis. Plant J. 69, 289–301. doi: https://10.1111/j.1365-313X.2011.04790.x

Havaux, M., Dall'Osto, L., and Bassi, R. (2007). Zeaxanthin has enhanced antioxidant capacity with respect to all other xanthophylls in Arabidopsis leaves and functions independent of binding to PSII antennae. Plant Physiol. 145, 1506–1520. doi: https://10.1104/pp.107.108480

Heigwer, F., Kerr, G., and Boutros, M. (2014). E-CRISP: fast CRISPR target site identification. Nat. Methods 11, 122–123. doi: https://10.1038/nmeth.2812

Hepworth, C., Wood, W. H. J., Emrich-Mills, T. Z., Proctor, M. S., Casson, S., and Johnson, M. P. (2021). Dynamic thylakoid stacking and state transitions work synergistically to avoid acceptor-side limitation of photosystem I. Nat. Plants 7, 87–98. doi: https://10.1038/s41477-020-00828-3

Hobe, S., Foerster, R., Klingler, J., and Paulsen, H. (1995). N-proximal sequence motif in light-harvesting chlorophyll a/b-binding protein is essential for the trimerization of light-harvesting chlorophyll a/b complex. Biochemistry 34, 10224–10228. doi: https://10.1021/bi00032a016

Horton, P., and Ruban, A. (2005). Molecular design of the photosystem II light-harvesting antenna: photosynthesis and photoprotection. J. Exp. Bot. 56, 365–373. doi: https://10.1093/jxb/eri023

Hu, C., Nawrocki, W. J., and Croce, R. (2021). Long-term adaptation of Arabidopsis thaliana to far-red light. Plant Cell Environ. 44, 3002–3014. doi: https://10.1111/pce.14032

Jansson, S. (1999). A guide to the Lhc genes and their relatives in Arabidopsis. Trends Plant Sci. 4, 236–240. doi: https://10.1016/s1360-1385(99)01419-3

Jansson, S., Pichersky, E., Bassi, R., Green, B. R., Ikeuchi, M., Melis, A., et al. (1992). A nomenclature for the genes encoding the chlorophyll a/b-binding proteins of higher plants. Plant Mol. Biol. Report. 10, 242–253.

Järvi, S., Suorsa, M., Paakkarinen, V., and Aro, E.-M. (2011). Optimized native gel systems for separation of thylakoid protein complexes: novel super-and mega-complexes. Biochem. J. 439, 207–214. doi: https://10.1042/BJ20102155

Jia, T., Ito, H., and Tanaka, A. (2016). Simultaneous regulation of antenna size and photosystem I/II stoichiometry in Arabidopsis thaliana. Planta 244, 1041–1053. doi: https://10.1007/s00425-016-2568-5

Johnson, M. P., Peìrez-Bueno, M. A. L., Zia, A., Horton, P., and Ruban, A. V. (2008). The Zeaxanthin-Independent and Zeaxanthin-Dependent qE Components of Nonphotochemical Quenching Involve Common Conformational Changes within the Photosystem II Antenna in Arabidopsis. Plant Physiol. 149, 1061–1075. doi: https://10.1104/pp.108.129957

Johnson, M. P., Vasilev, C., Olsen, J. D., and Hunter, C. N. (2014). Nanodomains of Cytochrome b 6 f and Photosystem II Complexes in Spinach Grana Thylakoid Membranes. Plant Cell 26, 3051–3061. doi: https://10.1105/tpc.114.127233

Johnson, M. P., and Wientjes, E. (2020). The relevance of dynamic thylakoid organisation to photosynthetic regulation. Biochim. Biophys. Acta Bioenerg. 1861:148039. doi: https://10.1016/j.bbabio.2019.06.011

Kim, E.-H., Li, X.-P., Razeghifard, R., Anderson, J. M., Niyogi, K. K., Pogson, B. J., et al. (2009). The multiple roles of light-harvesting chlorophyll a/b-protein complexes define structure and optimize function of Arabidopsis chloroplasts: a study using two chlorophyll b-less mutants. Biochim. Biophys. Acta 1787, 973–984. doi: https://10.1016/j.bbabio.2009.04.009

Kirchhoff, H., Mukherjee, U., and Galla, H.-J. (2002). Molecular architecture of the thylakoid membrane: lipid diffusion space for plastoquinone. Biochemistry 41, 4872–4882. doi: https://10.1021/bi011650y

Klimmek, F., Sjodin, A., Noutsos, C., Leister, D., and Jansson, S. (2006). Abundantly and rarely expressed Lhc protein genes exhibit distinct regulation patterns in plants. Plant Physiol. 140, 793–804. doi: https://10.1104/pp.105.073304

Kouřil, R., Zygadlo, A., Arteni, A. A., de Wit, C. D., Dekker, J. P., Jensen, P. E., et al. (2005). Structural characterization of a complex of photosystem I and light-harvesting complex II of Arabidopsis thaliana. Biochemistry 44, 10935–10940. doi: https://10.1021/bi051097a

Kramer, D. M., Johnson, G., Kiirats, O., and Edwards, G. E. (2004). New Fluorescence Parameters for the Determination of QA Redox State and Excitation Energy Fluxes. Photosynth. Res. 79:209.

Kramer, M., Rodriguez-Heredia, M., Saccon, F., Mosebach, L., Twachtmann, M., Krieger-Liszkay, A., et al. (2021). Regulation of photosynthetic electron flow on dark to light transition by ferredoxin: NADP (H) oxidoreductase interactions. Elife 10:e56088. doi: https://10.7554/eLife.56088

Krause, G. H., and Weis, E. (1984). Chlorophyll fluorescence as a tool in plant physiology. Photosynth. Res. 5, 139–157. doi: https://10.1007/bf00028527

Krol, M., Spangfort, M. D., Huner, N. P., Oquist, G., Gustafsson, P., and Jansson, S. (1995). Chlorophyll a/b-binding proteins, pigment conversions, and early light-induced proteins in a chlorophyll b-less barley mutant. Plant Physiol. 107, 873–883. doi: https://10.1104/pp.107.3.873

Leoni, C., Pietrzykowska, M., Kiss, A. Z., Suorsa, M., Ceci, L. R., Aro, E. M., et al. (2013). Very rapid phosphorylation kinetics suggest a unique role for Lhcb2 during state transitions in Arabidopsis. Plant J. 76, 236–246. doi: https://10.1111/tpj.12297

Leutwiler, L. S., Meyerowitz, E. M., and Tobin, E. M. (1986). Structure and expression of three light-harvesting chlorophyll a/b-binding protein genes in Arabidopsis thaliana. Nucleic Acids Res. 14, 4051–4064. doi: https://10.1093/nar/14.10.4051

Li, Z., Ahn, T. K., Avenson, T. J., Ballottari, M., Cruz, J. A., Kramer, D. M., et al. (2009). Lutein Accumulation in the Absence of Zeaxanthin Restores Nonphotochemical Quenching in the Arabidopsis thaliana npq1 Mutant. Plant Cell 21, 1798–1812. doi: https://10.1105/tpc.109.066571

Lokstein, H., Härtel, H., Hoffmann, P., and Renger, G. (1993). Comparison of chlorophyll fluorescence quenching in leaves of wild-type with a chlorophyll-b-less mutant of barley (Hordeum vulgare L.). J. Photochem. Photobiol. B Biol. 19, 217–225.

Lokstein, H., Härtel, H., Hoffmann, P., Woitke, P., and Renger, G. (1994). The role of light-harvesting complex II in excess excitation energy dissipation: an in-vivo fluorescence study on the origin of high-energy quenching. J. Photochem. Photobiol. B Biol. 26, 175–184. doi: https://10.1016/1011-1344(94)07032-6

Longoni, F. P., and Goldschmidt-Clermont, M. (2021). Thylakoid Protein Phosphorylation in Chloroplasts. Plant Cell Physiol. 62, 1094–1107.

Longoni, P., Douchi, D., Cariti, F., Fucile, G., and Goldschmidt-Clermont, M. (2015). Phosphorylation of the Light-Harvesting Complex II Isoform Lhcb2 Is Central to State Transitions. Plant Physiol. 169, 2874–2883. doi: https://10.1104/pp.15.01498

Longoni, P., Samol, I., and Goldschmidt-Clermont, M. (2019). The Kinase STATE TRANSITION 8 Phosphorylates Light Harvesting Complex II and Contributes to Light Acclimation in Arabidopsis thaliana. Front. Plant Sci. 10:1156. doi: https://10.3389/fpls.2019.01156

Malone, L. A., Proctor, M. S., Hitchcock, A., Hunter, C. N., and Johnson, M. P. (2021). Cytochrome b6f–Orchestrator of photosynthetic electron transfer. Biochim. Biophys. Acta 1862:148380.

Martinis, J., Glauser, G., Valimareanu, S., and Kessler, F. (2013). A chloroplast ABC1-like kinase regulates vitamin E metabolism in Arabidopsis. Plant Physiol. 162, 652–662. doi: https://10.1104/pp.113.218644

Mazor, Y., Borovikova, A., Caspy, I., and Nelson, N. (2017). Structure of the plant photosystem I supercomplex at 2.6 Å resolution. Nat. Plants 3:17014.

McGrath, J. M., Terzaghi, W. B., Sridhar, P., Cashmore, A. R., and Pichersky, E. (1992). Sequence of the fourth and fifth Photosystem II type I chlorophyll a/b-binding protein genes of Arabidopsis thaliana and evidence for the presence of a full complement of the extended CAB gene family. Plant Mol. Biol. 19, 725–733. doi: https://10.1007/BF00027069

Merchant, S., and Sawaya, M. R. (2005). The light reactions: a guide to recent acquisitions for the picture gallery. Plant Cell 17, 648–663. doi: https://10.1105/tpc.105.030676

Montague, T. G., Cruz, J. M., Gagnon, J. A., Church, G. M., and Valen, E. (2014). CHOPCHOP: a CRISPR/Cas9 and TALEN web tool for genome editing. Nucleic Acids Res. 42, W401–W407. doi: https://10.1093/nar/gku410

Murray, D. L., and Kohorn, B. D. (1991). Chloroplasts of Arabidopsis thaliana homozygous for the ch-1 locus lack chlorophyll b, lack stable LHCPII and have stacked thylakoids. Plant Mol. Biol. 16, 71–79. doi: https://10.1007/BF00017918

Nawrocki, W. J., Tourasse, N. J., Taly, A., Rappaport, F., and Wollman, F.-A. (2015). The plastid terminal oxidase: its elusive function points to multiple contributions to plastid physiology. Annu. Rev. Plant Biol. 66, 49–74. doi: https://10.1146/annurev-arplant-043014-114744

Nicol, L., Nawrocki, W. J., and Croce, R. (2019). Disentangling the sites of non-photochemical quenching in vascular plants. Nat. Plants 5, 1177–1183. doi: https://10.1038/s41477-019-0526-5

Ordon, J., Bressan, M., Kretschmer, C., Dall'Osto, L., Marillonnet, S., Bassi, R., et al. (2020). Optimized Cas9 expression systems for highly efficient Arabidopsis genome editing facilitate isolation of complex alleles in a single generation. Funct. Integr. Genomics 20, 151–162. doi: https://10.1007/s10142-019-00665-4

Pan, X., Cao, P., Su, X., Liu, Z., and Li, M. (2020). Structural analysis and comparison of light-harvesting complexes I and II. Biochim. Biophys. Acta 1861:148038. doi: https://10.1016/j.bbabio.2019.06.010

Pan, X., Ma, J., Su, X., Cao, P., Chang, W., Liu, Z., et al. (2018). Structure of the maize photosystem I supercomplex with light-harvesting complexes I and II. Science 360, 1109–1113. doi: https://10.1126/science.aat1156

Papageorgiou, G. C., and Govindjee, R. (2004). Chlorophyll a Fluorescence: a Signature of Photosynthesis. Germany: Springer.

Peter, G. F., and Thornber, J. P. (1991). Biochemical composition and organization of higher plant photosystem II light-harvesting pigment-proteins. J. Biol. Chem. 266, 16745–16754. doi: https://10.1016/s0021-9258(18)55364-3

Pietrzykowska, M., Suorsa, M., Semchonok, D. A., Tikkanen, M., Boekema, E. J., Aro, E. M., et al. (2014). The light-harvesting chlorophyll a/b binding proteins Lhcb1 and Lhcb2 play complementary roles during state transitions in Arabidopsis. Plant Cell 26, 3646–3660. doi: https://10.1105/tpc.114.127373

Porra, R. J. (2002). The chequered history of the development and use of simultaneous equations for the accurate determination of chlorophylls a and b. Photosynth. Res. 73, 149–156. doi: https://10.1023/A:1020470224740

Pralon, T., Collombat, J., Pipitone, R., Ksas, B., Shanmugabalaji, V., Havaux, M., et al. (2020). Mutation of the Atypical Kinase ABC1K3 Partially Rescues the PROTON GRADIENT REGULATION 6 Phenotype in Arabidopsis thaliana. Front. Plant Sci. 11:337. doi: https://10.3389/fpls.2020.00337

Pribil, M., Pesaresi, P., Hertle, A., Barbato, R., and Leister, D. (2010). Role of plastid protein phosphatase TAP38 in LHCII dephosphorylation and thylakoid electron flow. PLoS Biol. 8:e1000288. doi: https://10.1371/journal.pbio.1000288

Qin, X., Suga, M., Kuang, T., and Shen, J.-R. (2015). Structural basis for energy transfer pathways in the plant PSI-LHCI supercomplex. Science 348, 989–995. doi: https://10.1126/science.aab0214

Rantala, M., Rantala, S., and Aro, E. M. (2020). Composition, phosphorylation and dynamic organization of photosynthetic protein complexes in plant thylakoid membrane. Photochem. Photobiol. Sci. 19, 604–619. doi: https://10.1039/d0pp00025f

Ruban, A. V., Wentworth, M., Yakushevska, A. E., Andersson, J., Lee, P. J., Keegstra, W., et al. (2003). Plants lacking the main light-harvesting complex retain photosystem II macro-organization. Nature 421, 648–652. doi: https://10.1038/nature01344

Sattari Vayghan, H., Tavalaei, S., Grillon, A., Meyer, L., Ballabani, G., Glauser, G., et al. (2020). Growth Temperature Influence on Lipids and Photosynthesis in Lepidium sativum. Front. Plant Sci. 11:745. doi: https://10.3389/fpls.2020.00745

Shapiguzov, A., Ingelsson, B., Samol, I., Andres, C., Kessler, F., Rochaix, J. D., et al. (2010). The PPH1 phosphatase is specifically involved in LHCII dephosphorylation and state transitions in Arabidopsis. Proc. Natl. Acad. Sci. U. S. A. 107, 4782–4787. doi: https://10.1073/pnas.0913810107

Siefermann, D., and Yamamoto, H. Y. (1975). NADPH and oxygen-dependent epoxidation of zeaxanthin in isolated chloroplasts. Biochem. Biophys. Res. Commun. 62, 456–461.

Spicher, L., Glauser, G., and Kessler, F. (2016). Lipid antioxidant and galactolipid remodeling under temperature stress in tomato plants. Front. Plant Sci. 7:167. doi: https://10.3389/fpls.2016.00167

Suorsa, M., Rossi, F., Tadini, L., Labs, M., Colombo, M., Jahns, P., et al. (2016). PGR5-PGRL1-Dependent Cyclic Electron Transport Modulates Linear Electron Transport Rate in Arabidopsis thaliana. Mol. Plant 9, 271–288. doi: https://10.1016/j.molp.2015.12.001

Terao, T., and Katoh, S. (1996). Antenna sizes of photosystem I and photosystem II in chlorophyll b-deficient mutants of rice. Evidence for an antenna function of photosystem II centers that are inactive in electron transport. Plant Cell Physiol. 37, 307–312.

Toth, S. Z., Schansker, G., and Strasser, R. J. (2007). A non-invasive assay of the plastoquinone pool redox state based on the OJIP-transient. Photosynth. Res. 93, 193–203. doi: https://10.1007/s11120-007-9179-8

Trotta, A., Bajwa, A. A., Mancini, I., Paakkarinen, V., Pribil, M., and Aro, E.-M. (2019). The role of phosphorylation dynamics of CURVATURE THYLAKOID 1B in plant thylakoid membranes. Plant Physiol. 181, 1615–1631. doi: https://10.1104/pp.19.00942

Tyutereva, E. V., Evkaikina, A. I., Ivanova, A. N., and Voitsekhovskaja, O. V. (2017). The absence of chlorophyll b affects lateral mobility of photosynthetic complexes and lipids in grana membranes of Arabidopsis and barley chlorina mutants. Photosynth. Res. 133, 357–370.

Warren, S. C., Margineanu, A., Alibhai, D., Kelly, D. J., Talbot, C., Alexandrov, Y., et al. (2013). Rapid global fitting of large fluorescence lifetime imaging microscopy datasets. PLoS One 8:e70687. doi: https://10.1371/journal.pone.0070687

Wientjes, E., and Croce, R. (2011). The light-harvesting complexes of higher-plant Photosystem I: lhca1/4 and Lhca2/3 form two red-emitting heterodimers. Biochem. J. 433, 477–485. doi: https://10.1042/BJ20101538

Wientjes, E., Philippi, J., Borst, J. W., and van Amerongen, H. (2017). Imaging the Photosystem I/Photosystem II chlorophyll ratio inside the leaf. Biochim. Biophys. Acta 1858, 259–265. doi: https://10.1016/j.bbabio.2017.01.008

Wientjes, E., van Amerongen, H., and Croce, R. (2013). LHCII is an antenna of both photosystems after long-term acclimation. Biochim. Biophys. Acta 1827, 420–426.

Willig, A., Shapiguzov, A., Goldschmidt-Clermont, M., and Rochaix, J. D. (2011). The phosphorylation status of the chloroplast protein kinase STN7 of Arabidopsis affects its turnover. Plant Physiol. 157, 2102–2107. doi: https://10.1104/pp.111.187328

Wunder, T., Xu, W., Liu, Q., Wanner, G., Leister, D., and Pribil, M. (2013). The major thylakoid protein kinases STN7 and STN8 revisited: effects of altered STN8 levels and regulatory specificities of the STN kinases. Front. Plant Sci. 4:417. doi: https://10.3389/fpls.2013.00417

Xing, H. L., Dong, L., Wang, Z. P., Zhang, H. Y., Han, C. Y., Liu, B., et al. (2014). A CRISPR/Cas9 toolkit for multiplex genome editing in plants. BMC Plant Biol. 14:327. doi: https://10.1186/s12870-014-0327-y

Supplementary Material

The Supplementary Material for this article can be found online at: https://www.frontiersin.org/articles/10.3389/fpls.2022.833032/full#supplementary-material

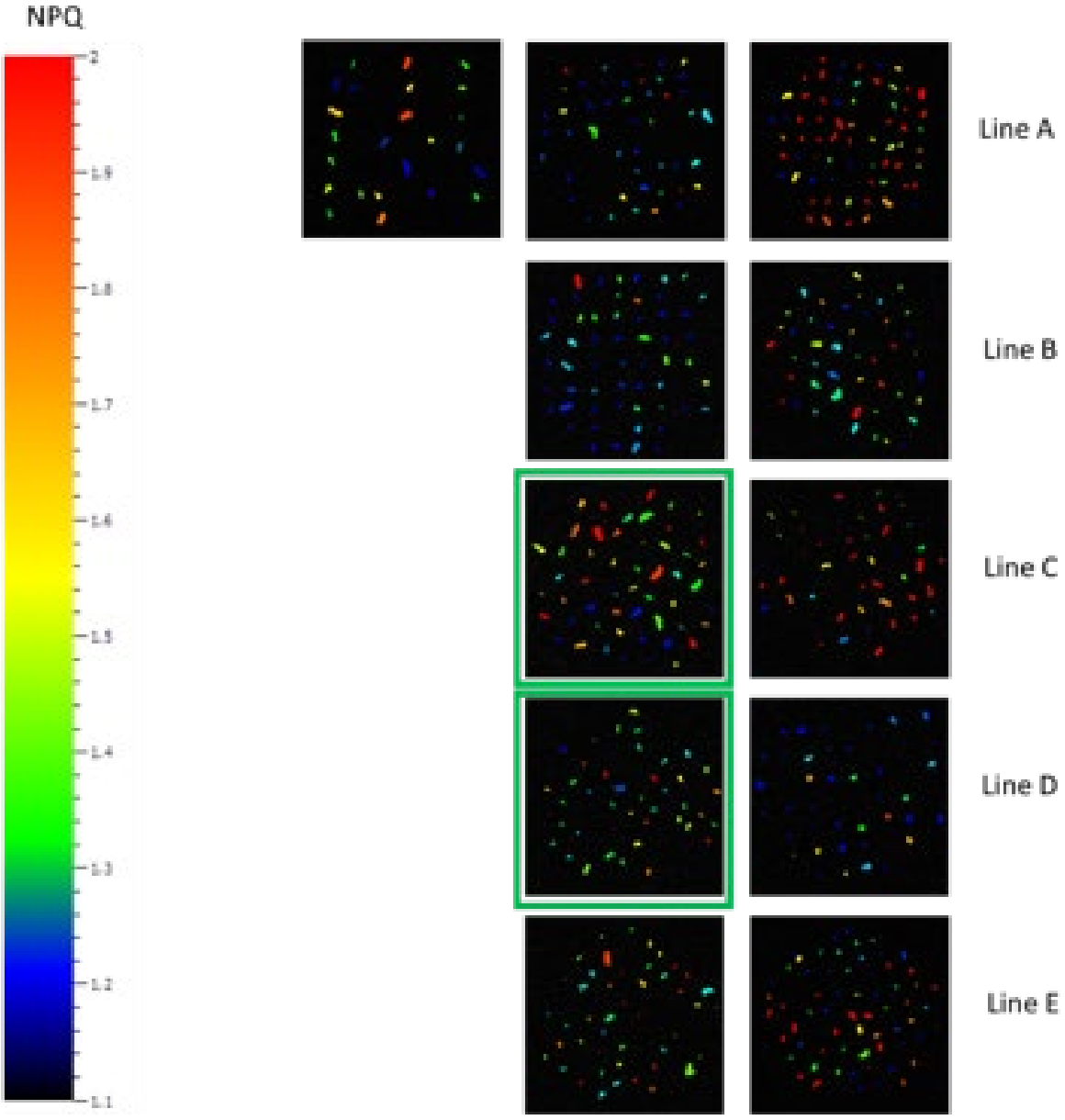

Figure S1. Screening of the T2 generation by NPQ. False color image of the calculated NPQ value per plant, the color scale with the corresponding values is shown on the left. Each row shows the plants generated from an independent T0 plant. The range of NPQ values was set between 1.1 (the NPQ value observed in a total Lhcb1 KO mutant) and 2 (the NPQ value of WT plants under this light condition). Plants with a low NPQ were selected from the two sets highlighted with green squares.

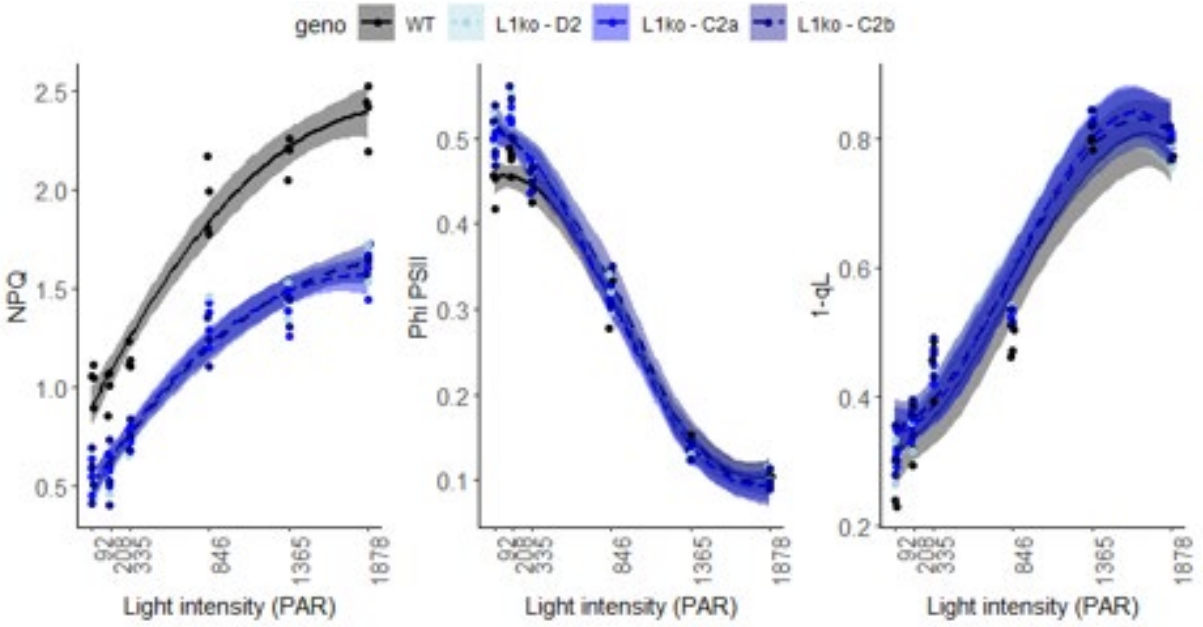

Figure S2. Different L1ko mutant lines have the same photosynthetic defects. Room temperature chlorophyll fluorescence analysis. Plates containing 14 days old WT and the three lines of L1ko mutant plantlets were analyzed with increasing actinic light intensities. The non-photochemical quenching (NPQ), the quantum yield of PSII (ΦPSII) and the fraction of closed PSII reaction centers (1-qL), measured at the end of each light step of 1 minute, are shown in the graphs as a function of the light intensity. The WT is shown in black, while the L1ko lines in a gradient of blue. The measured points were fitted with a second degree polynomial function for NPQ, and a third degree polynomial for 1-qL. The points of ΦPSII, were interpolated with a local polynomial regression to visualize a continuous estimate of the standard error. The standard error of the interpolations is shown as a colored area around the curves (n=4).

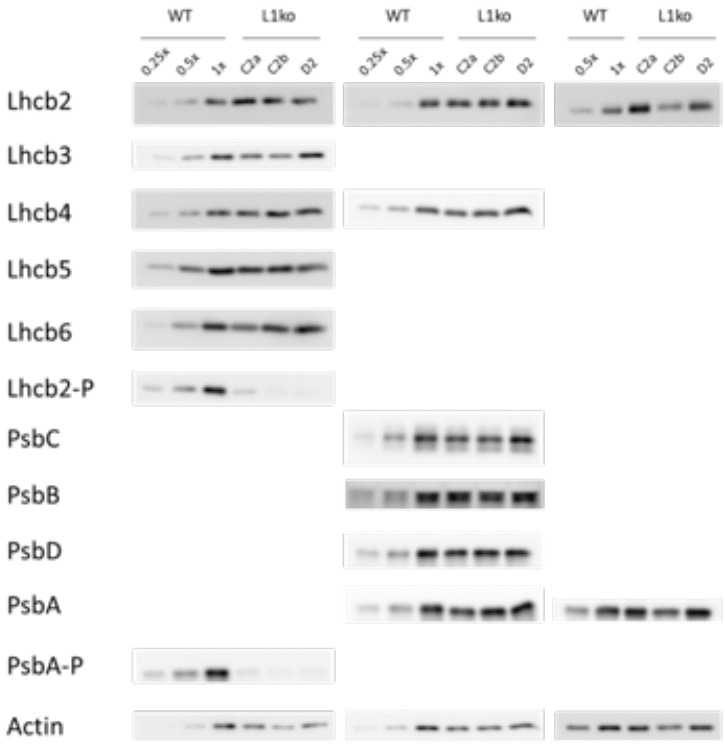

Figure S3a. Images of the immunoblot signals analyzed for Figure 3. The relevant protein is indicated in each row, each column represent an independent experiment and set of total protein extracts. WT 0.25x, 0.5x, 1x is the dilution scale used for the quantification of the protein based on signal intensity.

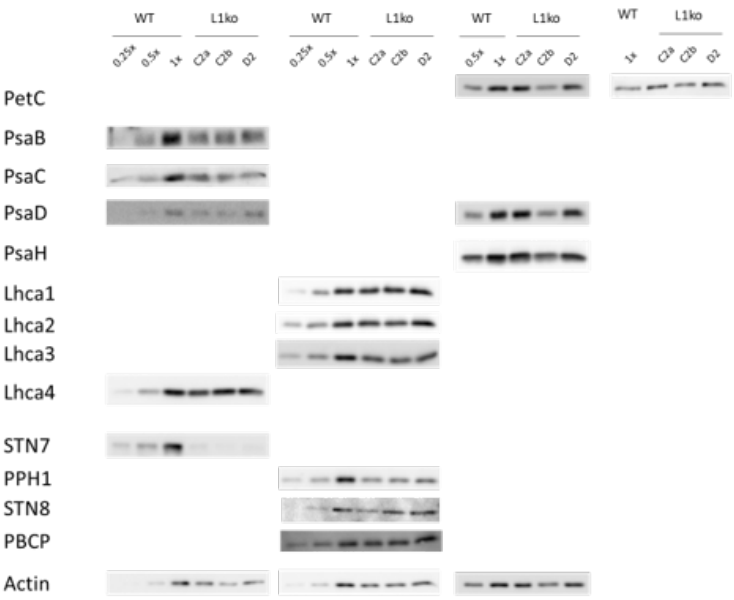

Figure S3b. Images of the immunoblot signals analyzed for Figure 3. The relevant protein is indicated in each row, each column represent an independent experiment and set of total protein extracts. WT 0.25x, 0.5x, 1x is the dilution scale used for the quantification of the protein based on signal intensity.

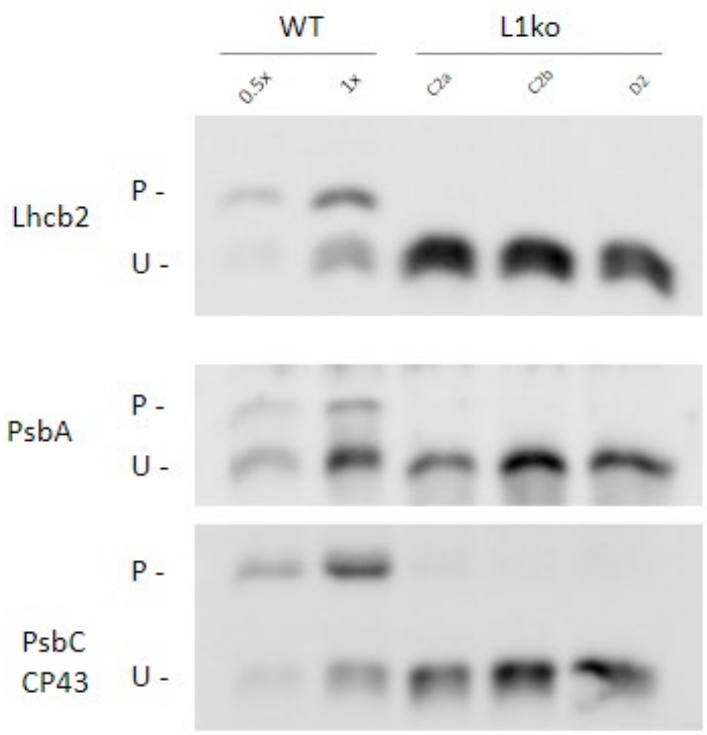

Figure S4. Phosphorylation of thylakoid proteins is altered in L1ko lines. Immunoblot of gels separated on a Phos-tag containing gel, separating the phosphorylated form (“P” band, above) from the unphosphorylated protein (“U” band, below). The detected protein is marked on the left, a dilution of the WT was used to assess if the signal was still detectable with 50% of the protein loading (0.5x).

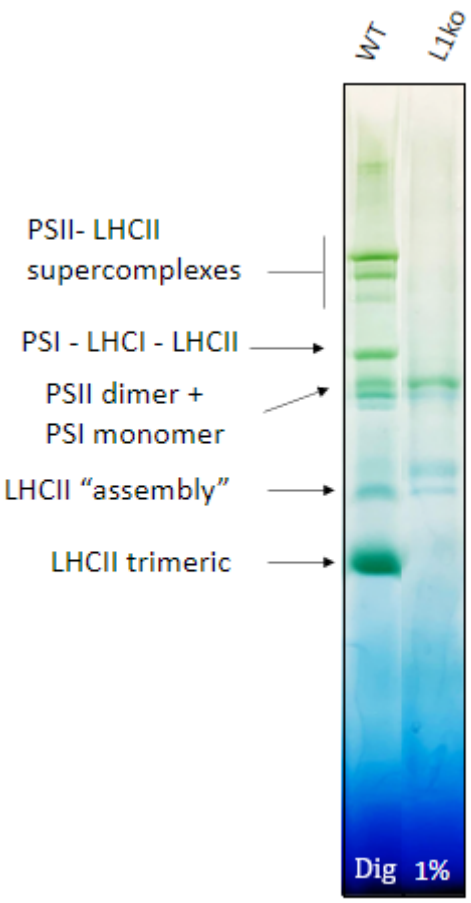

Figure S5. Mutation of LHCB1 affects the formation of supercomplexes and the LHCII trimerisation. A preparation of thylakoids from adult leaves of WT and L1ko plants was treated with 1% digitonin to solubilize the membrane and extract the photosynthetic complexes. The separation was performed in a blue native gel, the figure shows a representative lane of the two preparations. The supercomplexes were identified based on previous literature data and their position highlighted with an arrow.

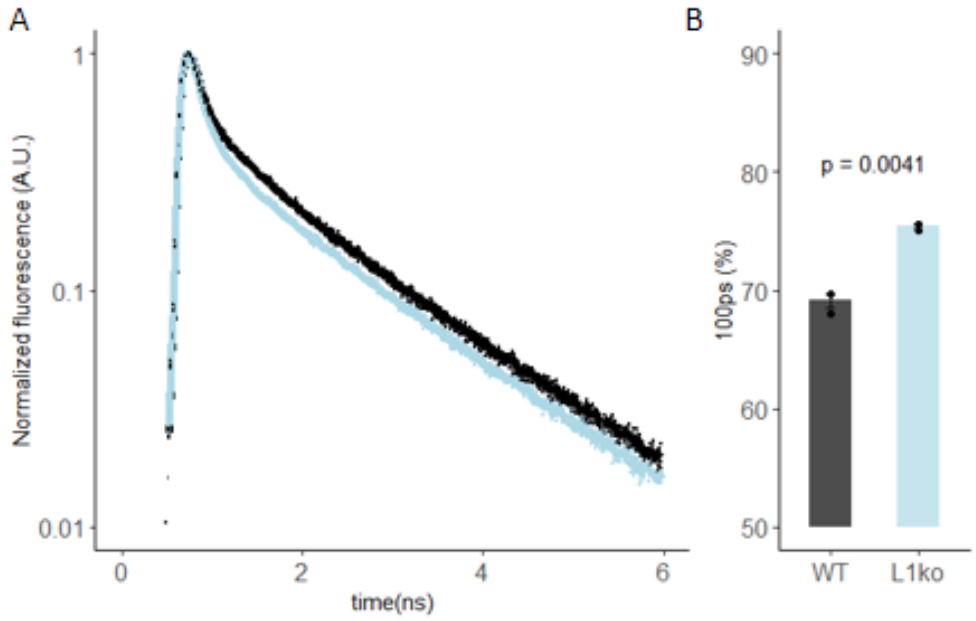

Figure S6. Fluorescence lifetime imaging microscopy (FLIM) for L1ko and WT. The FLIM measurement was performed on three individual leaves infiltrated with DCMU from adult plants of WT and L1ko, 116µm*116µm areas were measured. Sample were excited with 633 nm light (40 MHz rep. rate) and fluorescence emission was detected at 710-750 nm. A) Average fluorescence decay traces, with SD, from WT leaves WT (black) and L1ko (light blue). The decay traces were fitted with three exponentials (τ1 = 100ps (PSI) , τ1 = 900ps and τ1 = 2000ps (PSII)). B) Contribution of the fast (100ps) decay component in WT in the three measurement. The bar height shows the average contribution for each genotype and the error bar the SE. The 100ps contribution, was used for the calculation of the chlorophyll ratio of PSI/(PSI+PSII) shown in Figure 4 in the main text.

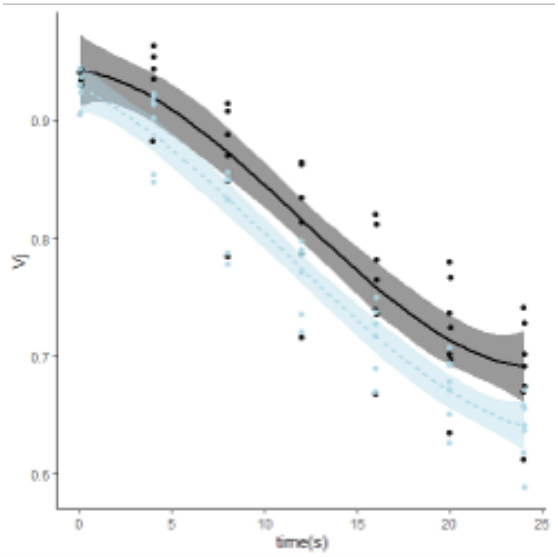

Figure S7. Rate of PQ oxidation in dark is similar in L1ko and WT lines. The redox state of the photoactive PQ was inferred from the fluorescence value measured at 3 ms during a 700 ms saturating pulse normalized over the maximal fluorescence (VJ), upon sequential incubations of the leaf samples in the dark for increasing time intervals (4-8-12-16-20 and 24 s). The points were fitted with a local regression algorithm based on a second degree function to visually represent the data distribution in function of the time with a continuous error estimate (black continuous line WT, gray line L1ko). The standard error of the interpolation is shown as a gray area around the curves.

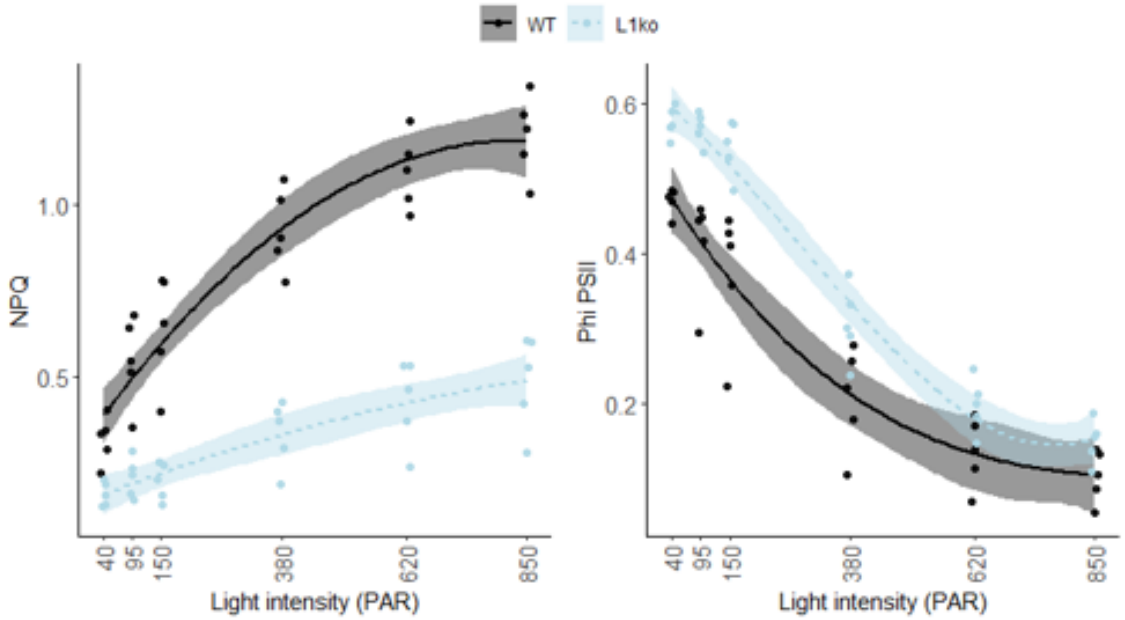

Figure S8. Measurement of non photochemical quenching (NPQ) and PSII quantum yield (Phi PSII) with a portable detector. The light curve in figure 4 was repeated with a handheld device (Multispeq v2) on the same 5 different plants. The NPQ and Phi PSII measured for each WT (black dots) and L1ko (Light blue dots) single leaves was plotted in function of the light intensity.The measured points were fitted with a second degree polynomial function for NPQ, and a third degree polynomial for ϕPSII to visually represent the data distribution and the standard error for WT (Black line and gray area) and L1ko (Blue dotted line and light blue area). Post-hoc analysis of the models for NPQ and ϕPSII show that there is a significant difference between L1ko and WT ($p<0.001$).

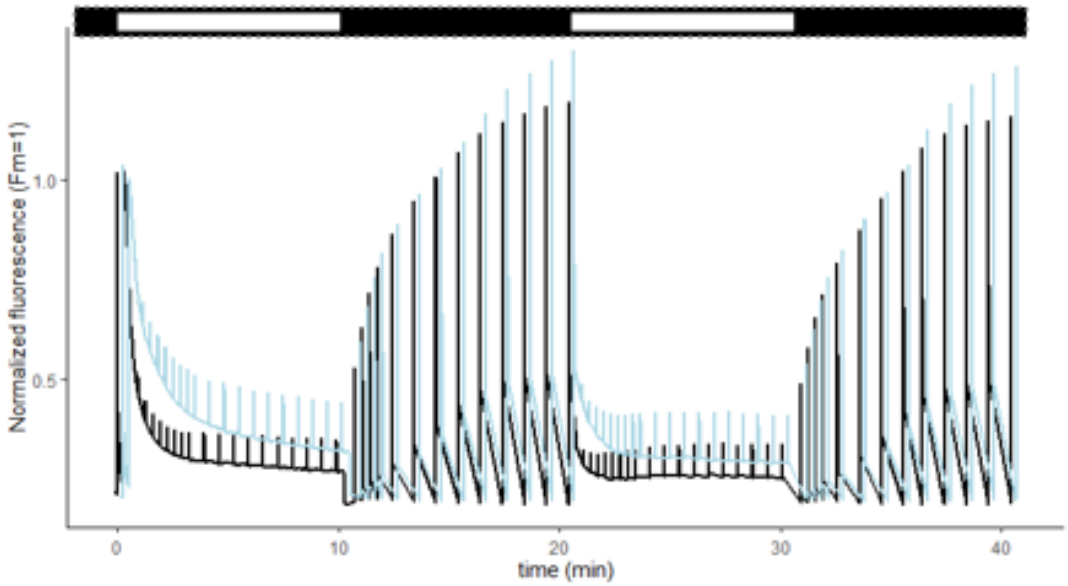

Figure S9. Chl a fluorescence traces used for the calculation of NPQ induction and relaxation shown in figure 5 normalized on the Fm value. Both light phases intensity is 1000 µmol photons m-2 s-1, measured in WT (Black line) and L1ko (Blue line) adult plants. The top bar shows the light exposition periods (white bars) and the dark relaxation (black bars). The lines correspond to the average Chl a fluorescence values from five biological replicates. The L1ko traces has been shifted forward of 30 seconds to allow the visualization of both traces on the same graph.

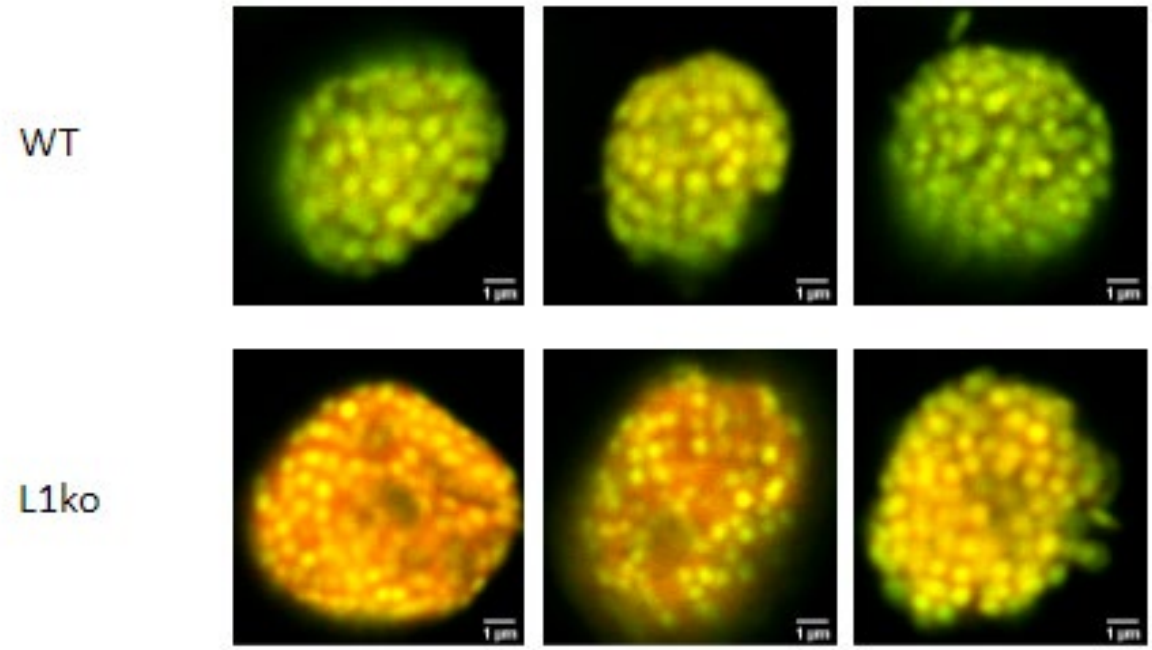

Figure S10. Images of the isolated chloroplast from WT and L1ko plants, acquired by confocal microscopy with an excitation at 633nm. The signal at 650-680nm is showed in green (PSII-maximum) while the signal at 710-750nm in red (PSI-maximum). Red channel intensity has been increased 10x in comparison to the green channel to compensate for decreased sensitivity of the detector and decreased fluorescence emission in the far-red region. Bar scale 1µm.

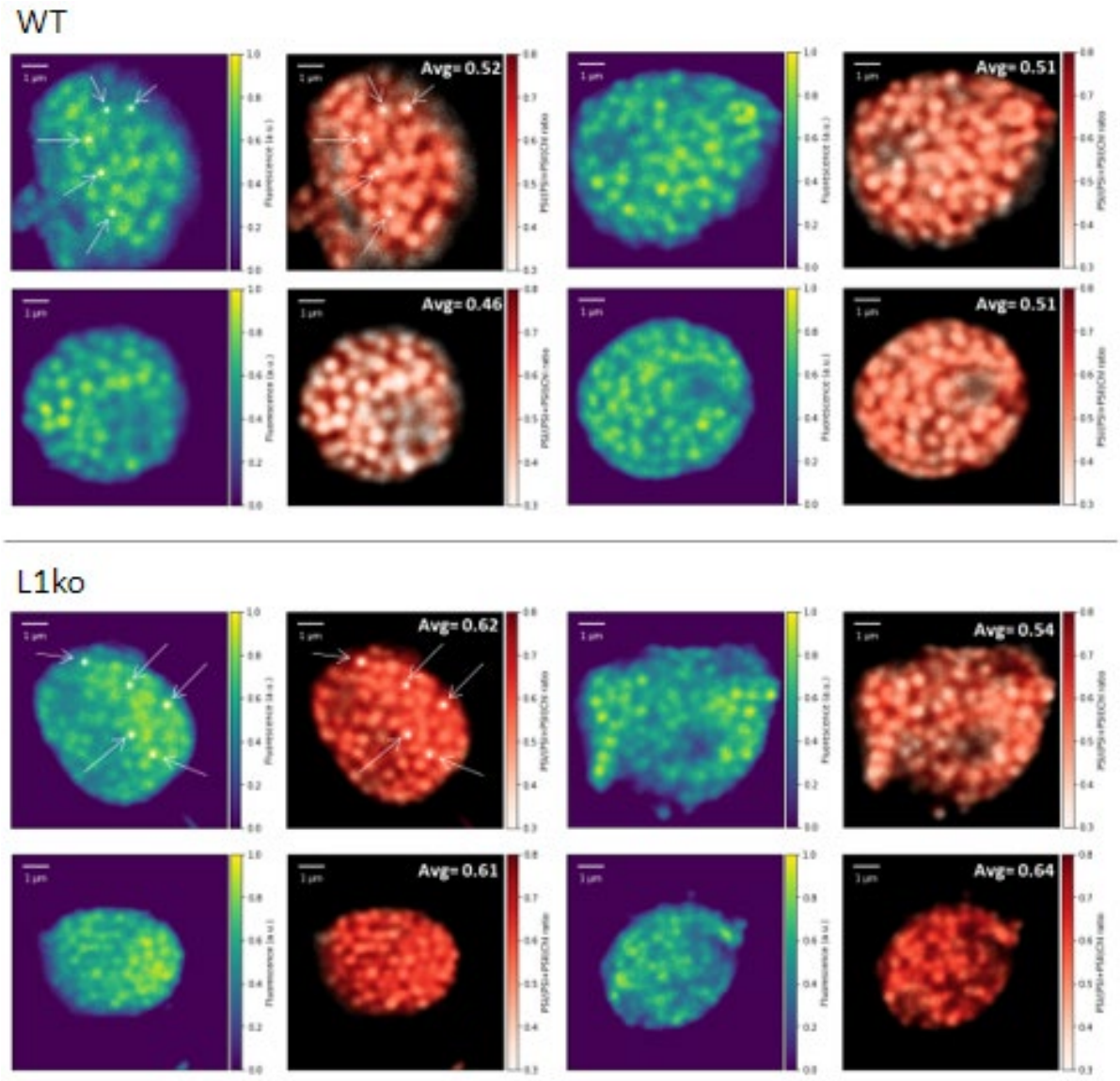

Figure S11. Fluorescence intensity and the PSI/(PSI+PSII) Chlorophyll ratio (calculated based on the FLIM measurements according to Wientjes et al. 2017) of isolated chloroplasts from WT and Lhcb1ko, incubated with DCMU. The images highlight the grana (lower PSI/(PSI+PSII)Chl ratios) and stromal (higher PSI/(PSI+PSII)Chl ratio) regions. As reference some of the grana are highlighted by an arrow and an asterisk in both the fluorescence intensity image and the PSI/(PSI+PSII) Chl ratio image. The overall PSI/(PSI+PSII)Chl ratio is higher in the WT compared to L1ko and the average ratios calculated, reported in the top right corner, correspond to the measurements made on intact leaves presented in Figure 4. Scale bar 1µm.

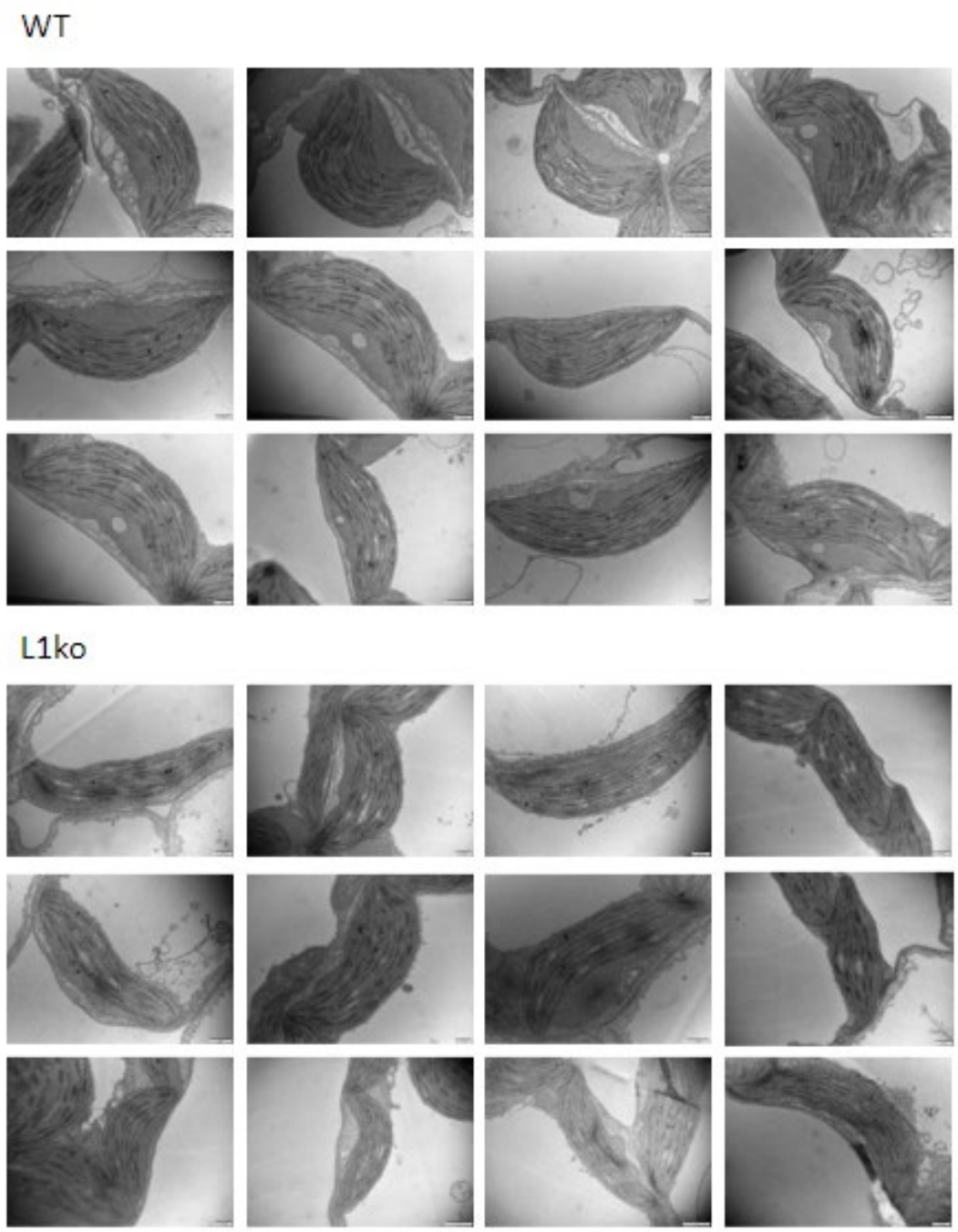

Figure S12. Collection of TEM images of chloroplasts observed in leaf sections of 15-days old WT and L1ko seedlings. The full set of collected images in the original resolution is available in the Zenodo repository (https://zenodo.org/record/5729177#.YaDZILrjKUk).

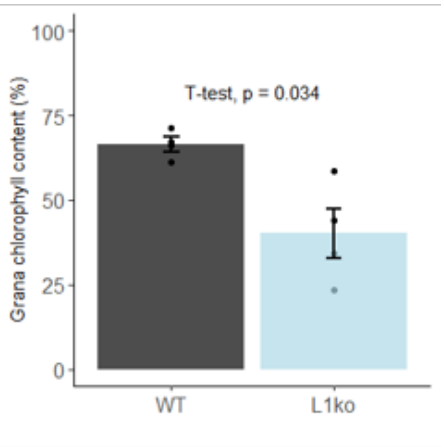

Figure S13. The chlorophyll repartition between grana and stroma lameallae is altered in L1ko line. Fraction of the chlorophyll contained in the grana stacks upon fractionation with 1% digitonin, the bar represent the average value for WT (black) and L1ko (Light blue), the error bars represent the standard error, the biological replicates (n=4) are plotted as individual points. The difference was tested by a t-test and the resulting p-value is displayed.

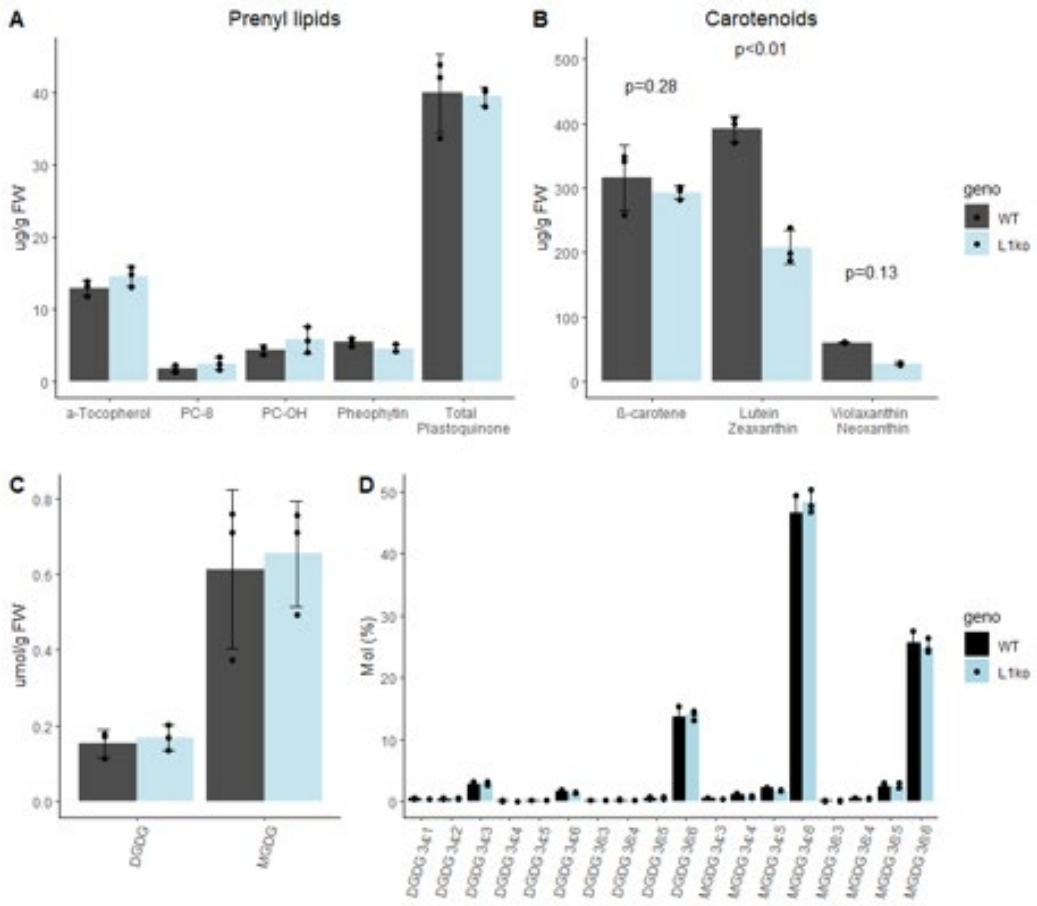

Figure S14. Effect of LHCB1 knockout mutation on lipid content. Samples were preparated from WT (Black) and L1ko (Light Blue) adult plants, and the result normalized on the FW used for the extraction. A) Quantification of prenyl-lipids, α - Tocopherol, Plastochromanol (PC-8), Hydroxyl-plastochromanol (PC-OH), Pheophytin and total Plastoquinone. B) Major carotenoids, β-carotene, Lutein and Zeaxanthin, and Violaxanthin with Neoxanthin. C) Galactolipids normalized on fresh weight combined in the classes digalagtosyl-diacyl glycerols (DGDG) and monogalactosyl diacyl glycerols (MGDG). D) detailed profile of the galactolipids divided by the saturation and lenght of the acyl chains. The bars show the average of three biological replicates, the error bars indicate the standard deviation of the mean. The p values in panel B derive from a Student's T-test.

Chapter IV

Role of LHCB2 phosphorylation in short- and long-term photosynthetic acclimation

Hamed Sattari Vayghan[1], Wojciech J. Nawrocki[2], Chen Hu[2], Roberta Croce[2], and Fiamma Longoni[1]*

[1]Laboratory of Plant Physiology, Institute of Biology, University of Neuchâtel, Neuchâtel, Switzerland.
[2]Department of Physics and Astronomy, Faculty of Science, VU Amsterdam, Netherlands

***Correspondence:** Fiamma Longoni, Fiamma.longoni@unine.ch, longonifiamm@gmail.com

The largest part of the light harvesting complex in higher plants is constituted by the trimeric protein complex Light harvesting complex II (LHCII). In *Arabidopsis thaliana*, three protein isoforms constitute these trimers: LHCB1, LHCB2 and LHCB3. The LHCB2 isoform has been shown to be essential for the dynamic association of LHCII trimer to photosystem I; a reversible process known as state transitions. This association is dependent on the phosphorylation of a threonine residue located in the N-terminal portion of the mature LHCB2 protein by the STN7 kinase. We generated a triple null mutant for the three Lhcb2 genes using CRISPR/Cas9. This line was complemented with recombinant forms of LHCB2 carrying a non-mutated line as control and point mutation to substitute the phosphorylated threonine with either a neutral amino acid, alanine, or a negatively charged amino acid, aspartate. This experimental system revealed that the complete removal of LHCB2 protein and substitution of its phosphorylation site by alanine or aspartate largely, but not completely, abolished the state transitions compared to non-mutated complemented line and the parental wild type plant. The absence of LHCB2 as well as the threonine substitutions decreased LHCII-PSI-LHCI
supercomplex formation slowing but not halting plant acclimation to fluctuating light. Our results show that only with the phospho-threonine group LHCB2 can fully accomplish state transitions and that the negative charge of the aspartate substitution is not sufficient for short-term photosynthetic acclimation. But in spite of its status as a conserved phospho-protein across higher plant lineages, LHCB2 is not required for long-term acclimation to fluctuating light.

Keywords: photosynthesis, light harvesting, LHCII, states transitions, NPQ, fluctuating light.

Introduction

Primary energy production to sustain life on Earth is largely fueled by photosynthesis (Galston, 1992; Janssen et al., 2014). The harvesting and conversion of the photon energy into chemical energy, via chlorophyll excitation, is a key step that allows this process to occur (Croce & van Amerongen, 2020). This process, at the interface between physics and biochemistry, is performed by a set of thylakoid membrane embedded pigment/protein complexes (J. D. Rochaix, 2011). The main pigment responsible for the light capture is chlorophyll (Chl). This pigment is highly abundant in photosynthetic organisms, and its role is central as it capable of undergoing charge separation, by donating an electron, when in an excited state (Park et al., 2019). This initial charge separation starts an electron transport chain spanning three different protein complexes: photosystem II (PSII), cytochrome b6f (Cyt b6f) and photosystem I (PSI)(J.-D. Rochaix, 2011). The electrons, obtained from the oxidation of water by PSII and flowing through plastoquinone (PQ), to the Cytb6f and PSI to be used, in the linear electron flow (LEF), for the reduction of NADP to NADPH (Kosourov et al., 2020) . Alternatively, from PSI the elections can be deviated by NDH (NADH dehydrogenase-like complex) or via a PGR5/PGRL1-dependent path back to the PQ pool (Ishikawa et al., 2016; Munekage et al., 2002), generating a cyclic electron flow (CEF) around PSI. CEF is required to regulate the ATP/NADPH ratio but has also a dynamic regulation that allows to optimize photosynthesis under unfavorable conditions (Ishikawa et al., 2016) . Inside the chloroplasts, all the photosynthetic complexes involved in the light dependent photosynthetic reactions are embedded in a membrane system called thylakoids (Friso et al., 2004). This membrane system is divided into two main domains: the grana stacks and the unstacked stroma lamellae. Due to the narrow gap between the appressed layers in grana stacks, almost exclusively LHCII, PSII and Cyt b6f are present in this region (Koochak et al., 2019). The not appressed part of the grana and the stroma lamellae embed also the PSI and the ATP synthase complexes. While PSII complexes are present mostly in the grana stacks, Cyt b6f is evenly distributed between these two thylakoid sub domains (Kirchhoff et al., 2017). The distribution of PSII and PSI in the thylakoids creates a topological separation of these two complexes, despite being functionally connected in the linear photosynthetic electron transport. Thus their activity requires to be coordinated by other actors in order to ensure the maximal photosynthetic efficiency in changing light conditions (Dekker & Boekema, 2005). One of the key complexes involved in this coordination is the Light Harvesting Complex II (LHCII). LHCII is a trimeric complex that is present in most photosynthetic eukaryotes, its appearance in the green lineage has been considered to have given the evolutive advantage to photosynthetic organisms to colonize terrestrial environments (Ballottari et al., 2012; van Amerongen & Croce, 2013). In most of the terrestrial higher plants, there are three main isoforms composing the LHCII trimer: LHCB1, LHCB2 and LHCB3. The core structure of these proteins is highly conserved across plant species and coordinates 8 molecules of Chl a and 6 molecules of Chl b along with a set of carotenoids that consists of two lutein, one 9'-cis neoxanthin and a violaxanthin molecules (Liu et al., 2004). This rich pigment repertoire allows these proteins to perform two main functions during the light-dependent phase of photosynthesis. The first one, is to extend the light capture ability of the photosystems (PSI and PSII) by connecting the Chls present in the LHCII trimer to those of the reaction centers (RCs) in a fashion that allows a rapid and highly efficient Chl to Chl excitation transfer (Caffarri et al., 2011; Croce, 2020). The second is to dissipate excess Chl excitation as heat. This process is an important part of the protective mechanisms collectively known as non-photochemical quenching (NPQ) and serves to protect the Chls of the reaction centers from over-excitation by transferring the Chl excitation energy towards accessory pigments (carotenoids), which have a much faster decay to the ground state by releasing thermal energy (Govindjee, 2002; Lauren Nicol et al., 2019). LHCB1 and LHCB2 are the products of multiple genes in higher plants. In *Arabidopsis thaliana* five genes encode quasi-identical LHCB1 proteins. Three genes code for LHCB2 and a single gene for Lhcb3 (Peter & Thornber, 1991; Wientjes et al., 2013). The most abundant isoform is LHCB1 constituting∼ 70% of the major LHCII, LHCB2 accounts for ∼20% and Lhcb3 for about 10% (Galka et al., 2012). The three isoforms composing LHCII have overlapping but distinct roles.

In Arabidopsis LHCB1 and LHCB" are both conditionally phosphorylated isoforms of major LHCII trimers. LHCB3 lacks an apparent phosphorylation site and is most likely involved in light energy transfer from the main LHCB1/LHCB2 antennae to the PSII core (Longoni & Goldschmidt-Clermont, 2021). LHCB2 has been found to be crucial for state transitions and it is almost completely in the phosphorylated form when present in a stable complex with PSI, the so-called state transitions complex (Longoni et al., 2015).
To gain a better understanding of the specific role of the LHCB2 isoform, beside the state transitions, we generated triple null mutants line using CRISPR/Cas9 in a T-DNA insertional line. A stable 3XL2KO null line was complemented with T-DNA constructs carrying a heterologous LHCB2 gene coding for the wild type LHCB2 with the phosphorylable threonine residue, or with an alanine or aspartate substitution of this threonine residue. These lines were used to investigate the role of LHCB2 phosphorylation in photosynthetic acclimation and complex organisation.

Materials and methods

Plant growth and stress conditions

The seeds were germinated on ½ Murashige-Skoog agar plates, grown under white light LEDs at an intensity of 120 µmol photons $m^{-2}s^{-1}$PAR with a 12/12-h-light/dark photoperiod in a climate chamber set at 22°C and 65% RH (ARALAB FitoClima 600 PL), thereafter referred to as "standard light condition". For the short-term fluctuating light experiments, seedlings were transferred after 2 days germination under constant light (120 µmol photons $m^{-2}s^{-1}$PAR 12/12-h-light/dark cycle) described above to the fluctuating light (4 min 50 µmol s^{-1} m^{-2} and 1 min 500 µmol s^{-1} m^{-2} 12/12-h-light/dark cycle) under custom LED panels (PHYTOTRONIC EVO Future LED) while the control seedlings were kept under normal light for 5 more days. For the long-term fluctuating light experiment seedlings, after 2 days germination on agar plate under standard light condition, were transferred to soil. One tray was kept under standard light condition and the second one was transferred to the fluctuating regime described above for 24 days. For chlorophyll measurements of each genotype, we used 14-day-old seedlings grown under standard light conditions. After recording fresh weight, the seedlings were flash frozen in liquid nitrogen. The frozen plants tissues were ground to fine powder using glass beads, mixing in an Ivoclar Vivadent shaker (Silamat) two times for 10 s. Extraction buffer (80% acetone buffered with Tris-HCl pH 7.4) was used to extract pigments. Chlorophyll a and b concentration were measured by multi-wavelength absorbance according to (Porra, 2002).

Engineering of Lhcb2 null lines and complementation

For the production of LHCB2 triple null lines we used an insertional mutant line for Lhcb2.1 from the SALK collection (SALK_005774C) as the genetic background. This insertional line was transformed with the binary vector containing the Cas9 gene under the control of the synthetic EC1 promoter described in (Xing et al., 2014) in which we inserted two sgRNAs (GGATTGTTGGATAGCTGATG for Lhcb2.2 (At2G05070) and GATGCGGCCACCGCCATTGG for Lhcb2.3 (At3g27690) under the control of the U6 promoter (Figure 1B). The transformants were selected on ½ MS plates containing hygromycin (33 µg ml^{-1}). Among the resistant plantlets those showing a slower fluorescence decrease upon state 1 to state 2 transition were selected and further analysed by immunodetection to confirm the decrease or the absence of the LHCB2 protein (for details of the immunodetection technique see below). The lines without detectable LHCB2 protein were then counter selected on hygromycin (*i.e.,* the hygromycin sensitive plants were selected), and screened by PCR, to confirm the loss of the T-DNA cassette together with the Cas9 gene (Table S1). For the complementation of the mutation, a line negative for Cas9 PCR amplification but showing no LHCB2 protein signal was used. This line will be referred to as 3XL2KO. All the amplifications for the cloning were performed with Q5® High-Fidelity DNA Polymerase (NEB).

The Lhcb2.2 gene, including the putative promoter and terminator, was amplified in two PCR fragments from the genomic DNA of Arabidopsis to insert a single HA sequence at the C-terminus of the protein. The two fragments were fused by overlapping extension PCR using the two external primers (L22HA_FRAG 1_For and L22HA_FRAG 2_Rev), thus producing the synthetic L22HA gene.
After 10 cycles of amplification with the GoTaq® DNA Polymerase (Promega) to add the terminal A to the amplicon, the PCR product was inserted into the cloning vector pTOPO-TA using the TOPO PCR Cloning kit (ThermoFischer Scientific). The sequence was verified by sequencing using the M13 primers (Microsynth), and cloned in the pCAMBIA 3300 vector (CAMBIA, Australia) using the *Hind*III and *Xba*I restriction sites, generating the pCAMBIA3300-L22HA vector. The mutations to change the codon for the threonine to alanine and aspartate were introduced by amplification of the pCAMBIA3300-L22HA fragment containing the L22HA gene in two fragments overlapping on the mutation site. The primers used (detailed in the supplementary table), allowed to re-insert the amplicon in the pCAMBIA3300 vector using *Xba*I and *Afl*II restriction sites to generate the pCAMBIA3300-L22HA-A and pCAMBIA3300-L22HA-D coding for an alanine and an aspartate in place of the threonine, respectively. The three constructs were verified by sequencing (Microsynth) and used for the transformation of the 3xL2KO mutant by floral dip(Clough & Bent, 1998).
The complemented lines were selected on glyphosate (30 mg ml^{-1}) and the resistant further analysed by western blot to assess the accumulation of the heterologous protein. The complemented lines showing a level of expression comparable to that of the WT were used for the subsequent analyses.

Thylakoid isolation and solubilisation

The organization of the photosynthetic complexes embedded in the thylakoid membrane was investigated by Blue Native (BN)–PAGE. Thylakoids were isolated from 4 weeks old rosettes acclimated to standard light condition with a 12/12-h-light/dark photoperiod (120 µmol photons m^{-2} s^{-1})(Arnold et al., 2014). Before extracting thylakoid in state 1 plants were acclimated to (30' Far-Red 40 µE) prior to state 2 (30' blue light 40 µE). Intact isolated thylakoids content was normalised based on chlorophyll (Chl) concentration to 1 µg/µl. Isolated thylakoid membranes were solubilized with 1%, 0.5% (w/v) Water-Soluble Digitonin or 1 % (w/v) α -dodecyl maltoside (α-DM) as previously described (Järvi et al., 2011). The complex separation was performed on SERVAGel™ N 3–12, Vertical Native Gels (Serva).

Protein Analysis and Immunodetection

After 14 days of growth on ½ Murashige-Skoog agar plates, total fresh weight of three plantlets per tube was recorded and plantlets immediately immersed in liquid nitrogen. Protein extraction was performed as previously described in (Sattari Vayghan et al., 2022). To study protein phosphorylation 30 µM Phos-tag™ Acrylamide (Wako) and 60 µM of divalent metal MnCl2 were added to a 12% polyacrylamide gel. For immuno-detection, proteins from the polyacrylamide gel were transferred to a nitrocellulose membrane. The membranes were stained with amidoblack as a loading control and incubated with the following blocking solution, TBS Tween (0.05%), skim-milk 5% for the detection with LHCB1 (AS09 522), LHCB1-P (AS13 2704), LHCB2 (AS01 003), LHCB2-P (AS13 2705), LHCB3 (AS01 002), LHCB4 (CP29) (AS04 045), LHCB5 (CP26) (AS01 009), LHCB6 (CP24) (AS04 010), LHCA1 (AS01 005), LHCA2 (AS01 006), LHCA3 (AS01 007), LHCA4 (AS01 008),STN7 (AS16 4098), PPH1 (AS16 4084) and anti HA (BioLegend 901513). The membranes were blocked for at least two hours before incubation with primary antibodies to probe targeted proteins. After primary antibody incubation the membranes were washed three times in TBS-Tween (0.01%) and then incubated with a (HRP)-conjugated secondary antibody (anti-rabbit (Merck, AP132P) or anti-mouse (Sigma, A5278) depending on the primary antibody's origin). After one hour of incubation in the secondary antibody and three washes, the membranes were soaked with enhanced chemiluminescence (ECL) reagents for HRP and signals recorded using a chemiluminescence imager (Amersham Imager 600, Amersham Biosciences, Inc.).

Chlorophyll Fluorescence Analyses

Room temperature Chlorophyll a fluorescence was measured using MF800 Fluorcam (Photon System Instrument). Different personalised protocols were applied as described in (Pralon et al., 2020). State transitions were measured using a MF800 Fluorcam (Photon System Instrument) essentially based on (Kramer et al., 2004) , using dark incubated plants (30 minutes).
Maximum fluorescence (Fm) in dark adapted plants was measured, then the plants were illuminated with red light (25 µmol photons m^{-2} s^{-1}) in order to induce State 2, far red (FR) light was added in the subsequent illumination step to induce State 1. Illumination used to induce either state lasted for 10 minutes and at the end of each a short saturating pulse (500 ms) was applied during which the maximal fluorescence was recorded. The values were used to calculate qT as (FmSt1-FmSt2)/FmSt1.
NPQ induction and relaxation was measured using a protocol adapted from (L. Nicol et al., 2019). Briefly, after 60 minutes of dark acclimation, plants were exposed to actinic light for 10 mins (1,000 µmol photons m^{-2} s^{-1} composed of 837 µmol photons m–2 s–1 470 nm blue combined with and 165 µmol photons m^{-2} s^{-1} 600 nm red light). For NPQ relaxation of the actinic light was turned off and the fluorescence measured for 10 minutes. Then the light and dark steps were repeated a second time. During both light and dark steps, the maximal fluorescence was measured with saturating light pulses (500 ms, 100% intensity) every 20s.
PSII functional antenna size was calculated using fluorescence induction beginning with dark adapted plants measurements with low light intensity on DCMU [3-(3,4-dichlorophenyl)-1,1-dimethylurea]-infiltrated leaves according to (L. Nicol et al., 2019). Considering the QA site blocking effect of DCMU, upon dark adapted plants illumination the rise of the fluorescence maximum (FM) represents a single, stable charge separation in PSII, the rate of the latter being directly proportional to the PSII absorption cross-section at a given light intensity. Maximal initial rate of PSII (when all PSIIs are open) is calculated from integrated area above the induction curves (Govindjee & Papageorgiou, 2004).

Results

Engineering of LHCB2 null mutant and its complementation.

Triple null mutants for Lhcb2 genes were obtained by CRISPR-Cas9 using two artificial gRNAs targeting Lhcb2.2 (AT2G05070) and Lhcb2.3 (AT3G27690) on the Lhcb2.1 (AT2G05100) T-DNA insertion mutant (Figure 1A, B). The mutations induced by the Cas9 endonuclease resulted in frameshifts that completely abolished the production of LHCB2 in the Lhcb2.1 T-DNA mutant background. Consequently, the LHCB2 isoform was no longer detectable by immunoblot (Figure 1C). The triple null mutant will be referred to as 3XL2KO. 3XL2KO was complemented separately with T-DNA constructs encoding either wild type (T-T line), T to A (T-A lines) or T to D (T-D lines) forms of a C-terminally HA-tagged Lhcb2.2 gene. The complemented 3XL2KO lines, regardless of the presence of the native threonine or an amino acid substitution, accumulated the HA-tagged form of Lhcb2.2 to levels similar to LHCB2 in the wild type when analysed by anti-HA western blotting (Figure 1C).
The T to D mutation changes the charge at the N-terminus of the mature protein affecting the epitope recognition by the anti-Lhcb2 antibody. A similar phenomenon has been observed when the threonine residue is phosphorylated (Longoni et al., 2015) . Therefore, the anti LHCB2 antibody was not suitable to compare the LHCB2 protein level between the complemented lines. The loss of LHCB2 in 3XL2KO did not result in any visible phenotype, nor did its complementation with either wild type or the mutated versions of the LHCB2 protein. Neither the total Chl nor the Chl a/b ratio were altered in 3XL2KO (Supplementary Figure S1). The lack of a visible phenotype prompted us to investigate whether the mechanisms of the photosynthetic acclimation in the triple knock-out mutant or the complemented lines were affected.

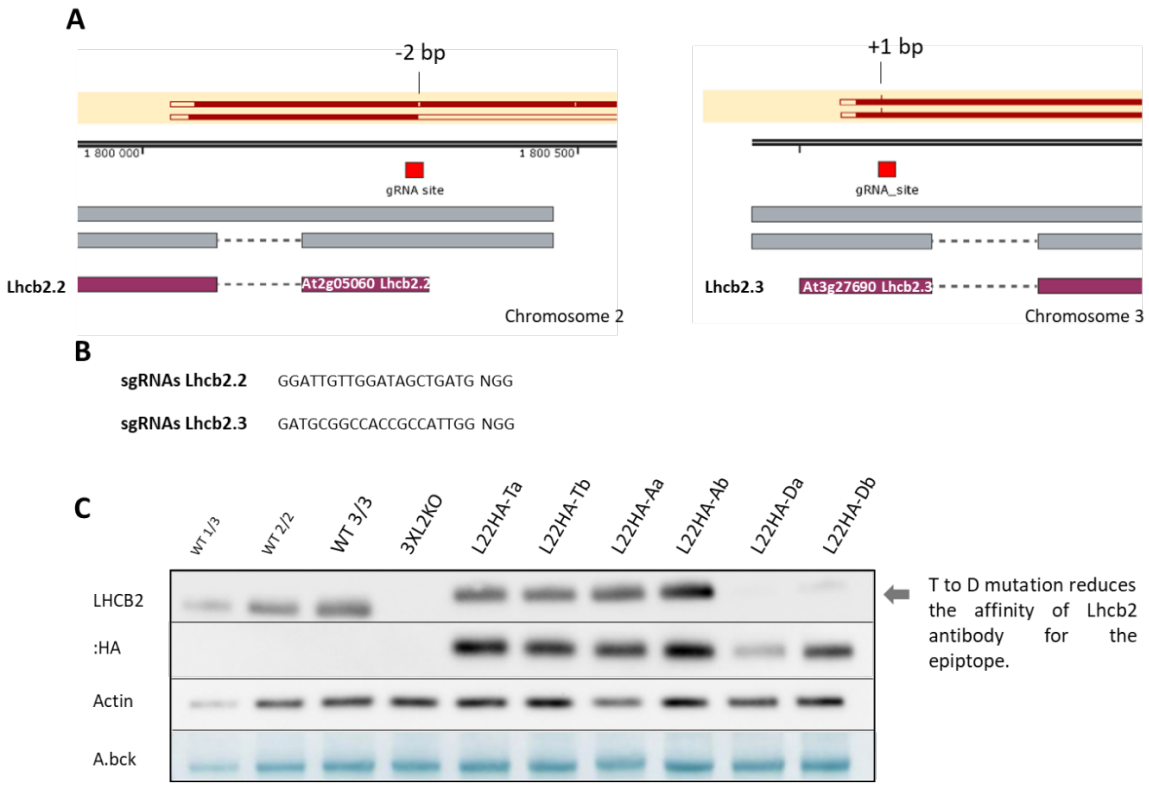

FIGURE 1| Engineering of null mutant lines for the three genes encoding LHCB2 and complementation with tagged versions of Lhcb2.2. A) Schematic representation of the Lhcb2.2 and Lhcb2.3 genes, the region targeted by the guide RNAs is highlighted in red. B) sequence of the two gRNAs. C) A representative immunoblots of total protein extracts from WT, 3XL2KO mutant and the 3XL2KO complemented lines with a C-terminal HA-tagged version of the wild type LHCB2 protein (L22HA-T (threonine)) or with a mutated version in which the phosphorylated threonine is mutated to alanine (L22HA-A) or aspartate (L22HA-D). The membrane was decorated with anti-LHCB2 antibody, anti-HA antibody recognizing the C-terminal tag present in the complemented lines. Actin antibody signal and amidoblack staining are shown as loading controls.

Mutation of Lhcb2 affects photosynthetic acclimation

The signature acclimation process in which LHCB2 is involved is state transitions (Crepin & Caffarri, 2015; Longoni et al., 2015; Malgorzata Pietrzykowska et al., 2014). Room temperature Chl a fluorescence was used to follow the acclimation of the mutant line 3XL2KO, and the derived complemented lines upon changes in the light spectrum inducing state transitions. These lines were compared with *stn7*, a mutant of the STN7 kinase, which is responsible for LHCII phosphorylation as well as state transitions (Bellafiore et al., 2005). Under normal growth conditions WT, 3XL2KO, derived complemented lines and *stn7* did not show any visible phenotype (Supplementary Figure S1), and the maximum quantum yield of PSII (Qy max) was unaltered. All of the tested lines had an average Fv/Fm value of ~0.80, which is the standard quantum yield expected for a healthy and not-stressed wild type plant (Maxwell & Johnson, 2000)(Figure 2A). The photosynthetic performance was measured by room temperature fluorescence upon shifts of the light spectrum inducing the so called State 1 and State 2. The steady state fluorescence was higher in the triple null mutant 3XL2KO as in the T-A and T-D lines (Figure 2B). Focusing on the State 1 to State 2 transition (Figure 2C) we observed that the fluorescence quenching was less pronounced in the 3XL2KO, T-A and T-D lines compared to WT and T-T lines, with potentially an even higher trace for T-A and T-D lines compared to 3XL2KO. The saturating pulses were used to calculate the quantum yield of PSII (ΦPSII) and the state transition related quenching (qT). Triple LHCB2 null mutation (3XL2KO) had a minimal impact on ΦPSII in both State 2 and State 1 lights (Figure 2D).

The mutation of the threonine residue to aspartate (T-D) or alanine (T-A) had a slightly larger effect, in terms ΦPSII of reduction, than knocking out LHCB2. However, none of the LHCB2 mutant lines were comparable to *stn7*, which had a lower ΦPSII in both State 1 and State 2 conditions (Figure 2D).
The state transitions related quenching was measured by room temperature fluorescence. The results (Figure 2E) showed that the 3XL2KO null mutation does not entirely inhibit state transitions as compared to the *stn7* mutant. In fact, the average calculated qT for the WT was 6.1% ± 0.3% while for 3XL2KO was 3% ± 0.4%. In comparison, the *stn7* mutant qT was 0.3% ± 0.2%. Complementation of 3XL2KO mutant with the HA-tagged version of LHCB2, in which the threonine of the phosphorylation site is maintained (T-T lines), restored the state transitions to WT levels (qT (5.8% ± 0.2%, 5.7%± 0.3%). Conversely, in the complemented T-A and T-D lines, the extent of state transitions was as low as in 3XL2KO (2.7% ± 0.3%, 2.2% ± 0.3% for T-A and 2.7% ± 0.4%,2.9% ± 0.5%, for T-D). The extent of state transitions was thus seemingly not affected by the charge of the amino acid used to substitute the threonine at the LHCB2 phosphorylation site.

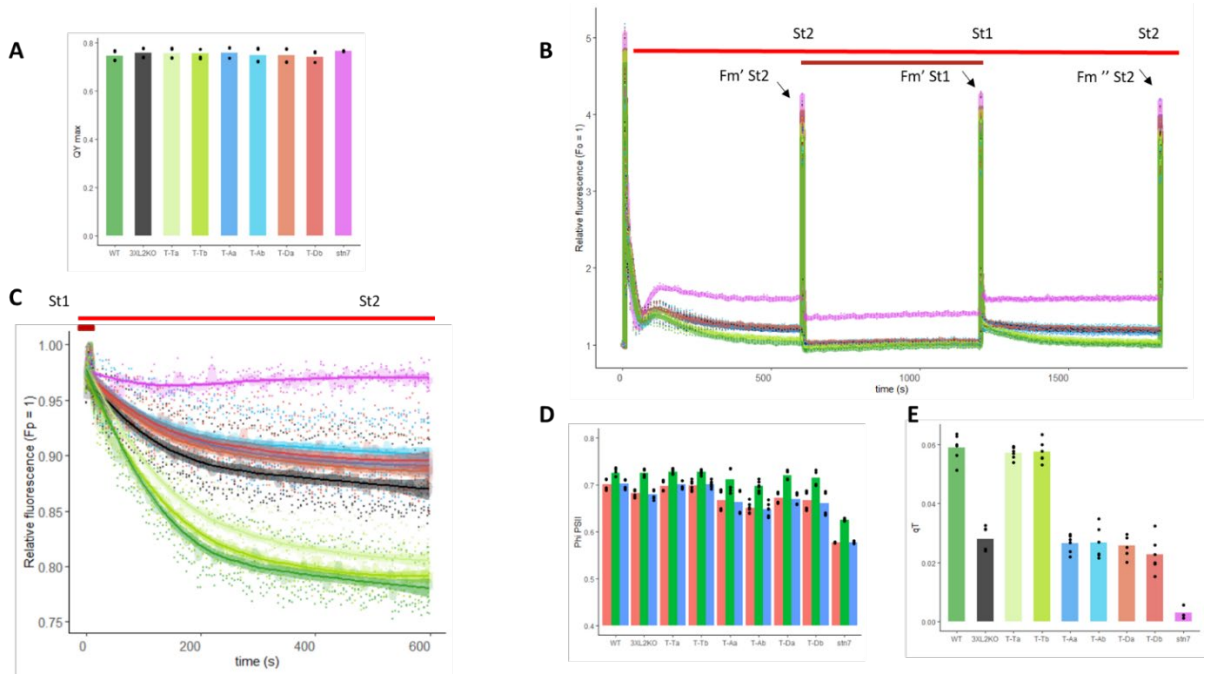

Figure 2| Loss of Lhcb2 or mutation of the threonine of the LHCB2 phosphorylation site impairs state transitions. A) Comparison of the maximum quantum yield of photosystem II (Fv/Fm = (Fm-F0)/Fm)) for the WT and the mutant lines. B) Fluorescence traces during state 2 to state 1 transitions and back induced by changing the light spectrum from red light to red + far-red as marked by the traits above the graph. C) Detail of the fluorescence traces during the State 1 to state 2 shift induced by red light normalized over the Fluorescence peak at the beginning of the state 2 light. The bars and curves are average of three replicates on a set of adult plant for each genotype. D) Comparison of the quantum yield of PSII Y (II): (Fm'-Ft)/Fm' at the end of the State 2, State 1 and the second State 2 phase. E) calculated qT= (FmSt1-FmST2)/Fm.

State transitions is an important mechanism at low light intensity, but its contribution is negligible in Arabidopsis under higher light intensities (Mullineaux & Emlyn-Jones, 2005). Hence, we analysed the NPQ induction and relaxation kinetics upon exposure to high light intensity comparing WT, 3XL2KO and the complemented LHCB2 lines. We observed that the two independent T-T complemented lines behaved like the WT control both in terms of induction and relaxation of the NPQ. 3XL2KO, T-A and T-D mutants had a tendency to show higher induction of NPQ compared to the WT, a phenomenon that is even more pronounced in the *stn7* mutant. No difference was observed in the relaxation phase, and all line behaved like WT and rapidly dissipated NPQ (Figure 4).

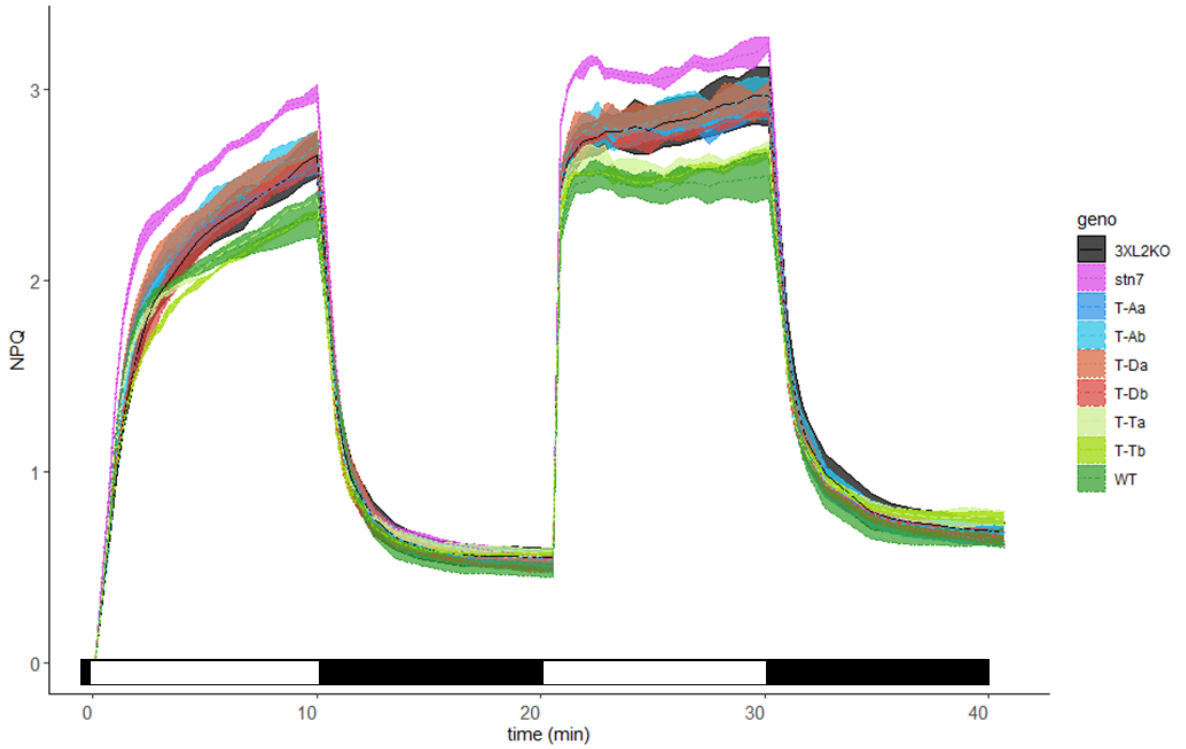

Figure 4| Induction and relaxation of the NPQ in WT and LHCB2 mutant lines. Calculated non-Photochemical Quenching (NPQ) = (Fm-Fm') /Fm'. is shown for each line (WT- dark green line, T-T light green, T-A blue, T-D red, stn7 violet). The line shows the average value of three biological replicates, and the area the standard deviation. The bar below shows in white the NPQ induction phase (1000 µmol photons m^{-2} s^{-1}) and in black the relaxation phase in the dark.

LHCII related proteins show minor changes in LHCB2 mutants.

The changes in the accumulation of the antenna proteins composing the LHCII and LHCI antenna complexes, were estimated by immunodetection. 3XL2KO as well as T-A and T-D lines only had a minor impact on the accumulation of other antenna proteins. A detectable change in the protein size was observed in complemented lines in which the phosphorylated threonine was replaced by alanine or aspartate due to the HA Tag fused to the C-terminal of protein. The other trimeric LHCII major antenna subunits (LHCB1 and LHCB3) did not show a significant increase in any of the lines and the accumulation of the minor antennae (LHCB4, LHCB5, LHCB6) was not affected either (Figure 5A). Despite the similar accumulation of LHCB1 its phosphorylation level, assessed by P-LHCB1 antibody, revealed an increase in 3XL2KO and the T-A and T-D lines, while in T-T lines the phosphorylated LHCB1 accumulation was close to WT. The T-A and T-D point mutations supress LHCB2 phosphorylation, which was clearly demonstrated with the P-LHCB2 antibody (Figure 5 B). As for the subunits of LHCI antenna, we could not detect a significant difference in (LHCA1, LHCA2, LHCA3 and LHCA4) (Figure 5C). Considering that the phosphorylation of LHCB1 in 3XL2KO and T-A, T-D lines was higher, we assessed the accumulation of the relevant kinase (STN7) and phosphatase (TAP38/PPH1). The accumulation of STN7 was higher in 3XL2KO and in the T-A and T-D lines compared to the WT. The same was observed for the phosphatase TAP38/PPH1 (Figure 5D). To confirm that the T-A and T-D lines had no other phosphorylation sites, and that LHCB1 was more phosphorylated in the 3XL2KO line as well as in T-A and T-D lines compared to the WT and T-T lines, we used Phos-tag containing gels to separate the phosphorylated form from the unphosphorylated protein. The following detection with anti-LHCB1 antibody and anti-HA for the recombinant LHCB2 allowed to detect the increased phosphorylation of LHCB1 in 3XL2KO, T-A, and T-D lines, as well as the absence of any phosphorylated bands for HA-tagged LHCB2 in T-A and T-D lines, while it was normally phosphorylated in the T-T lines (Figure 5 E, F).

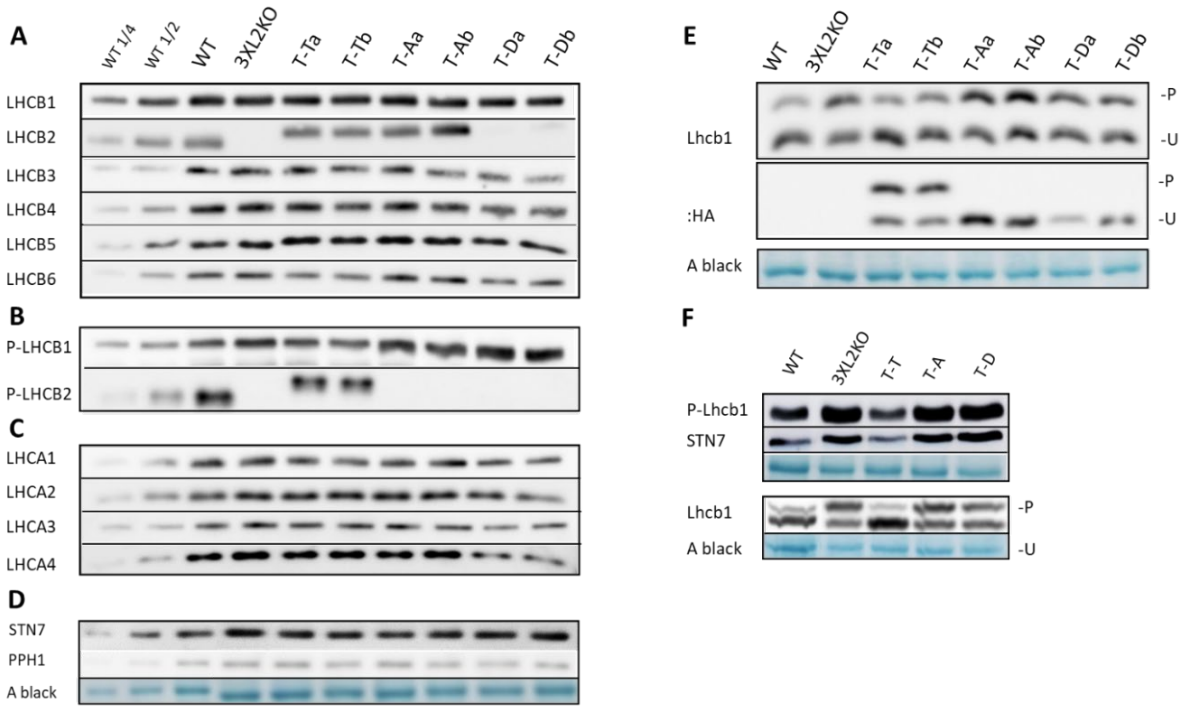

Figure 5|Representative immunodetection signal of the antenna proteins and antenna related kinase and phosphatases. Total protein extract of WT, 3XL2KO and 2 independent lines for each of 3 complemented lines (T-Ta-T-Tb; T-Aa T-Ab; T-Da-T-Db) were subjected to SDS-PAGE and immunoblotting. Fourteen -days-old seedlings were used to extract the protein. A) antisera against major and minor antenna of LHCII, B) antisera against phosphorylated form of LHCB1 and LHCB2, C) antisera against subunits of PSI antenna (LHCI), D) antisera against kinases STN7 and phosphatase PPH1 mainly involved in the regulation of the phosphorylation of LHCII and PSII. E, F) Phos-tag PAGE and immunoblot analysis, using antibody against LHCB1 and HA. The increase of the LHCB1 phosphorylation correlates with an increased accumulation of the STN7 kinase.

Supercomplex organisation in Lhcb2 mutated lines

Despite the marginal changes observed in the accumulation of the other antenna proteins, the mutation of LHCB2 resulted in an increased phosphorylation of the major LHCII subunit LHCB1. Changes in LHCII phosphorylation level may affect the structure and organization of the photosynthetic supercomplexes, this promoted us to analyse the supercomplex distribution and abundance using blue native PAGE (BN-PAGE) (Figure 6 A, B). The analysis was performed in plants acclimated to state 2 (30' blue light 40uE) or state 1 (30' Far-Red 40uE). The acclimation to state 2 and state 1 was confirmed by the analysis of LHCB1 phosphorylation, which is expected to be phosphorylated in state 2 and non-phosphorylated in state 1 (Longoni et al., 2015). Consistently, the phosphorylation status of LHCB1 changed in all the tested lines, including the 3XL2KO mutant and all the complemented lines (Figure 6 C, D). We used two detergents to have a more comprehensive view of the super complexes: Digitonin, that solubilizes mostly the stroma lamellae complexes, and alpha-DM, which solubilizes also the complexes present in the grana stacks (Ferroni et al., 2016; Järvi et al., 2011).
The LHCII-PSI-LHCI supercomplex, present in the WT only in State 2, was absent in the 3XL2KO mutant acclimated to state 2. The complementation of 3XL2KO with the native form of LHCB2 (T-T lines) resulted in the formation of this complex to WT level in State 2 only. In T-A and T-D lines the LHCII-PSI-LHCI complex was lost, in both State 1 and State 2 light. On the other hand, the separation of the other supercomplexes, and notably those resolved after solubilisation with alpha DM, did not show any major difference between the WT and the mutant lines (Figure 6 A, B).

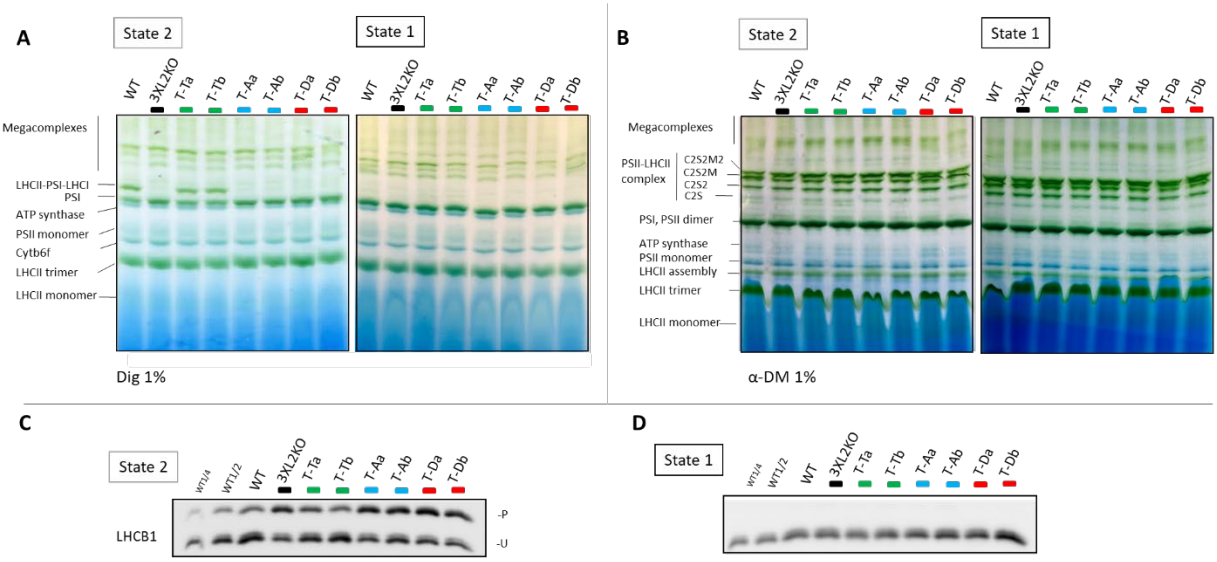

Figure 6 |BN-PAGE analyses of Arabidopsis thylakoid membrane protein complexes. 16 µg of chlorophyll of WT, (3XL2KO), mutants (L2.2: HA Threonine T_>T, L2.2: HA T_>A (Alanine), L2.2: HA. T_>D (Aspartate) thylakoid membrane subjected to state 2 and state 1 light were loaded. B) Thylakoid supercomplexes solubilized by 1% digitonin and C) 1% alpha-DM. C, D) The state transition was confirmed by the analysis of the phosphorylation level of Lhcb1.

Functional antenna size in state 1 and PSI/PSII reaction centres

To understand whether the observed changes in LHCII phosphorylation and the mutation of LHCB2 had an effect on the antenna association to the reaction centres, we performed an analysis of the maximal photochemical rate per reaction centre. The photochemical rate is expected to be higher if each reaction centre is connected to a larger antenna system. The analysis of PSII photochemical rate was conducted at 80 µmol photons m^{-2} s^{-1} light, measuring both the fluorescence rise and the ECS change upon induction. The resulting values are similar for the two measurements, confirming the validity of the approach. 3XL2KO, T-A and T-D had no impact on the photochemical rate of the PSII (Figure 7B). The photochemical rate of PSI was also measured by ECS at the same light intensity, as for the PSII, the resulting photochemical rate was identical for the WT and the mutant lines. Identical photochemical rates indicate that the WT and the LHCB2 null mutant and complemented lines have a similar number of chlorophylls functionally connected to each reaction centres (Figure 7 A). The ratio between PSII and PSI reaction centres was also not affected by the null or point mutation of LHCB2, indicating that WT and LHCB2 mutants have the same PS and LHC stoichiometry (Figure 7B).

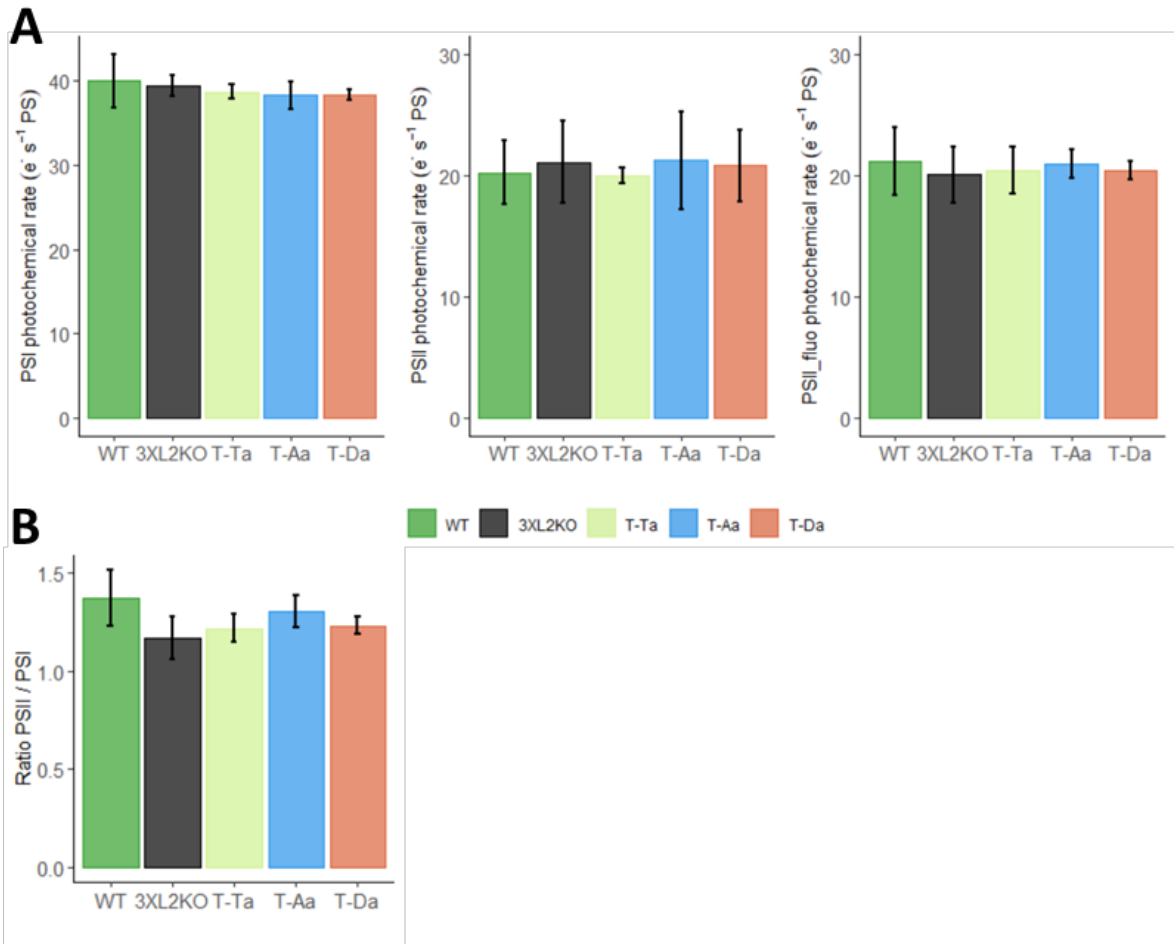

Figure 7| The PSI and PSII turnover rate are unaffected in the LHCB2 mutant lines. Reaction center stoichiometry and antenna size of the photosystems. A), The reaction centres ratio was measured in vivo using electrochromic shift (difference at 520 - 546 nm). Single-turnover, saturating laser flash was used to trigger charge separation in both photosystems; the same measurement was done with hydroxylamine and DCMU to block the PSII-related signal and to obtain PSI-dependent chromic shift. B), Light-limited photochemical rate of PSII and PSI was measured using fluorescence (PSII) and ECS (both for PSII and PSI).

LHCB2 and its phosphorylation are not essential to cope with fluctuating light in the long term

LHCII phosphorylation has been suggested to partially alleviate PSI over reduction under rapidly fluctuating light intensities (Grieco et al., 2012).It has been shown that LHCII phosphorylation, and mostly LHCB2 phosphorylation, favors antenna re-allocation between photosystems (Longoni et al., 2015), this allows to regulate the partition of the light-derived excitation energy between PSII and PSI. This, in the HL phase of fluctuating light, prevents the over reduction of the electron carriers of the electron transfer chain and thus having an electron excess arriving at PSI. Furthermore, by increasing PSI antenna cross section it may diminish PSI reaction center overreduction. This model has been used to explain the growth impairment of *stn7* under fluctuating light condition, but the details of this protective mechanism remain elusive. Considering that the loss of LHCB2, hampers the fast reallocation of LHCII between photosystem but not the steady-state LHCII association to the photosystems, we speculated that LHCB2 mutation may impair the ability of the plants to acclimate to light fluctuation. To test this hypothesis, the 3XL2KO mutant and the complemented lines with a point mutation at the LHCB2 threonine were exposed to light intensity fluctuation.
After 5 days of exposure to fluctuating light (50 µmol s^{-1} m^{-2} to 500 µmol s^{-1} m^{-2}), only the *stn7* mutant showed a clearly visible growth delay when compared to the other tested lines (Figure 8A).

To confirm that this delay was the result of a defect of the photosynthetic apparatus, the maximum quantum yield of PSII (QY Max) was measured by room temperature chlorophyll fluorescence in plants acclimated to constant and fluctuating light. QY Max does not vary under normal light conditions among different genotypes, however in fluctuating light a significant decrease was observed in *stn7* (Figure 8A). On the contrary, 3XL2KO and all the complemented lines were the same as WT. This suggests that the LHCB2 protein and its phosphorylation play no direct and essential role in the photoprotection of PSII from rapid light intensity fluctuation.

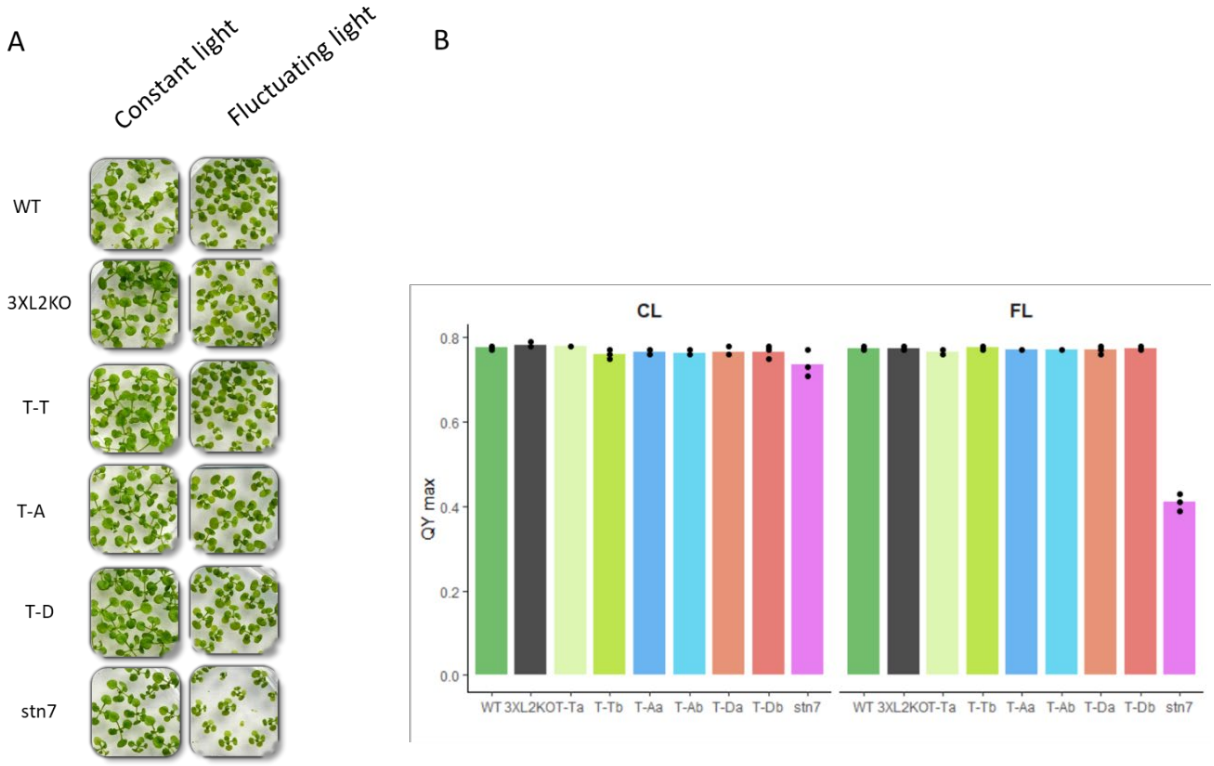

Figure 8| Delay in grown of *stn7* and reduced PSII efficiency under constant and fluctuating light condition compared to the WT. A) Phenotype of WT, 3XL2KO, complemented lines (L2.2: HA Threonine T_>T, L2.2: HA T_>A (Alanine), L2.2: HA. T_>D (Aspartate) and *stn7* mutant under 5-day constant and fluctuation light condition. Fluctuating light condition: low light (50 µmol photons m^{-2} s^{-1}) every 4 minutes interrupted by 1 minute of high light (500 µmol photons m^{-2} s^{-1}). As control, we used plants grown under constant light intensity (100-µmol photons m^{-2} s^{-1}). B), maximum quantum yield of photosystem II Fv/Fm :(Fm-F0)/Fm).

Prolonged exposure to fluctuating light resulted in a clear growth delay in *stn7.* However, we observed that, after twenty-four days of exposure to this light regime all the genotypes revealed a reduced rosette area. There was no detectable difference between WT, 3XL2KO and the complemented lines (Figure S2). To explain the lack of a visible photodamage to PSII in terms of photosynthetic acclimation, the seedlings were tested under the fluorcam using a protocol reproducing the same light intensity fluctuations during the fluorescence measurement (Figure 9A). This showed that the mutants have a slightly less efficient electron transport, visualized as a higher 1-qP, compared to the WT when exposed directly to the fluctuating light (Figure 9B). However, after 5 days of exposure to light fluctuation, the difference between WT and mutants, in terms of estimated electron transport, disappeared. Only in *stn7* the PSII reaction centers were always more closed, higher 1-qP, compared to the other lines resulting in clearly higher fluorescence trace (Figure 9C).
This observation suggests that the long-term acclimation mechanisms to fluctuating light intensity, independent on the phosphorylation and dephosphorylation of LHCB2, compensate entirely for the defect in the rapid acclimation.

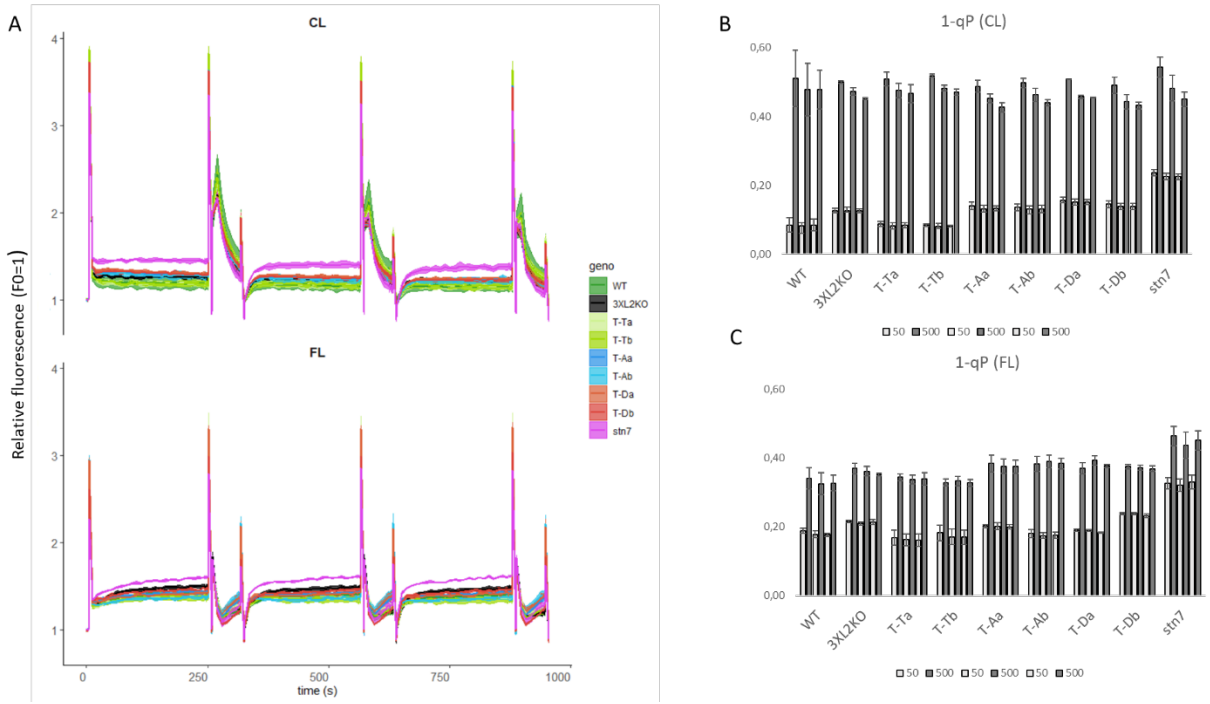

Figure 9: Short-term and long-term acclimation to fluctuating light. Room temperature fluorescence analysis under constant and fluctuating light regime. Plants grown under continuous white light (100 µmol photons m^{-2} s^{-1}), were exposed to a variable light intensity regime of blue light (450 nm) composed of 4 min of low light (50 µmol photons m^{-2} s^{-1}) and 1 min of high light (500 µmol photons m^{-2} s^{-1}) in a FluorCam (MF800 PSI - PhotoSystems Instruments). (A) The graph shows the average of the room temperature fluorescence measured during this period for the different lines, the values have been normalized on Fm = 1 and on FO = 0 (n = 5). B) Average value and standard deviation of the 1-qP parameter representing the excitation pressure on PSII measured at the end of each light phase.

Discussion

Previous attempts have been made to mutate a specific subunit of the LHCII using a Lhcb2 antisense RNA (asLhcb2), which resulted in a decrease of both Lhcb1 and Lhcb2 expression(Andersson et al., 2003); or by using artificial micro-RNA (amiLhcb1 and amiLhcb2), which managed to specifically deplete a single LHCII isoform (M. Pietrzykowska et al., 2014). These experiments revealed some important aspects of the role of the two most abundant LHCII isoforms in Arabidopsis: such as their role in state transitions, NPQ, thylakoid membrane structure and their partially complementary role. However, the RNA-based approaches have the drawback that they do not result in null mutants and are, for instance, less useful for the complementation with modified versions of the target LHCII protein. We, along with other groups, previously reported that targeted mutation via CRISPR/Cas9 resulted in the knockout of all five genes encoding a single LHCII isoform namely Lhcb1 (Ordon et al., 2020; Sattari Vayghan et al., 2022). In the present report we followed up on the CRISPR/Cas9 knock-out strategy for the Lhcb2 coding genes resulting in the triple null mutant 3XL2KO. The study includes the complementation of 3XL2KO with Lhcb2 versions carrying a point mutation at the phosphorylatable threonine residue. According to the literature the Lhcb2.2 gene (AT2G05070) is the most expressed amongst the Lhcb2-coding genes, and its mutation alone results in a reduction of 75% of the Lhcb2 protein (Xu et al., 2012). In this report we demonstrated that a single transgenic copy of Lhcb2.2 is sufficient to express LHCB2 at a WT level as confirmed by Western blotting. This proves also that the chosen sequences surrounding the CDS of Lhcb2.2 are capable to function as promoter and terminator (Figure 1) (Legen et al., 2001). It is also worth mentioning that the C-terminal fusion with a single copy of HA did not impair the functionality of LHCB2. In fact, 3XL2KO plants complemented with the native version of Lhcb2.2 fully restored state transitions to WT levels (Figure 2).

This result is consistent with our previous data where, using the same approach based on CRISPR/Cas9, we obtain a complete depletion of LHCB1 in a stable quintuple mutant (Sattari Vayghan et al., 2022). The CRISPR/Cas9 targeted mutation offers therefore a clear advantage over techniques based on miRNA and asRNA(Andersson et al., 2003; M. Pietrzykowska et al., 2014)resulting in specific and stable multiple null mutants, while the genes encoding even closely related isoforms are not directly affected. Plant growth and chlorophyll accumulation were not affected in the 3XL2KO (Figure S1). As the chl a/b ratio is unaltered other Chl b containing proteins should compensate for the loss of LHCB2. As the amount of LHCB2 protein is roughly 1/3 of that of LHCB1(Jansson, 1999), a relatively minor increase in the protein level of this isoform may suffice to compensate the defect. Such a small increase cannot be properly measured via a semiquantitative approach as the protein immunodetection used in this study (Heidebrecht et al., 2009). However, the amount of phosphorylated LHCB1 as detected by P-LHCB1 antibody and Phos-tag containing gels was increased in 3XL2KO and the T-A and T-D lines, while in T-T lines the phosphorylated LHCB1 was close to WT. STN7 kinase, the main kinase phosphorylating LHCII, had the same increasing tendency in above mentioned lines. As these mutants fail to fully connect LHCII to PSI and thus balance the excitation between PSI and PSII, the photoactive plastoquinone pool should be over reduced. This over reduction can trigger the accumulation of STN7 kinase and further activate it leading to the observed increase in LHCB1 phosphorylation. This phenomenon occurs in other state transition mutants in which STN7 is still present, for instance *psaH* mutant in which the LHCII docking site on PSI is impaired and thus the LHCII-PSI-LHCI supercomplex is missing (Lunde et al., 2000). It has been hypothesized that phosphorylation of LHCII, potentially of both LHCB1 and LHCB2 isoforms, favours its detachment from PSII and that undocked phosphorylated LHCIIs were shown to dissipate excitation energy(Iwai et al., 2008; Iwai et al., 2010; Ünlü et al., 2014). As in 3XL2KO PSI antenna cross section should not increase by docking of the LHCII trimer, the above mentioned LHCB1 over phosphorylation could be a mechanism to maintain equal functional antenna size of PSI and PSII in these mutants compared to WT.

The phosphorylation of LHCB1 does not fully complement the loss of LHCB2. This is in- agreement with previous literature data showing partial failure of state transitions (M. Pietrzykowska et al., 2014) Here we demonstrate that, the absence of LHCB2 protein in 3XL2KO or point mutation of its phosphorylation site in T-D or T-A disturbed stable LHCII binding to PSI while in 3XL2KO complemented with the native form of 3XL2KO T->T LHCII-PSI-LHCI supercomplex was detected by blue native gel electrophoresis. Despite the absence of this LHCII-PSI-LHCII supercomplex in 3XL2KO, T-D and T-A, state transitions is not fully blocked when compared to the STN7 kinase mutant (Figure 2 E). Indeed, *stn7* which lacks the major kinase of LHCII has almost no state transitions. This may suggest the existence of another LHCII-PSI binding site which requires neither LHCB2 nor its phosphorylated form (Bell et al., 2015; Bos et al., 2017). All the tested lines are capable of inducing and relaxing NPQ with a similar kinetic In terms of NPQ, this is consistent with the accepted hypothesis that phosphorylation is not expected to have a major role in this mechanism. Nonetheless, in increasing light intensities, LHCII tends to be dephosphorylated, and this should increase the NPQ level by increasing LHCII aggregation (Tang et al., 2007; Wu et al., 2021). This model may explain the higher level of NPQ observed in the *stn7* background, however 3XL2KO, T-A and T-D also have a potentially higher NPQ level. Therefore, if phosphorylation of LHCII plays a role in the NPQ level, it seems to be independent from LHCB2 and the charges present on its N-terminal region.

These observations led to the question whether any other supercomplex was (de-) stabilized in the lines lacking a phosphorylatable form of LHCB2. BN gel analysis revealed that except the LHCII-PSI-LHCI supercomplex lacking in 3X L2KO, T-A and T-D there were no apparent differences (Figure 6 A, B). However, even the relatively mild detergent solubilisation used in this study could be enough to disrupt atypical LHCII-PSI-LHCI supercomplexes. Such atypical supercomplexes may explain the low level of state transitions of 3XL2KO T-A and T-D lines.

The BN gel results confirm that the digitonin-resistant LHCII-PSI-LHCI supercomplex requires the phospho-threonine group of LHCB2 for stability (Crepin & Caffarri, 2015; Leoni et al., 2013) . The negative charge of the aspartate replacing the threonine in the T-D lines is not sufficient to allow stable docking of the LHCII trimer to PSI.

Another clue regarding the limited impact of the charge of the N-terminal amino acids of LHCB2 comes from the analysis of the antenna associated to PSI and PSII reaction centers. In fact, the 3XL2KO as well as the T-A and T-D lines show no detectable difference in the antenna distribution between photosystems. This is demonstrated by the measure of antenna cross-section in state 1 (Figure 7B). In state 1, in which LHCII is normally dephosphorylated (Longoni et al., 2015), should allow to detect any potential effect of the constitutive negative charge in the T-D lines, which may affect the three-dimensional structure of the LHCII trimers and thus decrease the LHCII affinity to PSII (Wood & Johnson, 2020). Also, in state 1 conditions, the electron transport imbalance due to the lack of phosphorylated LHCB2 in 3XL2KO is apparently too limited to induce a response at the level of the stoichiometry of the two photosystems (Figure 7A).

It appears that 3XL2KO, T->A and T->D result in a marginal defect on the photosynthetic apparatus under standard light conditions. The defects in state transitions, along with the absence of the LHCII-PSI-LHCI supercomplex, prompted us to challenge 3XL2KO, T->A and T->D with a rapidly fluctuating light intensity regime. Interestingly no growth defect or damage to PSII was observed compared to WT (Figure 8 A). To confirm that the conditions used in this experimental setup do indeed damage plants compromised in LHCII phosphorylation, we used the *stn7* mutant, which is known to be sensitive to light fluctuation and showed a severe growth delay and a decrease in PSII QY Max (Figure 8 B). The stunted phenotype observed in *stn7* was rationalized as an uneven distribution of light excitation between PSI and PSII leading to damage to PSI during the shifts in light intensity (Grieco et al., 2012). These authors had shown that LHCII phosphorylation under rapidly fluctuating light intensities alleviates the electron pressure on PSI by increasing its antenna cross section and thus protecting the photosynthetic apparatus. 3XL2KO, T-A and T-D do not have any detectable phosphorylated LHCB2. However, the higher phosphorylation of LHCB1, along with a higher level of STN7 kinase accumulation appear to be sufficient to equilibrate PSI and PSII excitation level and avoid severe damages to the photosynthetic electron transport chain, which would be reflected in a loss of PSII QY Max. A phosphate group in LHCB1 adds two negative charges to the protein(Hunter, 2012). Modelling data showed that phosphorylated LHCII, by the accumulation of negative surface charges creates a repulsive force that favors the LHCII dissociation from PSII thus reducing its antenna cross-section and excitation(Wood & Johnson, 2020). Furthermore, a previous publication correlated the activity of STN7 to long term acclimatory processes (Pesaresi et al., 2009; Węgrzyn et al., 2022) . The stunted phenotype of *stn7* could be the result of the sum of the missing LHCII phosphorylation combined with a defect in separate acclimatory processes dependent on STN7 activity. Supporting this hypothesis, we observed by fluorescence measurement taken during light intensity fluctuations the 3XL2KO, T-A and T-D had a less efficient electron transport, as inferred by the fraction of closed PSII reaction centers (higher 1-qP), compared to the WT and T->T lines (Figure 9B). This difference was reduced, in plants pre-acclimated for several days to fluctuating light before the measurement. Only in *stn7* the PSII reaction centers were always more closed, (higher 1-qP) in both conditions (Figure 9C) suggesting the presence of a long-lasting defect. In conclusion, the loss of LHCB2 or the mutation of the phosphorylatable threonine results in a transient defect in photosynthetic electron transport. This defect induces specific long term responses such as the over-accumulation of STN7 resulting in an increased phosphorylation of LHCB1 that may compensate for the loss of LHCB2 or mutation of its phosphorylatable threonine. Despite the defect in short term responses, the plants lacking LHCB2 can acclimate to lasting imbalances in the light spectrum, resulting in phenotypes similar to the WT.

References

Andersson, J., Wentworth, M., Walters, R. G., Howard, C. A., Ruban, A. V., Horton, P., & Jansson, S. (2003). Absence of the Lhcb1 and Lhcb2 proteins of the light-harvesting complex of photosystem II - effects on photosynthesis, grana stacking and fitness. *Plant J*, *35*(3), 350-361. https://doi.org/10.1046/j.1365-313x.2003.01811.x

Arnold, J., Shapiguzov, A., Fucile, G., Rochaix, J. D., Goldschmidt-Clermont, M., & Eichacker, L. A. (2014). Separation of membrane protein complexes by native LDS-PAGE. *Methods Mol Biol*, *1072*, 667-676. https://doi.org/10.1007/978-1-62703-631-3_46

Ballottari, M., Girardon, J., Dall'Osto, L., & Bassi, R. (2012). Evolution and functional properties of Photosystem II light harvesting complexes in eukaryotes. *Biochimica et Biophysica Acta (BBA) - Bioenergetics*, *1817*(1), 143-157. https://doi.org/https://doi.org/10.1016/j.bbabio.2011.06.005

Bell, A. J., Frankel, L. K., & Bricker, T. M. (2015). High Yield Non-detergent Isolation of Photosystem I-Light-harvesting Chlorophyll II Membranes from Spinach Thylakoids: IMPLICATIONS FOR THE ORGANIZATION OF THE PS I ANTENNAE IN HIGHER PLANTS. *J Biol Chem*, *290*(30), 18429-18437. https://doi.org/10.1074/jbc.M115.663872

Bellafiore, S., Barneche, F., Peltier, G., & Rochaix, J. D. (2005). State transitions and light adaptation require chloroplast thylakoid protein kinase STN7. *Nature*, *433*(7028), 892-895. https://doi.org/10.1038/nature03286

Caffarri, S., Broess, K., Croce, R., & van Amerongen, H. (2011). Excitation energy transfer and trapping in higher plant Photosystem II complexes with different antenna sizes. *Biophys J*, *100*(9), 2094-2103. https://doi.org/10.1016/j.bpj.2011.03.049

Clough, S. J., & Bent, A. F. (1998). Floral dip: a simplified method for Agrobacterium -mediated transformation of Arabidopsis thaliana. *The Plant Journal*, *16*(6), 735-743. https://doi.org/https://doi.org/10.1046/j.1365-313x.1998.00343.x

Crepin, A., & Caffarri, S. (2015). The specific localizations of phosphorylated Lhcb1 and Lhcb2 isoforms reveal the role of Lhcb2 in the formation of the PSI-LHCII supercomplex in Arabidopsis during state transitions. *Biochimica et Biophysica Acta (BBA) - Bioenergetics*, *1847*(12), 1539-1548. https://doi.org/https://doi.org/10.1016/j.bbabio.2015.09.005

Croce, R. (2020). Beyond 'seeing is believing': the antenna size of the photosystems in vivo. *New Phytologist*, *228*(4), 1214-1218. https://doi.org/https://doi.org/10.1111/nph.16758

Croce, R., & van Amerongen, H. (2020). Light harvesting in oxygenic photosynthesis: Structural biology meets spectroscopy. *Science*, *369*(6506), eaay2058. https://doi.org/doi:10.1126/science.aay2058

Dekker, J. P., & Boekema, E. J. (2005). Supramolecular organization of thylakoid membrane proteins in green plants. *Biochim Biophys Acta*, *1706*(1-2), 12-39. https://doi.org/10.1016/j.bbabio.2004.09.009

Ferroni, L., Suorsa, M., Aro, E. M., Baldisserotto, C., & Pancaldi, S. (2016). Light acclimation in the lycophyte Selaginella martensii depends on changes in the amount of photosystems and on the flexibility of the light-harvesting complex II antenna association with both photosystems. *New Phytol*, *211*(2), 554-568. https://doi.org/10.1111/nph.13939

Friso, G., Giacomelli, L., Ytterberg, A. J., Peltier, J. B., Rudella, A., Sun, Q., & Wijk, K. J. (2004). In-depth analysis of the thylakoid membrane proteome of Arabidopsis thaliana chloroplasts: new proteins, new functions, and a plastid proteome database. *Plant Cell*, *16*(2), 478-499. https://doi.org/10.1105/tpc.017814

Galka, P., Santabarbara, S., Khuong, T. T., Degand, H., Morsomme, P., Jennings, R. C., Boekema, E. J., & Caffarri, S. (2012). Functional analyses of the plant photosystem I-light-harvesting complex II supercomplex reveal that light-harvesting complex II loosely bound to photosystem II is a very efficient antenna for photosystem I in state II. *Plant Cell*, *24*(7), 2963-2978. https://doi.org/10.1105/tpc.112.100339

Galston, A. W. (1992). Photosynthesis as a Basis for Life Support on Earth and in Space. *BioScience*, *42*(7), 490-493. https://doi.org/10.2307/1311878

Govindjee. (2002). A Role for a Light-Harvesting Antenna Complex of Photosystem II in Photoprotection. *The Plant Cell*, *14*(8), 1663-1668. https://doi.org/10.1105/tpc.140810

Govindjee, G., & Papageorgiou, G. (2004). *Chlorophyll A Fluorescence: A Signature of Photosynthesis*. https://doi.org/10.1007/978-1-4020-3218-9

Grieco, M., Tikkanen, M., Paakkarinen, V., Kangasjärvi, S., & Aro, E.-M. (2012). Steady-State Phosphorylation of Light-Harvesting Complex II Proteins Preserves Photosystem I under Fluctuating White Light *Plant Physiology*, *160*(4), 1896-1910. https://doi.org/10.1104/pp.112.206466

Heidebrecht, F., Heidebrecht, A., Schulz, I., Behrens, S. E., & Bader, A. (2009). Improved semiquantitative Western blot technique with increased quantification range. *J Immunol Methods*, *345*(1-2), 40-48. https://doi.org/10.1016/j.jim.2009.03.018

Hunter, T. (2012). Why nature chose phosphate to modify proteins. *Philosophical Transactions of the Royal Society B: Biological Sciences*, *367*(1602), 2513-2516. https://doi.org/doi:10.1098/rstb.2012.0013

Ishikawa, N., Takabayashi, A., Noguchi, K., Tazoe, Y., Yamamoto, H., von Caemmerer, S., Sato, F., & Endo, T. (2016). NDH-Mediated Cyclic Electron Flow Around Photosystem I is Crucial for C4 Photosynthesis. *Plant and Cell Physiology*, *57*(10), 2020-2028. https://doi.org/10.1093/pcp/pcw127

Iwai, M., Takahashi, Y., & Minagawa, J. (2008). Molecular remodeling of photosystem II during state transitions in Chlamydomonas reinhardtii. *Plant Cell*, *20*(8), 2177-2189. https://doi.org/10.1105/tpc.108.059352

Iwai, M., Yokono, M., Inada, N., & Minagawa, J. (2010). Live-cell imaging of photosystem II antenna dissociation during state transitions. *Proc Natl Acad Sci U S A*, *107*(5), 2337-2342. https://doi.org/10.1073/pnas.0908808107

Janssen, P. J., Lambreva, M. D., Plumeré, N., Bartolucci, C., Antonacci, A., Buonasera, K., Frese, R. N., Scognamiglio, V., & Rea, G. (2014). Photosynthesis at the forefront of a sustainable life. *Front Chem*, *2*, 36. https://doi.org/10.3389/fchem.2014.00036

Jansson, S. (1999). A guide to the Lhc genes and their relatives in Arabidopsis/IT>. *Trends Plant Sci*, *4*(6), 236-240. https://doi.org/10.1016/s1360-1385(99)01419-3

Järvi, S., Suorsa, M., Paakkarinen, V., & Aro, E. M. (2011). Optimized native gel systems for separation of thylakoid protein complexes: novel super- and mega-complexes. *Biochem J*, *439*(2), 207-214. https://doi.org/10.1042/bj20102155

Kirchhoff, H., Li, M., & Puthiyaveetil, S. (2017). Sublocalization of Cytochrome b(6)f Complexes in Photosynthetic Membranes. *Trends Plant Sci*, *22*(7), 574-582. https://doi.org/10.1016/j.tplants.2017.04.004

Koochak, H., Puthiyaveetil, S., Mullendore, D. L., Li, M., & Kirchhoff, H. (2019). The structural and functional domains of plant thylakoid membranes. *The Plant Journal*, *97*(3), 412-429. https://doi.org/https://doi.org/10.1111/tpj.14127

Kosourov, S., Nagy, V., Shevela, D., Jokel, M., Messinger, J., & Allahverdiyeva, Y. (2020). Water oxidation by photosystem II is the primary source of electrons for sustained H₂ photoproduction in nutrient-replete green algae. *Proceedings of the National Academy of Sciences*, *117*(47), 29629-29636. https://doi.org/doi:10.1073/pnas.2009210117

Kramer, D. M., Johnson, G., Kiirats, O., & Edwards, G. E. (2004). New Fluorescence Parameters for the Determination of QA Redox State and Excitation Energy Fluxes. *Photosynthesis Research*, *79*(2), 209-218. https://doi.org/10.1023/B:PRES.0000015391.99477.0d

Legen, J., Miséra, S., Herrmann, R. G., & Meurer, J. (2001). Map positions of 69 Arabidopsis thaliana genes of all known nuclear encoded constituent polypeptides and various regulatory factors of the photosynthetic membrane: a case study. *DNA Res*, *8*(2), 53-60. https://doi.org/10.1093/dnares/8.2.53

Leoni, C., Pietrzykowska, M., Kiss, A. Z., Suorsa, M., Ceci, L. R., Aro, E. M., & Jansson, S. (2013). Very rapid phosphorylation kinetics suggest a unique role for Lhcb2 during state transitions in Arabidopsis. *Plant J*, *76*(2), 236-246. https://doi.org/10.1111/tpj.12297

Liu, Z., Yan, H., Wang, K., Kuang, T., Zhang, J., Gui, L., An, X., & Chang, W. (2004). Crystal structure of spinach major light-harvesting complex at 2.72 A resolution. *Nature*, *428*(6980), 287-292. https://doi.org/10.1038/nature02373

Longoni, F. P., & Goldschmidt-Clermont, M. (2021). Thylakoid Protein Phosphorylation in Chloroplasts. *Plant Cell Physiol*, *62*(7), 1094-1107. https://doi.org/10.1093/pcp/pcab043

Longoni, P., Douchi, D., Cariti, F., Fucile, G., & Goldschmidt-Clermont, M. (2015). Phosphorylation of the Light-Harvesting Complex II Isoform Lhcb2 Is Central to State Transitions *Plant Physiology*, *169*(4), 2874-2883. https://doi.org/10.1104/pp.15.01498

Lunde, C., Jensen, P. E., Haldrup, A., Knoetzel, J., & Scheller, H. V. (2000). The PSI-H subunit of photosystem I is essential for state transitions in plant photosynthesis. *Nature*, *408*(6812), 613-615. https://doi.org/10.1038/35046121

Maxwell, K., & Johnson, G. N. (2000). Chlorophyll fluorescence—a practical guide. *Journal of Experimental Botany*, *51*(345), 659-668. https://doi.org/10.1093/jexbot/51.345.659

Mullineaux, C. W., & Emlyn-Jones, D. (2005). State transitions: an example of acclimation to low-light stress. *J Exp Bot*, *56*(411), 389-393. https://doi.org/10.1093/jxb/eri064

Munekage, Y., Hojo, M., Meurer, J., Endo, T., Tasaka, M., & Shikanai, T. (2002). PGR5 is involved in cyclic electron flow around photosystem I and is essential for photoprotection in Arabidopsis. *Cell*, *110*(3), 361-371. https://doi.org/10.1016/s0092-8674(02)00867-x

Nicol, L., Nawrocki, W. J., & Croce, R. (2019). Disentangling the sites of non-photochemical quenching in vascular plants. *Nat Plants*, *5*(11), 1177-1183. https://doi.org/10.1038/s41477-019-0526-5

Nicol, L., Nawrocki, W. J., & Croce, R. (2019). Disentangling the sites of non-photochemical quenching in vascular plants. *Nature Plants*, *5*(11), 1177-1183. https://doi.org/10.1038/s41477-019-0526-5

Ordon, J., Bressan, M., Kretschmer, C., Dall'Osto, L., Marillonnet, S., Bassi, R., & Stuttmann, J. (2020). Optimized Cas9 expression systems for highly efficient Arabidopsis genome editing facilitate isolation of complex alleles in a single generation. *Funct Integr Genomics*, *20*(1), 151-162. https://doi.org/10.1007/s10142-019-00665-4

Park, S., Steen, C. J., Lyska, D., Fischer, A. L., Endelman, B., Iwai, M., Niyogi, K. K., & Fleming, G. R. (2019). Chlorophyll–carotenoid excitation energy transfer and charge transfer in Nannochloropsis oceanica for the regulation of photosynthesis. *Proceedings of the National Academy of Sciences*, *116*(9), 3385-3390. https://doi.org/doi:10.1073/pnas.1819011116

Pesaresi, P., Hertle, A., Pribil, M., Kleine, T., Wagner, R., Strissel, H., Ihnatowicz, A., Bonardi, V., Scharfenberg, M., Schneider, A., Pfannschmidt, T., & Leister, D. (2009). Arabidopsis STN7 kinase provides a link between short- and long-term photosynthetic acclimation. *Plant Cell*, *21*(8), 2402-2423. https://doi.org/10.1105/tpc.108.064964

Peter, G. F., & Thornber, J. P. (1991). Biochemical composition and organization of higher plant photosystem II light-harvesting pigment-proteins. *J Biol Chem*, *266*(25), 16745-16754.

Pietrzykowska, M., Suorsa, M., Semchonok, D. A., Tikkanen, M., Boekema, E. J., Aro, E.-M., & Jansson, S. (2014). The Light-Harvesting Chlorophyll a/b Binding Proteins Lhcb1 and Lhcb2 Play Complementary Roles during State Transitions in Arabidopsis *The Plant Cell*, *26*(9), 3646-3660. https://doi.org/10.1105/tpc.114.127373

Porra, R. J. (2002). The chequered history of the development and use of simultaneous equations for the accurate determination of chlorophylls a and b. *Photosynthesis Research*, *73*(1), 149-156. https://doi.org/10.1023/A:1020470224740

Pralon, T., Collombat, J., Pipitone, R., Ksas, B., Shanmugabalaji, V., Havaux, M., Finazzi, G., Longoni, P., & Kessler, F. (2020). Mutation of the Atypical Kinase ABC1K3 Partially Rescues the PROTON GRADIENT REGULATION 6 Phenotype in Arabidopsis thaliana [Original Research]. *Frontiers in Plant Science*, *11*. https://doi.org/10.3389/fpls.2020.00337

Rochaix, J.-D. (2011). Regulation of photosynthetic electron transport. *Biochimica et Biophysica Acta (BBA) - Bioenergetics*, *1807*(3), 375-383. https://doi.org/https://doi.org/10.1016/j.bbabio.2010.11.010

Rochaix, J. D. (2011). Regulation of photosynthetic electron transport. *Biochim Biophys Acta*, *1807*(3), 375-383. https://doi.org/10.1016/j.bbabio.2010.11.010

Sattari Vayghan, H., Nawrocki, W. J., Schiphorst, C., Tolleter, D., Hu, C., Douet, V., Glauser, G., Finazzi, G., Croce, R., Wientjes, E., & Longoni, F. (2022). Photosynthetic Light Harvesting and Thylakoid Organization in a CRISPR/Cas9 Arabidopsis Thaliana LHCB1 Knockout Mutant [Original Research]. *Frontiers in Plant Science*, *13*. https://doi.org/10.3389/fpls.2022.833032

Tang, Y., Wen, X., Lu, Q., Yang, Z., Cheng, Z., & Lu, C. (2007). Heat stress induces an aggregation of the light-harvesting complex of photosystem II in spinach plants. *Plant Physiol*, *143*(2), 629-638. https://doi.org/10.1104/pp.106.090712

Ünlü, C., Drop, B., Croce, R., & van Amerongen, H. (2014). State transitions in Chlamydomonas reinhardtii strongly modulate the functional size of photosystem II but not of photosystem I. *Proc Natl Acad Sci U S A*, *111*(9), 3460-3465. https://doi.org/10.1073/pnas.1319164111

van Amerongen, H., & Croce, R. (2013). Light harvesting in photosystem II. *Photosynthesis Research*, *116*(2), 251-263. https://doi.org/10.1007/s11120-013-9824-3

Węgrzyn, A., Krysiak, M., Kulik, A., Gieczewska, K. B., & Mazur, R. (2022). STN7 Kinase Is Essential for Arabidopsis thaliana Fitness under Prolonged Darkness but Not under Dark-Chilling Conditions. *Int J Mol Sci*, *23*(9). https://doi.org/10.3390/ijms23094531

Wientjes, E., van Amerongen, H., & Croce, R. (2013). LHCII is an antenna of both photosystems after long-term acclimation. *Biochimica et Biophysica Acta (BBA) - Bioenergetics*, *1827*(3), 420-426. https://doi.org/https://doi.org/10.1016/j.bbabio.2012.12.009

Wood, W. H. J., & Johnson, M. P. (2020). Modeling the Role of LHCII-LHCII, PSII-LHCII, and PSI-LHCII Interactions in State Transitions. *Biophysical Journal*, *119*(2), 287-299. https://doi.org/https://doi.org/10.1016/j.bpj.2020.05.034

Wu, G., Ma, L., Yuan, C., Dai, J., Luo, L., Poudyal, R. S., Sayre, R. T., & Lee, C. H. (2021). Formation of light-harvesting complex II aggregates from LHCII-PSI-LHCI complexes in rice plants under high light. *J Exp Bot*, *72*(13), 4938-4948. https://doi.org/10.1093/jxb/erab188

Xing, H. L., Dong, L., Wang, Z. P., Zhang, H. Y., Han, C. Y., Liu, B., Wang, X. C., & Chen, Q. J. (2014). A CRISPR/Cas9 toolkit for multiplex genome editing in plants. *BMC Plant Biol*, *14*, 327. https://doi.org/10.1186/s12870-014-0327-y

Xu, Y. H., Liu, R., Yan, L., Liu, Z. Q., Jiang, S. C., Shen, Y. Y., Wang, X. F., & Zhang, D. P. (2012). Light-harvesting chlorophyll a/b-binding proteins are required for stomatal response to abscisic acid in Arabidopsis. *J Exp Bot*, *63*(3), 1095-1106. https://doi.org/10.1093/jxb/err315

Supplementary methods and data

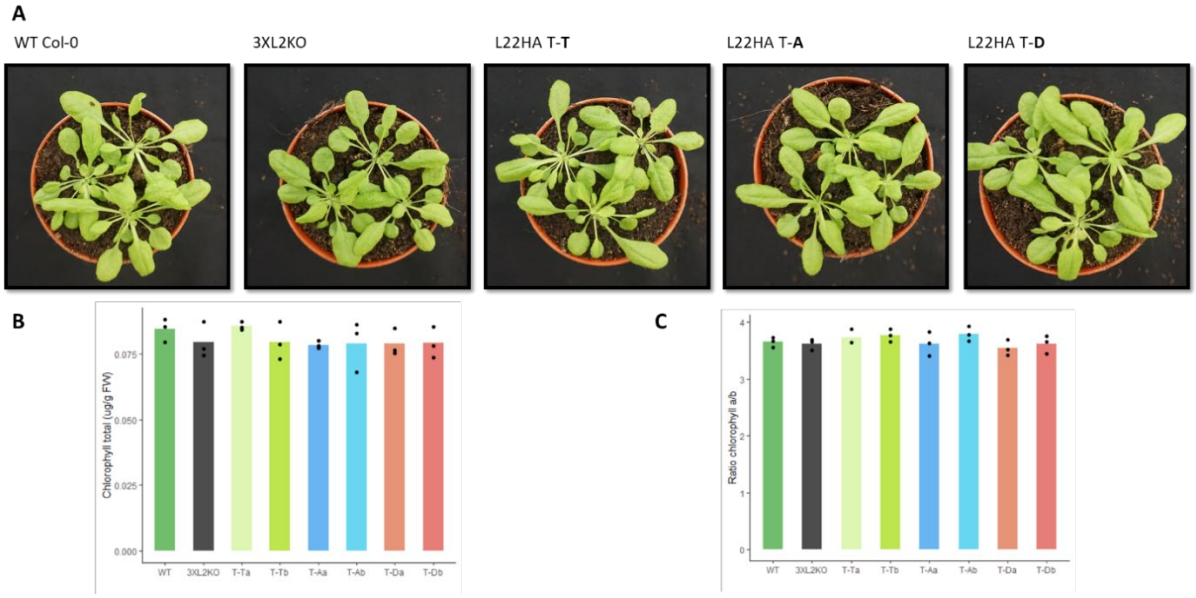

Figure S1| Mutation of Lhcb2 does not affect growth and chlorophyll accumulation. Plants were grown under standard conditions (100 µmol photons m−2 s−1, constant light, 16h light and 8h dark day cycle) for 6 weeks. A), Representative phenotype of WT, (3X L2KO), and the three 3XL2KO complemented lines with HA-tagged Lhcb2.2 construct. The phosphorylation site of the heterologous gene contains either a threonine L2.2HA T-T, an alanine L2.2HA T-A or an aspartate L2.2HA T-D (Aspartate). B), Total Chlorophyll and C), chlorophyll a/b ratios in mature leaves from these same plants. Error bars represent SE (n=3 biological replicates).

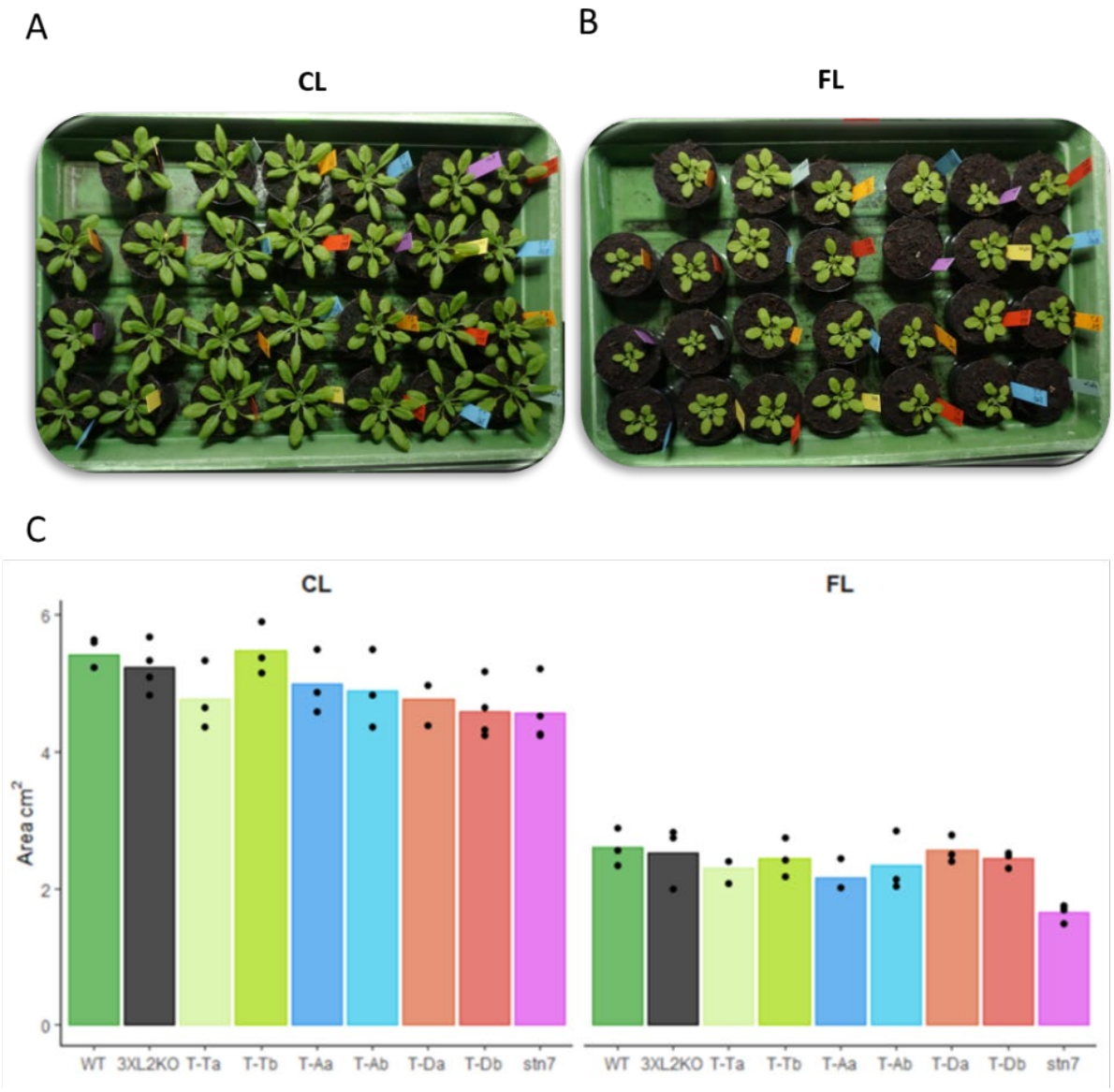

Figure S2|Growth of the plants and rosette area under constant and fluctuating light intensity. (A, B): Plants were grown under a long 12/12-h- day/night cycle. A) representative image of the plants grown under constant light intensity (120 µmol photons m^{-2} s^{-1}) B) representative image of the plants grown under fluctuating light intensity with 4 min at 50 µmol photons m^{-2} s^{-1} and 1 min at 500 µmol photons m^{-2} s^{-1}. C) Comparison of rosette size at day 24 for the different genotypes grown under the constant and fluctuating light regimes. The rosette surface was measured with ImageJ, using a colour threshold to distinguish the leaves from the background.

Name	Sequence	Notes
L22HA_FRAG1_FOR	AAGCTTtgcaatttttgttttgtttaatgagtcgttgtaatttttaatttatttga	Amplification Fragment 1 of Lhcb2.2
L22HA_FRAG1_REV	catatgataattaTGCATAGTCCGGGACGTCATAGGGATAGTCGAC ctttccggggacaaagttagtagcg	Amplification Fragment 1 of Lhcb2.2
L22HA_FRAG 2_For	ccccggaaagGTCGACTATCCCTATGACGTCCCGGACTATGCAtaa ttatcatatgtatttgcttcataatc	Amplification Fragment 2 of Lhcb2.2
L22HA_FRAG 2_Rev	GATCTAGAcatagagcctctcgtgaagagtaagaatt	Amplification Fragment 2 of Lhcb2.2
Lhcb2-2-1_LP	GCATTGTAATGGCTCATGACC	Cloning of L22HA to introduce T-A and T-D mutations
L22_REV	TGA CCA TGA TTA CGA ATT CGA GCT CG	Cloning of L22HA to introduce T-A and T-D mutations and sequencing
A-L2_REV	GGG AGT AGA CTT GAC GGC ACG ACG CAT GGT CAC ACG	Cloning of L22HA to introduce T-A mutation
D-L2_REV	GGG AGT AGA CTT GAC GTC ACG ACG CAT GGT CAC ACG	Cloning of L22HA to introduce T-D mutation
A-L2_FOR	CGT GTG ACC ATG CGT CGT GCC GTC AAG TCT ACT CCC	Cloning of L22HA to introduce T-A mutation
D-L2_FOR	CGT GTG ACC ATG CGT CGT GAC GTC AAG TCT ACT CCC	Cloning of L22HA to introduce T-D mutation
Cas9_For	ATG TAT GTG GAC CAG GAG CTG G	Genotyping cas9 in Arabidopsis transformed plants
Cas9_Rev	TTT GGG TAC TTC TTG ATC AGA GC	Genotyping cas9 in Arabidopsis transformed plants
L22_FOR	GGT TTT CCC AGT CAC GAC GTT G	Sequencing of L22HA, L22HA-A and L22HA-D

Table S1|Primer sequences to identify the mutation nature in Lhcb2.2-Lhcb2.3, complementation TAD, loss of Cas9 cassettes.

Discussion

Life on Earth depends on a complex and tightly regulated process called photosynthesis. Several physiochemical and biochemical reactions work in series enabling this process to fuel life using energy from sunlight. The overarching aim of my thesis was to elucidate how the photosynthetic apparatus responds to changes in the environment with a specific focus on the role of the light harvesting complex (LHCII) in the acclimation to changes in light conditions. The experimental system relied on Arabidopsis mutants missing specific isoforms of the trimeric LHCII. I attempted to elucidate the role of the two most abundant LHCII isoforms LHCB1 and LHCB2 in the dynamic organization of the LHCII network. LHCII plays a central role in regulating long and short-term acclimation responses but how each LHCII isoform contributes to these responses remains an important open question. Previous research highlighted important aspects of the role of the two most abundant LHCII isoforms in Arabidopsis: LHCB1 and LHCB2, using artificial micro-RNA in amiLhcb1 and amiLhcb2 (Pietrzykowska et al., 2014) and antisense RNA blocking both Lhcb1 and Lhcb2 expression in asLhcb2 (Andersson et al., 2003) . These experiments revealed the complementary roles of LHCB1 and LHCB2 in photosynthetic acclimation. However, these lines, as the RNA used to knock-down the genes may interfere with the expression of the heterologous protein or may be silenced itself resulting in a variable level of expression of the targeted genes, are not suitable for complementation experiments. The complementation experiments permit more detailed studies aiming at elucidating the role of specific amino acid residues of each LHCII isoform. In this work I have focused on the main post-translational modification occurring at the level of the LHCII: threonine phosphorylation. As this modification occurs at the level of a single and well described amino acid, it was possible to design experiments aiming at its mutation. The first step into this project was the production of stable knock out lines to be used as a platform for the complementation with the modified version of the targeted LHCII isoform. Furthermore, a stable knock-out line would allow to investigate the long term response of the plant to a constitutive lack of a given LHCII isoform.

LHCB1 and LHCB2 are encoded by multiple genes, 5 and 3 respectively (Leutwiler et al., 1986; McGrath et al., 1992) . The genes encoding each isoform are localized close to each other, making it nearly impossible to obtain a complete knock-out plant by crossing T-DNA insertional lines. The use of an approach based on the insertion of a heterologous Cas9 gene along with gRNA targeting simultaneously multiple genes for each isoform allowed to overcome this limitation. Stable multiple knockout lines were generated for each LHCII isoform. The two complete null lines were named 5XL1KO, for quintuple mutant of the genes coding for LHCB1, and 3XL2KO, which has a mutation in all the three genes for LHCB2. The technique proved to be highly efficient, so that, even lines heterozygous for the Cas9 T-DNA insertion were mutated in all the target genes. This was a key factor for the following complementation experiments, as these heterozygous lines could be counter selected for the T-DNA insertion and thus allowed the production of 5XL1KO and 3XL2KO lines without Cas9 that were thus exploitable for the complementation. This approach did not require back crossing of the mutants with the WT, a strategy that would have required a tedious screening procedure to obtain a stable and complete mutant.

The full knock out lines were the first products of this thesis work and their analysis already provided useful information on the role of the antenna and the compensatory mechanisms allowing to reduce the potential impact of these mutations.

Mutants of LHCB1 and LHCB2

Both multiple null mutants for LHCB2 and LHCB1 were analysed. Only 5XL1KO had a visible phenotype: the plants were pale green with a lower chlorophyll a/b ratio, the growth and flowering were delayed as reported in (Sattari Vayghan et al., 2022) . In contrast, 3XL2KO, despite the absence of detectable LHCB2 protein, did not show any obvious phenotype (Paper in chapter IV). At the molecular level the absence of LHCB1 resulted in an increased accumulation of LHCB2, while LHCB3 and the monomeric LHCII antennae show no major change. This suggests that only LHCB1, because of its structure or because of the level of gene expression, is capable to constitute roughly two third of the trimeric LHCII. This should be kept in mind when analysing the phenotype of 5XL1KO, as the defects observed in this line may as well derive from the sharp reduction of total LHCII content rather than the loss of a specific isoform. It is therefore useful to compare 5XL1KO with previously described mutants defective in chl b accumulation, which causes a decreased LHCII accumulation. In these mutants PSII-LHCII super complexes were not detected and LHCII trimers were missing, implying that the mutants had a smaller antenna size. The absence of LHCII resulted in an altered thylakoid structure with less stacked membranes and a reduced quantum yield of PSII (e.g., Reduced ΦPSII and Fv/Fm in ch1-3lhcb5)(Espineda et al., 1999; Kim et al., 2009; Murray & Kohorn, 1991) . Comparable to chlorina mutants, the pale phenotype of 5XL1KO is coupled with several defects in photosynthetic activity. Under control light, the PSII antenna absorption cross-section is smaller while no difference between mutant and WT was observed in PSI cross-section. This difference would favor PSI excitation over PSII, but was partially compensated by the lower PSI over PSII reaction center ratio and by the dephosphorylation of LHCII and PSII core subunits. No matter what, these stochiometric and post translational adaptations are not enough to fully compensate for the loss of LHCB1 and chlorophyll fluorescence analyses reveal that there is still an imbalance in the redox equilibrium of photosynthetic ETC in the 5XL1KO mutant.

Decreased levels of LHCII trimer in the absence of LHCB1 that limits PSII antenna cross-section also limits electron input from PSII. Consequently, the inability to over-reduce the plastoquinone pool can partially explain some defects such as a lower NPQ induction and the reduced capacity to perform state transitions. However, failure of state transitions and NPQ induction in 5X L1KO (even under very high intensity light conditions) may be also explained by an essential role of LHCB1 in the stability and/or conformation of the LHCII trimer capable of docking to PSI (L-trimer) and/or essential role for the conformational change of the antenna trimer during NPQ induction.

Phosphorylation of LHCB1 and LHCB2:

Thylakoid membrane proteins are post-translationally modified as part of the regulatory networks required for photosynthesis acclimation. Several proteins have post translational modifications (PTMs) but due to the abundance of the target proteins and the extent of the phosphorylation of the major isoforms of LHCII (LHCB1 and LHCB2) led to extensive research on the subject (Longoni et al., 2015; Longoni et al., 2019; Rantala et al., 2020) . The phosphorylation site of these isoforms has been confirmed by mass spectrometry and by the use of specific antibodies recognizing the target phosphorylated peptide (Bergner et al., 2015; Crepin & Caffarri, 2015; Leoni et al., 2013). The site is similar between LHCB1 and LHCB2 in both cases it's a threonine located close to the N-terminus of the mature protein(Longoni et al., 2015) . The same peptide, at a lysine residue, has also been proposed as an elusive acetylation site (Albanese et al., 2020).

Taken together these modifications and the slight but fundamental differences between LHCB1 and LHCB2 at the level of this terminal region hint at a very specific role of this domain and its PTMs during dynamic light acclimation. For instance, in a process known as state transitions qT, energy input equilibrium between two photosystems requires reversible association of LHCII. The phosphorylation of LHCB2 subunits of L-trimers has been suggested to play an important role in docking process of the trimer to PSI creating LHCII-PSI-LHCI supercomplex. Despite good knowledge about LHCB2, the specific role of PTM of LHCB1 have not been completely resolved. In addition to LHCII phosphorylation-mediated- regulation a newly characterized chloroplast acetyltransferase NSI/GNAT2 mutant has been suggested to have a role in acclimation to light changes, state transitions and thylakoid structure likely through chloroplast protein acetylation (Rantala et al., 2022) .

This work contributes towards the study of LHCII phosphorylation in the wider context of photosynthetic acclimation. In fact, LHCII phosphorylation level is not only linked to “State transitions” in sensu strictu but it’s also a means to manipulate LHCII dynamics in a range of environmental conditions. Our experiments conducted with Lepidium sativum offer an example of this wider regulation (Sattari Vayghan et al., 2020), where the level of phosphorylation, but not the antenna content, was shown to be dependent on the growth temperature. But there is increasing evidence, for instance (Węgrzyn et al., 2022) Showed that LHCII phosphorylation decrease in response to dark-chilling abiotic stress and increase in prolonged dark period along with decrease in Fv/Fm parameter. This is in line with the already proposed protective mechanism attributed to LHCII phosphorylation under fluctuating light (M. Grieco et al., 2012) .

The importance of LHCB2 phosphorylation in rapid acclimatory process known as state transitions has been widely investigated (Bellafiore et al., 2005; Delosme et al., 1996; Murata, 2009; Wollman, 2001). In agreement with previous studies our results imply that the light excitation balance between two photosystems does not solely rely on LHCB2 and its phosphorylation that allows to stabilize the LHCII-PSI-LHCI supercomplex. Interestingly, despite the absence of LHCB2 in 3XL2KO and the non-appearance of the LHCII-PSI-LHCI super complex in BN native gel, state transitions are not completely impaired. In fact, plants deprived of LHCB2 revealed an intermediate state between WT and the state transitions-dead mutant stn7.This difference confirms previously reported data using artificial micro-RNA amiLhcb2 to silence the Lhcb2 genes (Pietrzykowska et al., 2014) .

Compromised qT in 5XL1KO and 3XL2KO may have overlapping but distinct causes which is in line with the suggested distinct roles for either one. LHCII trimers the purified in LHCII-PSI-LHCI supercomplex are composed of two copies of almost entirely non-phosphorylated LHCB1 and one copy of almost completely phosphorylated LHCB2 (Longoni et al., 2015) . These specific and opposite phosphorylation levels may hint at parallel roles of each isoform in this specific configuration. However, this common defect to perform state transitions could also be rationalized differently: as LHCB2 is a requisite element the missing LHCII L-trimer may reduce the ability to dock to PSI and in 5XL1KO due consequence of dramatic loss of trimeric LHCII. Hence, it would be quite hard to assess whether LHCB1 and its phosphorylation have a specific role in qT. On the other hand, the smaller antenna size in 5XL1KO may directly affect the PQ redox state which is involved in STN7 activation.

Analyzing the failure of state transitions of both LHCII isoforms and shedding light on LHCII phosphorylation has become possible by complementing knock-out lines for LHCB1 and LHCB2 with the constructs containing mutant versions of a specific Lhcb gene. We have successfully produced a set of plants containing a gene encoding for LHCB1 and LHCB2 containing a phosphomimetic aspartate (T to D mutation; T-D) or the non-phosphorylatable alanine (T to A mutation; T-A) at the position of the N-terminal threonine which is the target of the STN7-dependent phosphorylation. Lines complemented with the native form of T->T were used as control.

Complemented lines with either of the point mutations at the third threonine of LHCB2 do not show any major defect in control light conditions. However, T-A and T-D are partially but not completely impaired in state transition. The complete depletion of 3XL2KO as well as the modification of the threonine residue result in the absence of the LHCII-PSII-LHCI supercomplex and increase the accumulation of STN7 kinase and phosphorylation of LHCB1. Due to the failure of the L-trimer in these mutants to connect to PSI and equilibrate light excitation between the two photosystems, the increase of STN7 kinase could be due to the over reduction of the plastoquinone pool which would further cause the observed increase in LHCB1 phosphorylation. This hypothesis is based on the over phosphorylation of LHCII in PsaH mutant in which state transition is impaired and the LHCII-PSI-LHCI supercomplex missing (Lunde et al., 2000). However, we cannot exclude that hyperphosphorylation of LHCB1 may be part of a compensatory process to alleviate the light excitation transfer by the PSII-surrounding light harvesting complex helping to maintain the equal excitation of PSII and PSI. It has been hypothesized that phosphorylation of LHCII is necessary to undocked from PSII and undocked phospho-LHCII have been shown to dissipate excitation energy(Iwai et al., 2008; Iwai et al., 2010; Ünlü et al., 2014). In 3XL2KO the PSI antenna cross section cannot increase by docking LHCII trimer. Therefore, the above mentioned LHCB1 over phosphorylation may be a mechanism to maintain equal functional antenna size of PSI and PSII in these mutants compared to WT.

LHCII phosphorylation and thylakoid structure

By promoting grana adhesion trimeric LHCII also plays a major role in thylakoid structure. A 'Velcro'-like model of grana stacking was proposed thanks to the negative charge of the stromal loop and the positive charge of the N-terminus of LHCII trimers on opposite membrane bilayers (Standfuss et al., 2005) . Phosphorylated LHCII at the N-terminal part of the protein adds an extra negative charge on the stromal gap of the thylakoid membrane. This negative charge may alter attractive and repulsive forces between the adjacent membranes and modulate thylakoid structure. Loss of LHCB1, which constitutes the largest portion of the trimeric LHCII, alters the organization of thylakoid membranes, in particular the grana have fewer stacks and a reduced width. These alterations may exclusively be due to the impact of the loss of LHCII trimers in 5XL1KO, however an exclusive role for LHCB1 cannot excluded. Furthermore, it is noteworthy that the minor thylakoid alterations in 5XL1KO are neither caused, nor compensated, by the structural lipid composition of the thylakoid membrane suggesting that there is no obvious correlation between the structural galactolipids of the thylakoid membrane and the LHCII proteins (Sattari Vayghan et al., 2022). Not surprisingly 3XL2KO mutants did not impede LHCII trimer formation and thylakoid topography is comparable to the WT plants (data not shown).

Future perspectives and preliminary results

During this PhD project, we generated total knockout lines for both the LHCB1- and LHCB2-encoding genes using CRISPR/Cas9 gene editing approach. These lines were called L1L2KO and were successfully screened to obtain the lines with no detectable protein of either LHCB1 and LHCB2 and without the Cas9 cassette in the genome. These now available lines will offer a great platform to study the importance of minor antenna and will give more insight into the role of these isoforms in PSII super complex structure. Furthermore, they could be used as a platform for future complementation and antenna engineering studies, as it allows to have a "neutral" background in terms of LHCII.

All generated lines in this project (5XL1KO, 3XL2KO and double mutant of LHCB1, LHCB2 (L1L2KO)) were challenged with fluctuating light stress, mild heat temperature and combinations thereof, LHCII phosphorylation has been suggested to have an important role ensuring photosynthetic efficiency notably under fluctuating light condition(Michele Grieco et al., 2012; Longoni et al., 2019) . Surprisingly and despite partial failure of 3XL2KO to do state transitions, and the inability to properly allocate LHCII trimers to the photosystems under rapid changes in light intensity, 3XL2KO did not show any growth impairment under light fluctuation, heat stress and the combined heat and light stress (Figure 1 A, B, C, D). The stn7 mutant was used as positive control as it has been reported to be vulnerable to fluctuating light (Michele Grieco et al., 2012). In brief, the observed stunted phenotype of stn7 under fluctuating light was explained by the absence of LHCII phosphorylation and antenna redistribution between two photosystems which is important to protect PSI and prevent harmful excessive overreduction of the photosynthetic electron transport chain (Michele Grieco et al., 2012).

5XL1KO and L1L2KO double mutants under fluctuating light conditions alone and heat stress, did not show any visible phenotype. However, the combination of light fluctuation stress with mild temperature stress resulted in a bleached phenotype for these genotypes as well as stn7 (Figure 1 A, B, C, D).

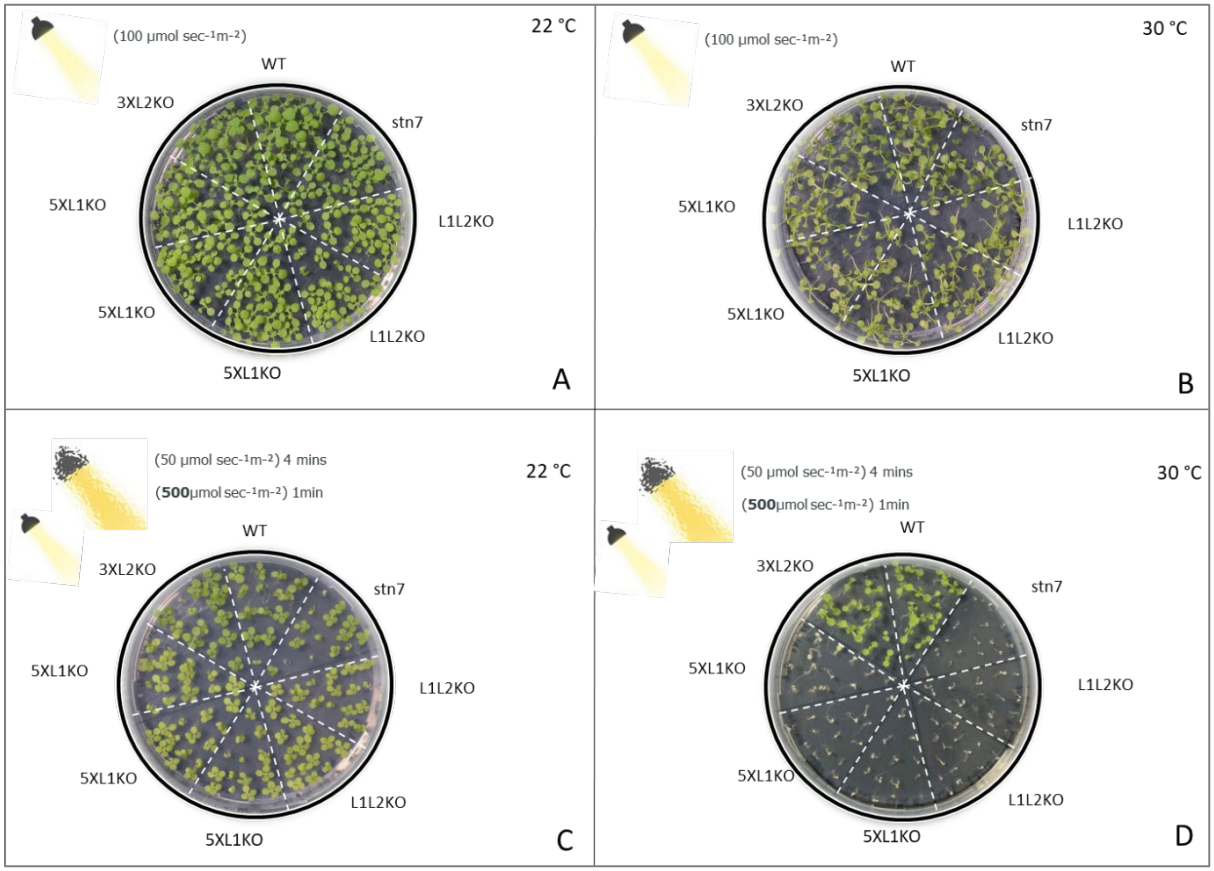

Figure 2 I Growth of the seedling constant light condition under fluctuating light, heat stress and combined heat and fluctuating light condition. (A, B): Plants were grown under a long day cycle with during the day under constant light intensity (100 µmol photons m^{-2} s^{-1}) after two days of germination under 22°C the plate was kept in 22°C in (A) and was transferred heat stress 30°C but the same light condition. (C-D) after two days of initial germination under constant light condition plates were transferred under a fluctuating light intensity with 4 min at 50 µmol photons m^{-2} s^{-1} and 1 min at 500 µmol photons m^{-2} s^{-1}. The growth chamber was settled to 22°C in plates (C) and 30°C in plates (D).

The lethal phenotype of 5XL1KO, L1L2KO and stn7 mutants under combined heat and fluctuating light stress points to the existence of a regulatory mechanism that is important to ensure photosynthetic efficiency and plant survival. LHCB2 is probably not a main contributor. But it appears that LHCB1 and/or its STN7-dependent phosphorylated form are important key player in this mechanism. Recently, we have obtained additional complemented lines in which the LHCB1 phosphorylation site is modified in the 5XL1KO background. These plants will allow to clarify the LHCB1's phosphorylation contribution in this acclimatory response. Our preliminary results revealed that modification in LHCB1 phosphorylation site, in which we point mutated the threonine to the non-phosphorylatable alanine T-A or the phosphomimetic aspartate T-D, allow to complement LHCB1 in terms of protein amount. Despite to the absence of phosphorylatable LHCB1 these plants do not show a bleached phenotype under combined heat and fluctuating light stress. However, additional replicates are required to confirm that the role of LHCB1 is structural in the formation of LHCII trimers, and that it is independent of its phosphorylation.
Further analyses are needed in other to conclusively assess the role of LHCB1 phosphorylation and its effect on the organization of the thylakoid membrane in the acclimation to the combined stress. To achieve this goal, it will be necessary to carry out transmission electron microscopy analysis. This allows to directly observe thylakoid structure after application of different stress conditions, specifically combined heat and fluctuating light. To further characterize the defects behind the combined stress phenotype, chlorophyll florescence of PSII and PSI, plastoquinone redox state and its re-oxidation kinetic as well as CO_2 assimilation rate will be measured and compared to control lines

In another future project it would be interesting to know whether the acclimatory properties of LHCB1 depend specifically on its N-terminal region. The different amino acid sequences of the N-terminal portion of each of the LHCIIs may underlie the specific regulatory and acclimatory roles of each isoform. To address this question, it would be interesting to complement the 5XL1KO total knockout with a chimeric LHCB1 protein in which the N-terminal part has been substituted by the one of LHCB2 and vice versa. Modification of the N-terminal region may have an impact on the stability and structure of the photosynthetic supercomplexes, hence, native gels will be used to characterize the super complex profiles in mutants expressing such chimeric LHCII isoforms. The complexes resulting from this separation will be analyzed by high-resolution Nano-Liquid Chromatography-Mass Spec (nLC-MS/MS). This will lead to a better understanding of the possible interactions amongst proteins in larger supercomplexes.
An additional question that I would like to answer is whether LHCB2 in sufficient amounts can complement the lack of LHCB1? To address this question, we would like to transform 5XL1KO with a construct containing two LHCB2 coding sequences under the control of the double Lhcb1.1-Lhcb1.3 promoter and terminator. The aim is to achieve levels of expression of the LHCB2 protein comparable to those of LHCB1. This should restore the chlorophyll, and thus the amount of total LHCII, to WT level, therefore allowing to address whether a single LHCN type is sufficient when maintaining the size of the LHCII.

Conclusion

Disentangling the distinct roles of each antenna isoform, LHCB1 and LHCB2 will shed light on short and long term acclimatory processes. This will lead to a better comprehension of how each isoform contributes to LHCII network organization and results in an optimal balance between light capture and photoprotection. The stable knock out lines produced in this project are an important tool for the investigation of LHCII and of interest to the scientific community. These lines open new research avenues including the fine engineering of the LHCII network. It is worth noting that the acclimation responses of the plants, and in particular the thermal dissipation of excess light, can be improved by targeted protein engineering. Modification of the dynamics of the antenna network, for instance by modifying the N-terminal regulatory domain, may lead to increased phosphorylation kinetics, and thus faster photosynthetic acclimation, a novel possible direction for photosynthesis improvement. Much focus was devoted to elucidating the role of LHCIIs posttranslational modifications, specifically N - terminal phosphorylation. This thesis indicates specific contributions of each isoform in the overall dynamics of LHCII and the precise and specific role of the negative charge of the phosphate group in long and short term acclimatory response and especially in state transitions. Clearly, it would be interesting to investigate the precise roles of LHCII and its PTMs more broadly in the maintenance of thylakoid organization and photosynthetic efficiency under non- optimal growth conditions.

References

Albanese, P., Tamara, S., Saracco, G., Scheltema, R. A., & Pagliano, C. (2020). How paired PSII–LHCII supercomplexes mediate the stacking of plant thylakoid membranes unveiled by structural mass-spectrometry. *Nature Communications*, *11*(1), 1361. https://doi.org/10.1038/s41467-020-15184-1

Andersson, J., Wentworth, M., Walters, R. G., Howard, C. A., Ruban, A. V., Horton, P., & Jansson, S. (2003). Absence of the Lhcb1 and Lhcb2 proteins of the light-harvesting complex of photosystem II - effects on photosynthesis, grana stacking and fitness. *Plant J*, *35*(3), 350-361. https://doi.org/10.1046/j.1365-313x.2003.01811.x

Bellafiore, S., Barneche, F., Peltier, G., & Rochaix, J. D. (2005). State transitions and light adaptation require chloroplast thylakoid protein kinase STN7. *Nature*, *433*(7028), 892-895. https://doi.org/10.1038/nature03286

Bergner, S. V., Scholz, M., Trompelt, K., Barth, J., Gäbelein, P., Steinbeck, J., Xue, H., Clowez, S., Fucile, G., Goldschmidt-Clermont, M., Fufezan, C., & Hippler, M. (2015). STATE TRANSITION7-Dependent Phosphorylation Is Modulated by Changing Environmental Conditions, and Its Absence Triggers Remodeling of Photosynthetic Protein Complexes. *Plant Physiol*, *168*(2), 615-634. https://doi.org/10.1104/pp.15.00072

Crepin, A., & Caffarri, S. (2015). The specific localizations of phosphorylated Lhcb1 and Lhcb2 isoforms reveal the role of Lhcb2 in the formation of the PSI-LHCII supercomplex in Arabidopsis during state transitions. *Biochim Biophys Acta*, *1847*(12), 1539-1548. https://doi.org/10.1016/j.bbabio.2015.09.005

Delosme, R., Olive, J., & Wollman, F.-A. (1996). Changes in light energy distribution upon state transitions: an in vivo photoacoustic study of the wild type and photosynthesis mutants from Chlamydomonas reinhardtii. *Biochimica et Biophysica Acta (BBA) - Bioenergetics*, *1273*(2), 150-158. https://doi.org/https://doi.org/10.1016/0005-2728(95)00143-3

Espineda, C. E., Linford, A. S., Devine, D., & Brusslan, J. A. (1999). The AtCAO gene, encoding chlorophyll a oxygenase, is required for chlorophyll b synthesis in Arabidopsis thaliana. *Proceedings of the National Academy of Sciences*, *96*(18), 10507-10511. https://doi.org/doi:10.1073/pnas.96.18.10507

Grieco, M., Tikkanen, M., Paakkarinen, V., Kangasjärvi, S., & Aro, E.-M. (2012). Steady-State Phosphorylation of Light-Harvesting Complex II Proteins Preserves Photosystem I under Fluctuating White Light *Plant Physiology*, *160*(4), 1896-1910. https://doi.org/10.1104/pp.112.206466

Grieco, M., Tikkanen, M., Paakkarinen, V., Kangasjärvi, S., & Aro, E. M. (2012). Steady-state phosphorylation of light-harvesting complex II proteins preserves photosystem I under fluctuating white light. *Plant Physiol*, *160*(4), 1896-1910. https://doi.org/10.1104/pp.112.206466

Iwai, M., Takahashi, Y., & Minagawa, J. (2008). Molecular remodeling of photosystem II during state transitions in Chlamydomonas reinhardtii. *Plant Cell*, *20*(8), 2177-2189. https://doi.org/10.1105/tpc.108.059352

Iwai, M., Yokono, M., Inada, N., & Minagawa, J. (2010). Live-cell imaging of photosystem II antenna dissociation during state transitions. *Proc Natl Acad Sci U S A*, *107*(5), 2337-2342. https://doi.org/10.1073/pnas.0908808107

Kim, E. H., Li, X. P., Razeghifard, R., Anderson, J. M., Niyogi, K. K., Pogson, B. J., & Chow, W. S. (2009). The multiple roles of light-harvesting chlorophyll a/b-protein complexes define structure and optimize function of Arabidopsis chloroplasts: a study using two chlorophyll b-less mutants. *Biochim Biophys Acta*, *1787*(8), 973-984. https://doi.org/10.1016/j.bbabio.2009.04.009

Leoni, C., Pietrzykowska, M., Kiss, A. Z., Suorsa, M., Ceci, L. R., Aro, E. M., & Jansson, S. (2013). Very rapid phosphorylation kinetics suggest a unique role for Lhcb2 during state transitions in Arabidopsis. *Plant J*, *76*(2), 236-246. https://doi.org/10.1111/tpj.12297

Leutwiler, L. S., Meyerowitz, E. M., & Tobin, E. M. (1986). Structure and expression of three light-harvesting chlorophyll a/b-binding protein genes in Arabidopsis thaliana. *Nucleic Acids Res*, *14*(10), 4051-4064. https://doi.org/10.1093/nar/14.10.4051

Longoni, P., Douchi, D., Cariti, F., Fucile, G., & Goldschmidt-Clermont, M. (2015). Phosphorylation of the Light-Harvesting Complex II Isoform Lhcb2 Is Central to State Transitions *Plant Physiology*, *169*(4), 2874-2883. https://doi.org/10.1104/pp.15.01498

Longoni, P., Samol, I., & Goldschmidt-Clermont, M. (2019). The Kinase STATE TRANSITION 8 Phosphorylates Light Harvesting Complex II and Contributes to Light Acclimation in Arabidopsis thaliana [Original Research]. *Frontiers in Plant Science*, *10*. https://doi.org/10.3389/fpls.2019.01156

Lunde, C., Jensen, P. E., Haldrup, A., Knoetzel, J., & Scheller, H. V. (2000). The PSI-H subunit of photosystem I is essential for state transitions in plant photosynthesis. *Nature*, *408*(6812), 613-615. https://doi.org/10.1038/35046121

McGrath, J. M., Terzaghi, W. B., Sridhar, P., Cashmore, A. R., & Pichersky, E. (1992). Sequence of the fourth and fifth Photosystem II type I chlorophyll a/b-binding protein genes of Arabidopsis thaliana and evidence for the presence of a full complement of the extended CAB gene family. *Plant Mol Biol*, *19*(5), 725-733. https://doi.org/10.1007/bf00027069

Murata, N. (2009). The discovery of state transitions in photosynthesis 40 years ago. *Photosynth Res*, *99*(3), 155-160. https://doi.org/10.1007/s11120-008-9389-8

Murray, D. L., & Kohorn, B. D. (1991). Chloroplasts of Arabidopsis thaliana homozygous for the ch-1 locus lack chlorophyll b, lack stable LHCPII and have stacked thylakoids. *Plant Mol Biol*, *16*(1), 71-79. https://doi.org/10.1007/bf00017918

Pietrzykowska, M., Suorsa, M., Semchonok, D. A., Tikkanen, M., Boekema, E. J., Aro, E.-M., & Jansson, S. (2014). The Light-Harvesting Chlorophyll a/b Binding Proteins Lhcb1 and Lhcb2 Play Complementary Roles during State Transitions in Arabidopsis *The Plant Cell*, *26*(9), 3646-3660. https://doi.org/10.1105/tpc.114.127373

Rantala, M., Ivanauskaite, A., Laihonen, L., Kanna, S. D., Ughy, B., & Mulo, P. (2022). Chloroplast Acetyltransferase GNAT2 is Involved in the Organization and Dynamics of Thylakoid Structure. *Plant and Cell Physiology*. https://doi.org/10.1093/pcp/pcac096

Rantala, M., Rantala, S., & Aro, E.-M. (2020). Composition, phosphorylation and dynamic organization of photosynthetic protein complexes in plant thylakoid membrane [10.1039/D0PP00025F]. *Photochemical & Photobiological Sciences*, *19*(5), 604-619. https://doi.org/10.1039/D0PP00025F

Sattari Vayghan, H., Nawrocki, W. J., Schiphorst, C., Tolleter, D., Hu, C., Douet, V., Glauser, G., Finazzi, G., Croce, R., Wientjes, E., & Longoni, F. (2022). Photosynthetic Light Harvesting and Thylakoid Organization in a CRISPR/Cas9 Arabidopsis Thaliana LHCB1 Knockout Mutant [Original Research]. *Frontiers in Plant Science*, *13*. https://doi.org/10.3389/fpls.2022.833032

Sattari Vayghan, H., Tavalaei, S., Grillon, A., Meyer, L., Ballabani, G., Glauser, G., & Longoni, P. (2020). Growth Temperature Influence on Lipids and Photosynthesis in Lepidium sativum [Original Research]. *Frontiers in Plant Science*, *11*. https://doi.org/10.3389/fpls.2020.00745

Standfuss, J., Terwisscha van Scheltinga, A. C., Lamborghini, M., & Kühlbrandt, W. (2005). Mechanisms of photoprotection and nonphotochemical quenching in pea light-harvesting complex at 2.5 A resolution. *Embo j*, *24*(5), 919-928. https://doi.org/10.1038/sj.emboj.7600585

Ünlü, C., Drop, B., Croce, R., & van Amerongen, H. (2014). State transitions in Chlamydomonas reinhardtii strongly modulate the functional size of photosystem II but not of photosystem I. *Proc Natl Acad Sci U S A*, *111*(9), 3460-3465. https://doi.org/10.1073/pnas.1319164111

Węgrzyn, A., Krysiak, M., Kulik, A., Gieczewska, K. B., & Mazur, R. (2022). STN7 Kinase Is Essential for Arabidopsis thaliana Fitness under Prolonged Darkness but Not under Dark-Chilling Conditions. *Int J Mol Sci*, *23*(9). https://doi.org/10.3390/ijms23094531

Wollman, F.-A. (2001). State transitions reveal the dynamics and flexibility of the photosynthetic apparatus. *The EMBO Journal*, *20*(14), 3623-3630. https://doi.org/https://doi.org/10.1093/emboj/20.14.3623